STOCHASTIC APPROACH FOR FINE SEDIMENT EROSION PREDICTION

By

FAEZEH BEHZADNEJAD

A dissertation submitted to the

Graduate School-New Brunswick

Rutgers, The State University of New Jersey

In partial fulfillment of the requirements

For the degree of

Doctor of Philosophy

Graduate Program in Civil and Environmental Engineering

Written under the direction of

Professor Ali Maher

And approved by

_____

_____

_____

_____

New Brunswick, New Jersey

October, 2015

ABSTRACT OF THE DISSERTATION

Stochastic Approach for Fine Sediment Erosion Prediction

By FAEZEH BEHZADNEJAD

Dissertation Director:

Dr. Ali Maher

This study aimed to characterize the erosion behavior of cohesive sediments in the Newark Bay, at flow velocities below 1 $\frac{m}{s}$ based on their index properties. The experimental methodology and data interpretation scheme of this research were devised based on the critical analysis of previous literature and aimed to reduce uncertainty, subjectivity, and arbitrariness. A comparison of erosion measurements obtained in this study with the results of some in-situ experiments conducted by other researchers revealed a strong consistency between these studies. The fact that this ex-situ study has been as successful as in-situ studies is quite an achievement. The success of the devised experimental methodology was also highlighted when the results were compared to similar ex-situ studies because the range of erosion rates measured in this study was well beyond the capability of those methods.

This research contributes to the literature on cohesive sediment erosion by offering new insights into three primary areas: regression, stochastic, and probabilistic analysis of erosion test results.

First, this study employed the regression technique to obtain the best linear unbiased estimator of erosion rates based on sediment index properties. The analysis resulted in the development of two fairly valid models for both fine- and coarse-grained sediments of the Newark Bay: (1) Newark Bay Fine Model (NBFM) and (2) Newark Bay Coarse Model (NBCM). These models were evaluated through cross-validation and cross-model comparison, as well as validation against a new dataset.

Second, a new methodology was developed for a stochastic analysis of erosion data by applying the Monte Carlo simulation technique. To the best of the author's knowledge, this technique had not been previously used in sediment erosion studies. This robust stochastic method enabled the researcher to investigate erosion over many artificially generated samples, in lieu of measured data, and make more realistic predictions. The confidence interval provided by stochastic simulations has a significant application in sediment erosion risk analysis.

Third, the framework developed for the probabilistic analysis of erosion data offers a standardized methodology for data analysis that paves the way for the comparison of different studies that use inconsistent methodologies.

ACKNOWLEDGEMENTS

I would like to convey my heartfelt gratitude to my PhD advisor Professor Ali Maher, Director of Center for Advanced Infrastructure and Transportation at Rutgers University. Without his unconditional support, guidance, and encouragement, this research would not have been possible. I have definitely learned the most from his visionary thinking and inspiring courage to tackle challenges.

I am also very grateful to the New Jersey Department of Transportation, particularly Mr. Scott Douglas for patiently providing strong support to this research. My thanks to Mr. Richard N. Weeks, the President of Weeks Marine Inc., as well for his major contribution to this research through his generous donations for establishment of the Weeks Soil and Sediment Management Laboratory.

I am indebted to Mr. Ryan Miller, the manager of Weeks Soil and Sediment Management Laboratory, whose contribution was integral to the establishment of the laboratory as well as timely completion of this research project. He always offered a helping hand when I encountered technical difficulties in my research. I would also like to convey my appreciation for the efforts of Mr. Dane Brosseau, our dedicated laboratory technician, as well as our laboratory interns Mr. Peter Katz, Mr. Cory Karinja, Mr. Brian Bersch, and Mr. Emre Imamoglu.

My warmest thanks go to Professor Nenad Gucunski, Chairman of Rutgers Department of Civil and Environmental Engineering, who provided me constant support and guidance since my first day at Rutgers. I am also thankful to my other committee members, Professor Mohsen Jafari, Chairman of Rutgers Department of Industrial and Systems Engineering, as well as Professor Trefor Williams, who kindly accepted the request to be my committee members despite their

busy schedules. Special thanks go to Professor Robert Miskewitz for his constructive feedback that improved my dissertation.

My gratitude too to the research team at J. Sterling Jones Hydraulics Research Laboratory of the Turner-Fairbank Highway Research Center, especially Dr. Kornel Kerenyi and Mr. Andreas Wagner, for their time and collaboration. I also owe many thanks to Professor Doyle Knight, Director of the Centre for Computational Design at Rutgers Department of Mechanical & Aerospace Engineering, for his support and advice throughout this study.

My thanks also to Ms. Azam Kalantari, the Administrative Coordinator of Center for Advanced Infrastructure and Transportation, not only because of her great assistance with my administrative needs, but also because she made me feel at home.

I have also been very fortunate to have the strong support of my advisors at the George Washington University School of Business, Professor Kristin Lamoureux and Professor Don Hawkins, in the past year. The completion of my thesis would not have been possible without the steadfast support of my mentor and supervisor at the World Bank, Dr. Hannah Messerli. Her encouragement and absolute support during the final stages were the catalysts for me to complete my thesis.

I owe all my success and achievements to my parents who fostered my creativity and self-confidence and gave me the courage to think big, aim high, and try hard. I would like to thank them as well as my best friend, sister, and role model, Fatemeh, for being my strongest supporters for longer than I remember.

Lastly, I would like to convey my sincere appreciation and gratitude to all my friends who have helped and inspired me during my doctoral study: Ms. Mehrnaz Tavan, Ms. Beheshteh Abdi, Mr. Alireza Aghasi, Ms. Sogol Fallah Moshfeghi, Mr. Farhad Fetrat, Ms. Nikoo Ghaffari , Mr. Amir Ghafoori, Ms. Soudeh Ghorbani , Mr. Munir Haggag , Ms. Donya Hajializadeh, Mr. Masoud

Janbaz, Ms. Golnaz Javaheri, Ms. Dominika Kanakova, Ms Tara K. Looie, Ms. Yuanrui Li, Ms. Niloufar Mirhosseini, Ms. Dharini Natarajan, Ms. Tina Nikou, Mr. Hooman Parvardeh, Ms. Maryam Salehi, Ms. Faranak Salman Nouri, Ms. Farahnaz Soleimani, Ms. Elaheh Taghaddos.

DEDICATION

This dissertation is dedicated to:

My parents, Mina and Mohammad

And my grandparents, especially my dearest Ziba and Iran

TABLE OF CONTENTS

LIST OF TABLES

LIST OF FIGURES

LIST OF ABBREVIATIONS

ANOVA	Analysis of Variance
cm	centimeter
EFA	Erosion Function Apparatus
EPS	Extracellular Polymeric Substance
ESETM	Ex-Situ Erosion Testing Machine
CFD	Computational Fluid Dynamics
Cov	Covariance
CV	Cross-Validation
d	Hydraulic diameter, Particle diameter
D	Depth of sediment (in the bed)
FHWA	Federal Highway Administration
gr	gram
K	Von Kármán constant
kg	kilogram
LL	Liquid Limit
m	meter
mm	millimeter
MSE	Mean Squared Error
NBFM	Newark Bay Fine Model
NBCM	Newark Bay Coarse Model
P	Rose Number
Pa	Pascal
PF	Percent Fines
PI	Plasticity Index
PL	Plastic Limit
SD	Standard deviation

SE	Standard error
SS	Sample size
v	Volume of the sample
V	Average Velocity ($\frac{\text{cm}}{\text{s}}$)

LIST OF SYMBOLS

μ	Shear viscosity of the fluid
μm	Micrometer
ρ	Pearson correlation
ρ_{Bulk}	Bulk density
ρ_{sed}	Sediment density
ρ_{water}	Water density
ρ_{d}	Dry bed density
ρ_{d0}	Dry bed density at the initial period of bed formation
τ	Shear stress
τ_{ce}	Critical shear stress for erosion
τ_{cr}	Critical shear stress
τ_{th}	Theoretical shear stress
ν	Kinetic viscosity ($\frac{m^2}{s}$)
λ	Friction factor
θ	Shields parameter or dimensionless critical shear stress
G_s	Specific gravity
u^*	Shear velocity
W_{i-air}	Initial weight
W_{ls}	Submerged weight loss
W_{lu}	Unsubmerged weight loss
W_{ns}	Non − submerged weight of the sample
w_s	Grain′s fall velocity
W_s	Submerged weight of the sample

1. INTRODUCTION

Statement of the Problem

Knowledge of cohesive sediment transport has found applications in many disciplines like geology and geography, as well as mechanical, geotechnical and environmental engineering. Waterways management and contaminant transport are two major interdisciplinary fields motivating exclusive research on cohesive sediment transport to address their challenges. In waterways management, maintenance and capital dredging are inevitable operations for maintaining competitive global networks. The fact that over 80 percent of the volume of global trade is handled by maritime transport indicates a high traffic concentration imposed on large ports (Rodrigue, Slack, & Notteboom, N.D.). Manufacturing of the giant post-Panamax generation of containerships is also an influential trend, obligating the creation of deeper and wider navigation channels. Hence, there is no surprise that dredging schemes and waterfront development projects are most in need of research on sediment transport.

Contaminant transport is the second field that emphasizes research on cohesive sediment transport. In only a few decades of industrial progress, a huge volume of toxic and hazardous chemicals has been accidently or deliberately released into the aquatic environment. As cohesive sediments can absorb a wide range of these pollutants, their accumulation in low energy environments, e.g. estuaries and coastal waterfronts, has produced hazardous contaminant repositories close to many developed areas. This explains why many of the studies on sediment transport are triggered by human health and ecological concerns, and aim to model contaminant

transport. Figure 1-1 illustrates historical profiles of globally averaged concentrations of three major groups of contaminants (Valette-Silver, 1993).

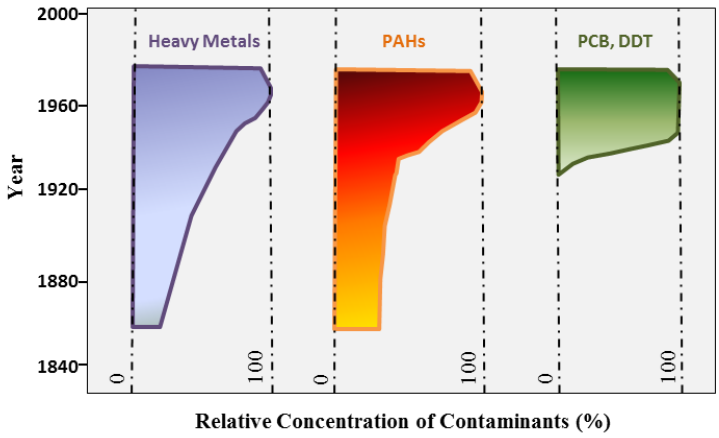

Figure 1-1. **Globally averaged profiles of historical sediment contamination in industrialized countries. Adapted from "The use of sediment cores to reconstruct historical trends in contamination of estuarine and coastal sediments," by N. J. Valette-Silver, 1993, Estuaries.**

The key processes constituting the dynamics of cohesive sediment transport are flocculation, deposition, consolidation, and erosion. Even though erosion is the most significant process in modeling sediment transport, there exists no theoretical erosion model that is universally accepted (Lick, 2008). However, several empirical methods have been developed to predict erosion in a wide range of circumstances using various devices.

Research Framework

The original objective of this research study was to better understand the dependence of sediment erodibility on shear stress using a novel erosion testing flume – Ex-Situ Erosion Testing Machine (ESETM). This linear flume (Figure 1-2) was innovatively designed to apply state-of-the-art technology to directly measure shear and weight forces exerted on a sample of sediment in real-time.

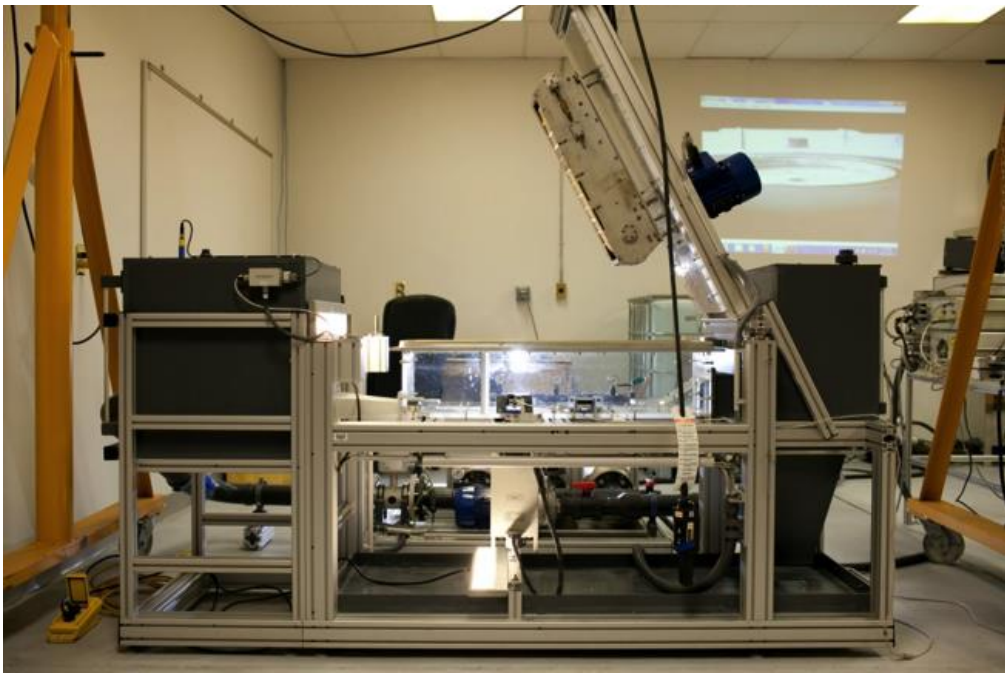

Figure 1-2. **The Ex-Situ Erosion Testing Machine assembled and installed in Weeks Soil and Sediment Management Laboratory**

The research framework used in this study consists of the four following main components: (1) device assessment, (2) experimental tests, (3) regression analysis of the experimental data, and (4) stochastic analysis. Figure 1-3 shows the flow chart of the main research activities accomplished in this study.

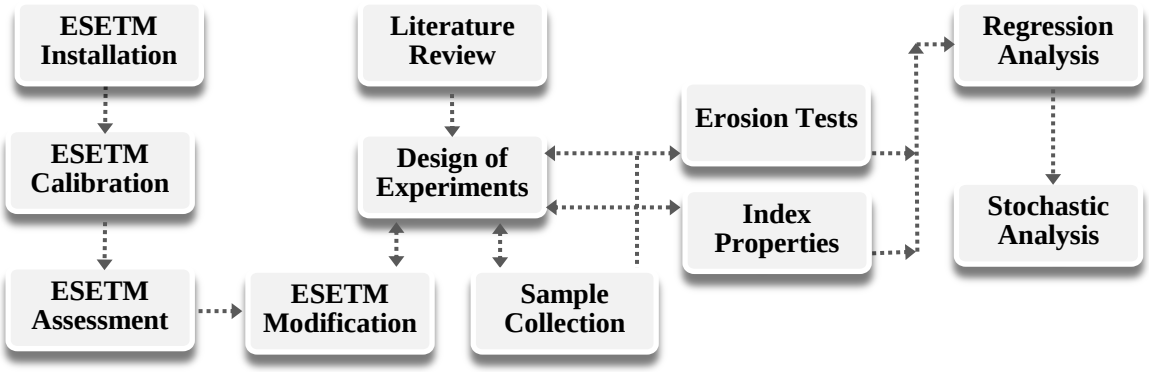

Figure 1-3. **The research methodology framework for the current study**

1- Device assessment: After the Ex-Situ Erosion Testing Machine was assembled, installed, and calibrated, extensive research was conducted to evaluate its performance. Significant effort was made in implementing a scientific methodology to identify the strengths and weaknesses of ESETM and evaluate the accuracy and reliability of its measurements. Due to the results of this assessment, the research objective was transformed into "**characterization of the behavior of cohesive sediments in the Newark Bay, at flow velocities below 1 $\frac{m}{s}$, based on their index properties."**

2- Experimental tests: In this study, 755 erosion rate tests were conducted on 142 fairly undisturbed samples taken from 24 cores extracted from the Newark Bay. Table 1-1 lists all the samples taken for various tests within this study.

Table 1-1. ***Itemization of samples in tests performed in this study***

Test	Count of samples
Erosion	**142**
Water content	**74**
Organic content	**68**
Bulk density	**77**
Specific gravity	**16**
Percentage of fines	**18**
Atterberg limits	**14**

3- Regression analysis of the experimental data: Regression analysis of the data resulted in the development of two fairly valid models for fine- and coarse-grained sediments of the Newark Bay: (1) Newark Bay Fine Model (NBFM) and (2) Newark Bay Coarse Model. Figure 1-4 compares NBFM's predictions to erosion rate observations for the Newark Bay samples based on their bulk density and water content.

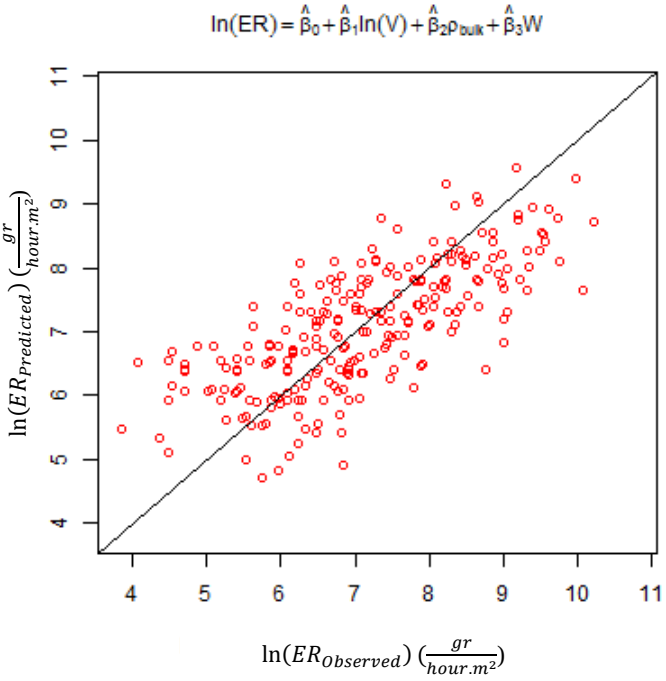

***Figure 1-4*. Observed erosion rates versus NBFM's predictions**

Both experimental and analytical results were compared with those obtained in similar studies in the literature. The comparison revealed that the experimental methodology had been as successful as in-situ studies in measuring low erosion rates occurring at flow velocities below 1 $\frac{m}{s}$. This is a significant achievement for an ex-situ study.

4- Stochastic analysis: Eventually, a new methodology was developed for the stochastic analysis of erosion by applying the Monte Carlo technique to NBFM and NBCM. The availability of such a robust stochastic method makes it possible to study the erosion behavior of sediments

over many artificially generated samples (in lieu of measured data), resulting in higher levels of confidence in predictions.

Organization of Thesis

This thesis is organized into six chapters as follows:

Chapter 1 (current chapter): This chapter introduces the research and outlines its objectives.

Chapter 2: This chapter reviews the literature on cohesive sediment erosion. It explains the essential concepts and serves as a background to understanding the remaining chapters. The first four sections of this chapter are on sediments and sediment transport dynamics and concepts. The review of the literature revealed the lack of sufficient attention to the issue of scale. Despite its significance, this concept had generally been used in an unclear or inaccurate manner in the field of sediment transport. The final section of the literature review is devoted to a comprehensive and insightful discussion of the concept of scale in cohesive sediment erosion.

Chapter 3: This chapter provides a thorough explanation of the methodology used in this study for sample collection, preservation, and preparation, as well as the experimental methodology for index property and erosion tests.

One of the main conclusions from the literature review was the strong dependence of the results of the erosion rate tests on the experimental design (selected levels of shear stress, duration of each step) as well as the interpretation method. This makes the interpretation of the experimental results very subjective and hinders the comparison of data from different experiments. In order to mitigate the above concerns, it was decided to explore this practical problem and investigate its consequences in more detail prior to designing the erosion experiments for the current study. Therefore, a methodology was developed for the analytical interpretation of the erosion test results. This method, which is based on the probabilistic modeling of erosion, applies an optimization technique to solve for the model's parameters probabilistically.

Chapter 4: In this chapter, the results of both erosion and geotechnical tests are presented.

Chapter 5: Chapter 5 addresses data analysis and explains the analytical methodology used in this research in two sections: regression analysis and stochastic analysis. The second section describes the regression analysis used to develop two models for erosion rate of both fine and coarse sediments in the Newark Bay. The third section describes the methodology developed to build upon these models and conduct stochastic simulations for cohesive sediment erosion. The main conclusions are discussed at the end of each section.

Chapter 6: This chapter concludes and addresses the main results of the thesis.

Appendix A: Appendix A includes the additional graphs, tables, and boxes that can be referred to for more details.

Appendix B: The scope of erosion rate experiments is presented completely in Appendix B.

2. LITERATURE REVIEW

This chapter serves as a background to understanding the remaining chapters. Section 2.1 defines cohesive sediments and followed by the definition of sediment flocculation, adsorption, transport, deposition, consolidation, and transport in section 2.2. Sections 2.3 and 2.4 are dedicated to erosion and the concepts relevant to it. Section 2.5 focuses on the concept of scale in cohesive sediment erosion. It investigates the causes and consequences of temporal and spatial variations in the erosion behavior of cohesive sediments and aims to shed light on the significance of the issue of scale.

2.1. Definition of Cohesive Sediment

Natural cohesive sediment is a heterogeneous and porous material containing all three phases of solid, liquid and gas (Winterwerp & Van Kesteren, 2004) with a form varying from suspended sediments to highly consolidated bed structures (Figure 2-1). The weight and volume proportions of the solid, liquid, and gas phases and the particle size distribution can be extremely variable in natural sediments as illustrated in Figure 2-2. In soil mechanics, particles smaller than 63 μm (including silt and clay) are generally considered as fine particles and mixtures with percentage of fines higher than 50% are generally categorized as cohesive (versus granular for mixtures with less than 50 percent of fines). However, Whitehouse et al. (2009) believe that only about 10% dry mass by weight of fines is required to convert a sandy bed into one exhibiting cohesive properties. Moreover, mineralogical composition of particles also has an important effect on sediment behavior. Particle size analysis and cluster analysis of samples taken from the

Newark Bay led to considering mixtures with percent fines higher than 60 percent as cohesive sediment for the purpose of this study.

The topmost portion of the sediment surface within which particles are accessible to the flow is called the active layer or mixing layer. The depth of this layer depends on the vertical structure of the bed and can vary from a few millimeters to a few decimeters. Mass transfer occurs through the active layer's top and bottom boundaries that separate it from the flow and the bottom bed. Sediments get into the active layer through deposition and mixing mechanisms and get out of this layer through erosion and consolidation. Flow properties, sediment composition, and transport rates are the factors that influence the vertical gradient of consistency in the bed.

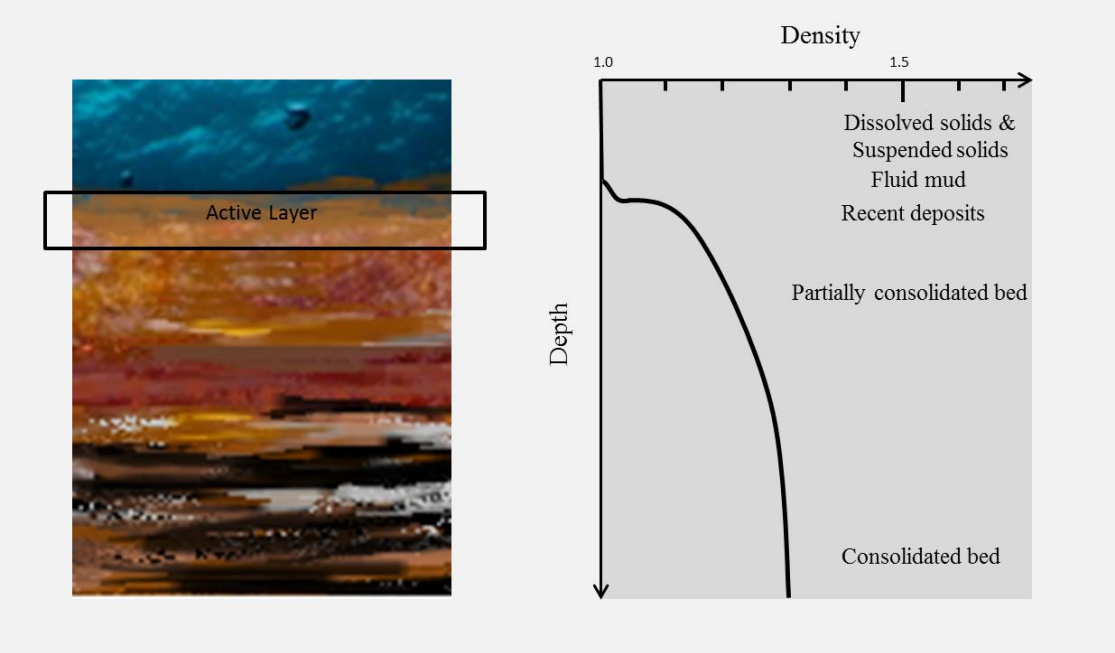

Figure 2-1. **Various natural forms of marine cohesive sediment**

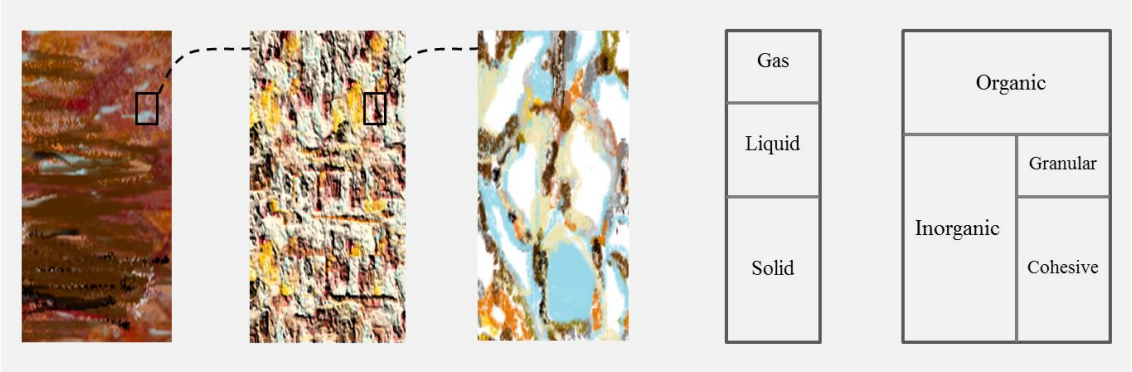

Figure 2-2. **Microstructure and composition of cohesive sediments**

2.2. Processes of Cohesive Sediments

This section describes the main processes of cohesive sediments including flocculation, adsorption, deposition, consolidation, and transfer. Erosion is discussed in detail in section 2.3.

2.2.1. Flocculation

Flocculation is the most characteristic property of cohesive sediments; when these sediments are brought in contact with a fluid, e.g. water, particle clusters (including enclosed water) named flocs, will be formed as a result of electrostatic aggregation (Winterwerp & Van Kesteren, 2004). Flocculation is the phenomenon that differentiates the behavior of granular and cohesive sediments. It is because of this process that sediment mineralogy and structure have a higher influence on the behavior of fine sediments compared to particle size distribution. In coastal regions, the dominant mode for deposition of fine cohesive material is flocculation (Lintern, 2003). However, “The mechanism of flocculation considerably complicates the task of modeling the transport of cohesive fine sediments, such as the ones found in estuaries” (Leupi, 2005). In certain environments similar to estuary heads, where salt and fresh water are mixed,

flocculation occurs more often and thus becomes a particularly important process to consider (Angelaki, 2006).

Clay particles have negatively charged external and interlayer surfaces. When these particles are in contact with an electrolyte, the charged surface absorbs polar water molecules and ions to form an ionic structure named the "double layer" referring to the two parallel layers of charge adsorbed to the surface. Figure 2-3 is a schematic of some clay particles surrounded by a double layer.

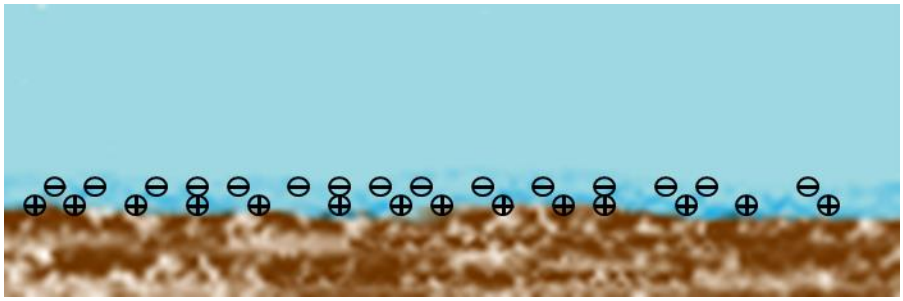

Figure 2-3. **The double layer formed in a suspension in contact with a negatively charged clay surface**

Sediment flocs have an open structure with several hierarchical orders of aggregation as displayed in Figure 2-4. First-order flocs consist of primary particles while higher-order flocs are made of lower-order aggregates and generally have lower strength (Partheniades, 1993). The low strength of larger flocs makes it difficult to measure floc size distribution from fluid samples as even sample extraction could lead to a disaggregation of the flocs (Angelaki, 2006).

Although the gravity force increases as a result of flocculation, floc' density generally decreases because of the open structure of the skeleton of the flocs formed in suspension. However, Lintern (2003) observed that the field settling velocity increases as a net result of these contracting actions. The floc settling velocity also depends on suspended solids concentration as it can be influenced by the interaction of other flocs present in the medium. For example, smaller particles can get trapped in a cluster of larger particles and settle at similar velocities (Been, 1980).

***Figure 2-4*. Hierarchical structure of flocs**

Several parameters are influential in the flocculation process including sediment size and mineralogy, suspended sediment concentration, turbulence intensity, organic coating, and salinity (Leupi, 2005). It should be noted that these factors are interactive, and their individual significance varies in different environmental conditions. For example, although the general assumption is that increasing suspended sediment concentration (SSC) increases the chance of floc formation, Van der Lee (1998) reported a different observation in his field study in the Dollard estuary. He investigated the impact of the fluid shear and suspended sediment concentration on the mud's floc size variation and discovered that the significance of SSC in floc formation varies with hydrodynamic conditions. He compared the role of fluid shear and SSC in the formation of flocs in a tidal channel and a nearby tidal flat; in contrast to the positive correlation between SSC and floc size in the tidal channel, there was a negative correlation between the two parameters above the tidal flat. He also recognized a diurnal pattern in the relationship between SSC and floc size: during the flood and ebb tides, higher levels of turbulence inhibited the development of larger flocs. A vertical concentration gradient also developed only when the flood current velocity started to decrease. However, some researchers agree that fluid shear is the main mechanism for floc formation in natural environments (Lintern, 2003).

Many studies have researched the effects of organic matter on the flocculation process with varied, complex results. For example, Whitehouse et al. (as cited in Angelaki (2006)) reported that the presence of organic material encourages organic binding, resulting in stronger and larger flocs. Lintern (2003), on the other hand, observed that organic sediment coatings could

potentially enhance, reduce or have no effect on the rate of the coagulation process in different settings.

The significance of flocculation in cohesive sediment transport is mainly derived from its continuous impact on the distribution of floc size and geometry and therefore, settlement velocity of sediments (Partheniades, 1993).

2.2.2. Adsorption

Adsorption in an intertidal system refers to the surface-based process through which ions, atoms, and molecules present in the water column adhere to sediment surface because of the physical or chemical attraction forces. A wide range of environmental contaminants (metals, toxic organics, radioactive particles etc.) are among the chemicals that get trapped in intertidal zones by adsorption due to the ionic nature of fine sediments.

Cohesive sediments provide a rich habitat for aquatic life that increases the chance of contaminant uptake by organisms and introduces them to the food web. Sediment resuspension (due to either an ordinary or an extreme event) and escape of contaminated pore water as a result of sediment consolidation are two other mechanisms that may lead to the separation of contaminants from the sediments introducing them into the marine environment.

2.2.3. Sediment Transport

Cohesive sediments, in general, do not have any standard form of existence. They can be suspended in the water column, recently deposited on the surface, attached to the fluid mud or consolidated into a structured bed with a depth-dependent stiffness degree. There are four principal processes that interactively and recursively work to transform these sediment states into each other (Figure 2-5): (1) Erosion (2) Deposition (3) Consolidation (4) Transfer. Flocculation and deflocculation are the processes that can occur simultaneously with almost each of these main

processes without directly changing the sediment state. In this study "sediment transport" is defined as the combination of all these extensively interrelated processes that together act toward shaping sediment dynamics in nature. It is important to note that many researchers use "sediment transport" to refer to both sediment transfer and what has been defined here as sediment transport. Figure 2-6 shows the flow chart of sediment transport processes. Most of the experimental studies on sediment transport have so far focused on each of the aforementioned processes in isolation (for simplification purposes).

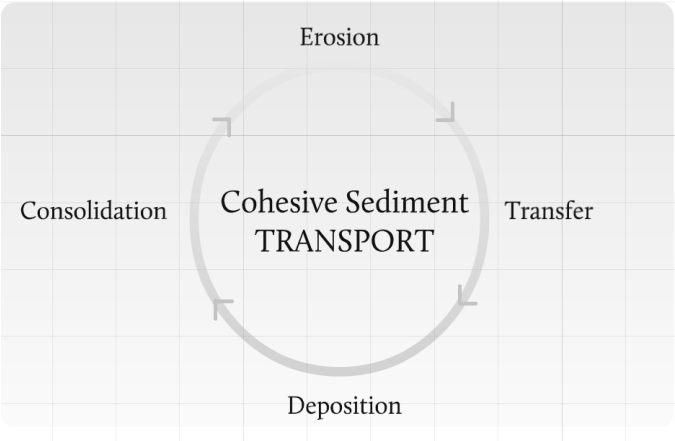

Figure 2-5. **Schematic of main processes involved in sediment transport dynamics**

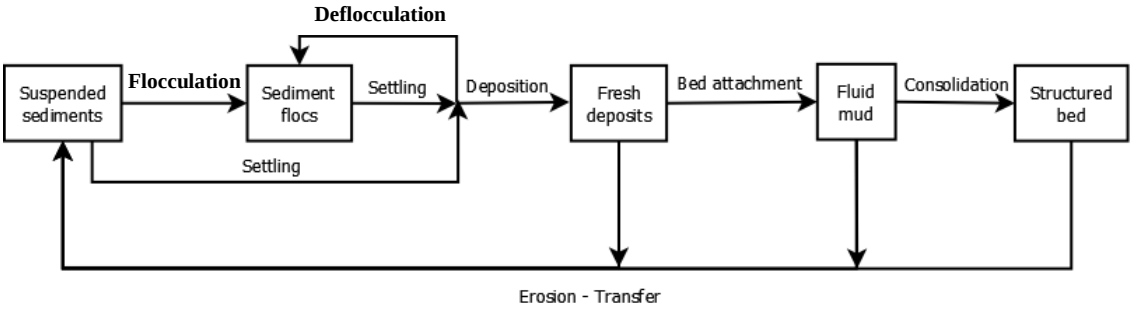

Figure 2-6. **Flow chart of sediment transport processes**

While deposition, consolidation, and erosion can be modeled as almost vertical processes, sediment transfer is a three-dimensional phenomenon due to the presence of complex turbulence

patterns in natural flows. Erosion and deposition are exchange processes occurring between the flow and the sediment bed. Consolidation, on the other hand, can be considered as a bed-based phenomenon while transfer is a problem in a two-phased flow. The forces acting upon sediments have a hydrodynamic, gravitational or electrochemical nature. Dependency of these forces on random factors (i.e. flow parameters, sediment characteristics, and environmental factors) introduces a source of randomness in time and space into all sediment transport processes. Therefore, each of these processes can be described as a problem in a random space-time field. Erosion, as the main subject of this research, is discussed in section 2.3 and the remaining processes are covered in the following three subsections.

2.2.4. Deposition

Deposition is a process wherein solid particles settlement (through a fluid) ends as they hit against the bed surface. Deposition can be considered as the polar opposite of erosion in bed development dynamics. Slurry column experiments, laboratory flume (linear and annular) experiments, and field (in situ) observations are the general methods for the measurement of deposition rate. The mud concentration in slurry column experiments is generally higher than in natural conditions, which makes it difficult to relate the settling rate and velocity observed within the slurry column to natural depositional behavior.

There are two main reasons to study deposition rate: (1) Deposition rate and pattern highly influence the void ratio and hence the texture of recent deposits. While slow deposition in still water leads to an open random fabric (high void index), rapid deposition from a dense suspension or sediment deposition occurring in the presence of a current give rise to a more uniformly oriented fabric with a lower void index (Lintern, 2003). (2) As a mechanism of material exchange between the flow and the bed, deposition rate should be directly taken into account to find the net sediment transport rate. Many researchers assume a depositional threshold

(flow velocity or shear stress) below which deposition occurs. Although it seems like a reasonable assumption for more uniform laboratory tests (such as homogeneous material, controlled flume geometry and flow characteristics), it is not the case in natural scenarios. Deposition and erosion can occur simultaneously (as depicted in Figure 2-7) and can be considered as two sides of a continuous two-way equilibrium. Variation in floc size and the presence of bedforms are two scenarios that can lead to simultaneous erosion and deposition. For example, a certain flow regime can be strong enough to erode smaller flocs and simultaneously weak enough to allow larger suspended flocs to be deposited, or various bedforms can create local depositional and erosional regions.

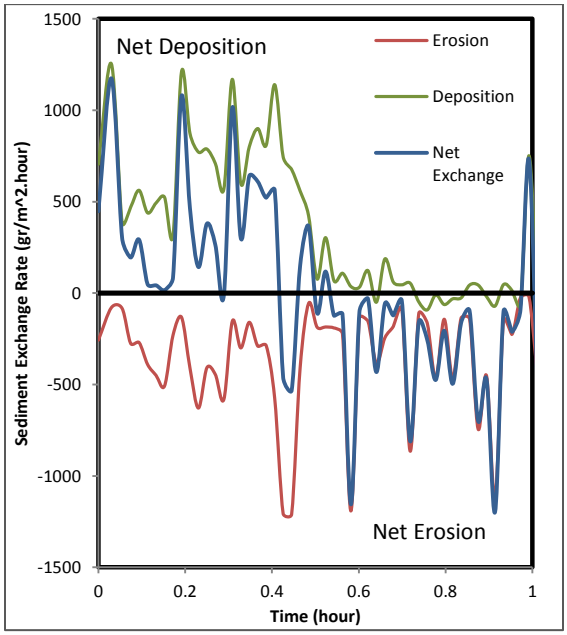

Figure 2-7. **Simultaneous erosion and deposition leading the system toward either an erosional or a depositional equilibrium**

There are three major factors that affect depositional behavior of marine sediments as displayed in Figure 2-8: (1) flow hydrodynamics (competence and capacity, location with respect to the estuarine turbidity maximum zone, etc.); (2) sediment supply in the flow and sediment characteristics: Subramanian (1993) studied several Indian rivers and suggested an inverse

relationship between the erosion rate upstream and deposition rate downstream of these rivers; and (3) flocculation dynamics, which has been previously discussed.

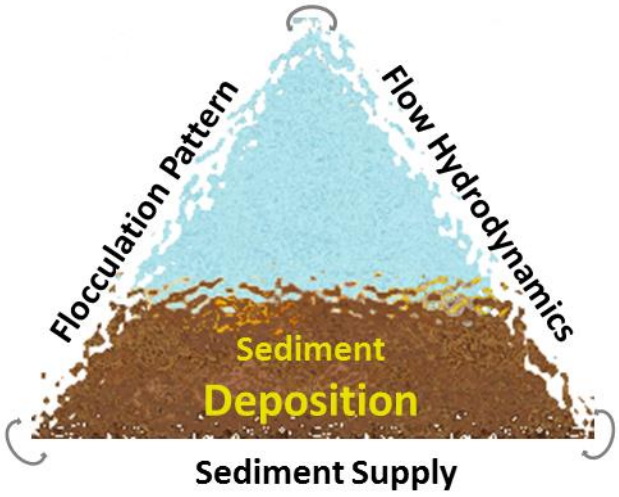

***Figure 2-8*. Main factors affecting sediments' depositional behavior**

There are different patterns of floc deposition as depicted in Figure 2-9. The same mass of sediments can deposit into layers of different thickness under various conditions (Lintern, 2003). Segregation of flocs while settling causes stratification in the bed with respect to density and erosion strength (Partheniades, 1993). The inter-particle bonds are rearranged as the settled flocs develop bonds with the bed, which is the main factor preventing the resuspension of deposited aggregates (Partheniades, 1993).

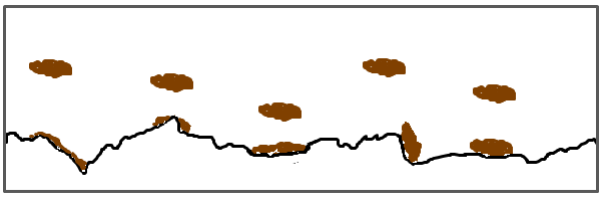

***Figure 2-9*. Random placement of floc deposition on the bed surface**

2.2.5. Consolidation

Karl Von Terzaghi, defines consolidation as any process that involves a decrease in water content of saturated soil without replacement of water by air. As new sediments overlay the bed surface, their submerged weight would be applied to the underneath layers as a static load. This gravitational loading causes an increase in the interstitial pore pressure, and as cohesive sediments have low permeability, the excess pressure can only be gradually transferred to solid particles through the expulsion of the fluid phase. This process will result in a reduction in the void ratio and hence a reorganization of sediment structure toward a more compacted state. The essential difference between the settling suspension and structured sediment matrix is an effective stress that develops during a transition phase (Been, 1980).

Although the driving force for consolidation (gravitational force from the overlying sediments) is mainly a physical force depending on the rate of deposition (Figure 2-10), there are also some chemical and biological factors that affect the soil permeability leading to complications in the consolidation process. Bioturbation (reworking of sediments by plants or animals) and gas production caused by decomposition of organic material are examples of such biochemical factors. Several investigations of consolidation have been conducted so far (although the presence of gas has been ignored in most cases); however, the effects of all the factors, especially the interaction between them, have not been considered (Lick, 2008).

Considering the factors affecting consolidation, different time scales should be involved when modeling this process in marine environments. In a self-weigh consolidation process, which normally occurs in natural environments, deposition and erosion rates and any time scale associated with them will influence the overburden pressure and hence consolidation. Deposition rate also influences the strength of fresh deposits by impacting the void ratio as more quickly deposited beds do not have time to strengthen before being bombarded and loaded by additional

flocs (Lintern, 2003). Biological activities, specifically gas formation (and gas movement within the matrix of flocs and aggregates) are additional time-dependent factors with rates varying in different environmental conditions.

In classic soil consolidation models, the rate of settlement on the surface is initially high, followed by lower rates, which is explained by the reduction in permeability. However, the presence, production, and movement of gas pockets in natural environments can create short-term and long-term irregularities in this pattern.

***Figure 2-10*. Interstitial water, squeezed out of marine sediments, travels upward due to gravitational loading caused by the weight of the overlying material**

2.2.6. Sediment Transfer

Marine sediment transfer (often referred to as sediment transport in the literature) is the movement of sediment particles or flocs by the flow. Flows carrying cohesive sediments in natural environments delineate a very complex problem in fluid mechanics not only because of the effect of solid particles in the turbulence structure, but also due to the strong interaction between the dynamic and movable sediment bed and the flow condition. Variations in the bed

geometry, bed roughness, and flow viscosity are examples of factors that are influenced by the flow and simultaneously affect the shear stress distribution at the boundary and hence the flow parameters in the near-bed region. “Description of sediment-laden flow becomes further complicated as suspended sediment includes smaller or larger vertical density gradients that can affect the efficiency of sweeps and ejections considerably” (Winterwerp & Van Kesteren, 2004).

Filip Hjulstrom (1935) proposed a graph to predict whether a particle of a certain size would be transferred (transported), deposited or eroded at different flow velocities (Figure 2-11). This graph includes two curves: (1) The lower curve presents the limit between transport and deposition. A particle being transferred by the flow would be deposited if the flow velocity falls below the limit suggested by this curve. (2) The upper curve marks the threshold beyond which the deposited sediment will erode. Any eroded sediment will continue to be transferred by the flow as long as its velocity is higher than the deposition limit.

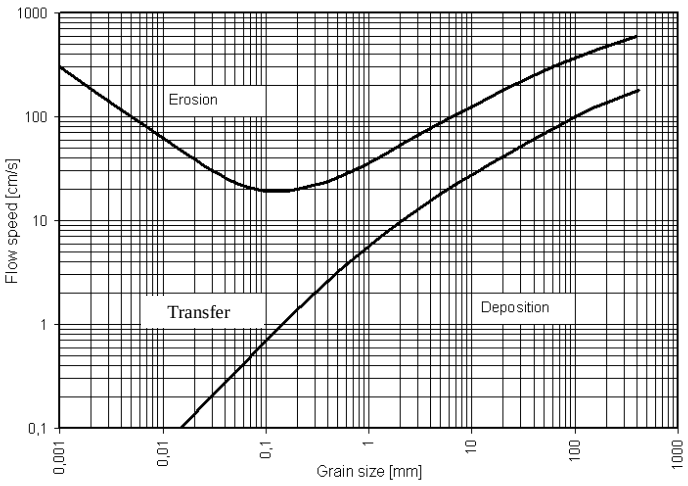

Figure 2-11. **Hjulstrom curve (source: unknown)**

There are three aspects to note about Filip Hjulstrom’s graph: (1) The erosion curve has a positive slope in the sand and gravel range (diameters larger than 0.05 mm) and a negative slope in the silt and clay range (diameters smaller than 0.05 mm). It means that a higher velocity

threshold is required for the erosion of a smaller clay particle compared to a larger clay particle and this is due to electrostatic forces. (2) The velocity range required to transfer fine particles is much larger than for coarse particles. (3) Flocculation and deflocculation are not taken into account in this curve; hence the results are valid for only granular sediments.

Albert Shields defined the ratio of driving forces (shear developed along the bed) to resisting forces (submerged weight of each particle) for sediment movement as a non-dimensional parameter called the Shields parameter. He empirically evaluated the critical Shields value at which the incipient motion occurs for different particle size ranges. In 1936, he plotted the resulting threshold values that he found together with the particles' Reynolds numbers to suggest a shaded region of critical shear stresses. Hunter Rouse later plotted a curve to produce what is now extensively used as the Shields curve (Figure 2-12). There are a few points to be noted about Shields' work:

(1) He made artificially flattened beds of uniformly-sized particles out of different materials (with a minimum diameter of 0.85 mm) for his tests. The range of boundary Reynolds numbers he generated during the tests is shaded in orange in Figure 2-12. The curve has been extended beyond this range by extrapolation.

(2) The force balance that he used to formulate the critical shear stress required for particle entrainment is only valid for granular material because: (i) electrostatic forces that have a significant role in cohesive sediment force balance, have not been considered in his formulation; (ii) cohesive sediments do not generally have the single spherical geometry as assumed in his formulation.

(3) Shields measured sediments transferred only as bedload while cohesive sediments are dominantly transferred as suspended loads.

(4) Because of practical reasons, Shields measured bedload transfer rate at different shear stress levels (all higher than the critical shear stress) and extrapolated his observed data to find the shear

stress associated with zero bedload rates. (5) Paintal (1971) reviewed the literature on critical shear stress and arranged some experiments to quantify bedload at shear stress values within close proximity of Shields' critical shear stress. He concluded that particle entrainment has a stochastic nature and hence there is no threshold below which no sediment movement occurs. (6) Even for granular particles, Shields ignored the effect of bedforms, bed armoring, and the degree of exposure of individual grains to the flow, which are all important factors (Fenton & Abbott, 1977). Shields defined a parameter representing the dimensionless critical shear stress as follows:

$$\boldsymbol{\theta = \frac{\tau_{cr}}{g(\rho_s - \rho)d} = f(\frac{u_* d}{\nu})}$$

θ: Shields parameter or dimensionless critical shear stress

τ_{cr}: critical shear stress at incipient motion

ρ_s: sediment density

ρ: fluid density

d: particle diameter

u_*: shear velocity

ν: fluid's kinematic viscosity

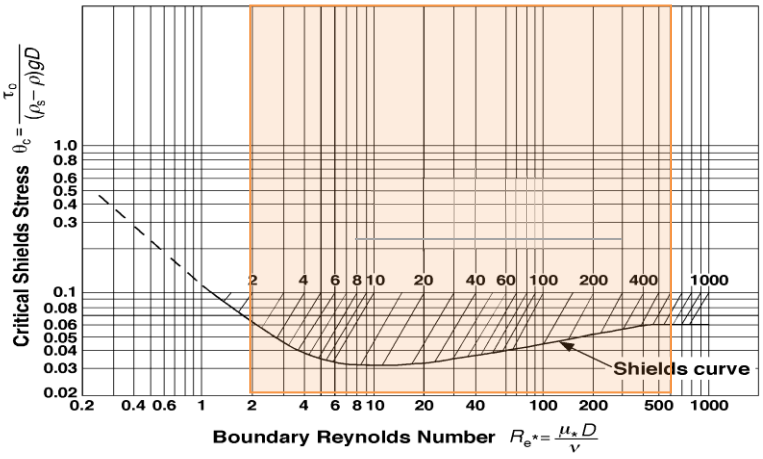

Figure 2-12. **Shields diagram modified by Rouse**

Different transfer modes have been recognized for natural sediments (summarized in Table 2-1): (1) Dissolved load is defined as ions and molecules dissolved in a water column. (2)

Suspended load includes particles and flocs kept in suspension by turbulent diffusive forces. (3) Wash load is the portion of suspended solids that are very tiny in size (clay range) and are kept in suspension by Brownian motion. (4) Bedload includes particles and flocs that move (roll, slide, saltate) while partially or completely supported by the bed.

Hickin (1995) collected data on various major rivers in all continents to compare the mean dissolved load to the mean suspended load and found ratios between 2% and 80% in these rivers (Hickin, 1995). Even though the high volume of wash load has a huge significance for land erosion studies at the watershed level, it does not directly affect river/estuarine morphology because the solute remains within the flow unless it is saturated. However, the wash load can have an indirect effect on erosion/deposition by altering the water column chemistry.

In order to predict the transfer mode for a particle of a certain size, we need to consider its vertical force balance. Figure 2-13 compares a floc of sediment with a certain settlement velocity (in static water) at three different turbulence levels. At lower velocities, eddies are smaller than the floc which causes smaller flow velocity fluctuations around the particle compared to the average settlement velocity. At higher velocities, on the other hand, larger eddies create bigger velocity fluctuations compared to the average fall velocity causing greater distortions in the particle's trajectory.

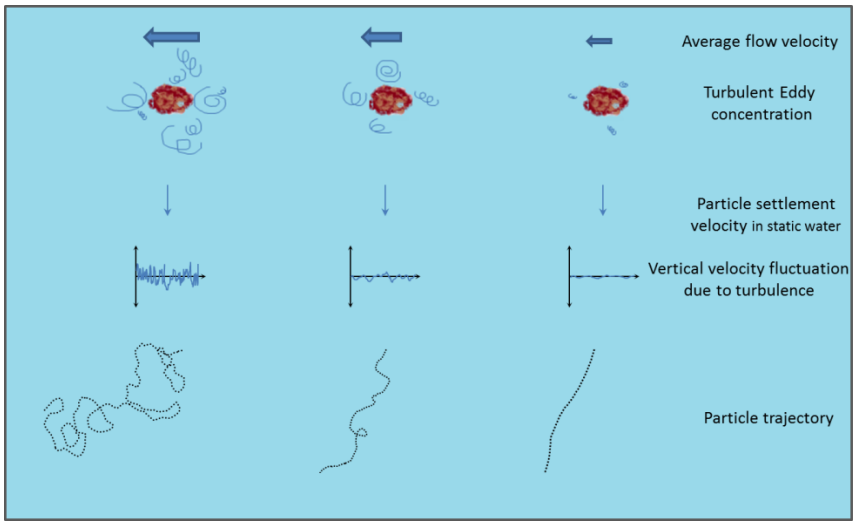

Figure 2-13. **Effect of the level of intensity and size of eddies on a suspended particle's trajectory**

The Rouse number (P) is a non-dimensional number defined to determine the transfer mode of a grain by comparing its settlement velocity with its upward velocity caused by turbulent velocity fluctuations.

$$\mathbf{P} = \frac{\mathbf{w_s}}{\boldsymbol{\beta\kappa u^*}}$$

w_s: grain's fall velocity

β: a constant to relate eddy viscosity to eddy diffusivity, typically taken to be equal to 1

κ: Vom Kármán constant, typically taken to be equal to 0.4

u^*: shear velocity

Table 2-1 compares different transfer modes and their typical ranges based on the Rouse number values. Cohesive sediments may experience repetitive cycles of resuspension, transfer, and resettlement before their final embedment as illustrated in Figure 2-14. The duration and number of these cycles depend both on flow dynamics and sediment characteristics.

Table 2-1. ***Description of different transfer modes for marine sediments***

Transfer Mode	Material	Transfer Mechanism	Distribution in Water column	Rouse Number
Dissolved Load	Solute chemicals	Flow advection	Uniform	-
Wash Load	Clay particles	Flow advection	Uniform	P < 0.8
Suspended Load	Silt and sand, Clay flocs	Gravitation, Mechanical turbulence	Variable with depth	0.8< P <2.5
Bedload	Mainly sand and gravel, Cohesive flocs	Gravitation, Boundary shear stress.	Sediment-water interfacial region	2.5< P <7.5

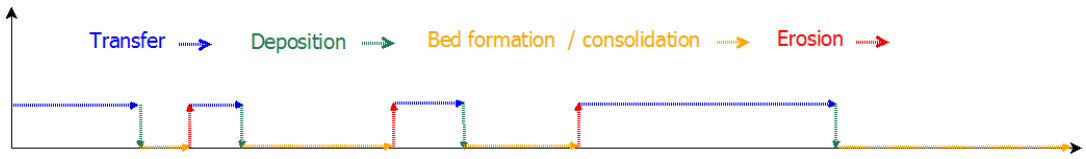

Figure 2-14. **Repetitive cycles of resuspension, transfer, and resettlement in cohesive sediments**

2.3. Erosion

Section 3 is dedicated to the study of literature on the subject of erosion. The definition of erosion, critical shear stress for erosion, erosive capacity of water, and erosion resistive forces and mechanism are reviewed in sections 2.3.1-2.3.4 and section 2.3.5 describes different types of erosion models developed for cohesive sediments.

2.3.1. Definition of Erosion

Erosion in marine environments (also referred to as incipient motion, entrainment or resuspension) can be defined as the detachment of particles, flocs, or mud clusters from the bed by flow. In granular materials, grain size distribution and grain density are the main factors affecting erosion behavior. Table 2-2 provides a list of influential factors for the erosion of cohesive sediments and categorizes them into intrinsic and extrinsic properties. Moreover, in cohesive sediments, particles are not identified individually, and both their properties and behavior are generally defined for bulk samples. Annandale (2005) highlights this characteristic by modeling cohesive sediments as chemical gels consisting of elements in occupied spaces that are connected to each other by fixed bonds. He then analogizes the erosion process to the failure mechanism of these chemical bonds, arguing that the energy required to separate a particle from the matrix of cohesive sediments follows the same pattern as the typical energy required for chemical reactions.

Table 2-2. ***Influential factors in cohesive sediment erosion***

Type	Influential factors in cohesive sediment erosion
Intrinsic properties	Specific density, Mineralogy, Particle size distribution
Extrinsic properties	Sediment Composition: (organic content, gas content, water content), Void ratio, Permeability, Bioturbation and other biogenic influences e.g. biofilm , Maturation period, Consolidation time, Deposition rate, Aerial exposure, Shear stress history, Pore water composition (salinity, PH)

Mehta (Mehta, 1988) identified three different modes of erosion depending on sediment structure and bed shear stress magnitude (Figure 2-15): (1) floc erosion, (2) mass erosion, and (3) re-entrainment of fluid mud (a high density suspension). Winterwerp and Van Kesteren (2004) considered a fourth mode as well-surface erosion.

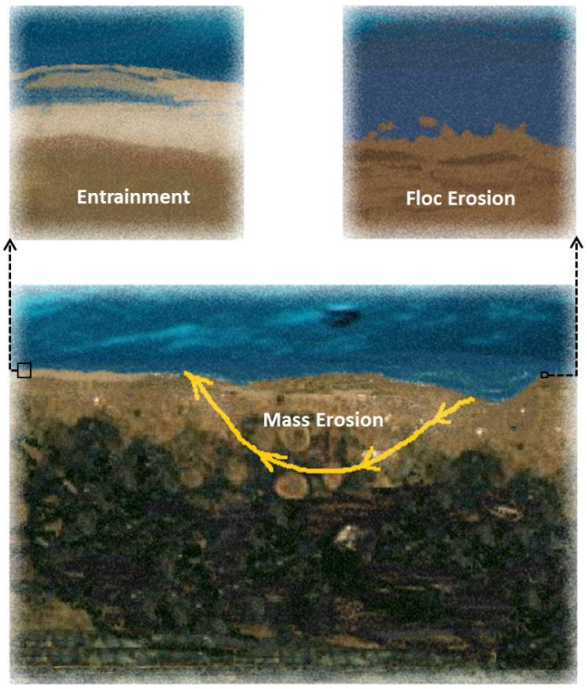

***Figure 2-15*. Three major modes of erosion: entrainment, floc erosion, and mass erosion**

Individual disruption of flocs/particles from the bed is defined as floc erosion. When a floc reaches a bed of consolidating soil, it may immediately be broken up into smaller pieces or may maintain its original structure. Fresh deposits are surrounded by a boundary layer of water (double layer) and before they can come into close contact with other flocs to create a frictional resistance, they should overcome repulsive forces and expel some excess trapped water. This explains the presence of a density gradient (density increases with depth) in the top few centimeters of the bed. It also explains why the morphology of such sediments is easily disturbed by environmental factors and reshaped into new forms. In floc erosion, the fluid forces exceed either the internal strength of a floc or the overall adhesion to the bed. As a result, the surface material is washed away particle by particle. This mode does not normally have large magnitudes of erosion but as a continuous process, it can be a major contributor to the total erosion rates. Recognition of this erosion mode and detection of its threshold (if it exists) is not simple.

Mass erosion (sometimes referred to as bulk erosion) occurs when erosive forces are large enough to detach chunks/clods of sediment from the bed. The failure process can be either instantaneous (brittle fracture) or continuous (fatigue). While the former requires the forces to exceed the fracture resistance instantaneously, the latter involves cyclic (fluctuating) loading applied for a long enough period. Natural surface imperfections, local strength deficiencies, and bioturbation are among the factors that can enhance the formation and growth of ruptures. Surface irregularities can also create stress concentrations leading to the removal of a piece of the bed. Although this erosion type is poorly understood, some researchers relate it to flow-induced pressures and believe that it occurs when the mean flow and/or wave induced stagnation pressures are much larger than the critical shear stress (Winterwerp & Van Kesteren, 2004).

Lick (2008) used particle size to explain different modes of erosion. For particles smaller than 200 microns (in diameter), he suggested that as cohesive effects become significant, particles start to erode in the form of chunks. Critical shear stress in this situation becomes a function of

both bulk density and particle diameter. He mentions that as sediment diameter decreases even further, cohesive forces become more dominant which results in the frequent occurrence of chunk erosion and a simultaneous increase in both bulk density and size of chunks.

As suspended sediments settle toward the bed they may experience a transition state in which they can neither form a structure to develop effective stresses nor can they still be considered as suspended particles. This static, high density, viscous fluid mud can be formed when rapid sedimentation occurs or as a result of bed liquefaction. Fluid mud can be considered as a thick liquid with some behavior like a soft solid. For example, there is a shear stress that if exceeded, will cause a permanent displacement of sediment particles resulting in the flow of the structured fluid (yield stress). When a turbulent flow applies shear stresses higher than the yield stress to a layer of fluid mud, it will be entrained, and the particles/flocs within it will be resuspended back into the flow. This mode of erosion is called entrainment.

Two general modes of erosion have been recognized by many researchers: Type I erosion (depth limited) and Type II erosion (steady state or unlimited). In the depth limited erosion, within each shear stress level, the erosion rate exponentially decays with time (Sanford & Maa, 2001). This type of erosion is observed in the upper portion of natural sediments where the degree of consolidation is very depth-dependent. Unlimited erosion (type II) occurs in uniform beds when the time scale of sediment depletion is longer than that of shear stress change. This type of erosion is generally observed in more consolidated sediments where the bed shear strength does not have a vertical gradient. However, a mixture of these two behaviors is what is observed most frequently. With any increase in flow strength, the erosion rate increases initially and then reduces to reach zero if the test duration is long enough. It can be concluded that a combination of two factors determines the erosion mode: (1) sensitivity of sediment strength to depth (due to factors like sediment properties, deposition history and consolidation history); (2) experiment design (duration and organization of different test steps).

Figure 2-16 shows the flaky structure of three common clay minerals and Figure 2-17 shows the topographic structure of a natural cohesive bed at a micron scale. Although fine sediments are generally described to be smooth, in fact, they have a jagged surface consisting of numerous clusters of fine particles with various orientations and packing states. While some of these clusters can be easily distinguished as flocs, the rest have a stronger attachment to the bed. Floc erosion depends on the flow turbulence structure (especially in the viscous sub-layer), the nature of chemical bonds (internal strength and adhesion to the surface), and the surface topography in small scale (surface morphology). Figure 2-18 is an illustration of a floc with a flaky structure (with water filling the interlayer space) overlying the surface. The forces acting on the floc are flow-induced erosive forces (drag and lift) and resistive forces (weight and friction resistance). The force balance determines whether the failure plane will be inside the flake (internal failure), or the flake will separate from the bed as a whole body due to the weak adhesion to the surface.

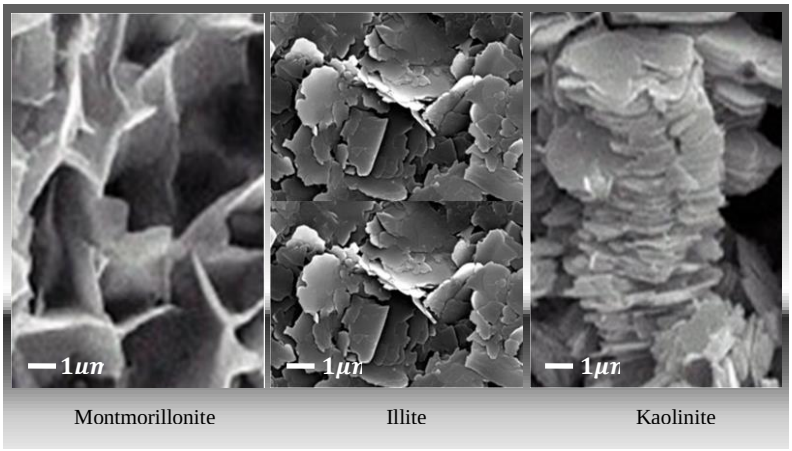

***Figure 2-16*. Flat flakes of three clay minerals (source: unknown)**

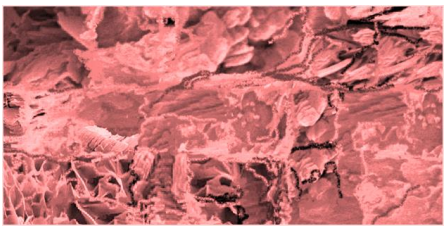

Figure 2-17. **Topographic structure of a cohesive bed at a micron scale**

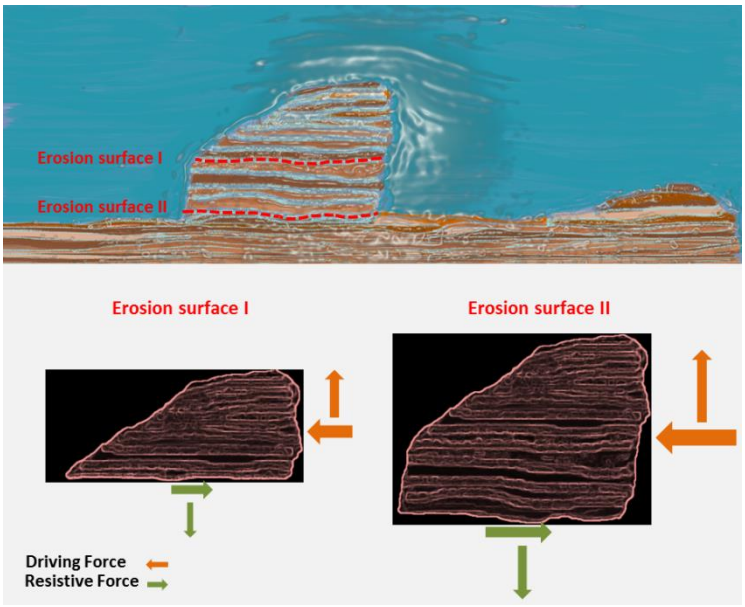

Figure 2-18. **Two possible erosion alternatives for a flaky chunk of cohesive sediment**

Erosion is the displacement of sediment solids (silt and clay, granular, and organic material) as a result of interaction with fluid and gravitational forces. Surface erosion is defined as the slow mobilization of a large area of surface sediment. It is a drained failure process in which the top of the bed liquefies as a result of swelling when the bed is locally over-consolidated. It may also occur as a result of hydrodynamic pressure fluctuations induced by the turbulent flow and/or waves (Winterwerp & Van Kesteren, 2004). Water flows into the bed when the surface swells and this process results in a reduction in the bed strength; leading to a removal of the weakened surface by flow.

Sediment transport in regimes with low shear stresses is very poorly understood. Pintal (1971) studied bedload transport for granular particles (with diameters in the range of 2-22 mm) in the proximity of the sediment critical shear stress and could not find a threshold for the movement of particles. He observed that incipient motion was possible at any shear stress level if the sediment was exposed for a long enough period to initiate the particles' motion. This is consistent with the lower probability of movement at lower shear stress levels. While bedload rate was found to be proportional to the 2.5th power of (dimensionless) bed shear stress in relatively higher shear stresses by different researchers and confirmed by Paintal (1971), he found a 16th power correlation in very low shear stress levels. This means that sensitivity to shear stress is very high in low shear stress regimes. In contrast to the mindset that assumes erosion has a threshold, some researchers consider erosion to be a continuous process that is influential in creating the balance between deposition and entrainment. However, there is not much data in support of this hypothesis (Wiltshire et al., 1998).

2.3.2. Critical Shear Stress for Erosion

It can be concluded from the above discussion that there is no universal definition of the onset of sediment erosion. Sutherland et al. (1998) reported the following incompatible observational definitions that they found in the literature for the entrainment of non-cohesive sediments: (1) "simultaneous movement of ten or more inorganic grains"; (2) "simultaneous movement of both organic and inorganic grains"; (3) occurrence of erosion "at four distinct stages"; and (4) "a reduction (>30%) in" light transmission." The definition of a threshold gets even more complicated for cohesive marine sediments because of the impossibility of studying individual particles, variability in the size of flocs, existence of different modes of erosion, and complexities caused by surface topography among other reasons. Table 2-3 presents some common definitions of critical shear stress in fine sediments.

Table 2-3. ***Various definitions of critical shear stress***

	Critical Shear Stress Definition
1	The stress at which initiation of particle motion first occurs
2	The stress at which significant erosion first occurs
3	The intercept of erosion rate versus stress data
4	An entire depth sequence of increasing critical shear stress
5	An empirical function of soil physical parameters

Source of items1-4: (Sanford & Maa, 2001)

Definitions 1 and 2 in Table 2-3 are very sensitive to the visual recognition of the onset of erosion. Among the three major modes of erosion (floc erosion, mass erosion and re-entrainment of fluid mud), only mass erosion can be easily recognized through observation. This mode of erosion generally occurs at shear stresses which are much larger than the critical shear stress. Sutherland et al. (1998) also mention that the movement of larger particles can cause bias in the detection of motion and introduce an element of subjectivity in critical shear stress determination. All efforts to provide clear definitions of the onset of erosion (like number of grains eroded within a certain period for larger granular particles) have not gained much success for cohesive sediments. The onset of floc erosion and re-entrainment cannot be easily detected and involves a high degree of the observer's personal judgment. The results of field studies on natural sediments (or laboratory studies in which deposition is allowed) are also very dependent on the deposition history of the surface. Almost all methods to determine the critical shear stress rely on the behavior of the most erodible surface particles. Some experiments suggest that erosion commences almost simultaneously with the initiation of any flow over the cohesive sediment surface (Annandale, 2005). This is probably due to the re-entrainment of recently deposited particles and is evidence for the presence of hysteresis (history affects measured critical shear stress). Definition 3 reduces the role of personal judgment by providing a less subjective guideline to be followed. However, the methodology used for erosion measurements results in significant variation in the shape and intercept of the erosion rate-versus-stress curve. Even for a

certain methodology, changes in arbitrary factors (e.g. the sequence of shear stress levels and duration of each step) cause variation in the curve shape and its intercept.

Definition 4 is helpful in modeling the effect of the consolidation process which makes erodibility a function of time and depth. Sanford and Maa (2001) for example assumed a locally constant rate of increase in the critical shear stress with depth. Definition 5 takes some physical properties of the sediments into account. However, relating sediment physical properties to the critical shear stress for erosion is still a central problem in bedload mechanics (Kirchner et al., 1990). The equation obtained empirically by Thorn and Parsons based on laboratory tests on partially consolidated cohesive sediments is as follows (Thorn & Parsons, 1980):

$$\boldsymbol{\tau_{ce} = E_1 \rho_{Dry}^{E_2}}$$

τ_{ce}: critical shear stress for erosion

E_1 and E_2: site − specific dimensional coefficients

The units for this equation should be in SI. Nicholson and O'Conner's formula (1986) is another example:

$$\boldsymbol{\tau_{ce} = \tau_{ce0} + K_t(\rho_d - \rho_{d0})^{n_t}}$$

τ_{ce}: critical shear stress for erosion

τ_{ce0}: critical shear stress for erosion at the initial period of bed formation

ρ_d: dry bed density

ρ_{d0}: dry bed density at the initial period of bed formation

k_t and n_t : empirical parameters

Different fractions of a sediment mixture have different thresholds for incipient motion. Kirchner et al. (1990) measured the critical shear stress for particles of different diameters. He observed that grain projection, exposure, and friction angle strongly affect the motion threshold

of single-sized particles. The distribution of erosion probability that he assigned to each particle size became broader with the decrease in the size of particles. Estimation of critical shear stress becomes more complex when considering the interaction of fractions of different sizes due to the protective influence of larger particles/flocs on smaller ones.

It can be concluded from the above discussions that even for a single grain size, there is no determinant and single threshold shear stress value for erosion. Winterwerp and Van Kestern (2004) suggest that as the onset of sediment movement is governed by the peaks in the bed shear stress, the measured shear stress underestimates the true values and hence should be called the "apparent critical shear stress". Hickin (1995) believes that the fluctuation about the mean value is more important than the mean velocity (shear stress) in initiating sediment motion. Considering the stochastic nature of both resisting and driving forces active in sediment incipient motion, it seems that a comparison of probability frequency distribution of these forces can offer a promising solution. However, the measurement and prediction of turbulent forces in the field conditions is still not feasible.

Another aspect worth mentioning is the dependency of observed values of critical shear stress on the choice of experimental time frame and sample size. As stated by Sutherland et al. (1998) "Given an extended observation period or working area, the probability of particle movement would increase." This can be explained by the stochastic nature of hydrodynamic forces and the high levels of non-homogeneity in natural sediments.

Despite all the aforementioned ambiguities, critical shear stress – the shear stress associated with the onset of erosion – is a factor typically present in most erosion models (e.g. models 3, 4, 6 in Table 2-6). The definition of this concept is also very qualitative, and there is no universally accepted method for its quantification (Paintal, 1971). The presence of different definitions of critical shear stress (presented in Table 2-3) has led to considerable inconsistencies in the experimental results reported in the literature (Sutherland et al., 1998). This is why the direct

comparison of different studies (using different criteria or methods for determination of critical shear stress) is generally not possible.

2.3.3. Erosive Capacity of Water

The most influential part of the flow regarding sediment erosion is the bottom boundary layer. The fluid energy can be dissipated through two mechanisms when in contact with a boundary: skin friction and form drag. Skin friction is caused by the shear stress induced at the bed by the flow. It has for long been considered as the main factor determining the erosive capacity of water. Different methods have been developed for the estimation of the boundary shear stress depending on the technical constraints of the measurement methods. Almost all of these methods are obtained for particle-free, hydraulically smooth flows over impermeable and rigid beds. Although flows over cohesive sediments are typically considered as hydraulically smooth, factors like bed permeability and elasticity, surface irregularities and bedform creation, and the presence of suspended solids in the flow make natural field conditions sophisticatedly different from the theoretical assumptions behind these methods. For example, previous studies have proved that a low concentration of suspended clay ($< 10\ \frac{g}{l}$) reduces the skin friction significantly and results in higher erosion thresholds (because of the increase in mixture viscosity). On the other hand, a higher concentration of suspended clay can make a fluid diverge from the Newtonian response toward a Bingham-like behavior (Angelaki, 2006).

Regarding laboratory studies, Heuvelink and Webster (2001) compared the shear stress distribution in various erosion testing devices and found differences between them and the field condition. Presently, no theory exists for the prediction of the actual shape of the bed shear stress probability density function (Winterwerp & Van Kesteren, 2004).

Form drag is caused by stochastic turbulent ejections and sweeps along the boundary layer. Even though the form drag is a major contributor to the total forces on the bed, only skin

friction is assumed to be relevant to the erosion of single grains by many researchers. Partitioning the shear stress into form drag and skin friction is largely motivated by this hypothesis (Garcaia, 2008). However, if each particle/floc is studied individually, a form drag can be associated with its geometry that generates pressure fluctuations. Pressure fluctuation has also been proved to affect erosion (Lopez & Garcia, 2001) and has even been considered as the prime driver of incipient motion by some researchers (Annandale, 2005). It has been argued that such pressure forces are also correlated with shear stress, but there is no strong evidence to prove the presence of adequate correlation between them (Hickin, 1995).

Presently there is no unique way of quantifying erosion capacity of water because bed instability processes are not sufficiently understood. The indicator parameters that are generally used for the estimation of flow erosion capacity are average velocity, shear stress, and stream power (Annandale, 2005).

A vertical velocity gradient in the near-bed region – through which the fluid velocity reduces down to zero – forms the flow structure named the "boundary layer". This layer consists of three regions in smooth-turbulent flows (which is the type of flow expected in natural flows over hydraulically smooth surfaces): (1) Viscous sub-layer, (2) Buffer zone, and (3) Logarithmic turbulent zone.

Viscous sub-layer is a thin layer within which viscous effects are dominant. This layer lies in direct contact with the boundary, and the velocity gradient is almost constant within this layer. If roughness elements exceed the thickness of the viscous sub-layer, this layer diminishes, and the flow will be considered as a rough-turbulent flow. The bottom shear stress in smooth-turbulent flows can be calculated by the gradient method based on Newton's viscous stress equation:

$$\boldsymbol{\tau = \mu \frac{du}{dy}}$$

τ: shear stress in the fluid

μ: shear viscosity of the fluid

$\frac{du}{dy}$: derivative of the velocity component

The flow in the viscous sub-layer is non-turbulent. The slender longitudinal vortices advected at low velocities within this layer become unstable at specific moments and form hairpin or horseshoe vortices that are ejected into the boundary layer (Winterwerp & Van Kesteren, 2004). The transition between viscous and logarithmic sub-layers occurs, is called buffer zone. Within this zone, the momentum is comparably transferred via both viscosity and turbulence and the linear relationship between velocity and depth in the viscous sub-layer merges to the logarithmic velocity profile.

Logarithmic turbulent zone is the sub-layer within which the momentum is transferred mainly through turbulence. The average flow velocity in this region can be calculated based on the *law of the wall* which relates the average velocity to the logarithm of the distance from the boundary as follows:

$$\mathbf{u} = \frac{\mathbf{u_*}}{\mathbf{k}} \mathbf{ln} \frac{\mathbf{y}}{\mathbf{y_0}}$$

u_*: shear velocity $u_* = \sqrt{\frac{\tau_w}{\rho}}$

K: Von Korman constant

Y: distance from the wall

y_0: distance from the wall at which velocity reduces to zero

The net force applied to each particle/floc is generally resolved into a vertical component (lift) and a horizontal component (drag). The term drag used here is an effective force on individual sediments and should not be confused with “form drag” which is a source of hydraulic resistance resulting from pressure distribution over an entire bedform. Incipient motion occurs

when the combination of lift and drag forces applied to a floc/particle exceeds the resistive forces. The relative importance of drag and lift forces is highly variable with the degree of exposure and the impact of neighboring flocs/particles. It means that even for a single particle size, no single force (either lift or drag) can be determined as the erosion threshold.

Lift forces can originate from three sources: (1) Buoyancy: Buoyancy force is understood well and easily estimated for granular particles. However, as this force is dependent on the volume of the particles, estimation of its magnitude is not very straight forward for cohesive material with all its structural complexities. Connectivity of the fluid trapped within the internal voids to the flow can also affect the buoyancy force. (2) Upward turbulence forces: Diffusion of eddies within the flow superimposes some random velocity fluctuation on the flow average velocity (in all directions including the vertical direction). Eddy creation can be intensified by the presence of local bedforms and an increase in roughness. (3) Vertical velocity gradient: Fluid velocity reaches zero at any solid boundary to match the boundary velocity. According to Bernoulli's principle, any decrease in the flow speed is simultaneous with an increase in fluid pressure. It can be concluded that a vertical pressure gradient also exists in the boundary layer with higher pressure values occurring closer to the bed. As a consequence, an upward lift force is applied to particles in this region, thus facilitating motion initiation. The direct measurement of lift and drag forces has been the focus of several experimental investigations; however, almost all of them concentrate on granular particles.

Researchers have studied turbulent flow through pipes extensively and developed some empirical functions that relate the mean flow rate to the wall shear stress. An implicit formula relating the wall shear stress to the mean flow in a smooth pipe of arbitrary cross section can be obtained from Prandtl's universal law of friction and expressed as (Schlichting, 1979):

$$\frac{\mathbf{1}}{\sqrt{\boldsymbol{\lambda}}} = \mathbf{2.0}\,\mathbf{log}\left[\frac{\mathbf{Vd}\sqrt{\boldsymbol{\lambda}}}{\boldsymbol{\upsilon}}\right] - \mathbf{0.8}$$

V: average velocity $(\frac{m}{s})$

ν: kinetic viscosity $(\frac{m^2}{s})$

$\lambda : \frac{8\tau_{th}}{\rho V^2}$ friction factor

d: hydraulic diameter $d = \frac{2hw}{(h+w)}$

W: duct width (m)

ρ_w: density of water $(\frac{kg}{m^3})$

τ_{th}: theoretical shear stress at the wall (Pa)

As water density and kinetic viscosity are temperature-dependent as presented in Table 2-4, a sensitivity analysis was conducted to see the effect of temperature on theoretical shear stress. As illustrated in Figure 2-19, temperature has a significant effect on shear stress, so temperature measurements were taken into account by using the values in Table 2-4 and interpolation. The temperature was assumed to be $20°C$for those tests missing temperature measurements.

Table 2-4.*Variation of density and dynamic viscosity with temperature for water*

Temperature (℃)	**Kinematic viscosity** $(\frac{m^2}{s})$	**Density** $(\frac{Kg}{m^2})$
0	1.787e-6	999.8
10	1.307e-6	999.7
20	1.004e-6	998.2
30	0.801e-6	995.7
40	0.658e-6	992.2

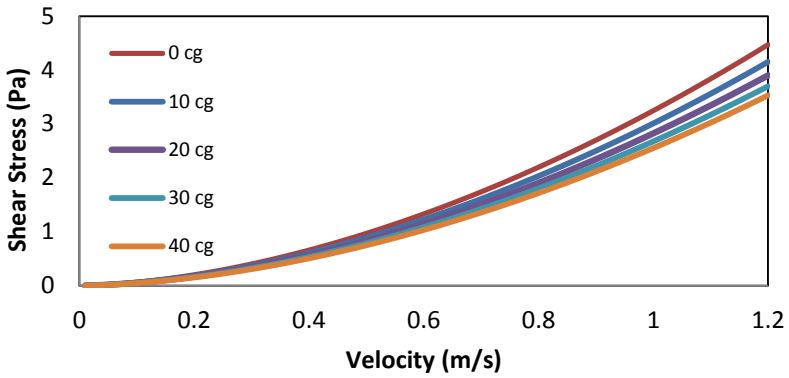

Figure 2-19. **Variation of theoretical shear stress with velocity at different temperatures**

2.3.4. Erosion Resistive Forces and Mechanisms

Relating the bed strength to flow characteristics has been the goal of many researchers without any deterministic solutions achieved so far. Most of the research focusing on fundamental processes leading to erosion has been conducted on granular particles. Resistive forces in cohesive sediments can originate from particles' submerged weight, adhesive forces, biofilm coverage, and the protective effects of bedform structures. Except for the submerged weight, the rest of factors are of dynamic nature and are very difficult to be quantitatively assessed. Annandale (2005) proved that the relationship between erosion rate and shear stress is a function of clay properties. His experiments suggested that clay erosion rate can be affected more by pH or salinity variation than by shear stress variation (Annandale, 2005). Even though such material properties have not been integrated into most of the erosion models, there is a general consensus among researchers that all models require material–specific (site-specific) validation and calibration based on their intended scale of application.

2.3.5. Erosion Studies of Cohesive Sediments

Erosion quantification of cohesive sediments has been studied intensely since 1960. Researchers have made numerous simplifying assumptions, developed various experimental set-ups, and applied approximate analytical methods to overcome the inadequacy of a basic understanding of this type of erosion and mitigate the high variability in sediment properties. The variability in both experimental protocols and data analysis procedures has also been considered as important factors contributing to uncertainty in these studies (Sanford, 2006). Researchers have used a wide range of devices for the quantification of erosion. These devices employ different methods for flow generation such as use of a pump, rotating disk or cylinder, water jet, oscillating grid, and rotating propeller. In both laboratory and field tests, flow has generally been formed in either flumes (straight or annular) or cylindrical chambers. Lee and Mehta (1994) have provided a comprehensive review of the devices and assemblies used for cohesive sediment erosion tests. None of these devices guarantee that the pressure gradients (or turbulent intensity spectrum) generated in the sediment interface will have a structure similar to those created by natural flows, and this presents a major barrier toward scientifically valid experimental protocols.

Additionally, different types of samples have been used in erosion testing devices as summarized in Table 2-5. The mutual interaction between the deformable sediment boundary and the sediment-carrying flow makes the measurement of the shear stress and quantification of erosion difficult. Various experimental methodologies have been used by researchers for the quantification of erosion. They can be categorized as: (1) total suspended solids measurement (densimetric, acoustic, and optical methods) (2) volume loss estimation (visual, total suspended solids, image analysis) (3) weight loss estimation. Several shear stress evaluation methods can also be found in the literature including (1) empirical equations, (2) direct shear stress measurement, (3) pressure differential, and (4) velocity profile in the laminar layer.

Table 2-5. ***Types of samples used in erosion tests***

Sample type	Description
Natural bed	In-situ tests
Placed bed	Natural sediment is mixed and placed on bed or remolded
Deposited bed	A dilute suspension of natural sediment settles to forms a consolidated bed
Undisturbed samples	Undisturbed cores of sediment

Most of the erosion experiments were designed to simulate layer-by-layer erosion under different shear stress levels. The duration of each test step, shear stress at each step, and the order of successive steps were arbitrarily chosen by researchers. The simultaneous occurrence of each of the aforementioned factors made the comparison of different studies very challenging and sometimes impossible. Thus, it is no surprise that there is no consistency in the way the critical erosion values have been reported in the literature. For example, some studies report the critical erosion values in terms of flow velocity at a specific height above the bed, or revolution speed (of a propeller, duct cover or concentric cylinders) while others use the pressure of a vertical jet, or a spatial and time-averaged bed shear stress among other ways (Sutherland et al., 1998).

As erosion is a time-dependent process (except for type II erosion occurring in uniform beds) the duration of exposure to each shear stress level affects the quantity of material eroded at that step in a non-linear fashion. Figure 2-20 illustrates a typical erosion rate-versus-time graph for a test with four successively increasing shear stress levels. The shear stress levels were applied to the sediment sample for 20-minute intervals.

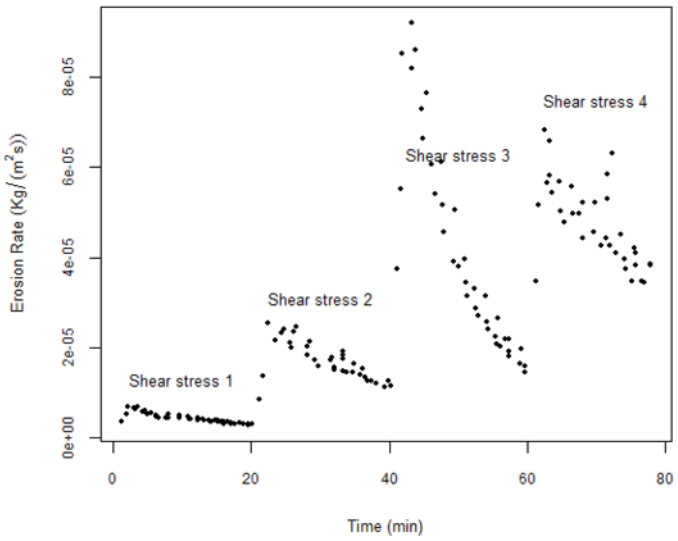

***Figure 2-20*. Typical pattern of data generally observed in erosion experiments**

Lee et al. (1981) demonstrated an attention-grabbing hysteresis effect by combining erosion and deposition sequences in their experiments (Lee et al., 1981). They measured the steady-state concentration of suspended solids in an annular flume bedded with consolidated cohesive sediments. The tests were implemented in two orders: step-up (increasing) followed by step-down (decreasing) sequences of shear stress levels. The steady-state sediment concentration, reached at each shear stress level, was observed to be higher in the decreasing order. This undermines the idea that there is a specific erosion rate for each shear stress level.

Research approaches to study fine sediment erosion can be generally classified as (1) empirical, (2) physics-based, and (3) probabilistic. There is no sharp distinction between these models, and a mix of these components may be found in some studies. Theoretical studies generally lead to more complex models based on laboratory tests that eliminate uncontrolled factors. Hence, they usually have low potential to be used for field condition predictions because of insufficient data available the behavior of sediments in natural environments.

2.3.6. Erosion Models for Cohesive Sediments

The three major types of erosion models found in the literature – empirical, theoretical, and stochastic – are presented in the following sections.

2.3.6.1. Empirical Models

Empirical models are the most simplistic type of models that are generally developed under the assumptions of stationarity and homogeneity and have the least computational complexities among other models. It is a common approach in erosion studies to create empirical models based on observed data (either in the laboratory or field). Generally, a simple form of an equation relating selected causal variables to the response variable is assumed, and the characteristic coefficients are determined experimentally for each site based on observations. Many different devices and testing protocols have been used to estimate cohesive sediments' erosion rate, but there is no unique standard procedure and guideline on how to sample and test cohesive sediments for this purpose. Even with one specific device and a standard material and test protocol, it is still possible to generate different incompatible results due to the over-dependency of experimental results on the operator's subjective assessment. Some popular forms of the empirical models developed in the literature are listed in Table 2-6. The characterizing parameters obtained by different researchers reflect a wide range in the values' orders of magnitude. Even for a specific mud sample, it is possible to obtain coefficients that vary within one order of magnitude (Kronvang et al., 2006). Despite the shortcomings of empirical models, one main advantage is their capability to cope with limited measurements.

Table 2-6. ***Typical forms of empirical erosion models found in the literature***

	Erosion Model	Characterizing Parameters
1	$E = \alpha \lvert\tau\rvert^{\eta}$	α, η
2	$E = A\tau^{n}\rho^{m}$	n, m
3	$E = M(\frac{\tau_b}{\tau_c} - 1)$	M
4	$E = M(\tau_b - \tau_c)^{n}$	M, n
5	$E = A\tau_b(t)^{n}e^{-k\rho(z)}$	A, n, k
6	$E = \epsilon_f . \exp(\alpha[\tau_b - \tau_c]^{\beta})$	$\epsilon_f, \alpha, \beta$

2.3.6.2. Theoretical Models

Another approach is to look for more theoretical and physics-based erosion models. As cohesive sediment erosion cannot be completely explained by fundamental physics equations, this approach requires breaking down the problem into individual processes that involve fewer measurable parameters, and that can be studied in smaller scales. Development of such models involves numerous assumptions, and hence, it is not possible to generalize the results without testing for the validity of these assumptions. As the significance of some processes may be scale dependent, a process may even loose its physical significance at larger scales. The possibility of interactions between different factors is also a point of concern that has been overlooked so far but should be investigated at some point.

The derivation of physics-based expressions requires a careful design of experiments to control for the known factors that are not of interest. As properties of natural sediments and environmental conditions in the field cannot be controlled, manufactured samples tested in well-specified laboratory environments are very popular in such studies. Even though this strategy is very helpful in providing a better understanding of the erosion phenomenon, the generated results cannot be generalized for any other circumstance/material since such experiments are heavily

simplified. More surprisingly, it is common in erosion literature to see similar studies with contrasting results. For example, increasing the fluid's PH has been proven to both increase and decrease erosion resistance in different studies. Such a complex behavior can be explained by the dependence of chemical forces between clay particles on the temperature, salinity, and PH of the ambient and interstitial water (Annandale, 2005). Not only does this reasoning justify the observation of contrasting results, but it also gives rise to a serious question: Even if we assume to know the erosion behavior of all natural minerals deterministically, is it practical or reasonable to include details at a mineralogical level in erosion prediction models? The answer may be "yes" if we are interested in the erosion behavior of a certain material with uniform chemical properties; but what about natural sediments with all their complexities? The large scale of typical erosion problems and sparsity of available data impose severe limitations on the applicability of models developed at small scales.

Although most of the factors in Figure 3-7 have been extensively studied and their significance in erosion has been proved, we are still far from understanding the true physics behind erosion. As a result, there is no physical formulation for fine sediment erosion and most of the proposed forms originate from empirical studies. Many physics-based models are developed based on small-scale tests and under very controlled conditions while their application is generally at higher scales and under different (and variable) conditions. Although many such models have been proven to match the experimental results well, the numerous assumptions involved do not guarantee the functionality of the model in predicting erosion behavior under new conditions and for larger scales of variability in data. Moreover, the physics-based models fall short as the results they provide are deterministic in nature as compared to the stochastic character of erosion.

2.3.6.3. Stochastic Models

It can be concluded from the previous discussions that random processes have a significant role in sediment transport. Even though a deterministic approach is not sufficient for modeling and predicting such processes, they are still frequently conceptualized deterministically. This is mainly because of "lack of enough experimental and / or field information to perform stochastic analysis" (Lopez & Garcia, 2001), which is a common practice in other research areas.

A popular approach in stochastic erosion modeling efforts found in the literature is to assign a probability distribution function to either erosive forces or erosion strength (or both). Van Prooijen and Winterwerp (2010) analyzed sediment erosion by using stochastic bed strength and shear forcing in a linear erosion formulation. They used a formulation suggested by other researchers to calculate the probability density distribution based on the mean bed shear stress. Their analytical method could reproduce the time-varying erosion rates reported in two other studies. Winterwerp et al. (2012) also assumed a probability density function for both the eroding shear stress and bed strength and validated their results against a limited set of experimental data. They derived the average bed strength from soil mechanics theory.

Another approach for stochastic modeling of erosion is to assign a probability density function to the flow-induced shear stresses and to compare that with the distribution of sediments' critical shear stress. For example Zanke (1990 as cited in (Lopez & Garcia, 2001)) used the erosion risk concept defined as the risk for a particle to be eroded and estimated as:

$$\mathbf{Ri} = \int_{\mathbf{0}}^{\infty} \mathbf{pdf}_{\boldsymbol{\tau f}} \left[\int_{\mathbf{0}}^{\boldsymbol{\tau f}} \mathbf{pdf}_{\boldsymbol{\tau f}}\, \mathbf{d}_{\boldsymbol{\tau c}}\right] \mathbf{d}_{\boldsymbol{\tau f}}$$

$pdf_{\tau f}$: probability density function of the flow − induced wall shear stress

$pdf_{\tau f}$: probability density function of the critical stress for the initiation of motion

2.4. Other Factors Contributing to Erosion

Three major factors that impact erosion are investigated in this section: biological factors, sediment structure, and extreme events.

2.4.1. Biological Factors

Studies prove that an intense two-way interaction exists between biological and geomorphological processes in intertidal mudflats (Herman et al., 2001). Even though this review mainly focuses on the effect of biological activities on sediment transport, it should be noted that sediment transport can also affect the biological nature of sediments by changing the bed composition and flow characteristics. Estuarine ecosystems are extremely dynamic areas combining marine, fluvial and terrestrial ecosystems to create a highly productive environment. Salinity gradient, the hydrodynamic interaction of tidal and non-tidal flows, and partial exposure to air and the sun are some major factors creating a wide variety of local ecosystems in coastal estuaries.

Remarkable variations in habitats and species occur over very short distances in intertidal environments (Meadows et al., 1998). Population and composition dynamics of the biota can influence cohesive sediment dynamics through various mechanisms (toward both stabilization and destabilization (Riethmüller et al., 1998)) and over a wide range of spatial and temporal scales. Although many researchers have studied this influence at small scales, the large-scale effects of small-scale biological activities have very rarely been quantified (Borsje et al., 2008). Even at a small scale, there still remain many uncertainties about the interaction of organisms and flow. As stated by Paterson and Black (1999), living organisms are not simply affected by the

flow since they also shape and mediate the flow in a manner that generally enhances their survival chances.

In order to have a dynamic interaction, processes should act on the same temporal and spatial scales, otherwise they will be considered as either noise or boundary conditions (Borsje et al., 2008). For example, Ruddy et al. (1998) compared the potential erosion and deposition depths with the photosynthesis depth and as they both occurred in the order of a few hundred microns, they suggested that ecological and sediment dynamics occur at a similar physical scale (Ruddy et al., 1998).

A bed of natural cohesive sediments is often densely colonized by assemblages of bacteria and microphytobenthos (Wiltshire et al., 1998). The top few (~10) centimeters of the cohesive sediments are exposed to aerobic conditions while the deeper zones are anaerobic (Winterwerp & Van Kesteren, 2004). Only the top few hundred microns (300-3000 microns according to (Ruddy et al., 1998)) of sediment surface in the intertidal zone are euphotic. Thus, photosynthesizing microorganisms accumulate in this region only (Wiltshire et al., 1998).

There are various dynamic mechanisms through which biological activities affect sediments' physical properties: (1) Organic compounds decrease the sediment bulk and dry density because their density is almost 60 percent that of natural minerals. (2) The organic content of deeper sediments (also known as carbon storage) is mainly a result of the burial of the highly dynamic uppermost layer (Ruddy et al., 1998)). (3) Reworking and restructuring of sediments by living organisms (also called bioturbation) affects sediment porosity and texture. Specifically, bioturbation can keep a (generally thin) layer of surface sediments from becoming a part of the bed (Luettich et al., 1990). The bottom shear stress required to resuspend the material in this layer is generally small due to the low consistency caused by mixing the liquid (flow) and solid phases. (4) The degradation of organic matter under aerobic or anaerobic conditions produces gases, mainly methane and carbon dioxide. The amount of gas produced in many natural types of

sediment is sufficient to significantly affect both the erosion rate and density (Lick, 2008). If the pore water is saturated with dissolved gas (in a time frame of weeks, years or centuries), small bubbles are created to constitute a gas phase (Winterwerp & Van Kesteren, 2004). Production of gas bubbles affects sediment porosity and density. Besides, migration of gas bubbles due to pressure and temperature variation can disturb sediment structure and affect the consolidation rate. (5) Aquatic vegetation reduces the flow energy transferred to the bed. Fibrous plant structures can also stabilize the bed and increase the effective particle size. (6) Fine sediments are agglutinated in the presence of exopolymers. Sutherland et al. (1998) observed a variation in the eroded aggregate size explained by the biofilm development stage. (7) Experiments have shown a significant correlation between the shear stress erosion threshold and presence of biofilm on sediment surfaces (Widdows et al., 2000). Biofilm is the protective deformable layer of extracellular polymeric substance (EPS) – mainly consisting of polysaccharides – formed when microorganisms adhere to wet surfaces. Its life cycle, as typically observed in intertidal mudflats, is presented in Figure 2-21. Biofilm regeneration and recycling are generally fast processes (Malcolm et al., 1997), and can occur within 1 hour of exposure to seawater (Lintern, 2003).

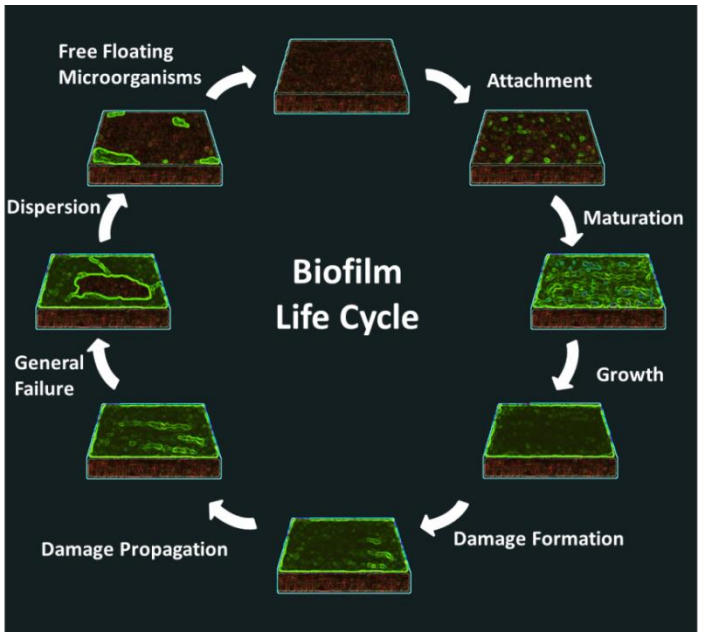

***Figure 2-21*. Life cycle of biofilm**

A biofilm-covered sediment surface can be considered as a thin film in contact with a less deformable sediment structure. Different failure mechanisms can be recognized in this system: (1) Hydrodynamic forces or biological activities can cause local damages in the biofilm matrix. Fluid forces help the biofilm skin to be peeled off the surface near the damaged zone. The continuous nature of such forces widens the crack and finally releases the patch of biofilm surrounded by the developed cracks. (2) The variation in the environmental conditions (e.g. temperature, light, nutrients concentration, biota composition, etc.) may lead the system toward a new equilibrium in which EPS secretion is stopped, and available polysaccharides are consumed as a food source by microorganisms. (3) Wiltshire et al. (1998) reported the presence of loose pieces of biofilm on top of its structure which suspend into the flow easily. Sutherland et al. (1998) also found that the biofilm's strength has a stratified structure with respect to depth (increasing downward). These observations suggest a continuing mode of failure associated with the gradually increasing fluid forces that dissolve looser parts of the biofilm matrix layer by layer. (4) Freund and Suresh (2003) suggested that the biofilm may buckle and separate from the sediment interface where the compressive stresses are large enough (Freund & Suresh, 2003).

An intact and mature layer of biofilm acts as a force absorbent and controls the exposure of the underlying sediments to the fluid forces. Not only does this prevent the resuspension of freshly deposited sediments, but it also provides a chance for such particles to establish bonds with the surface and enhances the consolidation of the top sections of sediment. If fluid forces cannot penetrate through the biofilm layer to break it up, erosion will not initiate regardless of the sediment's strength (Hickin, 1995). Wiltshire et al. (1998) also measured the pigments derived from the biofilm in the water column during erosion tests and concluded that the general failure of the bed occurs after biofilm separation, confirming the strong dependence of the sediment erosion threshold on biological factors.

Some researchers have compared the erosion threshold of sediments in the presence and absence of biogenic influences. The ratio of these values is called the stabilization coefficient (Sutherland et al., 1998). For example, Neumann et al. (1975) observed a stabilization coefficient equal to 5 in their study. Kornman and De Deckere (1998) studied the temporal variation of biofilm effects on sediment erodibility in the Dollard Estuary, England in 1996. They found erosion thresholds of 0.2, 0.5, 0.6, 0.1 and 0.1 Pa, in March, April, May, June, and July respectively. As they could not explain this variation by observed differences in grain size, water content and density of samples, they concluded that the presence of biofilm caused the strong increases and decreases in the erosion threshold (that could take place within a period of two weeks).

Some undisturbed samples taken from the Newark Bay mudflats during the period of this study were covered by a layer of intact and elastic biofilm easily observed by the naked eye. This layer could be separated and peeled off from the surface using tweezers because of its consistent structure as seen in Figure 2-22. However, it is not always as easy to detect biofilm. Wiltshire et al. (1998) used electron microscopy to observe and measure the thickness of a biofilm layer to be less than 10 microns.

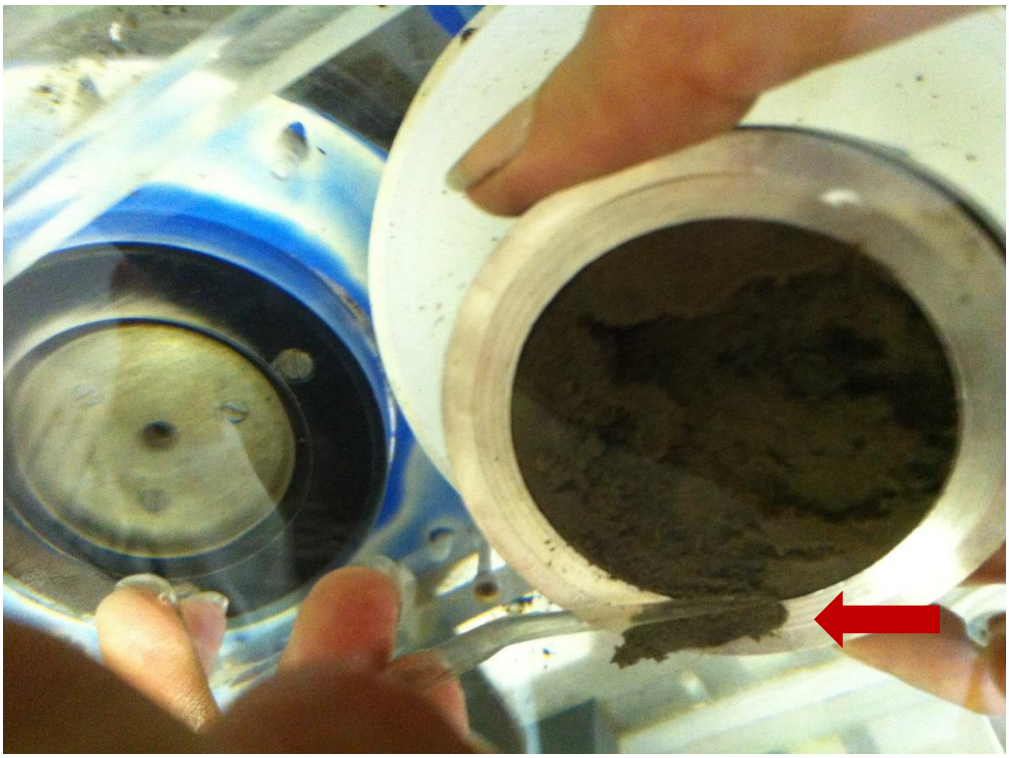

***Figure 2-22*. A fresh layer of biofilm peeled off from the surface**

Riethmüller et al. (1998) studied the dependence of erosion shear stress on the chlorophyll-a (a photosynthetic pigment that has widely been used as a tracer for the extracellular polymeric substance in biofilm studies) concentration for a wide range of sediment types and found that this dependence is strong only in sediments with percentages of fines higher than 50 percent.

The data obtained in biological studies should be interpreted cautiously. Different biological communities may reflect contrasting adaptations to the environmental conditions. It follows that no single equilibrium state can be associated with such environmental systems. In fact, Herman et al. (2001) found a simultaneous occurrence of contrasting equilibrium states within a single intertidal mudflat: “one with low mud and low microalgal biomass occurring at low shear stress levels and the other with high mud and high microalgal biomass observed at lower shear stress levels”. Interestingly, Borsje et al. (2008) could distinguish between the impact

of stabilizing and destabilizing organisms. The stabilizing organisms were found to be mainly responsible for seasonal variation in the suspended sediment concentration while the destabilizing organisms were the primary cause of spatial variation in the fine sediments present in the bed. The overall conclusion is that the results obtained at a certain spatial or temporal scale and under a specific environmental setup, should not be generalized or extrapolated to other situations without additional experiments.

Borsje et al. (2008) made research endeavors to understand the large-scale effects of small-scale biological activities in the North Sea. They hypothesized that if the biological parameters were well-documented and averaged over small support units, their basin-wide effects on sediment dynamics could be sufficiently estimated. Given all the difficulties in modeling the biological activities, they concluded that even though not all the biological and transport parameters could be prescribed for the entire study area, trends and orders of magnitude of biological influence on sediment transport could be estimated (Borsje et al., 2008).

Even though it has been proven that abiotic conditions are not representative of natural environments for erosion studies (Sutherland et al., 1998), many laboratory studies completely eliminate biota from the system to control for unknown factors. Biological cycles are also very sensitive to seasonal, tidal, and diurnal variations. For example, Malcolm et al. (1997) found a dramatic change in the system's balance between summer (when benthic production of organic material is dominant) and winter (when the organic material is being degraded). Despite all the difficulties in simulating estuarine natural processes in the laboratory, many successful cross-disciplinary studies have investigated the interaction between geotechnical variables and biological factors. However, innovative methods for the measurement of biological and geotechnical parameters with high accuracy are still missing (Meadows et al., 1998).

2.4.2. Sediment Structure

Bed evolution is a rather slow and intermittent process that can be highly impacted by intense events. There is no direct pathway for the transformation of the loose discrete elements recently deposited on the surface to deeper sediments possessing an established structural strength. Sediment particles/flocs may experience repetitive cycles of deposition and erosion before being buried downward. Current- and wave-induced forces, biological influences (limited to the upper bed layer), exposure to air and light, and gas production and migration are among the active processes that can either enhance or diminish the bed formation trends. Therefore, water-worked sediment deposits are the result of a complex chain of events, and their future behavior depends on the conditions at the time as well as past events.

It is not possible to study the long-term development of sediment deposits through direct observation. A very valuable source of information specially for understanding the chronological evolution and long-term patterns in sediment transport is geochemical analysis performed by high- resolution absolute and relative dating (such as Pb[1] and Cs[2] dating) techniques. Herman et al. (2001) used radionuclides' profiles for estimation of both long- and short-term sedimentation rates. Additionally, Cundy et al. (1998) proved that palaeoecological and geochemical analysis can be combined to reconstruct environmental changes that previously occurred in the fluvial and estuarine wetland settings. While these methods are very informative of sediment accumulation rate, they provide no clue of erosion rates because of their exclusive dependence on the available particles.

---

[1] lead
[2] caesium

Halonen (2011) performed a historical bathymetric analysis for the Newark Bay and realized that between 1934 and 2008, significant changes had occurred in the hydraulic geometry of the Newark Bay. During this period, most of the flats (except known areas of human disturbance) had experienced a net deposition of less than 1 meter with annual deposition rates less than 1.2 cm/year. He also found the accumulation patterns to be complicated and correlated to the channel deepening activities.

Meadows et al. (1998) analyzed the small-scale differences in sediment properties (particle size, organic content, load resistance and in-situ shear strength) by taking replicate cores from four adjacent sites on the Clyde Estuary in Scotland. Their cluster analysis revealed a break in the data at a depth between 40 and 70 mm (Meadows et al., 1998). They explained it to be due to either biological activity within the sediment, the impact of the water column across the sediment-water interface, or the influence of deeper sediments.

The sediment structure has a direct relevance to its physical properties e.g. water content and bulk density. Penetration of fluid into the surface material is also very dependent on the level of interconnectedness of void spaces which is a function of particle arrangement. Fluid penetration through the surface boundary can be influential in two ways: (1) exerting physical forces through shear stress and pressure fluctuation; or (2) changing the chemistry of interstitial water. This change can either strengthen or weaken the chemical bonds in sediments depending on the chemical properties of the water (Annandale, 2005). The level of dissolved oxygen in the interstitial water can also affect biological activities.

As cohesive sediments have low permeability, pressure pulses caused by flow are not dissipated immediately; hence gradients are established in the pore water. This makes the estimation of internal forces within the upper bed layer very complicated. Furthermore, cohesive sediments constitute an elastic porous medium, which has a mutual interaction with the flow, thus presenting an additional complication. As the boundary, the sediment surface shapes the near-bed

flow, and the flow-induced shear, in turn, deforms the bed surface and modifies the hydraulic roughness. For example, erosion of sediments in spots of surface imperfection increases the surface roughness which causes higher turbulence levels followed by a progressive erosion.

As discussed above, there are various factors that affect sediment structure during bed formation and evolution. It is not possible to quantify the relationship between sediment structure and its erosion behavior without obtaining samples with uniform and similar structures. As natural samples cannot be controlled for their structure, many researchers manufacture replicate samples for this purpose. However, most artificial samples are not prepared by the action of flowing water which eliminates many complexities naturally present in water-worked sediments.

2.4.3. Extreme Events

Rare meteorological events (e.g. severe storms, extreme floods, tsunamis, and hurricanes) are processes highly compressed in time that are responsible for significant amounts of sediment transport. Lack of data on the effects of such extreme events on local and global sediment flux is a fundamental problem (Syvitski, 2003). Small and shallow waterways are highly susceptible to the impacts of these events as deposits of several years can be disturbed and relocated within few minutes of wave activities intensified by extreme events.

In order to reflect the intense sediment transport patterns and increase the model's responsiveness to extraordinary forces, some event-based models were developed to increase the temporal resolution of data analysis during extreme events. Even though the ongoing improvements in computation power has made it possible to move toward more continuous simulations of reality (Merritt et al., 2003), the data collection techniques have not improved as much. For example, most tests used to determine sediment index properties still require laboratory investigation of samples obtained from the field. The extreme post-event conditions pose a practical barrier against performing such site studies immediately after the events. Even

the use of automated sampling devices, as suggested by Quinton (2005) is a viable solution only for some factors e.g. flow velocity and depth.

The global climate trend toward more frequent extreme weather events and a more vigorous hydrologic cycle (Amore et al., 2004), indicates a growing significance for studying the effects of intense nonstationarities caused by such events. It can be concluded that the contribution of episodic events to the total sediment transport is very sensitive to the length of time series, data frequency, and number of events recorded. For instance, Subramanian (1993) measured 12% of the annual sediment load of the Godavari River occurring in a single day. Calculation of the mean annual load based on this measurement overestimates the Godavari's annual sediment load fortyfold. This is true even for longer records: a yearlong study will result in very different results based on the occurrence or absence of extreme events during the study period.

2.5. The Concept of Scale in Sediment Erosion

Section 2.5 focuses on the concept of scale in cohesive sediment erosion. It investigates the causes and consequences of temporal and spatial variations in the erosion behavior of cohesive sediments and aims to shed light on the significance of the issue of scale. In this context, the term "scale" refers not to any specific number, but to a rough indication of the order of magnitude (Blöschl & Sivapalan, 1995). Scale in cohesive sediment transport is classified into three categories: process, observational, and modeling scales, which are discussed in sections 2.5.2, 2.5.3, and 2.5.4, respectively.

2.5.1. Introduction

Scale is considered one of the most fundamental aspects in almost all research endeavors and simultaneously one of the most ambiguous ones (Goodchild et al., 1997). However, the concept of scale in the sediment transport field, if not completely ignored, has generally been

used in an unclear or inaccurate manner. For example, the temporal and spatial scales are often not distinguished from each other and are both referred to as scale.

Sediment transport occurs in a wide range of temporal (Figure 2-23) and spatial (Figure 2-24) scales. Nano-scale inter-particle forces, micro-scale turbulence structures, mezzo-scale tidal currents, and macro-scale regional and global climate patterns are examples of processes within that range. While moving from small scales to large scales, the contribution of individual processes to erosion behavior may either increase or decrease. This could be due to the introduction of new processes to the system and/or the presence of scale-sensitive processes e.g. reciprocal cyclic forces.

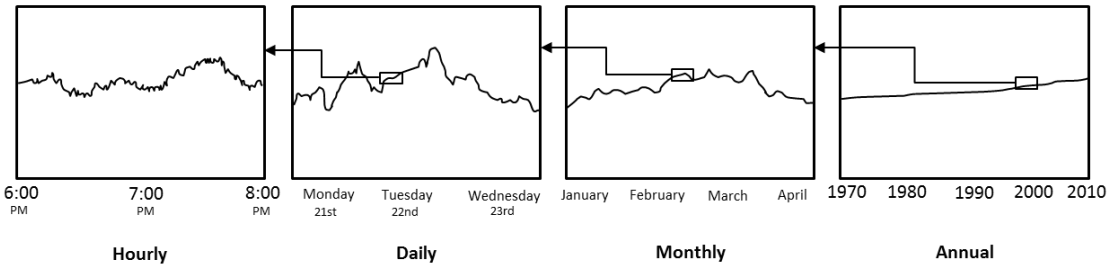

Figure 2-23. **Temporal scales associated with cohesive sediment processes**

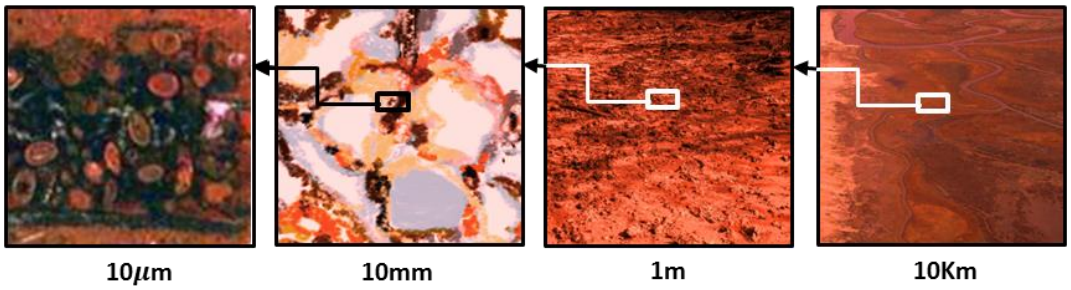

Figure 2-24. **Spatial scales associated with cohesive sediment processes**

Scale has numerous definitions and in the sediment transport context it may refer to any of the following concepts (applicable to both temporal and spatial aspects): (1) **Support**: Support is a measure of the finest level of spatial or temporal data resolution (McBratney, 1998). Support

is sometimes also referred to as "grain". Within each support unit, the measured or predicted variable is assumed to be homogeneous (in space) or time-invariant (in time). (2) **Extent**: Extent refers to the domain of study in either space (area/volume) or time (duration) delineated by the boundaries imposed by the rest of reality. If the study extent is thought of as the target population from a statistics viewpoint, support will be the sub-unit of the population selected for observation. As typical with statistical studies, only a sub-set of support units are observed in each study. **Coverage** is defined as the ratio of observed support units (area, volume or duration) to all possible non-overlapping units within the study extent. In most environmental studies, the support size is much smaller than the project extent, resulting in very small coverage ratios; thus, coverage is sometimes reported as the number of observations per a certain area or duration (Bierkens et al., 2000). (3) **To scale (as a verb):** Scale may also be used as a verb to refer to the act of transferring information across different support units (to scale up or down). In this study, to avoid any confusion due to the inconsistent use of the term "scale", the terms "support" and "extent" are used when possible.

Progress in the sediment transport field requires simultaneous advancements in three distinct yet conceptually sequential phases: (1) process identification and phenomenological investigation; (2) observation and evaluation; and (3) modeling and prediction. The three major interrelated constraints that are associated with almost any approach to cohesive sediment erosion modeling can also be related to this classification: (1) In the process phase, the complex spatiotemporal variation of sediment and flow properties in a wide range of scales necessitates extensive field studies making the interpolation of parameters between the sampling points inevitable. (2) Data scarcity is still a critical concern in sediment erosion studies especially at the regional or global levels. Despite all the advancements in the remote sensing technologies (which seem to be the solution for collecting high-resolution data in heterogeneous fields), they still cannot measure many sediment parameters successfully, especially below the surface. Sampling

and testing sediments in the laboratory are still necessities for quantifying some parameters even though it may reduce the accuracy of results due to sample disturbance. (3) The resolution of the input data, the extent of the study site, relative dominance of different processes and variability of input parameters at different scales, are some factors affecting model uncertainty. As sediment erosion is considered to be a local phenomenon (both erosive forces and resistive forces are highly dependent on local factors), most models developed so far have been obtained and calibrated under laboratory conditions or based on field data obtained at small temporal and spatial scales. Model predictions, however, are generally required and used at larger scales. Although system behavior at larger scales is to a great extent the outcome of processes taking place at smaller scales, the scale of study can still seriously affect a model's predictions (Heuvelink, 1998).

Scale can be defined and used at three levels corresponding to the aforementioned phases: (1) **process scales** are the scales of different phenomena operating within the study area; (2) **observational scales** include all the scales associated with experimental measurements and observations; and (3) **modeling scales** or working scales are the scales over which the model is assumed to represent reality. The process scales are controlled by the nature and intensity of environmental forces. Observational and modeling scales are generally imposed by the study's technical and financial resource constraints. The modeling scales, constrained by computational limitations, should be compatible with the process and observational scales.

It is interesting to note that the process scale is considered as an abstract idea rather than a physical reality by some researchers e.g. Bierkens (2000). They believe that no clear distinction can be made between the process and modeling scales because our understanding of reality can only be presented through some form of a model. In this study, however, process scales are studied with a focus on models' inputs and state variables while the modeling scale mainly focuses on the process of modeling erosion. Another type of scale that is defined and used by

some researchers is the “policy scale” or “operational scale”. This is the scale of information required by policy makers to make decisions (Karstens, 2009) and (Bierkens et al., 2000). It is worth mentioning that operational scale is sometimes used in lieu of process scale (Zhang et al., 2005).

2.5.2. Process Scale

The process scale (sometimes referred to as operational scale) is the characteristic time (or length) at which processes occur in the system (environment). For example, a seasonal flow pattern operates at a larger scale than tidal fluctuations. While natural process scales are generally beyond the researcher's control (with the exception of controllable factors in laboratory or field experiments), understanding these scales seems to be helpful when designing the experiments and interpreting the results. However, environmental systems consist of numerous interlinked processes such that the processes operating at small (fast) scales are constrained by the ones operating at large (slow) scales (Zhang et al., 2005), making it impossible to recognize and understand all the operation scales.

As previously discussed, the key processes in cohesive sediment transport are flocculation, deposition, consolidation, erosion, and transport by flow. Even though these processes are linked together extensively, most of the experimental studies on erosion have so far primarily focused on a single process in isolation Another fundamental issue is that cohesive sediments, in general, do not have a standard form of existence. One other issue to be noted is that the forces acting upon sediments can be hydrodynamic (frictional or form drag), gravitational or electrochemical in nature. The dependence of these forces on flow parameters, sediment characteristics, and environmental factors, among others, introduces a source of randomness into all sediment transport processes. Variation in the medium’s properties in space is generally referred to as “heterogeneity” while the term “variability” is often used for variation with time (Blöschl & Sivapalan, 1995).

The relationship between spatial and temporal scales is ambiguous. Bloschl (1995) argues that there is a direct relationship between the length and time scales of a certain process, meaning that large time scales are associated with large length scales (similarly for small scales). However, this statement might not always be true. For example, a long-term climate variation may affect transport processes in small as well as large dimensional scales. The emphasis in the following subsection is to explore the variability of different factors (influencing erosion) with time and space as found in the literature.

2.5.2.1. Temporal Variation

Variability of sediment transport processes with time occurs at a very wide range of time scales – from fractions of a second to years – with a spectral gap in between (referred to as separation of scales). "The influence of temporal variability (including tides as well as lower-frequency processes) on the time-averaged estuarine regime is one of the most important topics in estuarine physics" (Geyer, 2010). The ratio of the time period of the recorded data to the forecast period strongly affects the reliability of the predictions (De Vriend, 1991) due to superposition of components with different frequencies. Another challenge in the detection and tracking of different temporal scales is caused by the time lag between input variations and the response of some processes.

Temporal variations can be classified into the following three categories based on their nature of variation: cyclic, pulsed, and ramped. **Cyclic** variations are periodical fluctuations with certain frequencies such as the variability caused by tidal and seasonal trends. The characteristic time scale of such variables is generally the period of the cycle. When intense variations occur in a short period of time, for example in floods, tsunamis and storms, they are considered to be **pulsed** variations and can be modeled as a point phenomenon in long-term modeling. Although the characteristic time-scale of such events is generally their recurrence interval (or return period), the duration of these events can also be taken into account for a more detailed analysis.

Ramped variations (e.g. climatic change) occur continuously and often gradually throughout time and are usually considered as integrating processes.

Reaction and relaxation time are two additional concepts relevant to temporal variations that must be defined when observing process scales are reaction time and relaxation time. (1) **Reaction time** is defined as the amount of time between an external stimulation to a system and its corresponding response. (2) **Relaxation time** is defined as the time required for a system to return to its original state or to adjust toward new equilibrium state post stimulation.

2.5.2.1.1. Hydrodynamics

The variation of hydrodynamic forces in tidal estuaries covers a wide range of time scales. The random velocity fluctuations occurring in fractions of a second mark the minimum in this range while long-term climate patterns affecting global hydrological cycle and sea level for instance represent the largest scales. Tidal and seasonal cycles fall somewhere in the middle of this range.

There exists a circular cause-and-consequence relationship between flow hydrodynamics, bed morphology, and sediment transport patterns (erosion and deposition) as illustrated in Figure 2-25. This relationship can be illustrated using the example of a deeply dredged shipping channel. In such a channel, a bathymetric discontinuity leads to a complicated hydrodynamic behavior (Burke at al., 2002), which results in a complex sediment transport pattern. Incorporating this relationship in sediment transport models is challenging specifically because of the dependence of the bottom shear stress on the surface roughness. For example, in low-shear-stress regimes, a muddy environment generally dominates, and the deposition of fine particles creates a hydrodynamically smooth muddy surface (Herman et al., 2001). The continuous deposition of sediments in such regimes can eventually alter the bed's morphology to reach a new equilibrium between the bed elevation and the flow condition by imposing higher velocities (as a result of

reduction in the depth of the flow). Climate change and extreme meteorological events are two factors that directly affect flow hydrodynamics independent of the other factors in the cycle.

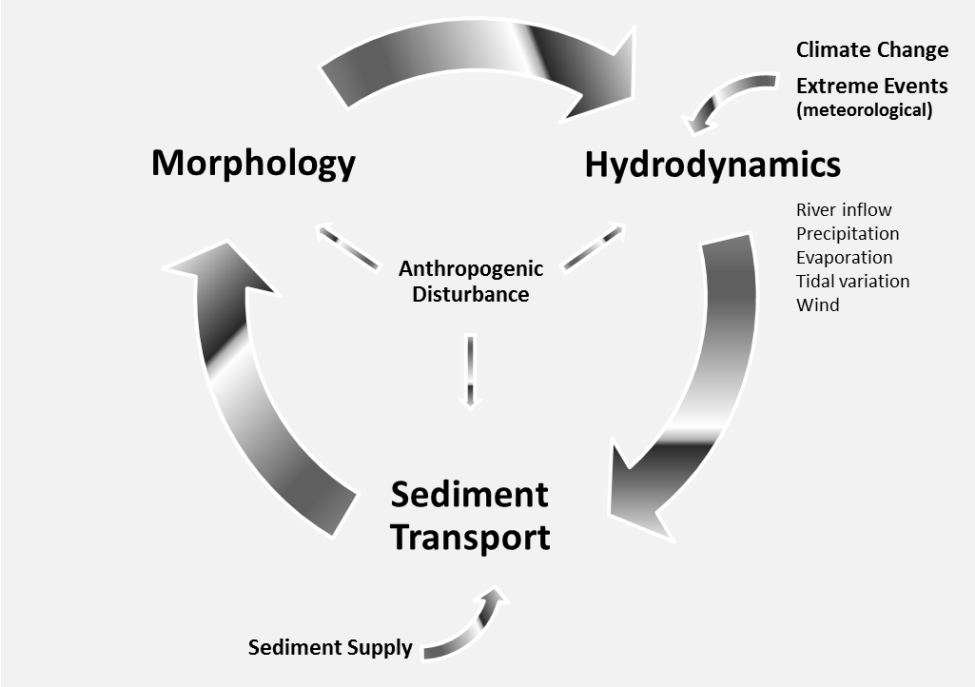

***Figure 2-25*. The circular cause-and-consequence relationship between flow hydrodynamics, bed morphology, and sediment transport patterns**

If hydrodynamic conditions are not uniform in a study area, it is important to detect the discontinuities and patterns and to identify the reasons for their occurrence. For example, the Newark Bay belongs to a larger estuarine system, consisting of the tidal portions of the Passaic and Hackensack Rivers and the Arthur Kill and Kill Van Kull straits. As a result, Halonen (2011) divided this system into nine zones to emphasize the variation of hydraulic geometry between the shipping channels and flats in his bathymetric change analysis.

The hydrodynamics of tidal estuaries is more complicated than that of unidirectional fluvial channels due to the presence of tidal currents and salinity differences between marine and fluvial waters. Geyer (2010) considers the salinity gradient to be the key variable differentiating estuaries from other lacustrine or marine environments. The salinity gradient (in both horizontal and vertical directions), freshwater inflow, and meteorological forcing are the prominent factors

that shape the circulation regime in estuaries. The regime is influenced mainly through the tidal propagation pattern and the location of the estuarine turbidity maximum (ETM). In a recent hydrodynamic study in the Newark Bay, Kill Van Kull strait, and southern part of the Arthur Kill strait, the seaward surface currents and landward bottom currents (primarily restricted to shipping channels) were observed to form a classic gravitational circulation (Chant, 2005).

2.5.2.1.2. Tidal Cycle

Recently deposited sediments are very susceptible to erosion until they get a chance to gain some strength as a result of self-consolidation, biostabilization, and evaporation (in air-exposed areas in intertidal zones). Variation of water depth during tidal cycles also affects the significance of wave climate as an erosive force. Whitehouse and Mitchener (1998) observed that a large portion of the change in the bed level occurred at the initial and final stages of the tide cycle when the shallow depth of water (<0.5m) and wave actions could exert a strong controlling influence on the sediment surface. The reversing of direction in tidal currents can also complicate the behavior of fine sediments during each tidal cycle. Consequently, a certain particle can be resuspended and repeatedly resettled before it either becomes part of the bed or exits the estuary.

Burke et al. (2002) performed a frequency analysis on the flow data from the Newark Bay and distinguished the semidiurnal tide to be the dominant force exerted by the current (Burke at al., 2002). They also observed in their study channel that the predominant bed suspension occurred twice per month during spring tides. Van (1998) studied the floc size of mud in the Dollard Estuary in October 1995 and found strong variations in floc size during the tidal cycle. The observed floc size correlated positively with the suspended solids concentration and negatively with the current velocity. He also detected a vertical concentration gradient during periods of lower velocity that occurred due to the settling of larger flocs (Van der Lee, 1998).

The detailed measurements of waves, suspended sediment concentrations (SSC), and boundary-layer currents made by Green et al. (1997) in an estuary in New Zealand revealed an

interesting tide-dependent trend in the origin of suspended sediments (Green et al., 1997). During ebb tides, a majority of sediments were derived from upstream but during the flood tides, most of the particles originated from the local seabed. Whitehouse and Mitchener (1998) reported a similar phenomenon during the fortnightly tidal cycle. They studied bed level variations in an intertidal mudflat (in the Severn Estuary, England) during 31 tidal immersions (15 days) in the winter of 1995. During the spring tides, the soft mud supplied to the intertidal zone they studied was easily resuspended, whereas during the neap tides, the data reflected the behavior of a more consolidated bed. It can be concluded that the stage of the tidal cycle should be taken into account when analyzing the current velocity and SSC data. On a tide-by-tide basis, the range of variations in the bed level was between 10 and 20mm. Whitehouse and Mitchener (1998) found the bed level to be generally 10mm higher during the spring tide compared to the preceding and following neap tides. They also observed a net increase of at least 3mm in the bed level over all 31 tides. On an annual timescale, the bed level variation was found to be in the order of 100mm. However, they emphasized that the phasing of the spring-neap cycle and the tidal elevation with periods of low- or high-wave activity has a strong control on tidal and fortnightly trends. The surface wave activity, which is a tide-independent factor, can also influence the bed elevation data.

Mariotti et al. (2013) explored the long-term behavior of cohesive sediments under intermittent and moderate-energy disturbances e.g. tidal currents (and winds). They subjected a placed bed of montmorillonite to consecutive cycles of erosion and deposition for an 80-day period and found patterns of temporal variation for sediment resuspension occurring on scales of weeks to months (Mariotti et al., 2013).

2.5.2.1.3. Waves

Although steady currents play the main role in the horizontal transport of sediments, the main causes of sediment suspension in shallow estuarine flats are intermittent processes such as

wind waves (Burke at al., 2002). Wave-induced sediment transport has very rarely been studied analytically (Xiao, 2009). Both local and distant winds can create surface waves in estuaries. Short, sharp-crested waves originate from local winds while slow, gently rolling waves (called swell) have a distant source (Beer, 1996). Although the effect of waves on the marine sediments in shallow water has been studied extensively in the past decades (Jeng et al., 2000) wave-induced erosion is not understood well yet (Winterwerp & Van Kesteren, 2004). Waves may simultaneously influence the estuarine sediment transport through several mechanisms, including but not limited to the following.

(1) Increasing bed shear stress and causing pressure fluctuations at the sediment-flow interface: Wave-induced shear stresses in the bed surface can easily exceed flow-induced shear stresses by an order of magnitude because of the non-linear nature of the interaction between currents and waves (Winterwerp & Van Kesteren, 2004). Subtidal waves can also cause pressure fluctuations at the sediment surface (Meysman et al., 2003).

(2) Affecting the salinity structure and estuarine circulation by enhancing the mixing throughout the water column: A sufficiently strong wind can totally mix the water column from top to bottom, inducing a windward flow on top and a reverse flow underneath (Beer, 1996).

(3) Generating a seepage flux into and out of the sediment bed: The sediment bed is a three-phase porous medium and waves passing over it can induce a seepage flux into and out of this medium (Jeng et al., 2000). The micro-scale velocity variations within the top portion of the bed depend on the compressibility, permeability, and saturation level of the bed.

(4) Affecting the size and strength of suspended flocs: Waves can influence the flow's capacity to entrain cohesive sediments and its competence to keep the flocs/particles of a certain size suspended. The large turbulence intensity caused by waves can also inhibit the development of large flocs (Van der Lee, 1998)

Currents and waves have different temporal scales; hence, in order to take both current- and wind-induced shear stresses into account, combined shear stress is generally defined. Natural surface waves, however, are composed of a whole spectrum of waves originating from different sources rather than a simple train of waves (Beer, 1996). Although one option to overcome this complexity is to replace the whole spectrum with an average value, Winterwerp and Van Kesteren (2004) found that the mean bed shear stress may not be the parameter describing the surface sediment dynamics most accurately. Therefore, they proposed the peak values as a more suitable parameter for sediment transport analysis. There are also some phase-resolved models that compute the details of wave propagation and its effects on current (and sediment transport) at each phase of the cycle (Wu & Wang, n.d.). Such models, however, require extensive computational resources.

Sediment transport rates in the presence and absence of intermittent waves have been compared in both laboratory and field studies. In field studies, as the level of control over sediment sources is very low, care should be given to distinguish between the wave-induced local suspension and sediments of non-local origins. Green et al. (1997) suggested examining concentrations of suspended sediments at different elevations above the bed for this purpose. Laboratory studies also have pitfalls as a result of limitations associated with scaling down the field conditions.

The ratio of the magnitude of wave-induced velocities to current velocities is an important factor contributing to the observed spatial variation morphology and sediment composition in tidal flats of Strangford Loch (Ireland) (Ryan & Cooper, 1998). This ratio also varies with time (following the wave cycle pattern) causing temporal variations in the turbulence structure. The relative contribution of currents and waves to the total sediment transport is such a significant factor that it can be used to classify the cross-shore profiles of mud flats (Kirby, 2000). Erosional flats dominated by wind waves fall at one end of this classification range while tidally

dominated flats lie at the other end (Pritchard et al.). Whitehouse (2009) suggested that the depth of the water column, shallow enough to let waves create oscillatory velocity at the bed level, is approximately$10H_s$, where H_s is the significant wave height.

2.5.2.1.4. Seasonal Variation

Seasonal trends affect sediment transport in a variety of ways. The fresh water discharge rate has an obvious seasonal trend, which impacts the tidal propagation pattern, average salinity, and salinity intrusion length. The phasing of the air exposure period, that is when sediments in intertidal zones are exposed to air, with daylight hours also has a seasonal pattern, which affects the subaerial self-consolidation (hardening) and biological activities in sediments (Whitehouse & Mitchener, 1998).

Herman et al. (2001) report an interesting example of a seasonal cycle which does not leave any long-term trace. They observed fine sediment accumulation up to 10 cm in an intertidal flat in the Westerschelde Estuary (The Netherlands), between the months of March and June in 1997 (Herman et al., 2001). However, radionuclide profiles could only detect long-term sand deposition in that area. They deduced that the mud deposition in that region was a temporary phase being reversed (washed away) during the winter probably due to storms. Another seasonal study in the Oues Estuary (England) also revealed a seasonal cycle of (sand-sized) sediment redistribution operating between summer and winter (due to variations in the discharge) in both the subtidal and intertidal zones (Uncles et al., 1998). In this study, up-channel banks, which were covered by fine sand during the summer and autumn, were eroded back to a stronger, cohesive bed over the winter.

Subramanian (1993) studied sediment load in India's peninsular rivers, looking for temporal trends. He observed that 95% of the annual sediment loads were delivered to the mouth of the rivers during the monsoon months coinciding with peak discharges. This implies that

during the remaining seasons, rivers generally deposited sediments at extremely low rates. He also discovered a negative correlation between the upstream erosion rate and the downstream deposition rate in different Indian rivers. When he compared the variation of annual sediment load of these rivers across different years, he found loads differing by factors as large as 20 over a period of 5 years in the Godavari river, and 12 over a 10-year period in the Mahandi river (Subramanian, 1993).

Whitehouse et al. (1998) compared the bed elevation measured in the tidal and annual time scales at the Severn Estuary (England). They concluded that the annual trends in the data could be explained by integrating the tide-by-tide behavior and superposing the impacts of seasonal variations on the biological activity, climate, and storminess.

The volume of sediments delivered to an estuary by rivers depends on the availability of sediments, the erosive power of flow, and the capacity of flow to carry sediments of different sizes along the river. The last two factors are strongly related to the river's discharge rate which is a season-dependent variable. However, it is worth noting that a higher availability of particles in the water column does not necessarily result in a higher siltation rate. Herman et al. (2001) suggested that research be conducted at the estuarine level to determine if there is a causal link between the total availability of mud in an estuary and the siltation rate.

Whitehouse and Mitchener (1998) did an extensive survey of bed levels in an intertidal mudflat at the Severn Estuary (England) over a period of 22 months. They observed a seasonal pattern for the reworking and redistribution of sediments, which reached a peak between August and October, and was followed by an erosion period caused by waves during the winter.

The sediment structure can be divided into microstructure and macrostructure. While sediments' microstructure strongly depends on their depositional and stress history; their macrostructure is also dependent on the biological activities of the ecosystem's flora and fauna, which is also a season-dependent factor.

2.5.2.1.5. Suspended Solids

In mudflats, more than 98 percent of the sediment flux (to the bed) can potentially be resuspended (Ruddy et al., 1998). Measuring suspended solids concentrations is relatively easier and cheaper than measuring other physical properties of sediments. This is why SSC time series are generally long and have high frequencies. However, even the acquisition of accurate SSC data can be problematic in environments with multiple sediment sources and variable grain sizes and compositions (Green et al., 1997). It is also important to note that the size distribution of suspended sediments is different from that of the bed sediments at the same location (Lick, 2008). This is because the suspended sediments' measurements do not exclusively reflect the local and immediate conditions as they are highly influenced by sediments suspended in other locations and transferred in the system through advection (Mikkelsen & Pejrup, 1998).

2.5.2.1.6. Basin Geology and Geomorphology

The geological formation of each basin and its contributing watershed plays the dominant role in determining the available sediment supply that could potentially be transported by the flow. The spatial variation of a fluvial basin's lithology evidently impacts the sediment load in large rivers (Subramanian, 1993).

Bedforms, as small-scale topographic structures, can also create spatial and temporal variations in the system. In cohesive beds, bedforms can be caused by factors such as fluid forces, bioturbation, and collision of hard objects (shells, pieces of wood, etc.) with the surface. Bedforms control the relative projection of flocs above the average bed level and hence their degree of exposure to the fluid and the surface roughness. They can also modify the local flow field and turbulence level. Additionally, large-scale geologic formations can create inhomogeneities and erosion trends as well (Wood et al., 1988).

Analysis of bathymetric change and sediment geochronology are two useful methods for the investigation of long-term morphological changes and recognition of net sediment transport patterns (Halonen, 2011). Variability of sediment characteristics with depth is a strong indicator of long-term trends and patterns in sediment transport.

The volume, timing, and composition of sediments carried by a river are to some extent a function of flow hydrodynamics. They are also highly influenced by the soil erosion in the subaerial zones of the watershed. The amount and size of sediments available for transport is referred to as sediment supply, which can be a limiting factor for sediment transport capacity when the supply of sediments of a certain size are limited (Hickin, 1995). Many researchers have studied soil erosion using the Universal Soil Loss Equation, which is the most popular mathematical model for the estimation of long-term average annual soil loss due to an overland flow. This model has been developed based on empirical studies and is not event-responsive.

$A = RKLSCP$ Universal Soil Loss Equation

R: rainfall erosivity factor

K: soil erodibility factor

L and S: topographic factors

C and P: cropping management factors

Each of the factors in the Universal Soil Loss Equation introduces a new source of temporal or spatial variation into the cycle represented in Figure 2-25 by directly affecting the sediment supply (independent of hydrodynamic and morphological factors).

2.5.3. Observational Scale

Observation is a fundamental step in environmental sciences that includes both direct observations (primary research) and historical data obtained from other sources (secondary research). Karstens (2009) defines observation scale as the scale at which humans choose to study

natural phenomena. Bierkens et al. (2000) defined it as the scale for which an observation provides an average value. Observational scale in this study refers to both the resolution and extent of observed data (spatial or temporal). Choosing the scale of measurements is a matter of personal judgment. Researchers should choose the observational scale based on their prior knowledge and the purpose of study while also considering the logistic and technical measurement constraints and the nature of processes they study. Ideally, the observational scale should be similar to the process scale because the process scales larger than the observational scale appear as trends in the data and those smaller appear as noise (Blöschl & Sivapalan, 1995). However, the simultaneous operation of multiple processes at different scales and the infeasibility of making continuous, direct observations at large scales make researchers choose observational scales that are practical but not ideal.

Most studies in the field of sediment transport provide an Eulerian description of variables by collecting data from fixed points. This is why the spatial resolution of collected data is generally poorer than its temporal resolution. Some additional issues specific to studying sediment properties are lack of access to subsurface material, difficulty in estimation of sediment properties with depth, and necessity of destructive sampling in determining some properties including grain size distribution and density.

Determining the proper observational scale that provides sufficient detail for a new site is a difficult task due to the lack of prior knowledge about significant scales. The impact of changing observational scales on the interpretation of sediment transport data and development of models has very rarely been studied. Erosion and deposition thresholds are very significant parameters in most sediment transport models. The methods that measure these parameters in a certain location (sample) have strong stochastic components. For a sample of fixed area A, examined under a specific flow level, the longer the duration of observation, the more likely it is that the threshold is exceeded within the testing period. The same argument is valid regarding the

sample's area. For an observation of a fixed duration, as the sample area is enlarged, the sediments are more likely to reach the erosion threshold during the test. This can be explained by the stochastic nature of flow turbulence, probabilistic sediment characteristics (size and composition), and dependence of measurement techniques on the volume of sediments tested compared to the flow discharge rate. Another concern when choosing the observation duration for studying natural sediments' behavior is the dynamic processes occurring at the time scales similar to the observation period. A perfect example in this context is the dependence of sediment erodibility on the stage of the biofilm development in a mudflat resulting in unstable thresholds for observations of short duration. Another example is the multi-scale variability caused by waves and currents. The oft used coastal process models either compute the wave propagation details at each phase (phase-resolved) or only take the average effect of waves on current and sediment transport into account (phase-averaged) (Wu & Wang, n.d.).

A crucial question that can be raised is whether we can find a "Threshold Observation Scale" that leads to an acceptably realistic representation of a site. This threshold should definitely be set for the combination of support and coverage. Inspired by the concept of "Representative Elementary Volume" used in the porous media literature, Wood et al. (1998) introduced the concept of "Representative Elementary Area" for hydrologic models. They defined it as the smallest discernible point that is representative of the continuum. This seems to be analogous to the following assumption, previously used in the definition of support: the predicted variable is assumed to be homogeneous (if spatial) or time-invariant (if temporal) within each support unit. For each study, the minimum required size of the support unit depends on the technical methodology for making the measurements as well as the scale of variability of the measured parameters. The average value of the parameters measured for each support unit should not vary significantly with increasing the sample size. Even after finding the minimum support size, we need to understand the proper coverage (i.e. number of samples) that informs us about

the distribution of the measured parameters within the whole site. Investigating the underlying distribution of the variability between different samples can also guide us toward partitioning the site into homogeneous sections for further analysis.

Laboratory experiments provide a major source of observational learning in sediment transport studies. A great advantage of laboratory tests is the higher level of control over the desired factors and the possibility of running tests on duplicate samples. However, any laboratory study inevitably involves some degree of change in scales and is accompanied by the introduction of some new factors to the system and the elimination or alteration of some natural processes. Moreover, not all the natural processes can be simulated in their original scale. An ideal example to prove the importance of scale considerations in the design of laboratory experiments is the dependence of cohesive sediments' erosion mode on the time scale of the change in the shear stress relative to the time scale of sediment depletion. As stated by Sanford and Maa (2001), the ratio of the rate of shear stress change to the sediment depletion rate controls the erosion behavior and determines which type of erosion (I or II) is dominant.

In all environmental studies, some measurements are made using very small quantities of material (of the size order of cubic centimeters) as compared to the huge volume of material included in the study scope (in the size order of cubic kilometers). This is also true in the time domain: while most of the environmental processes vary continuously, most observations are measured, summarized, and reported discretely or intermittently. As the point behavior may deviate significantly from the block behavior, block predictions made based on point measurements should be examined carefully (G. B. Heuvelink, 1998). Measurements also tend to oscillate if the coverage is too small. To increase the coverage of a study and attenuate such measurement oscillations, different strategies can be used including:

(1) Take more samples and test them individually.

(2) Mix several samples and create a single composite sample on which the tests are conducted. This method requires sample disturbance and only measures an average value for all samples without any estimate of the variability between the samples.

(3) Find auxiliary variables, which are correlated with the parameter of interest (at the scale of interest) and more easily measurable. Using optical remote sensing methods to measure the surface chlorophyll-a concentration in exposed mudflats as an indicator of surface stability (because of its correlation with the biofilm concentration) is an example of this approach (Murphy at al., 2004).

Point samples are generally widely separated apart by distances which are larger than the sample's dimensions by several orders of magnitude. Observational experiments should be designed to reflect the environment and maximize our understanding of the variability in sediment properties given all the technical and financial limitations. The selection of sampling locations can be a random, systematic, or judgment-based process or may include a combination of these methods. Random sampling requires the least design effort as it follows the procedures for simple random sampling. It gives all possible points the same chance of being tested. Systematic sampling involves a systematic randomization technique e.g. presenting a geometric configuration for the points to be sampled. To ensure that estimates are unbiased, an element of randomization that provides a probabilistic basis for the inference should be applied (Webster & Oliver, 2007). Partitioning the study area into fairly homogeneous grid cells is often a necessary step in studies of large scope including those examining different sediment types. A single value is generally assigned for each of the grids to be used within the models.

In order to deal with complexities at very small scales, a fundamental question is if there exists a threshold scale that attenuates the small-scale, undefinable complexities in sediment heterogeneities without losing a realistic perspective of the variations. In practice, however, the number of samples and the sample size are generally determined based on the measurement

techniques and sampling methods used, site conditions, study purposes, and other technical considerations.

2.5.4. Modeling Scale

Modeling (working) scale is the scale of predictions made by the model outputs. For instance, an estuarine annual sediment transport model provides the average annual sediment transport for that estuary. What some researchers categorize as policy scale is also treated as a modeling scale in this study. The modeling scale should be determined based on both the model applications and the observation scales. The typical temporal modeling scales for sediment transport are long-term, annual, seasonal, monthly, weekly, daily and event-based. Similarly, the spatial scales of data can vary from pore-scale to local, regional, and global scales. In environmental studies, it is typically easier to increase the support and extent of a study in the temporal dimension compared to the spatial dimension; this explains why spatial data is often widely dispersed. The modeling scale is generally much larger or smaller than the observation scale; therefore, the data needs to be scaled to bridge this gap (Blöschl & Sivapalan, 1995). Models representing a process at different scales are unlikely to be linearly related and thus, the data will carry different information at various scales. For example, a model developed at the pore scale is not applicable at the regional scale without adjustment.

The following factors cause considerable differences between models at different scales:

(1) The significance and dominance of processes vary at different scales. The relationships derived at one scale may not be valid at other scales. For instance, tidal and seasonal variations in suspended solids, which are significant factors in short-term transport rates may have no effect on annual transport rates.

(2) The heterogeneity and variation of model inputs in space and time make them scale-invariant and adds a source of nonlinearity to all processes including linear ones.

(3) The temporal and spatial scales of most observations are much smaller than the scales at which predictions are required for the system. This necessitates aggregating small-scale observations to represent larger-scale processes. However, Goodchild et al. (1997) believe that when data are aggregated, new properties may emerge. The quality and quantity of data available for doing large-scale analysis is generally poor and insufficient, which makes the use of simpler models with fewer parameters inevitable. For a fixed experimental design, the coverage (ratio of observed support units to the study extent) varies based on the extent for which the model is used. This ratio significantly affects the reliability of the model at different scales.

(4) Most of the models used for sediment transport analysis have a strong empirical nature because of a lack of understanding of the physics of the processes. The model coefficients and constants as well as the form of the statistical models heavily depend on the set of measurements over which the model is developed and calibrated.

(5) Some properties of the system may be correlated only at certain scales (Webster & Oliver, 2007). Consequently, if a model depends on such correlations, it cannot simply be transferred across different scales.

The development and modification of models for different scales are not straight- forward tasks. The advent in technology (both computational and observational) has made it possible to concentrate on fine-scale erosion processes (with the aim of understanding the physics behind them). The general improvement in observation scales in recent years makes it even more critical to clarify the relationship between larger and smaller scales. There are two extreme viewpoints regarding this relationship. The first one assumes that the significance of each process is limited only to the scale at which it operates and that there is no transfer of influence across scales. The second thinks of larger-scale processes as being shaped by and extended from processes occurring at smaller scales. In reality, each of these views partly explains the relationship between the scales, and the contribution of each process to the overall sediment transport is generally a

scale-dependent variable. The fact that flocculation occurs at fine scales never undermines its significance at larger scales while some processes occurring during the course of a tidal cycle may not remain as contributory in models operating on large scales.

The inherent relationship between the process scales and observation scales on one hand and the observation scales and modeling scales on the other hand, makes it important to design experiments bearing these relationships and the end use(s) of the results in mind. Future studies and additional measurements can also be improved based on the model requirements and previous measurements.

Bierkens et al. (2000) divided the scale transfer operations into three categories. A combination of these methods is generally used to transfer data between the observation and modeling scales.

(1) Change of extent (extrapolation versus singling out): when the extent of the observations and the model do not match, the data should be either extrapolated (to increase the extent) or singled out (to decrease the extent) should be performed.

(2) Change of support (upscaling versus downscaling): An Examples of upscaling include calculating the annual sediment transport rate based on the measured daily rate or measuring erodibility in a single location and assuming that it applies to the surrounding area. On the other hand, an example of downscaling is estimating the net sediment deposition in a section of a channel based on suspended sediment concentration measurements made at the input and output points for the entire channel. Another example is when a monthly sediment transport rate is derived from an annual record.

(3) Change of coverage (interpolation versus sampling): For instance, while sediment organic content is determined for a few small samples taken from the basin, an erosion model may require the organic content value for each of the model grids. This necessitates increasing the coverage of

the input data by interpolation. If a model requires fewer data points than the collected measurements, sampling should be performed to reduce the coverage of input values to be used in the model.

It may be necessary to partition a site into smaller areas and model them as interacting adjacent systems. The suitable scale for analysis of the observed data, in this case, is the scale that tolerably lowers the response variability between various sufficiently large areas. Zhang et al. (2005) suggested the following methods for determining a relevant homogeneous size to be used as the optimal scale in environmental models.

(1) Analysis of the variogram change with variation in spatial resolution

(2) Estimation of the average local variance from a moving window for different measurement scales and finding the scale at which the variation is maximized

(3) Plotting the semi-variance at a lag of one pixel versus different spatial resolutions

(4) Using the dispersion variance of a variable within a specific region that is defined on a spatial scale

These techniques along with prior knowledge of the site can also be used for site partitioning. The process for selecting the optimum analysis scale – as discussed above – is independent of the scale of the model outputs required by decision makers. This problem is viewed as a discrepancy between the observed data, the analysis efforts, and the required outputs in the literature. In order to align the model output with the scale of the environmental measures decision makers need to know, a scale transfer mechanism should also be built into the model.

One approach to reduce the scaling complexities is to break different model components apart. Bierkens et al. (2000) defined model components as follows: **Inputs** are the measured variables that are fed into the model. **State variables** are all the variables that are necessary to describe the system. They should be known along with the input variables to describe the system's response

and they can vary in both time and space. These variables are independent of the path and only depend on the current status of the system. **Parameters** represent the intrinsic properties of the model; they are invariant in time (may vary in space) and relate the input variables to output variables. **Constants** are the scale-invariant model properties that do not change in either time or space.

As presented in Figure 2-26, e is an erosion model obtained through a small-scale study with sets of inputs (i), state variables (v), and parameters (p) and E is the model adjusted for a larger scale with I, V, P as model components. To completely adjust the erosion model to the new scale, the general structure of the model ($e \leftrightarrow E$) and the model components ($i \leftrightarrow I$, $v \leftrightarrow V$, $p \leftrightarrow P$) may be transferred. Very often, only one component is modified for scale transfer and it is very rare for all the components to be adjusted. Although this method does not eliminate all possible effects of scaling, identifying a few scalable elements within any complex system definitely reduces modeling uncertainties (Zhang et al., 2005).

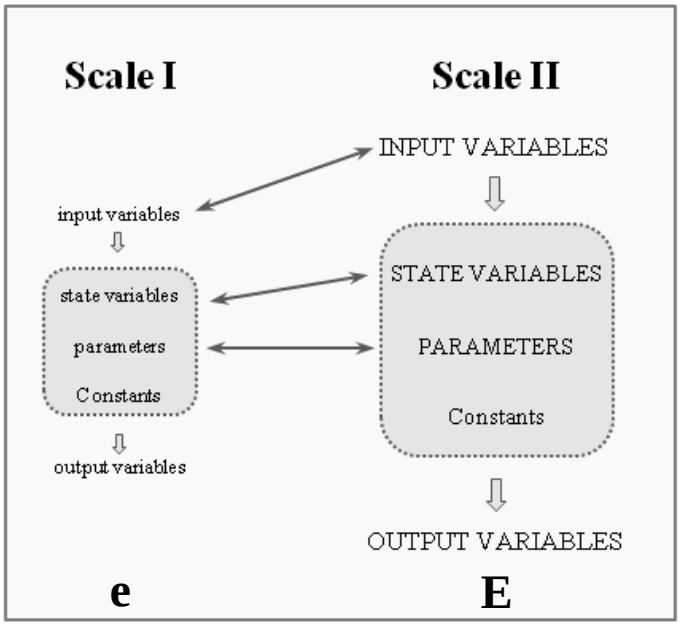

Figure 2-26. **Transfer of model components between two scales**

Adjusting the general structure of a model across scales involves using statistical techniques and background knowledge (mostly empirical), to develop a new model structure that is more suitable for the new scale (often a larger scale). The state variable is the model component that appears to be neglected the most in sediment transport studies. To the best of the author's knowledge, no model in the literature has explicitly included this component so far. This variable represents those elements of the system that cause different responses to identical inputs. The modification of model parameters across different scales can be considered as a special type of model structure adjustment in which the form of the model does not change, and only the parameters are modified.

A large body of literature has been developed on scale transfer methods in the past three decades (Bierkens et al,, 2000) providing guidance for linking the observation and modeling efforts across different scales. Some of these methods are presented here:

(I) Calibration: This technique finds empirical relationships between available fine-scale and large-scale data (generally using regression techniques). It can be applied to any of the model components (inputs, parameters, state variables) or used to form a new model structure at the modified scale. Despite its computational simplicity, this method postulates that sufficient data is available for calibration which is rarely the case. The model's reliability should also be validated in different conditions to ensure the validity of the statistical assumptions.

(II) Estimation Interpolation: There are a wide range of interpolation techniques available for generating new data based on available information for the surrounding points. An interpolation technique that is widely used in geostatistics to estimate a single realization of a random field is Kriging or Gaussian process regression. Under suitable assumptions, Kriging results in the best linear unbiased estimator of a variable at an unmeasured location based on point observations at other locations. Similar to other interpolation algorithms, Kriging calculates the weighted sum of the surrounding data points. The main difference between this technique and other interpolation

methods (splines, inverse distance squared, etc.) is that instead of using an arbitrary function, the weight assignment procedure for Kriging is data-driven and weights are assigned based on the level of spatial continuity in the data. However, creating a model that describes the spatial dependence of the data, still involves an arbitrary selection of a mathematical form and values of the associated parameters. Another difference between Kriging and other linear estimation methods is that it minimizes the error variance and gives an estimation of the variable along with approximate values of the estimation error (Kriging variance). There are different types of Kriging: (1) Simple Kriging: The whole dataset is assumed to have a constant mean. (2) Ordinary Kriging: This is the most widely used type of Kriging in which the mean is assumed to be constant only in the local neighborhood of each estimation point. (3) Universal Kriging: It is very similar to ordinary Kriging with the only difference that it fits a trend to estimate the mean value at each point. (4) Cokriging: This is a multivariate Kriging that uses the correlation between variables (as a function of lag) to improve predictions. It is considered as a reliable framework to incorporate auxiliary information into predictions (Zhang et al., 2005).

The spatial continuity in a dataset can be estimated and modeled using any of the following methods:

(a) Correlogrom: This graph depicts the auto correlation of the dataset at varying time lags or distance lags. If there is no spatial or temporal dependence between different points, the autocorrelation will be approximately zero for all lags.

(b) Covariance function: This function is defined as:

$$\mathbf{Cov}(\mathbf{h}) = \boldsymbol{\rho}(\mathbf{h}).\boldsymbol{\sigma}_{\mathbf{x}}.\boldsymbol{\sigma}_{\mathbf{x+h}}$$

ρ(h): The correlation between any two points separated by lag h

(c) Semi-variogram: The semi-variance between points i and j is defined as

$$\frac{\mathbf{1}}{\mathbf{2}}[\boldsymbol{Z}(\boldsymbol{x_i}) - \boldsymbol{Z}(\boldsymbol{x_j})]^{\mathbf{2}}$$

If the semi-variance between all the pairs of data is plotted against the distance that separates the two locations, a semi-variogram cloud is created which generally consists of many points. If the data has spatial dependence, closer points will have lower semi-variance. In order to make it easier to interpret the data, the distance range is divided into lag classes $[h-\delta, h+\delta)$ represented by the mid-range value h. The semi-variance values between all n pairs of data separated by a lag h are averaged as follows to obtain the variogram:

$$\boldsymbol{\gamma(\mathbf{h}) = \frac{1}{2n}\sum_{1}^{n}(Z_i - Z_{i+h})^2}$$

Models fitted to variograms can have different forms (spherical, exponential, etc.) but the following parameters are common to all of them: **Nugget** ($\boldsymbol{C_0}$): the semi-variance at extremely small separation distances (or times). Theoretically, this value should be zero but because of short-scale variations and measurement errors it is possible to have different observations at very close locations, creating a discontinuity at the origin of the curve. **Range:** the lag at which the semi-variogram reaches its plateau. **Sill** ($\boldsymbol{C_0 + C_1}$) : the maximum semi-variogram value which is the semi-variance between any two points with separation lags larger than the range value.

(III) Stochastic simulation: Stochastic simulation has been previously discussed in Section 2.5.3. While the main goal in estimation is optimizing the local estimates (for example, Kriging minimizes the local error variance), stochastic simulation focuses mainly on the global statistics to better reproduce the spatial variability. This is why simulation, in general, is a much better method (compared to estimation) to preserve statistics such as variance, the shape of the histogram, and the spatial continuity of the variogram. Despite resulting in larger mean prediction errors, simulated values better represent the spatial variations in the field because estimation methods like Kriging reflect a smoothed representation of the reality.

2.5.5. Conclusion

Scaling issues have been previously brought into focus for environmental (Bierkens et al., 2000), (João, 2007), (João, 2000), (G. B. Heuvelink, 1998), (Zhang et al., 2005)), hydrological (Blöschl & Sivapalan, 1995), (Bergström & Graham, 1998), and soil erosion (Amore, et al., 2004) studies. However, there have been no investigations exclusively examining the scale problem in marine sediment transport studies. Presently, there is no clear indication of the different scales associated with most sediment transport studies especially in the case of modeling scales. This can be considered a serious barrier to comparing results from different studies. There is a need for a framework that guides researchers through dealing with the issue of scale in their erosion studies. This study investigates various scale-related aspects in cohesive sediment transport based on the current literature. Defining and understanding these aspects can be considered as the first step toward developing a holistic framework.

3. METHODOLOGY

"A good data collection scheme can ensure a simplified analysis and a generally more applicable model. A poor data collection scheme can induce serious problems for the analysis and its interpretation."(Montgomery et al., 2012)

In the first three sections in Chapter 3, the methodology used for sample collection, transportation and preservation, and preparation is described. Undisturbed samples from two sites (Figure 3-1) in the Newark Bay were obtained between February 20, 2012 and July 24, 2012 and transported to Weeks laboratory to be tested in the Ex-Situ Erosion Testing Machine.

Section 3.4 explains the procedures used for determining sediment index properties (bulk density, water content, organic content, Atterberg limits, particle size analysis, and specific gravity). The final section defines the methodology used for conducting erosion tests. It starts with a comprehensive assessment of the Ex-Situ Erosion Testing Machine. The next section is dedicated to developing a framework for probabilistic analysis of erosion rate measurements. Through this analysis, this section provides a better understanding of the impact of experimental design on erosion studies. A detailed description of the methodology used for erosion tests in this study concludes this chapter.

3.1. Sample Collection

In this study, 142 fairly undisturbed samples were obtained from 24 cores which were extracted from the Newark Bay, New Jersey between February 20, 2012 and July 24, 2012. The locations of the sampling sites are shown on the map in Figure 3-1.

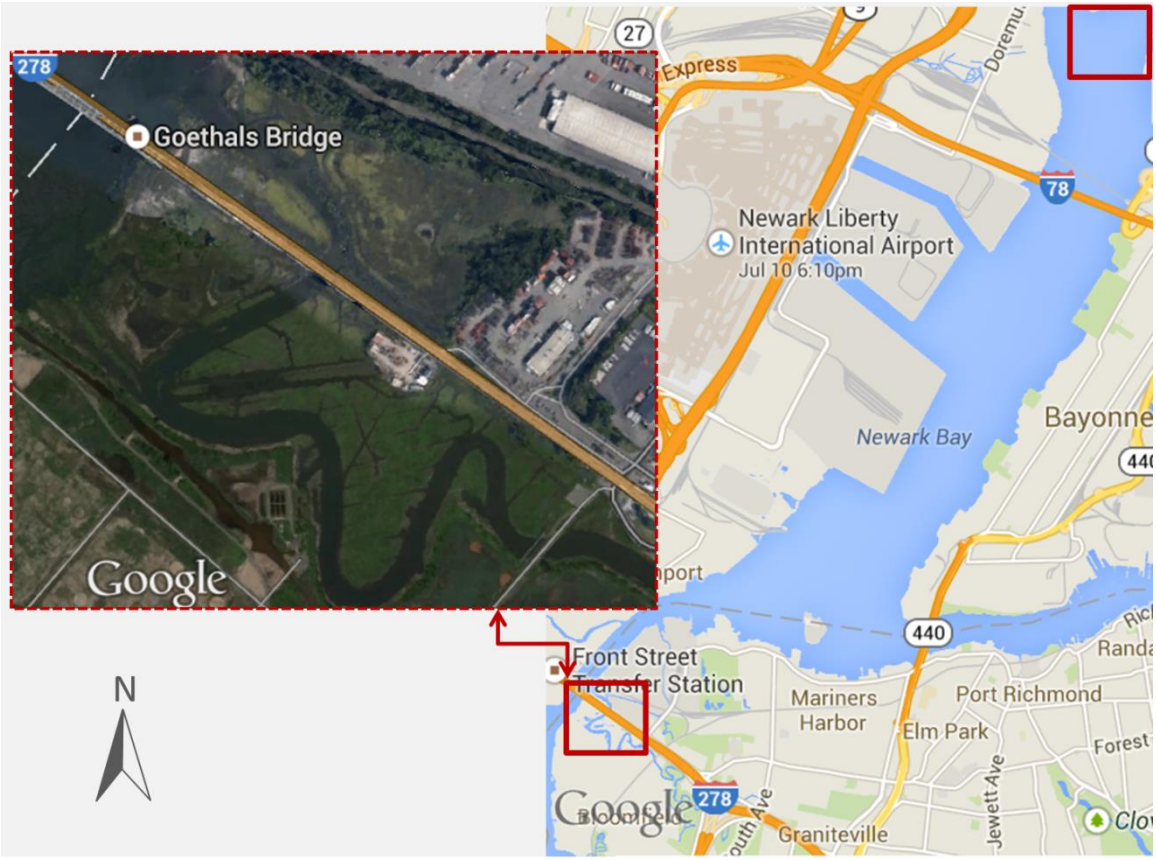

***Figure 3-1*. Sampling sites in the Newark Bay, New Jersey**

The bottom corer (Figure 3-2) used for sample collection in this study employs both gravity and suction forces to push a Lexan tube, 10 cm in diameter, into the bed. It seals the core bottom to prevent disturbance while elevating the frame to the boat deck. A winch, installed on the deck of the study boat, is used to haul the sampler up and down. On a few occasions when the operator can walk on the surface of the shallow mudflats, the tube is separated from the main frame and manually pushed into sediments. The wall friction does not let the core slide down while being retracted from the bed. Eventually, the water collected from the sampling location is decanted to fill the tube before sealing its top. Figure 3-3 shows the undisturbed surface of a sample taken from the bay.

Figure 3-2. **The bottom corer used in this study**

Figure 3-3. **Undisturbed surface of a sample extracted from the bay**

3.2. Sample Transportation & Preservation

In this study, four sediment cores were collected during each of the six field trips. The cores were then labeled (Figure 3-4) and vertically submerged in ten-gallon barrels filled with the site water and transported to the laboratory. The main consideration during sample transportation

and preservation was to minimize physical disturbance and maintain the system's natural balance. The cores were transported to the laboratory within a three-hour time frame. Upon arrival at the laboratory, the distance between the bottom and top of each core was recorded as the thickness before submerging the tube into a cool chamber filled with the site water. The cool environment reduces the biological activity and helps the cores to maintain their integrity for a longer period. The biofilm layer that was originally visible on the surface of some of the samples lost much of its strength (consistency) in the first few hours after being removed from the site. There was no visible biofilm on top of the samples after 24 hours. This was consistent with the observations of Sutherland et al. (1998). Their biostabilization studies proved that sediment stability is affected by the physiological state of the biofilm and its composition (influenced by nutrient status and growth phase). They also found a correlation between the biofilm's age and eroded particles' shape and size. The storage chamber was aerated with an air pump, and a light source was added to the system to simulate natural daylight.

3.3. Sample Preparation

Sample preparation is an essential part of performing reliable erosion tests. After removing the top and bottom lids, the tube was placed on a sample ejector and a 2.5-cm-thick extension ring (Figure 3-5) was placed and pushed tightly over that. The ejection piston was then pushed upward to slide the sediment core outward into the extension ring. When a sufficient amount of sediment was pushed into the ring, it was detached from the rest of the core using a thin cutter plate (Figure 3-6). A smaller cutter (a metal ring with an external diameter of 61 mm) was then used to obtain up to 2 sub-samples from this sediment section as shown in Figure 3-6. Ejection, cutting, and trimming of the sample tend to disturb the sediment structure, especially at the periphery of the sample and along the cutting surfaces when roots are present. Hence, care was taken to minimize sediment disturbance as much as possible. The disturbance potential was the highest on the surface where the sample had its lowest consistency. The final samples were

then submerged in the site water for a few minutes before being tested for erosion. Bulk samples were also taken from the remaining material in the original sediment ring and stored in tightly sealed plastic bags for index properties tests. Up to eight sections of sediment were obtained from each core at various depths.

Figure 3-4. **A sediment core obtained from the Newark Bay on 06/19/2012**

Figure 3-5. **Extension ring and cutter used to trim a section of sediment**

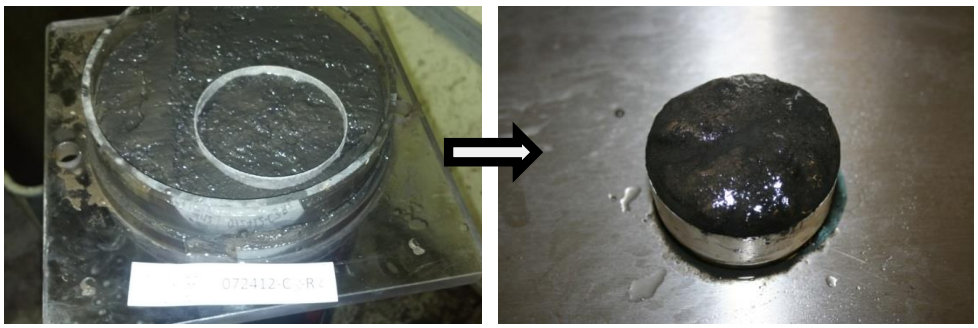

Figure 3-6. **A sample obtained from a trimmed section of the original sediment core**

All samples were labeled, and their specifications were filed according to the protocol developed for this study. The forms designed to facilitate data management are presented in Figure A. 1 - Figure A. 3. A description of the data management methodology employed is as follows:

Form 1: Core Acquisition Data (Figure A. 1): This form was used to record information on sample ID, sampling date, location, thickness, sample description, sampling method, water

depth, and the names of image files. It was filled out during sample preparation. The format for the sample ID (example: 020112-C1) was “date of sampling-C Core Number” where the prefix “C” denoted “core” and the Core Number was a number from 01 to 04 that distinguished between the four cores collected on that date.

Form 2: Ring Identification Data (Figure A. 2): This form was designed to keep track of each sample’s depth with respect to the bed level. As previously explained, each core was divided into various sections (rings). The sections derived from each core were numbered according to their depth starting from 1 for the uppermost section. The thickness of each section and its extraction date were recorded in form 2.

Form 3: Undisturbed Sample Identification Data (Figure A. 3): This form included the sample ID and the top and bottom depths of the sample. The format for the sample ID (example: 022412-C03-R07-S2) was “date of sampling-C Core Number-R Ring Number-S Sample Number. The age of the sample (indicating the time lag between the coring and sampling procedures measured in days, and the time between the sampling and testing steps indicated in hours) were also recorded in this form.

3.4. Index Properties

Many parameters have been proven to affect the erosion behavior of cohesive sediments so far. Many researchers including Winterwerp and Van Kesteren (2004), Whitehouse et al. (2009), and Grabowski et al. (2011) have provided comprehensive lists of factors influencing erosion. These researchers often classified the contributing factors into physical, chemical, or biological categories.

A summary of the most important parameters studied more or less extensively in the literature is presented in Figure 3-7. They are classified according to their domain: fluid; interface; and sediment. Lick (2008) and Whitehouse et al. (2009) are good references that

discuss many of these parameters in detail. Climatic and hydrological variations, biological activities, physical processes, and chemical reactions are the main driving forces that cause variations in these parameters both interactively and independently. While a few of these parameters can be measured in the field (e.g. flow properties and interface specifications), most of them require laboratory measurements. This means that field tests alone cannot measure such parameters without complementary laboratory tests.

It is neither possible nor useful to measure all sediment properties known to influence erosion behavior simultaneously. Considering the Ex-Situ Erosion Testing Machine's requirements for sediment testing including specifications for experiment configuration, sample size, fluid characteristics, and sample preservation methods, the following tests were conducted in this study as complementary laboratory tests: (1) bulk density; (2) water content; (3) organic content; (4) Atterberg limits; (5) particle size analysis; and (6) specific gravity. Given the quantity of material required for each of these tests as compared to the material available within each ring, the last three tests were performed on homogenized samples obtained from the whole core. While the bulk density was measured for individual samples, water and organic content were measured for each sediment ring. These tests will be discussed in sections 3.4.1 through 3.4.6.

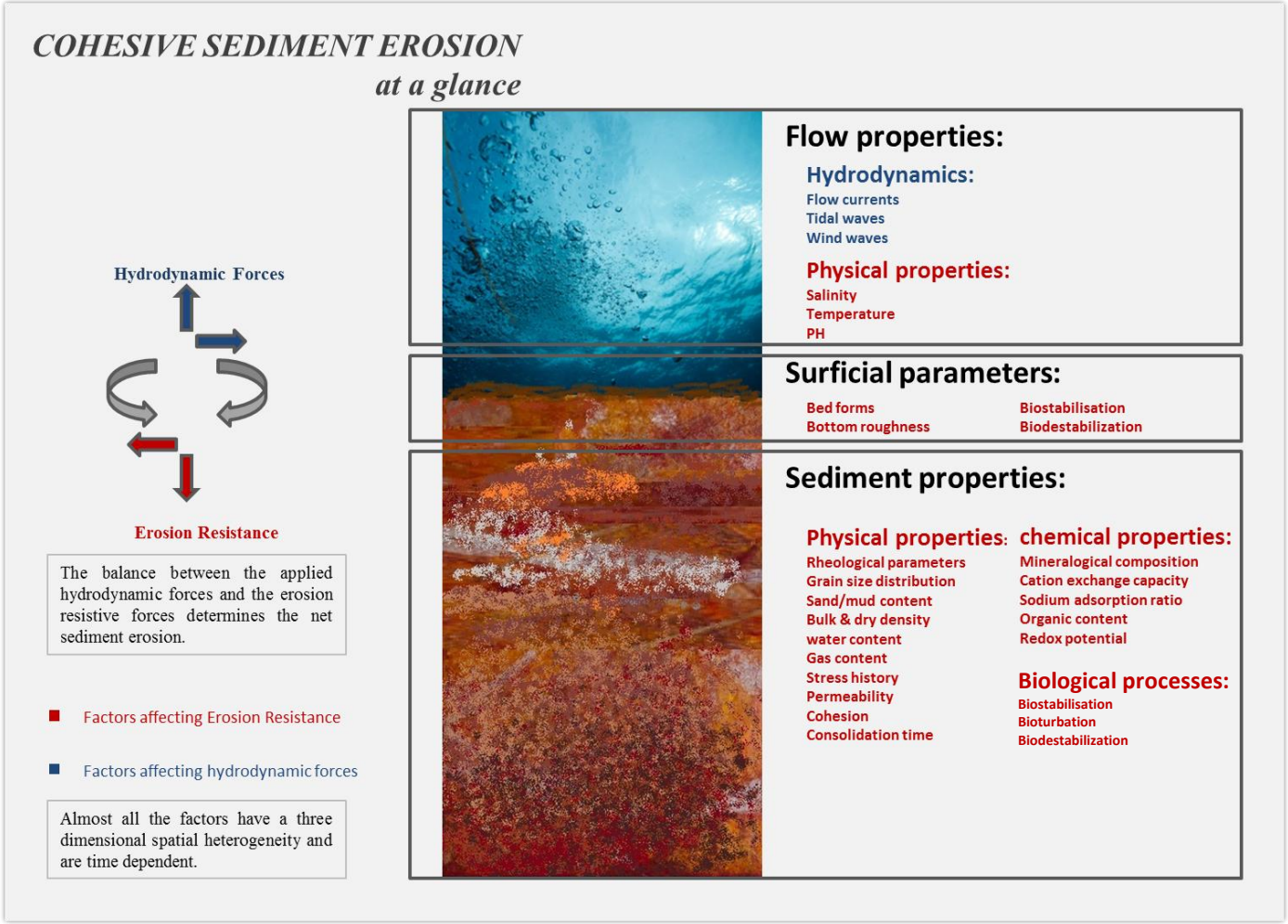

Figure 3-7. **Parameters influencing erosion of cohesive sediments**

3.4.1. Bulk Density

Bulk density has frequently been recognized to have a negative relationship with the erosion behavior of cohesive sediments. There are generally large density variations within each study site as well as between different sites (Dyer, 1998); hence many studies have focused on the prediction of sediment density based on other properties. For example, Lintern (2003) studied the relationship between the floc size and the bed density. He observed that the effect of the rate of floc deposition on bed density is more significant than the size of individual flocs.

In most cohesive sediment studies (including McNeil et al., 1996; Jepsen et al., 1997; Roberts et al., 2000; and Borrowman et al., 2006 among others), bulk density has been determined through the measurement of water content and without any volume measurements. This method makes an important assumption that the sample is saturated and uses the following equation to estimate bulk density based on water content. As specific gravity of sediment is not measured in most cases, a typical value is generally assumed (e.g. 2.6 in Jepsen et al., 1997).

$$\boldsymbol{\rho_{Bulk}} = \frac{\mathbf{G_s}\cdot\boldsymbol{\rho_w}}{\boldsymbol{\rho_w} + (\mathbf{G_s} - \boldsymbol{\rho_w})\mathbf{W}}$$

ρ_w: density of water $(1\ \frac{gr}{cm^3})$

W: water content

G_s: specific gravity

In order to experimentally verify this assumption for the Newark Bay samples, submerged samples were placed into a vacuum chamber. The sudden release of bubbles from the sample, revealed its unsaturation thereby questioning the validity of the assumption. This observation was in line with Lick's (2008) discovery that in natural cohesive sediments, the decay of organic matter often produces enough gas to affect density (Lick, 2008).

Another shortcoming of the aforementioned method (based on water content) is its dependence on the sample's specific gravity value. The presence of a variable amount of organic content makes it difficult to have a reliable estimation of specific gravity for each sample without conducting the specific gravity test. Sensitivity of this method to the value assumed for specific gravity is presented in Figure 3-8. According to this figure, the calculated bulk density for finer sediments is more sensitive to the assumed specific gravity value.

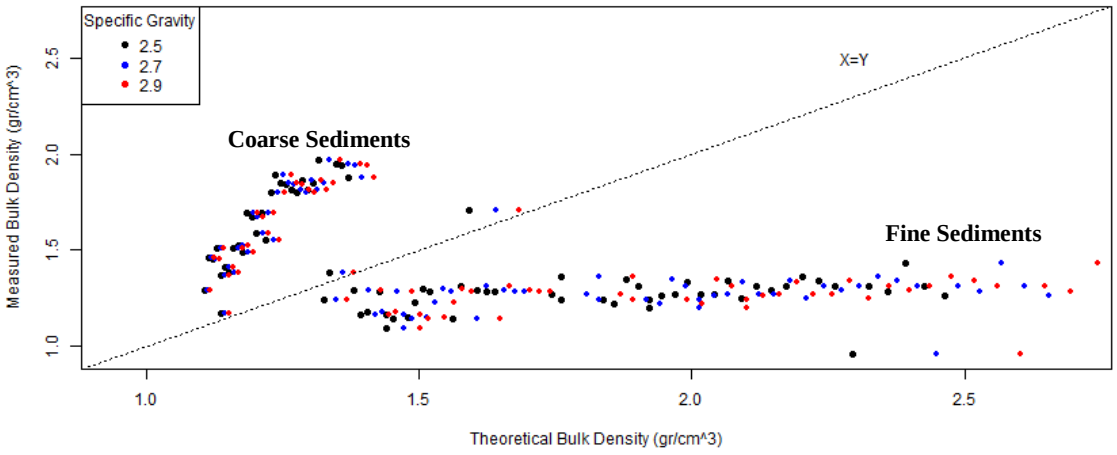

***Figure 3-8*. Comparison of bulk density measurements of this study with theoretical values calculated based on three assumptions for specific gravity (2.5, 2.7, and 2.9) – The samples are assumed to be saturated**

In this study, in order to avoid the inaccuracies that could have resulted from the saturation assumption, the bulk density of each sample was determined by two other methods to find a reliable average value. The first method is based on measuring the sample's volume and weight as follows:

$$\boldsymbol{\rho_{bulk} = \frac{W_{ns}}{v}}$$

ρ_{bulk}: Sediment bulk density

W_{ns}: non − submerged weight of the sample

v : volume of the sample v = Sample area × sample thickness

The second method calculates the bulk density based on the difference between the submerged and non-submerged weights of the sample as presented here:

$$\mathbf{W_{ns} = W_s \times \left(\frac{\rho_{bulk}}{\rho_{bulk} - 1}\right)} \quad \mathbf{\rho_{bulk} = \frac{W_s \times \left(\frac{\rho_{bulk}}{\rho_{bulk} - 1}\right)}{v}} \rightarrow \mathbf{1 = \frac{W_s \times \left(\frac{1}{\rho_{bulk} - 1}\right)}{v}}$$

$$\rho_{bulk} = 1 + \frac{W_s}{v}$$

W_s: submerged weight of the sample

The results of the bulk density measurements in this study are presented in Figure 4-4. Figure 3-9 compares the bulk density measurements of this study with theoretical values calculated based on specific gravity measurements with the assumption that the samples are saturated. According to this figure, the theoretical method significantly underestimates the bulk density of fine sediments and overestimates the bulk density of coarse sediments.

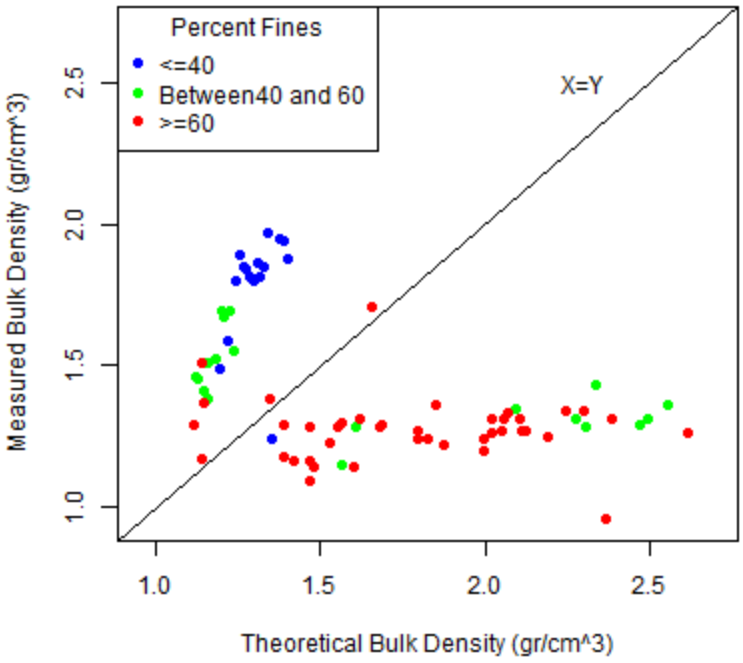

***Figure 3-9*. Comparison of bulk density measurements of this study with theoretical values calculated based on the specific gravity and water content measurements made in this study – The samples are assumed to be saturated**

3.4.2. Water Content

ASTM D-2216 was the test procedure used for the determination of the water content in this study. The samples obtained for water content tests were taken from each of the rings and dried for 24 hours at a temperature of $94^{\circ}C$. The same water content value was used for both samples if two erosion samples were obtained from one ring.

3.4.3. Organic Content

The loss-on-ignition method was used for the determination of organic content. The residual material from the water content tests was burned for 24 hours at $600^{\circ}C$ to determine the organic content. Dyer (1998) set five percent as a rough division between the low and high organic contents in natural sediments. He also suggested that sediments with low organic content (with an olive grey to blue grey color) are generally aerobic while those with high organic content (with a typically black color) are anaerobic.

3.4.4. Atterberg Limits

Atterberg limit tests were carried out on mixed samples taken from the whole core according to the ASTM D-4318 procedure. These tests were conducted only on samples with fine percentages greater than 60 percent.

3.4.5. Particle Size Analysis

The ASTM D-422 procedure was used for particle size analysis. As the quantity of the remaining material within each ring was not sufficient to run individual particle size analysis tests per ring, equal portions of sediment were taken from each ring and mixed to represent the whole core. After drying the sediments, the wet screening procedure was used to determine the particle size distribution.

3.4.6 Specific Gravity

The specific gravity determination tests were performed according to the ASTM D-854 procedure. Figure 3-10 shows two of the samples prepared for the specific gravity test and Figure 4-3 presents the results for Newark Bay samples.

***Figure 3-10*. Samples of granular (left) and cohesive (right) sediments prepared for the specific gravity test**

3.5. Erosion Tests

Erosion rate, as a stochastic variable, was assumed to be a function of flow characteristics and sediments' physical parameters. The average flow velocity in the test channel was measured to represent the flow characteristics, and sediment index properties of sediments (bulk density, water and organic content, specific gravity, grain size distribution and Atterberg limits) were measured as physical factors possibly affecting sediment erosion. This section provides information on the device and procedure used for conducting erosion tests in this study.

3.5.1. Ex-Situ Erosion Testing Machine (ESETM)

The Ex-Situ Erosion Testing Machine (Figure 3-11 and Figure 3-12) was originally developed by Prechtl Laboratories (Austria) and refined by researchers in J. Sterling Jones Hydraulics Research Laboratory (at Turner-Fairbank Highway Research Center). This linear

flume was innovatively designed to apply state-of-the-art technology to directly measure shear and weight forces exerted on a sample of sediment in real time as well as to enhance the flow velocity profile in erosion tests. Compared to most other flumes and devices used for sediment erosion studies, ESETM was considered a major innovation that could help push the boundaries in experimental erosion studies.

As indicated in Figure 3-13, the dimensions of the test channel are 110x800x21 mm and the sediment probe has an internal diameter of 61 mm. The sample probe's elevation can be set by an internal elevator that has a full 30 mm range of vertical movement (Figure 3-14). The force sensor can measure shear stresses of up to 100 Pa. Vertical forces in the range of 0-1N can also be measured by the weight sensor, which is shown in (Figure 3-14).

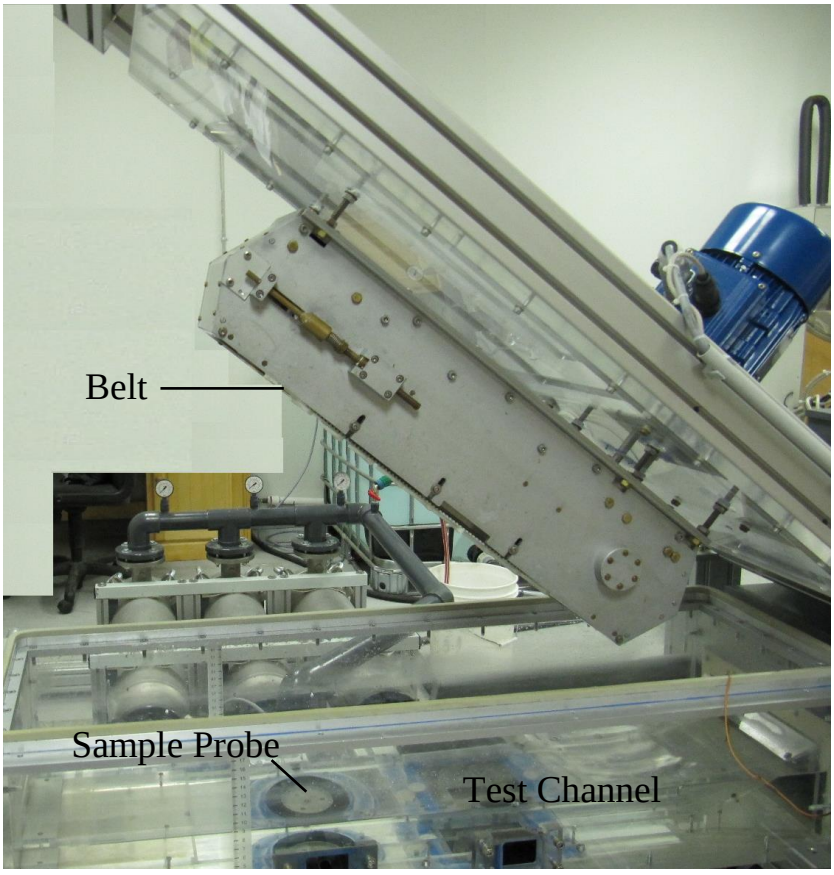

***Figure 3-11*. Side view of ESETM**

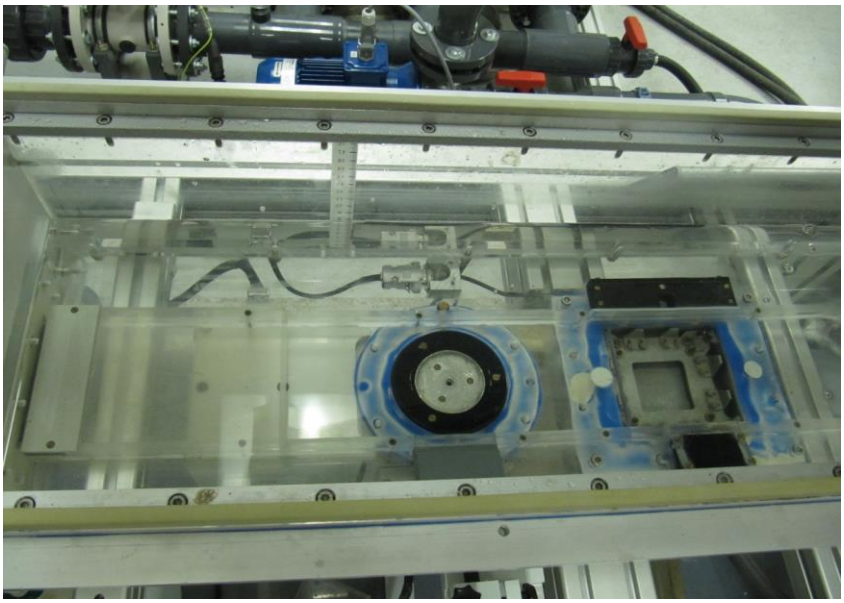

Figure 3-12. **Top view of ESETM**

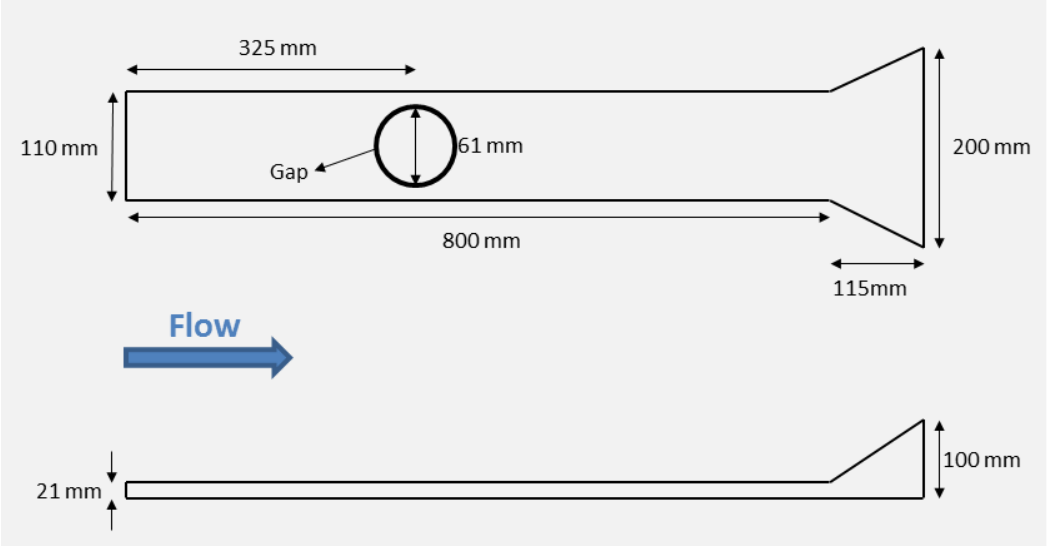

Figure 3-13. **Top and side views of the Ex-Situ Erosion Testing Machine (ESETM) testing duct**

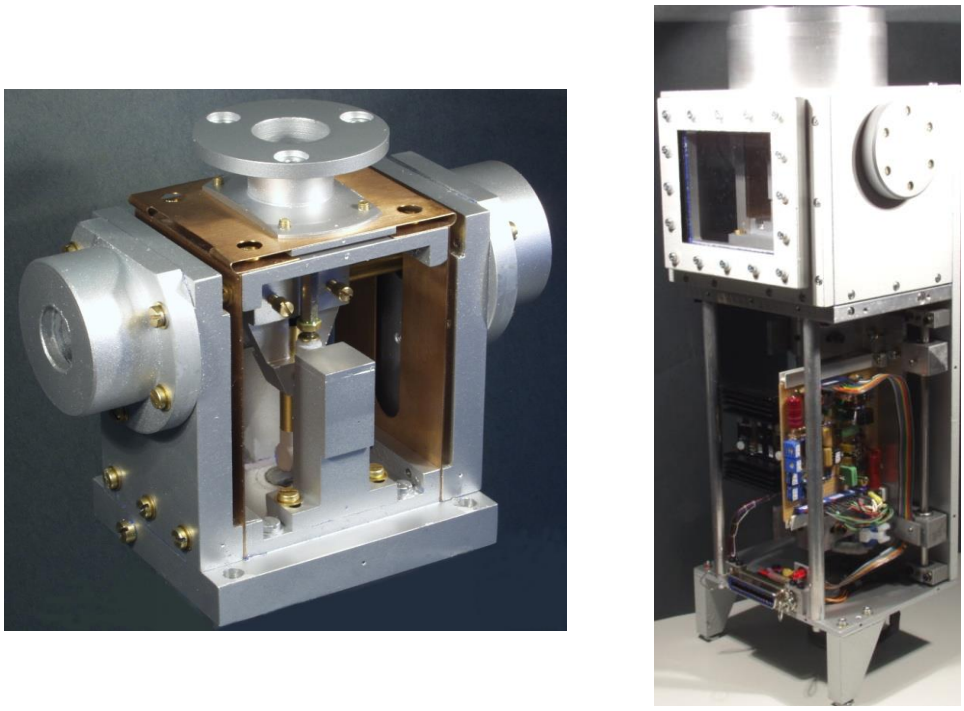

Figure 3-14. **The internal structure of ESTEM's force measurement sensors**

As ESETM was the second version of the only two available versions, a significant amount of time was spent on the calibration of the device and evaluating its functionalities. While the device was able to provide several force measurements, there were issues of reliability with three of the parts: the shear stress sensor, weight sensor, and belt. The following assessment of the device resulted in four main corrective actions: (1) The revolving belt, which was designed to simulate more realistic flow velocity profiles, produced unwanted errors in force measurement. Consequently, to reduce this error, the belt was replaced with a smooth PlexiGlass cover. (2) The shear stress measurements were disregarded. (3) Instead of using the measurements recorded by the weight sensor, a new methodology was designed to obtain weight measurements using a scale at the end of each test step. (4) Unconfined cohesive samples hindered the operation of the device due to the escape of material into the sensor. As a result, a ring with a sliding bottom plate was designed to confine cohesive sediment samples (Figure 3-15). This new design allowed the test

instructor to maintain the sediment surface level with the bed as much as possible. A brief explanation of the methodology used for the device assessment in addition to some major findings are presented in sections 3.5.1.1-3.5.1.3.

***Figure 3-15*. The ring and sliding bottom plate designed to confine the sediment sample**

3.5.1.1. Weight sensor assessment

Two tests were conducted to evaluate the accuracy and reliability of weight sensor measurements. In the first test, a standard ten-gram weight was placed on the plate attached to the weight sensor 24 times at predetermined spots as displayed in Figure 3-16. The entire procedure was repeated three times with the plate set at different elevations. The results presented in Figure 3-17 show a large spatial variance in the accuracy of the measured weight. The measured values ranged between 5 and 17 grams in this test and between 75 and 120 grams for the same test using a 100-gram weight. This could be explained by the torque created due to non-uniform loading on the plate that caused a swing in the central rod and the magnet attached to it. In conclusion, the high variation in weight measurements negatively impacts the ability to estimate the weight of sediments being eroded as samples do not erode uniformly during erosion tests.

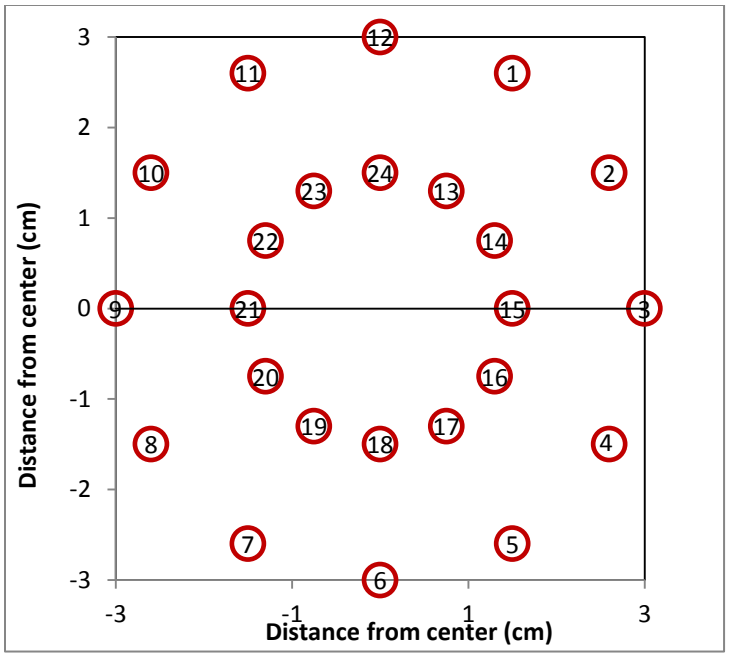

Figure 3-16. **Map of sample locations for spatial sensitivity analysis of ESETM**

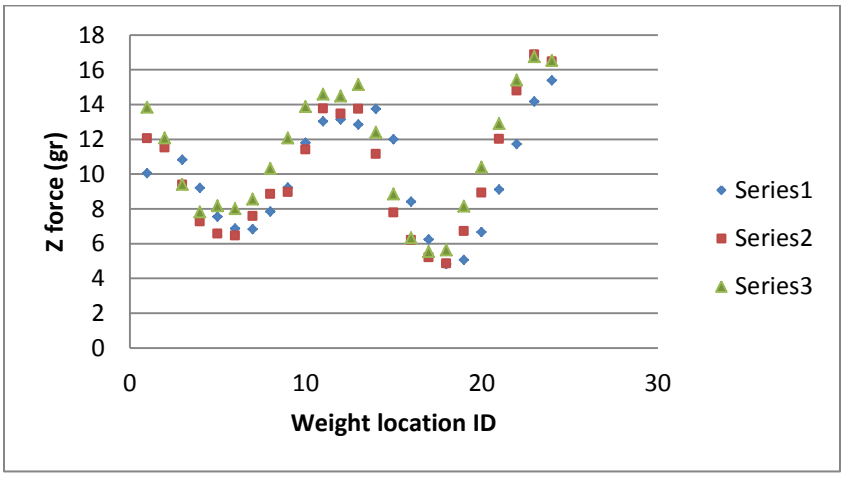

Figure 3-17. **Weight sensor measurements for a 10-gram weight located at different points on the sensor**

The second test to assess the weight sensor was designed to study the drift observed in signals generated by the sensor. This drift was temperature-independent and seemed to be a linear phenomenon caused by variable aging rates. For example, Figure 3-18 shows the signals

generated by the weight sensor during a two-hour test without any weight being actually placed on the plate. The sensor measured 5 grams after two hours, a very large weight compared to the expected amount of erosion during the 5-10 minute tests (Figure 3-19).

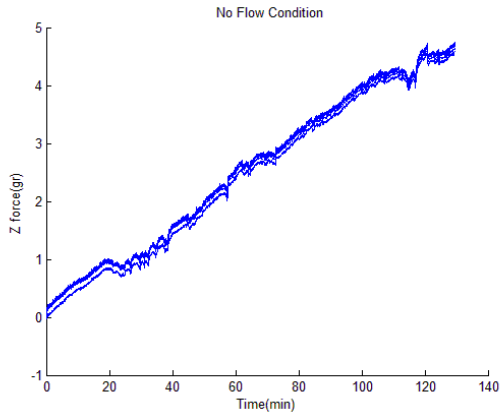

Figure 3-18. **Typical drift observed in the signals generated by the weight sensor**

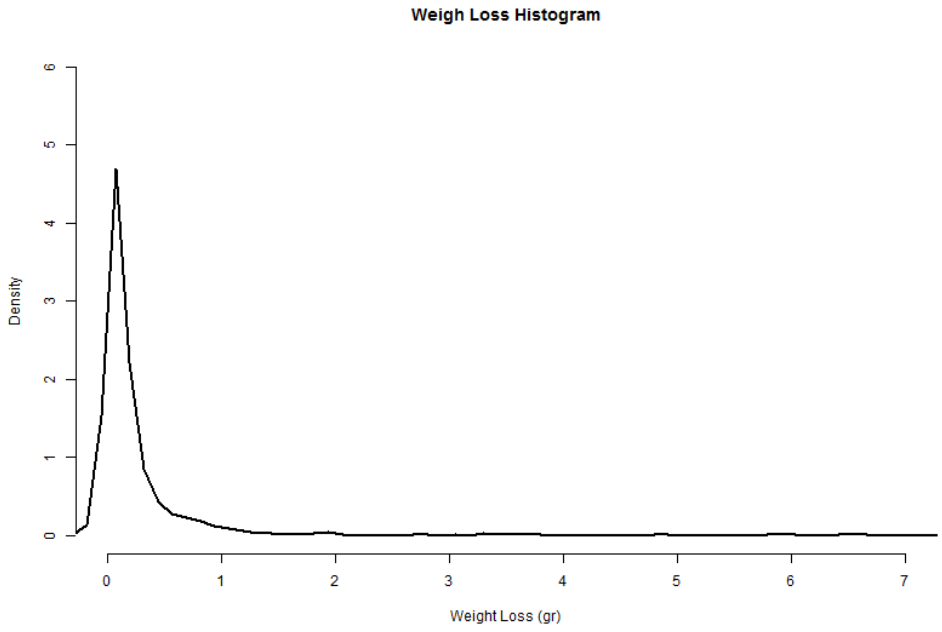

Figure 3-19. **Histogram of all the measured weight losses**

Figure 3-20 shows the weight measurements during a two-hour test on a manufactured sediment sample. While the sample lost eight grams during the test, the sensor detected only three grams of weight loss.

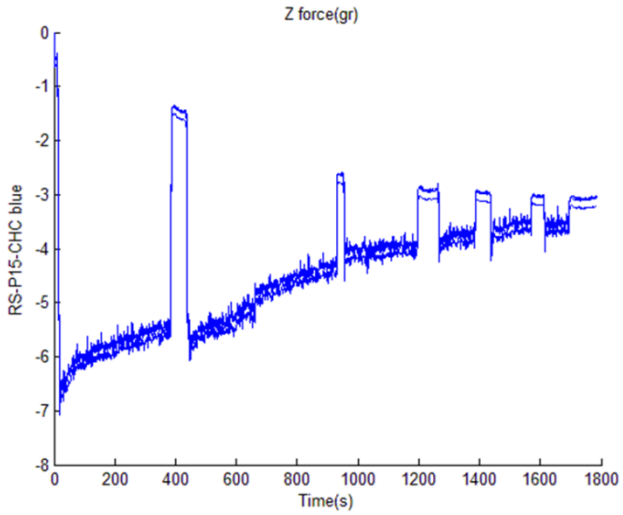

Figure 3-20. **Weight measurements for a typical erosion test on a manufactured sample**

3.5.1.2. Shear Stress Sensor Assessment

A test was designed to compare the measurements derived from the shear stress sensor with those available in the literature. Following the same methodology used by Briaud et al. (2001), an aluminum disk (Figure 3-21) was placed over the sensor probe (leveled with the channel's bed) to evaluate the measurements made by the shear stress sensor and the result was compared with two other methods used in the literature: (1) estimation based on pressure measurements taken before and after the sample as used in the Erosion Function Apparatus (Briaud et al., 2001); (2) calculation based on the average velocity in the duct using Prandtl's

universal law of friction., The shear stress measurements provided by the shear stress sensor for the aluminum disk (leveled with the channel's bed) fall in the range of other observations/calculations as illustrated in Figure 3-22.

Figure 3-21. **The flat aluminum disk used to create a smooth surface for device assessment**

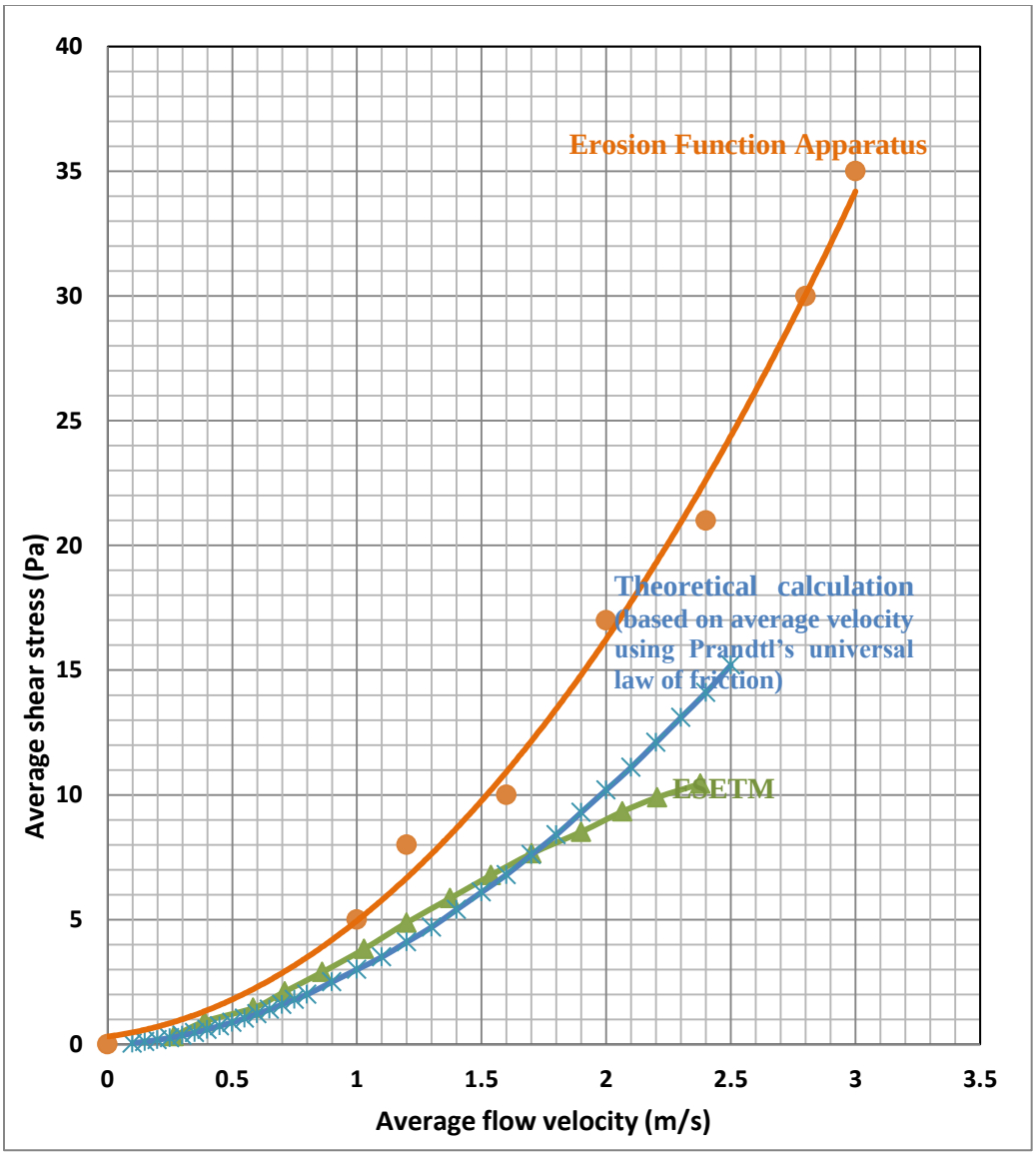

Figure 3-22. **Comparison of shear stress measurements obtained from three methods: (1) indirect measurements in Erosion Function Apparatus (Briaud et al. , 2001); (2) direct measurements in ESETM; (3) calculated based on Prandtl's universal law of friction**

The shear stress sensor seemed to work more accurately in very short tests (e.g. the calibration tests). However, this was not the case for longer tests. Figure 3-23 shows the sensor's measurements for the same sample tested under a no-flow condition for two hours (long test). While no physical forces were applied to the sensor during this test, it measured a shear stress as large as 0.5 Pa as a result of a non-linear drift.

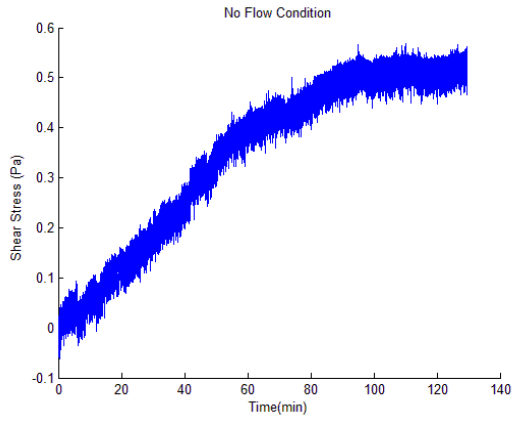

Figure 3-23. **A typical drift observed in the signals generated by the shear stress sensor**

Another anomaly observed in the shear stress data was the presence of negative shear stress measurements, (Figure 3-24) which suggested the presence of a force in the direction opposite to the flow. Further investigation revealed that uneven erosion (more erosion occurring at the edges of unconfined manufactured samples) might let the flow face into the aperture ring and cause this negative force as shown in Figure 3-25.

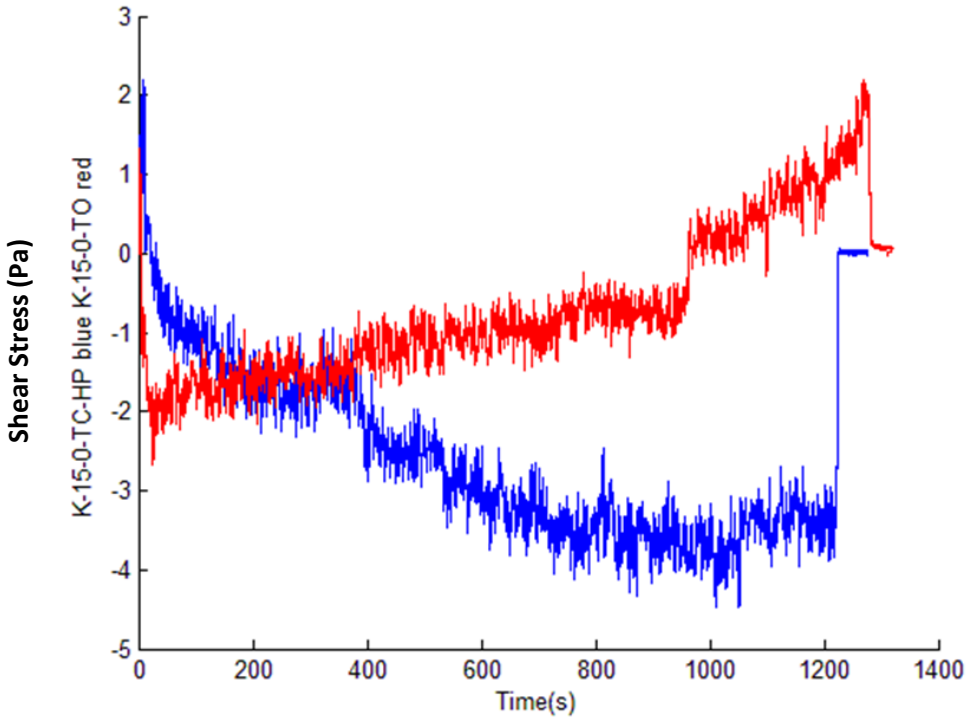

Figure 3-24. **Results of two typical erosion tests performed on manufactured kaolinite samples in which negative shear stress values were observed**

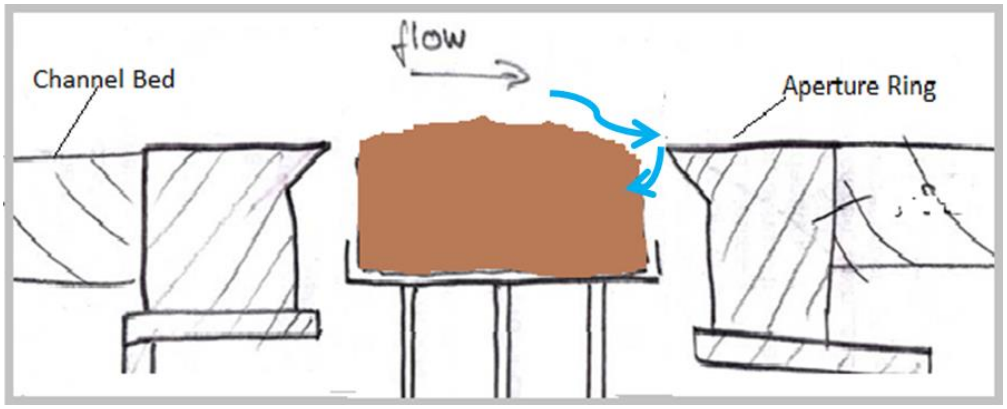

Figure 3-25. **Vertical cross-section of a sample surrounded by the aperture ring. Non-uniform erosion around the edges of the sample disturbs the flow and creates forces in the direction opposite to the flow**

One other point of concern regarding the accuracy of shear stress measurements is the shear forces caused by the form drag exerted on the walls of the sample when it is mildly extended into the flow as shown in Figure 3-26.

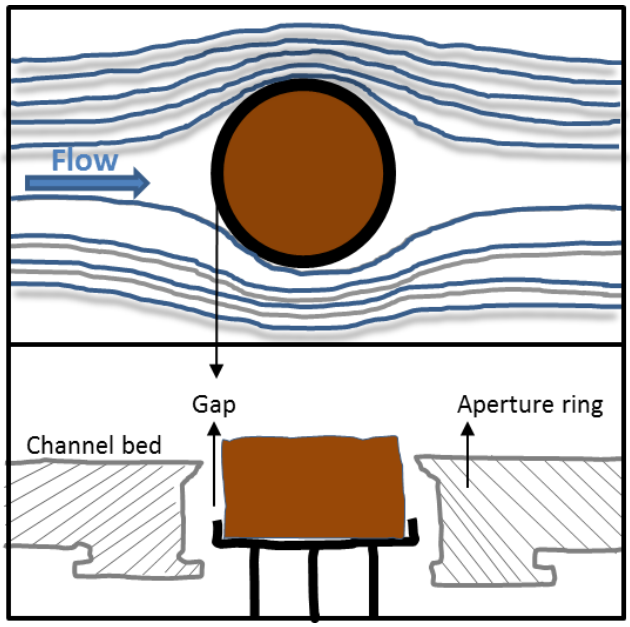

Figure 3-26. **Top view and vertical cross-section of the sample probe surrounded by the aperture ring**

To further study the effect of sample protrusion on shear stress measurements, a series of tests were conducted on the aluminum disk, the results of which are provided in Figure 3-27. In these tests, a rigid Plexiglas strip tool was used to level the disk with respect to the bottom of the channel very carefully. The elevator was then used to extrude the disk by different amounts to measure shear stress values for different flow velocities. As shown in Figure 3-28, protrusions smaller than 1 mm can create high variations in the shear stress values. This high variation occurs not only because of the sensor error but also because the shear stress sensor is measuring skin friction and form drag simultaneously.

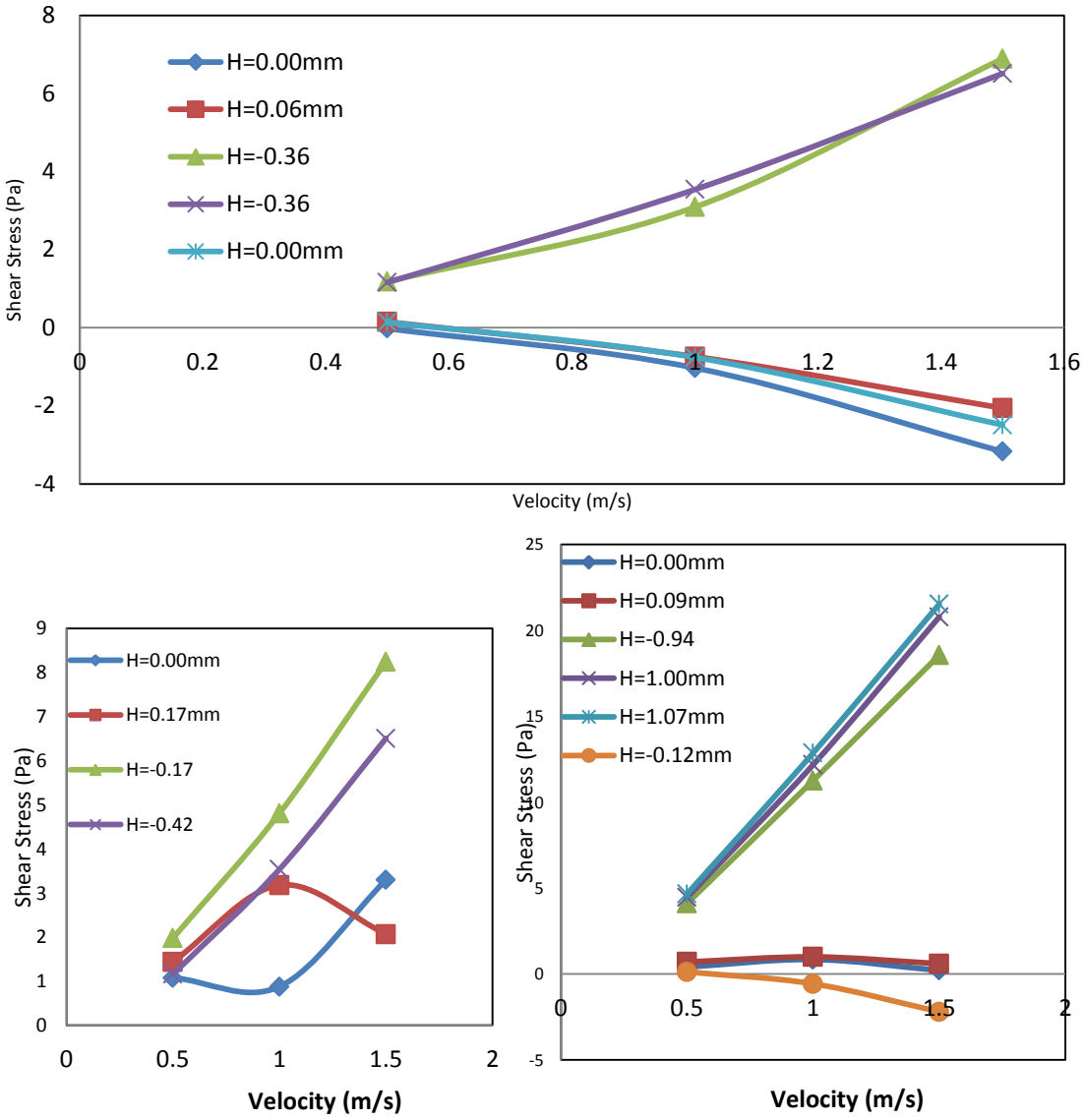

***Figure 3-27*. Reliability analysis of the shear stress sensor using the aluminum disk tested at different elevations (0.00 is the bed level)**

In order to evaluate the reliability of the shear stresses sensor more extensively, Anderson and Knight (2012) performed a computational fluid dynamic analysis to simulate the ESETM tests on the aluminum disk as conducted in this study. Figure 3-28 shows the velocity profile in the channel for an average flow velocity of 1m/s. Figure 3-29 compares the shear stress

measurements obtained from the shear sensor for a series of replicated tests on the aluminum disk (leveled with the bottom of the channel) with the results computed by the CFD model. To identify the impact of the instructor's judgment in leveling the disk, the same experiment was conducted five times, and the test was replicated twice in each of them. All the tests involved three steps with average velocities equal to 0.5, 1, and 1.5 m/s as can be seen in Figure 3-29.

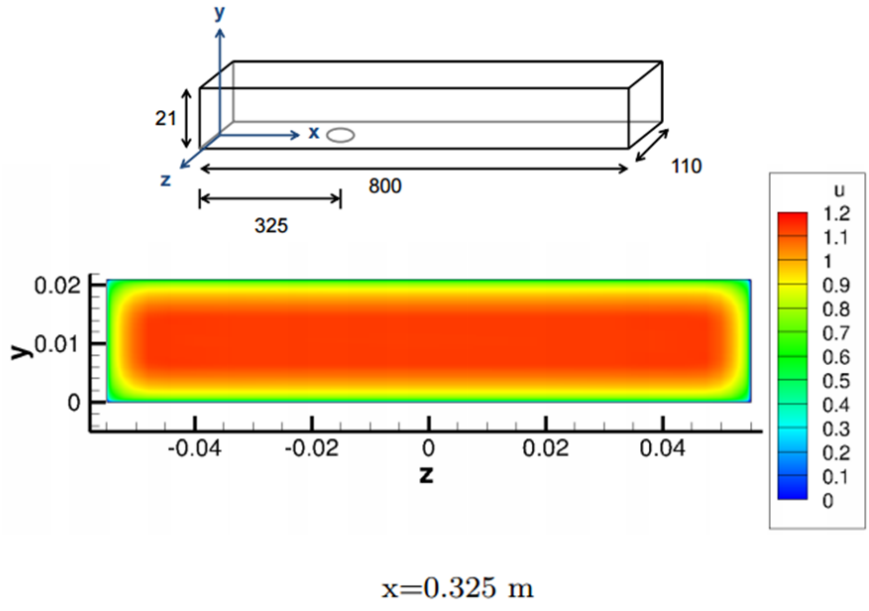

***Figure 3-28*. Velocity profile in ESETM's testing channel at the section passing through the center of the sample probe. The average velocity in the channel is 1 m/s. Calculations are based on computational fluid dynamic analysis conducted by Anderson and Knight (2012). Adapted from (Anderson and Knight, 2012).**

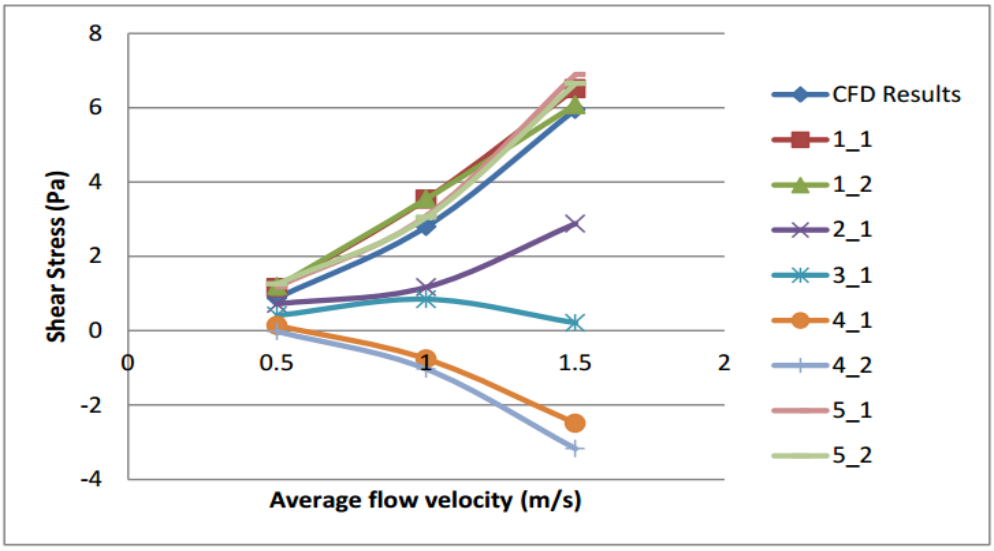

Figure 3-29. **Comparison of CFD computations with five experiments (each replicated twice) conducted on the aluminum disk leveled with the bed (0.00 mm protrusion)**

As can be seen in Figure 3-29, the fourth test resulted in negative shear stresses which could be attributed to a minimal degree of tilt in the disk which was practically unavoidable. Figure 3-30 and Figure 3-31 show the results of numerous runs of tests performed at velocities between 0.1 and 1.5 m/s for protrusions of 0.00 and 1.00 mm respectively. It can be concluded from all these tests that the measured shear stresses depended on how perfectly the disk was leveled (considering both tilt and elevation) and hence introduced a serious source of subjectivity into the tests. Consequently, it was decided to not depend on the shear stress values measured by the sensor and to use the average velocity instead as a measure of erosive forces.

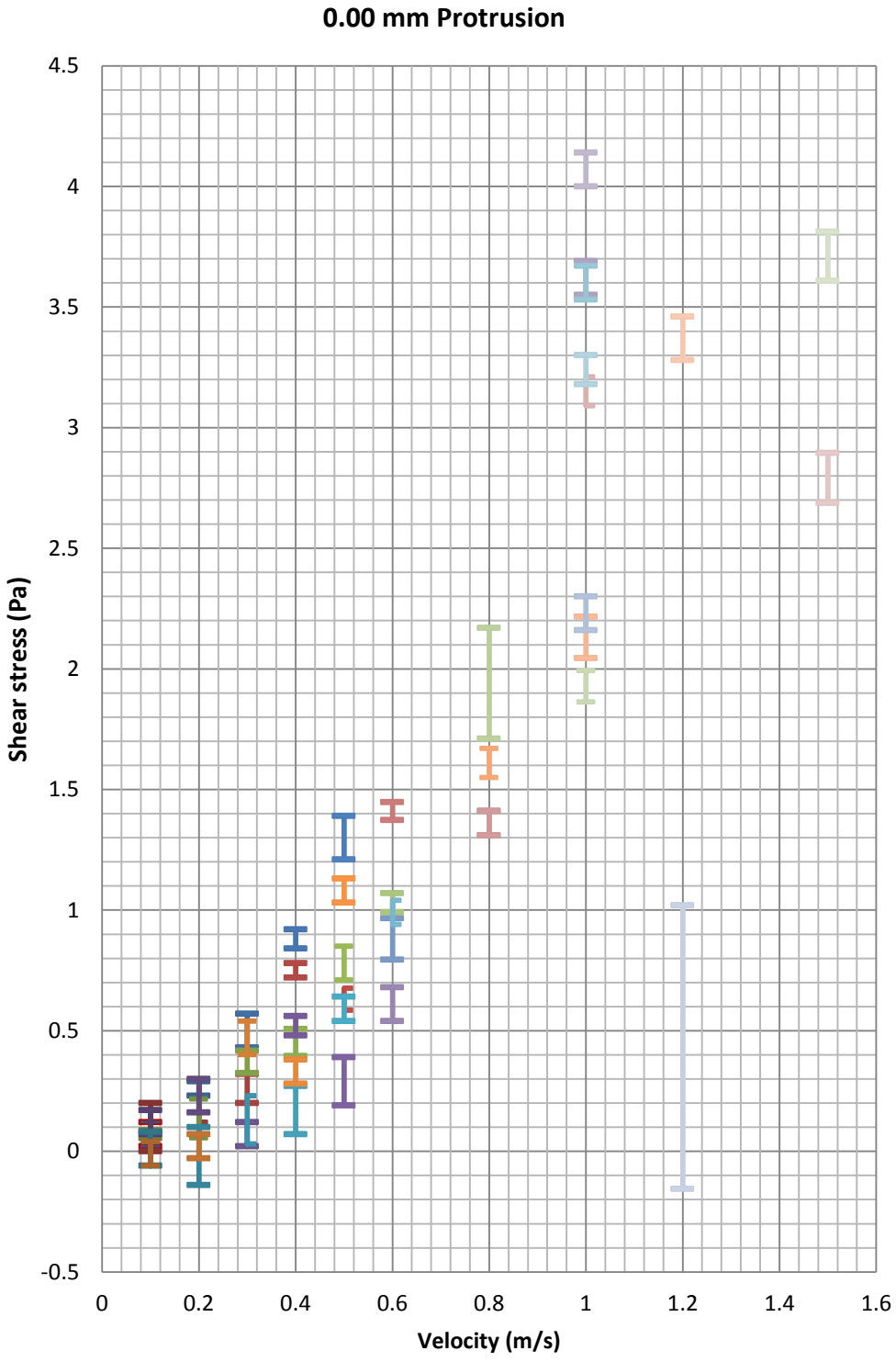

Figure 3-30. **Measured shear stresses for the aluminum disk leveled with the channel's bed (replications of the same test)**

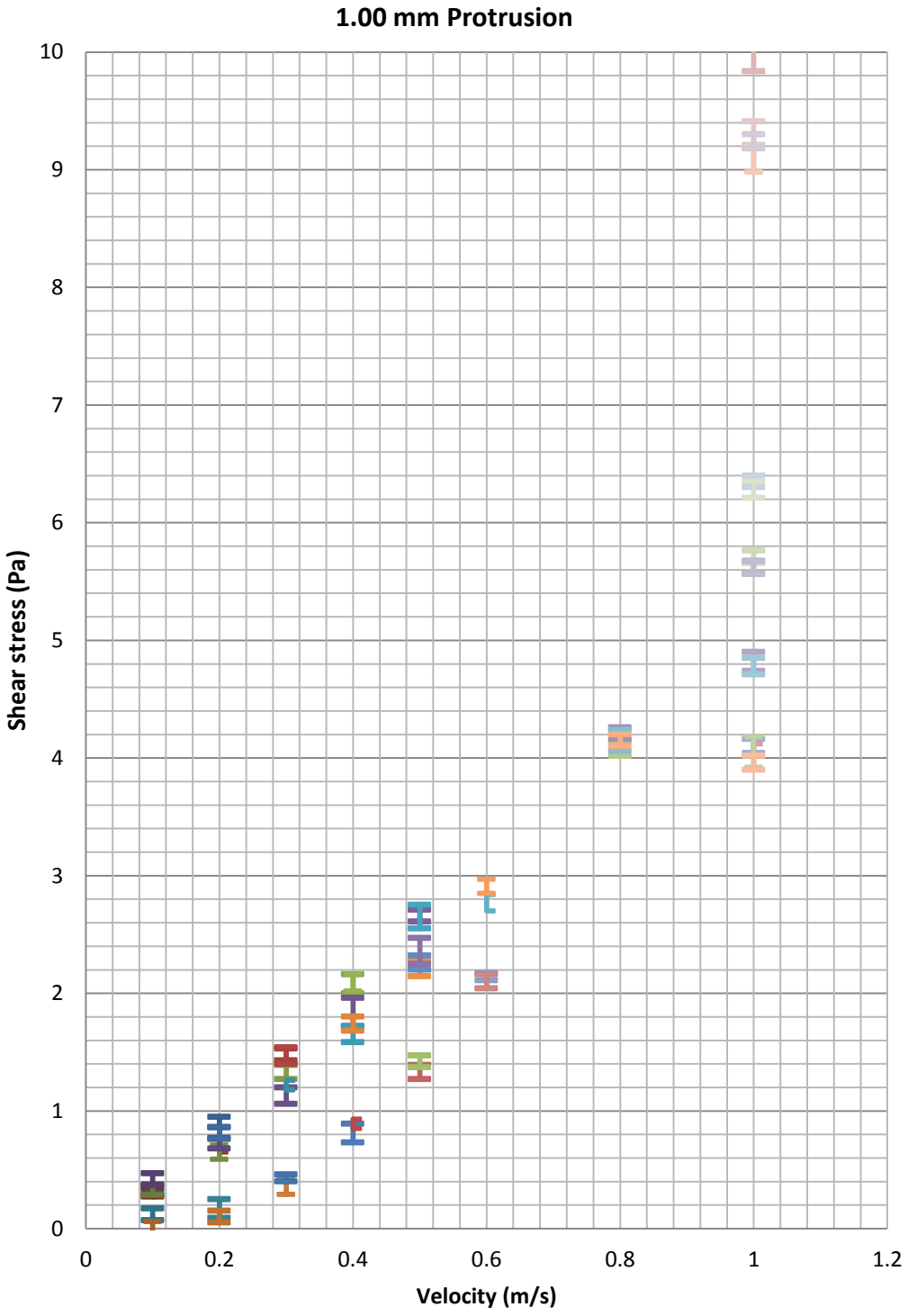

Figure 3-31. **Measured shear stress values on the aluminum disk extruded by 1.00 mm into the flow (replications of the same test)**

Figure 3-32 compares the average shear stress values measured by the device with the theoretical shear stress values calculated based on Prandtl's universal law of friction. It is obvious from this figure that the measured shear stress values were significantly higher from the theoretical values which can be partly attributed to the inclusion of form drags.

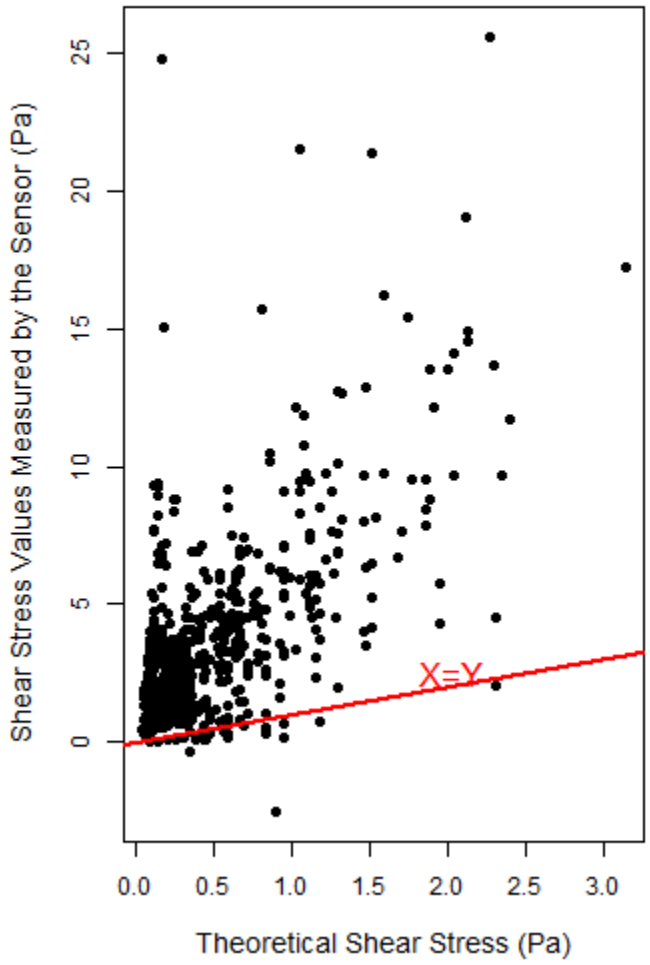

Figure 3-32. **Comparison of shear stress values measured by the sensor with theoretical values calculated based on average velocity**

3.5.1.3. Belt Assessment

The revolving belt (Figure 3-11) was originally designed to innovatively modify the velocity profile in the testing channel (Figure 3-28) to make it more similar to natural flows (Figure 3-33).

Figure *3-34* shows the velocity profile measured in the channel through 2-dimensional particle image velocimetry (PIV).

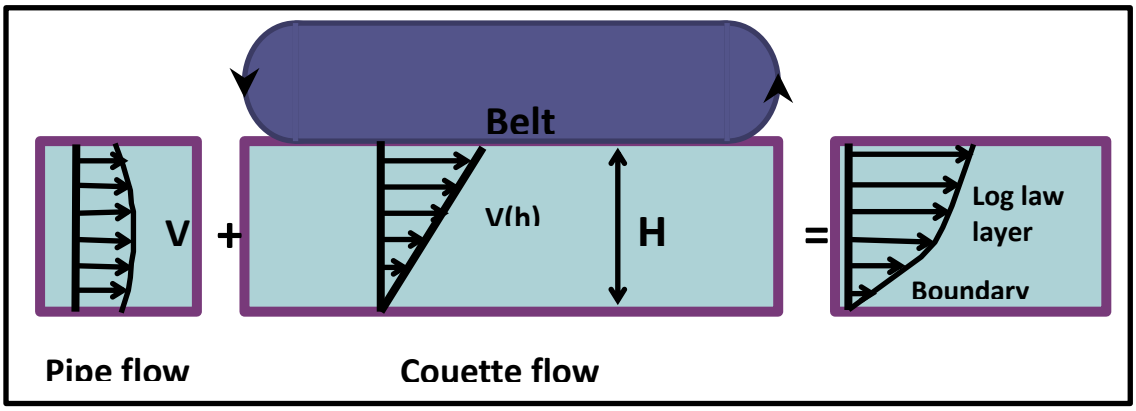

***Figure 3-33*. The Couette flow created by the belt can be combined with the pipe flow profile to create a more realistic velocity profile**

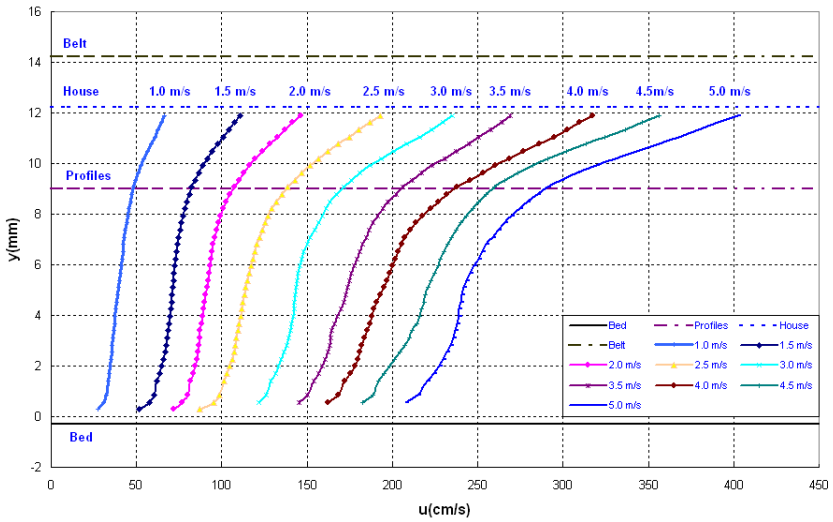

Figure 3-34. **Velocity profile in ESETM's testing duct measured through 2-dimensional particle image velocimetry in the J. Sterling Jones Hydraulics Research Laboratory at the Turner-Fairbank Highway Research Center (used with permission).**

Closer assessment of the belt system revealed that it introduced some factors into the tests which were difficult to control. For example, Figure 3-35 compares the results of two sets of experiments on the aluminum disk. In the first experiment (red points) the channel was covered by the belt while in the second experiment (green points), the channel was covered by a smooth plate. As can be seen in this figure, in the presence of the belt (even if it is not working) the measured shear stress values increase significantly which can be attributed to the dents that were responsible for modifying the flow profile. For each of the experiments, shear stress values were measured under different velocities for protrusion levels of 0.00 and 1.00 mm (indicated by different shapes). In addition to the impact on the shear stress values, the belt also introduced some noise into the shear stress and weight sensor signals when in operation.

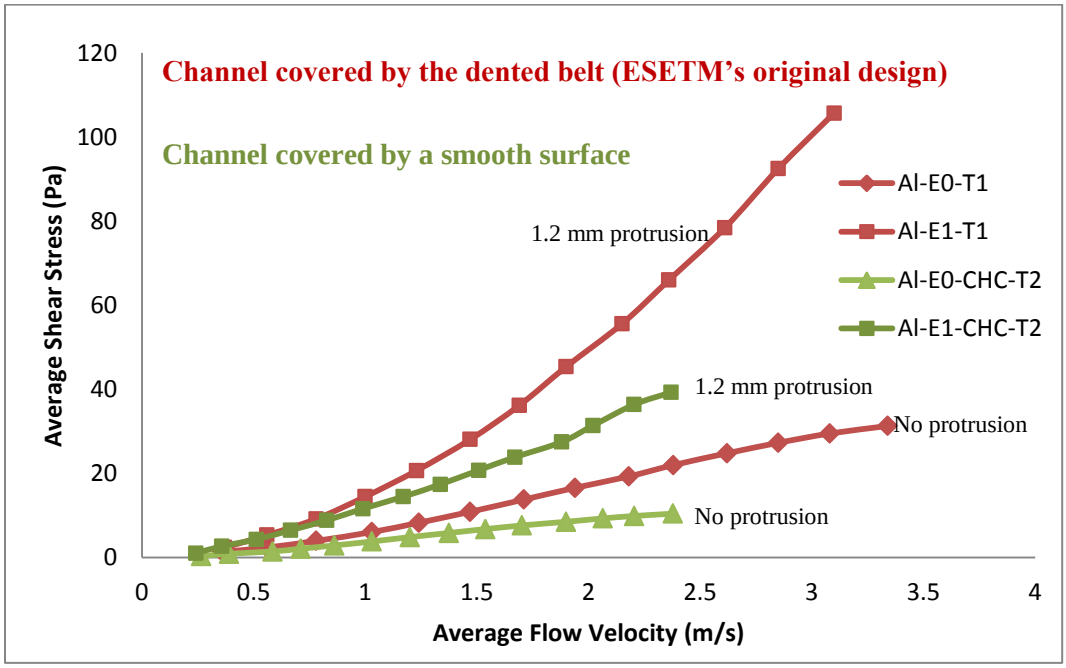

***Figure 3-35*. Impact of the roughness of channel cover on the measured shear stress values for the aluminum disk (smooth surface) at different levels of protrusion**

3.5.2. Probabilistic Analysis

3.5.2.1. Introduction

One of the main conclusions of the literature review for this study was that the results of erosion rate tests are highly dependent on the design of the experiment (sequence or arrangement[3] of the shear stress levels applied to the sediment, and duration[4] of each step) as well as the interpretation method.

Aberle et al. (2004) categorized the various interpretation approaches for the evaluation of erosion rates in the literature as: (1) the initial peak erosion rate after application of a new bed shear stress, (2) the rate of erosion after some initial response has passed, (3) the average erosion rate over the entire test interval, and (4) the inclusion of a time factor in the erosion rate prediction equations. These sources of uncertainty and their consequences have made it very difficult to compare different studies.

In order to mitigate the above concerns, it was decided to define this practical problem and explore its consequences prior to designing the erosion experiments for the current study. Therefore, a methodology was developed (section 3.5.2.2) for analytical interpretation of erosion test results. This method, which is based on the probabilistic modeling of erosion, applies an optimization technique to solve for the model's parameters probabilistically. The algorithm developed for this method is presented in section 3.5.2.3 and is followed by the results and conclusions in sections 2.5.2.3 and 2.5.2.4 respectively.

---

[3] For example, in Figure 2-20, if the third step of the test has a shear stress level that is very close to the stress level in the second step (or even equal to it), the observations in the third step will follow the pattern of points in the second step, resulting in a lower average erosion rate for the same shear stress level.

[4] For example, in Figure 2-20, If the third step of the test continues for longer than 20 minutes, a smaller peak value will be observed for the erosion rate at the beginning of the fourth step because less material will be available to erode at this stage.

3.5.2.2. Analysis Framework

In this section, an analysis framework has been developed and used to reanalyze the datasets published by different researchers. This approach is proved to be capable of generating results that are comparable to empirical data from different studies.

Van Prooijen and Winterwerp (2010) classified a bed of sediment according to critical shear stress to take the time dependency of erosion rate into account. Similarly in this study, the portion of cohesive sediment eroded during each erosion test (the top layer of sediment with thickness h) was assumed to consist of an array of n different material clusters (Figure 3-36). However, particles or flocs in each cluster are taken to have similar erosion behavior. An average probability of erosion is assigned to each of these clusters for all stress (or velocity) levels to which the sediment is exposed for a specific duration.

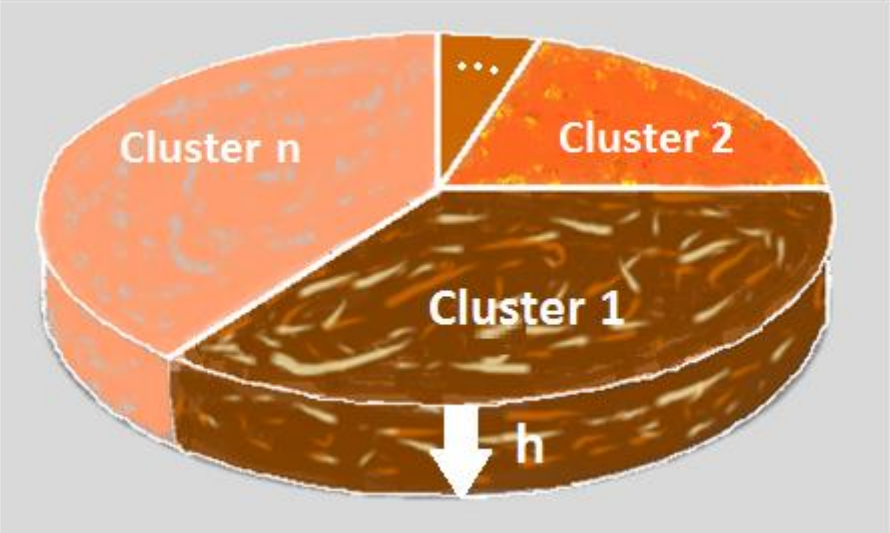

Figure 3-36. **Surface sediment partitioned into clusters with similar erosion behavior**

The probability matrix P is defined as

$$\boldsymbol{P} = \begin{bmatrix} \boldsymbol{p_{1,1}} & \cdots & \boldsymbol{p_{1,n}} \\ \vdots & \ddots & \vdots \\ \boldsymbol{p_{m,1}} & \cdots & \boldsymbol{p_{m,n}} \end{bmatrix}$$

where p_{ij} is the probability of a particle in cluster j being eroded during the i_{th}step of the test. If any two test steps a and b in this matrix have similar shear stress or velocity levels, then rows a and b in this matrix will be equivalent.

The vector S consists of velocity or shear stress levels at the i_{th} step of the test such that $s_i \in \{1,2,\dots,L\}$

$$\boldsymbol{S} = \begin{bmatrix} \boldsymbol{s_1} \\ \vdots \\ \boldsymbol{s_m} \end{bmatrix}$$

For example, if the sediment is eroded under shear stress (or velocity) levels (1, 2, 3) for (20,10,30) minutes successively, and the probabilities in matrix P are set for a 5-minute long exposure, then $S = [1,1,1,1,2,2,3,3,3,3,3,3]$. The length of matrix S is assumed to be m.

The ratio matrix R consists of r_{ij} entities equal to the proportion of particles in cluster j at the beginning of step i of the test. Hence, the sum of the entities in each row is equal to 1. The first row of this matrix includes the initial weight proportion of particles in each of the available **n** clusters and should be provided as an input to the code. The values in the remaining rows are unknown and are calculated within the suggested framework.

$$\boldsymbol{R} = \begin{bmatrix} \boldsymbol{r_{1,1}} & \cdots & \boldsymbol{r_{1,n}} \\ \vdots & \ddots & \vdots \\ \boldsymbol{r_{m+1,1}} & \cdots & \boldsymbol{r_{m+1,n}} \end{bmatrix}$$

Available material vector, AM, is a vector of length $m + 1$ with entities am_i equal to the material available for erosion at the beginning of the i_{th}step of the test. am_1 represents the total material eroded during the whole test and should be provided as an input to the program.

$$\mathrm{AM} = \begin{bmatrix} \mathrm{am}_1 \\ \vdots \\ \mathrm{am}_{\mathrm{m+1}} \end{bmatrix}$$

Cluster erosion matrix, CE, consists of entities ce_{ij} equal to the material eroded from cluster j during step $i - 1$. All the first-row entities are equal to zero.

$$\mathrm{CE} = \begin{bmatrix} \mathrm{ce}_{1,1} & \cdots & \mathrm{ce}_{1,\mathrm{n}} \\ \vdots & \ddots & \vdots \\ \mathrm{ce}_{\mathrm{m}+1,1} & \cdots & \mathrm{ce}_{\mathrm{m}+1,\mathrm{n}} \end{bmatrix}$$

Eroded material vector, EM, has entities em_i equal to the total material (from all clusters) eroded during the $i-1^{th}$ step. As no material is eroded before the first step of the test, $em_1 = 0$.

$$E\mathrm{M} = \begin{bmatrix} \mathrm{em}_1 \\ \vdots \\ \mathrm{em}_{\mathrm{m}+1} \end{bmatrix}$$

3.5.2.3. Algorithm

The following algorithm is used to calculate the unknown variables:

Require: $\mathrm{P}, \mathrm{R}_{1,:}, \mathrm{am}_1$

For i in 1: m

For j in 1: n

$\mathrm{CE}_{\mathrm{i}+1,\mathrm{j}} = \mathrm{P}_{\mathrm{i,j}}.\mathrm{R}_{\mathrm{i,j}}.\mathrm{AM}_{\mathrm{i}}$

End For

$\mathrm{EM}_{\mathrm{i}+1} = \sum \mathrm{CE}_{\mathrm{i}+1,\mathrm{j}}$

$\mathrm{AM}_{\mathrm{i}+1} = \mathrm{AM}_{\mathrm{i}} - \mathrm{EM}_{\mathrm{i}+1}$

For j in 1: n

$\mathrm{R}_{\mathrm{i}+1,\mathrm{j}} = \dfrac{(\mathrm{R}_{\mathrm{ij}}.\mathrm{AM}_{\mathrm{i}}.(1-\mathrm{P}_{\mathrm{k,j}}))}{\mathrm{AM}_{\mathrm{i}+1}}$

End For

End For

All the entities in the probability matrix, P, and the initial weight proportion values in the first row of the ratio matrix, R, are considered as entities of the unknown variable matrix x. An optimization problem is defined to minimize the difference between the observed values and the erosion rates predicted by the model.

$$\mathbf{x} = \begin{pmatrix} \mathbf{P_{1,1}} \\ \vdots \\ \mathbf{P_{m,n}} \\ \mathbf{r_{1,1}} \\ \vdots \\ \mathbf{r_{1,n}} \end{pmatrix}$$

The minimization is subjected to the following constraints:

1. All the variables in the x vector should be in the $[0,1]$ range as they are either probability or weight ratio values.

2. $\forall i \in [1, m]\ \&\ \forall j \in [2, n]\ \ P_{i,j-1} \leq P_{i,j}$

3. If the shear stress level in step i is larger than in step j, then $\forall k \in [1, n]\ \ P_{j,k} \leq P_{i,k}$

4. $\sum_{i=1:n} r_{1,i} = 1$

$$\min_{x} f(x) \text{such that} \begin{cases} Ax \leq b & \text{Linear inequality constraints} \\ lb \leq x \leq ub & \text{Upper and lower bound constraints} \end{cases}$$

3.5.2.4. Results

The proposed methodology was applied to data published by Zerik, Krishnappan, Germaine, and Madsen (1998), Parchure and Mehta (1985), and Sanford and Maa (2001). Figure 3-37 depicts the results obtained by the proposed probabilistic framework compared to the data observed by Zerik et al., (1998). The set of parameters used for simulation 1 are presented in Table 3-1. Simulation 2 uses the same parameters but applies a different arrangement of shear stress levels starting at the highest level. It is interesting to note that the weight of material eroded in the first step in simulation 2 is greater than the weight of the total material eroded in all nine steps with the same shear stress level (level 4) in simulation 1. This can be attributed to the fact that in the first simulation, the original weight proportion of clusters with different erosion resistances is altered through 16 testing steps at shear stress levels 1 to 3 before reaching shear stress level 4. This example proves that simple parameterization of erosion behavior (regardless

of shear stress history) does not have the capacity to describe the temporal changes in the erosion resistance of the remaining flocs.

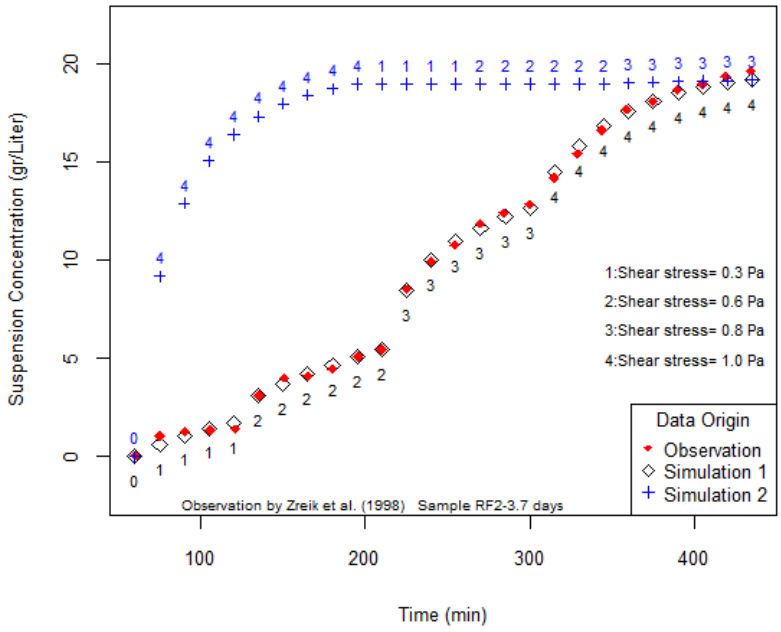

***Figure 3-37*. Comparison of data from Zerik, Krishnappan, Germaine, and Madsen, (1998) with data predicted by the model**

Table 3-1 Parameters used in simulations 1 and 2 presented in Figure 3-37 (15-minute-long test steps)

	Material cluster		
	I	II	III
	Weight proportion		
	0.13	0.36	0.51
Level	**Probability of erosion**		
1	0.239	0.000	0.000
2	0.962	0.084	0.000
3	0.964	0.580	0.060
4	0.978	0.580	0.259

Figure 3-38 illustrates the total and cumulative erosion at each step in simulation 1 broken up by cluster at each step. Figure 3-39 compares the data observed by Zreik et al. (1998) (for a sample of the same material as in Figure 3-37 but with different consolidation duration) with the predictions of three different sets of probabilistic parameters (all resulting from the optimization problem solved). As the figure shows, all three simulations are capable of capturing the main pattern in the observed data. Thus, access to data obtained by different arrangements of shear stress levels can be helpful in choosing the best model among different possible options.

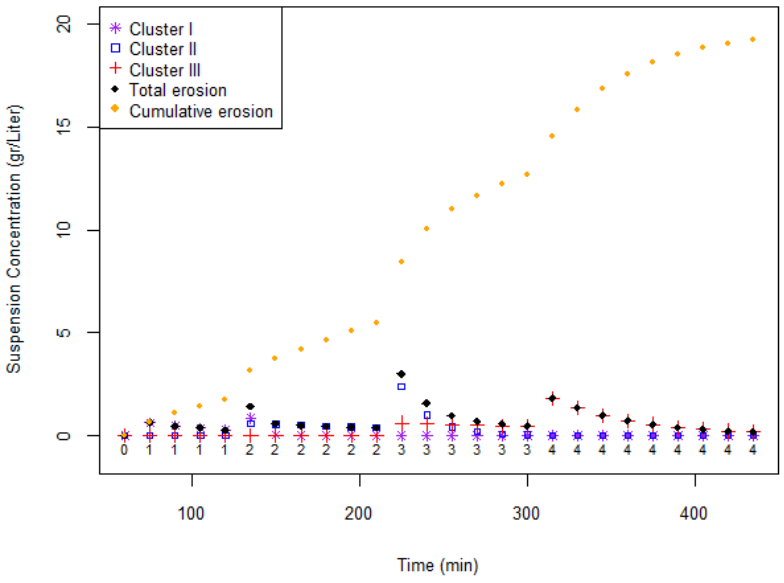

***Figure 3-38*. Breakup of erosion observed by Zerik et al. (1998) into different clusters at shear stress levels 1-4**

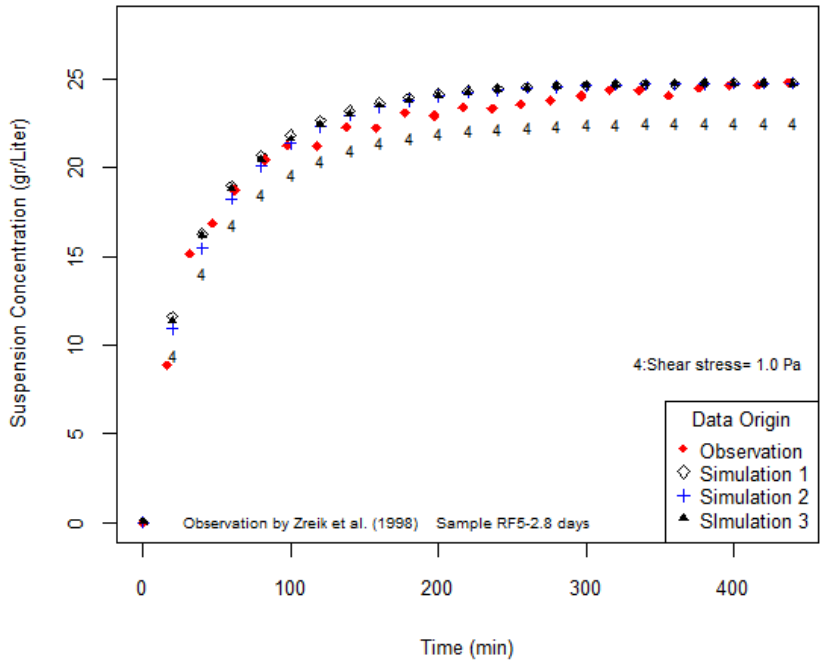

Figure 3-39. **Comparison of data observed by Zreik et al. (1998) with predictions of models calibrated based on data presented in Figure 3-37**

Figure 3-40 compares the simulated results with the data measured by Parchure and Mehta (1985). In simulations 1 and 2, the material is assumed to be composed of three and four clusters respectively. The derived parameters are provided in Table A. 4.

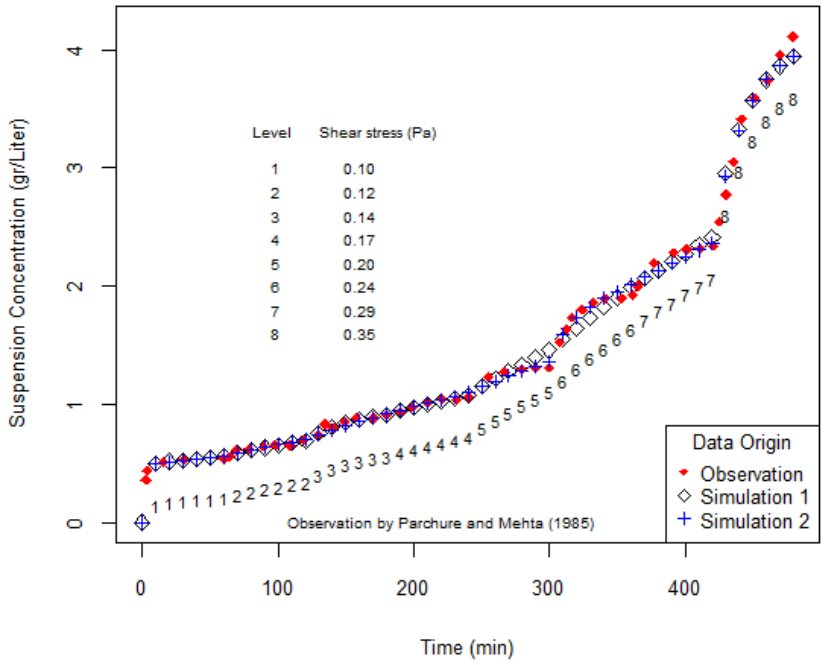

***Figure 3-40*. Comparison of data observed by Parchure and Mehta (1984) with the model predictions**

Figure 3-41 compares the results of two probabilistic simulations with the data published by Sanford and Maa (2001). In simulations 1 and 2, the material is assumed to be composed of three and four clusters respectively. The derived parameters are summarized in Table A. 5.

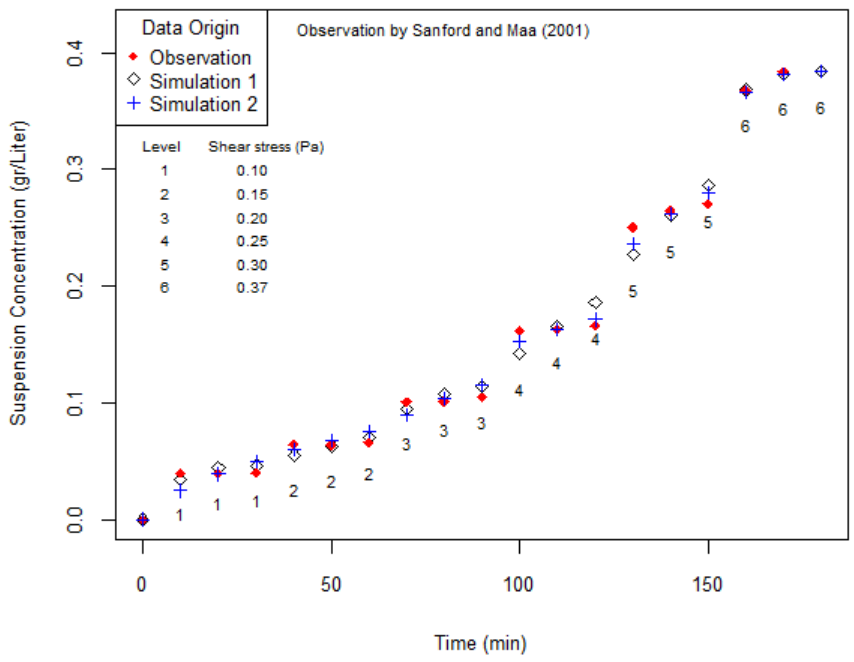

Figure 3-41. **Comparison of data observed by Sanford and Maa (2001) with the probabilistic model predictions**

3.5.2.5. Conclusion and Discussion

1. The analysis framework developed in section 3.5.2.2 solved an inverse problem to convert erosion rate data to information about erosion probability of different material clusters assumed to constitute the studied sediment. This problem is ill-posed, as typical for inverse problems and has no unique optimal solution.
2. The great advantage of this approach is that the results obtained by this methodology are not dependent on any particular testing arrangement and can be used to make predictions for new arrangements of flow levels to which the material is exposed.
3. This framework also offers the opportunity to compare the results obtained by different devices by standardizing the analysis methodology.

4. The probabilistic analysis conducted in this section clearly indicated the significant impact of the design of erosion experiments – specifically the length and order of different shear stress levels applied to sediments – on experimental outcomes.
5. Ideally, it is best to run only one test on each sediment sample. However, as only one erosion rate per sample does not reveal much about the overall behavior of sediment at different shear stress levels, testing a sample under different shear stress levels is inevitable. The main conclusion of this section for the purpose of this study is that if the sample is tested for shorter periods at each shear stress level, the effect of shear stress history on the observed erosion rates will be lower. This is because less sediment will be eroded during each step, and hence the sediment will retain its original composition.
6. The probabilistic analysis clearly demonstrated that the validity of measurements decrease as more tests are conducted on one sample because of the impact of shear history. It can be concluded that for the purpose of this study, the number of shear stress steps to which a sample is exposed to should be limited to avoid unrealistic results.

3.5.3. Erosion Testing Methodology

The erosion tests conducted in this study exposed the samples to a sequence of increasing flow velocities, each of which were followed by a stage of no-flow for a few minutes. The tests were designed based on the conclusions derived in section 3.5.2.5.

In order to minimize the effect of sudden flow generation at the beginning of each test step, the pump power was programmed to increase at a low rate. The samples' submerged weights were measured during the no-flow intervals to determine the weight loss occurring in the preceding stage. The operator set the elevation of each sample (to be flushed with the channel bottom) at the beginning of each test cycle using the device's elevation control feature. Each test step lasted for 5, 10, or 15 minutes depending on the rate and extent of the observed surface disturbance. All the

tests were performed in the temperature range of $17 - 27^{\circ}C$ with a mean temperature of $21^{\circ}C$ and a standard deviation of $3^{\circ}C$. Table 3-2 and Table 3-3 summarize all the factors and parameters used for the erosion experiments. Figure 3-42 shows two of the samples taken from the Newark Bay after the erosion tests.

Figure 3-42. **Two Newark Bay samples after the erosion test**

Table 3-2. ***Summary of measurements made for erosion tests***

Quantity	Symbol	Unit	Definition	Measurement Method	Measurement Accuracy
Initial thickness	h_i	mm	Average thickness of the sample	Calipers	0.1
Initial weight	W_{i-air}	gr	Non-submerged weight of the sample (in air)	Digital scale	0.01
Submerged weight	W_s	gr	Submerged weight of the sample	Digital scale	0.01
Depth	d	mm	Sum of the thickness of all the above rings	Calipers	1
Age1	-	day	Number of days between field sampling and lab. sampling	Form 3 data	1
Age2	-	hour	Number of hours between sample preparation and testing	Form 3 data	0.5
Average flow velocity	V	cm/s	Average flow velocity in the channel	Magnetic flow meter flowmeter	1
Temperature	T	℃	Temperature of water during the tests	Thermometer	1
Step duration	-	min	Duration of each step of the erosion test	-	$1/60$
Weight loss	WL	gr	Sample's weight change during each step of the erosion test	-	0.01

Table 3-3. ***Summary of factors/properties measured for erosion tests***

Factors/Properties	Time
Initial thickness, Initial weight (in air), Initial submerged weight, Depth, Age	Determined before erosion experiments
Flow velocity, Submerged weight, Shear stress, Z force, Tank level, Temp, Step duration, Elevation	Measured during erosion experiments
Water content, Organic content, Particle size distribution, Specific gravity, Atterberg limits	Determined through complementary tests
Erosion rate, Theoretical shear stress, Bulk density, Void ratio, Weight loss	Calculated based on other measurements

Calculation of average velocity in the channel:

The mean velocity measured by the magnetic flow meter was corrected for the increase in the elevation of water occurring in the storage tank. The corrected mean velocity was calculated by subtracting the volume of water stored in the tank during each step from the total discharge into the channel.

$$\mathbf{V = V_{flowmeter} - \left(\frac{\frac{\Delta TL}{\Delta t} \times area_{tank}}{Duration \times area_{channel}}\right)}$$

$\frac{\Delta TL}{\Delta t}$: time gradient of the level of water in the tank

The following dimensions were used for the calculation of areas:

$area_{tank} = 0.573 \times 0.508 = 0.29108 m^2$

$area_{channel} = 0.11 \times 0.021 = 0.00231 m^2$

Erosion rate calculation:

The erosion rate was calculated as follows:

$$\mathbf{W_{ls} = W_{lu} - V_l \times \rho_{water}}$$

$$V_l = \frac{W_{lu}}{\rho_{sed}}$$

$$W_{ls} = W_{lu} - \frac{W_{lu}}{\rho_{sed}} = W_{lu} \times (\frac{\rho_{sed} - 1}{\rho_{sed}})$$

$$W_{lu} = W_{ls} \times (\frac{\rho_{sed}}{\rho_{sed} - 1})$$

W_{ls}: submerged weight loss

W_{lu}: non − submerged weight loss

V_l: volume of eroded sediment

ρ_{water}: water density

ρ_{sed}: sediment density

The non-submerged weight loss during each test step was used to calculate the erosion rate for that step which is defined as the mass of sediments (including liquid and solid phases) eroded from a surface of one square meter per hour.

$$\mathbf{ER}(\frac{\mathbf{gr}}{\mathbf{m^2.hour}}) = \frac{\frac{\mathbf{WL_{ns}\ (gr)}}{\mathbf{1 + \frac{w(\%)}{100}}}}{\mathbf{Sample\ area\ (m^2) \times Test\ duration\ (hour)}}$$

$$WL_{ns} = WL_s - V \times \rho_w$$

$$\text{Sample area} = \frac{\pi \times 0.061^2}{4} = 2.9224\text{e} - 3\ \text{m}^2$$

4. TEST RESULTS

The results of the tests for determination of index properties are presented in this section. More details are provided in Figure A. 6 - Figure A. 27 and Appendix B includes the data obtained from erosion tests.

4.1. Index Properties

Table 4-1 summarizes all the index properties measured for tested samples.

Table 4-1. ***Summary of measured index properties***

Quantity	Symbol	Unit	Measurement Method
Water content	W	%	ASTM D-2216
Organic content	O	%	Loss on ignition method
Particle size distribution	-	-	ASTM D-422
Specific gravity	G_s	-	ASTM D-854
Atterberg limits	PL,LL	%	ASTM D-4318
Bulk density	ρ_{bulk}	gr/cm^3	Volumetric measurements

In the case of the Newark Bay, samples from the northern section of the Bay (near the mouth of the Hackensack River) were granular – with the percentage of fines less than 60% – whereas samples from southern mudflats (Kill Van Kull) had cohesive behavior.

Table 4-2 summarizes the pairwise correlation values between sediment properties for different classes of sediment size. These correlations can also be seen in Figure 4-1 and Figure 4-2. The results of specific gravity and bulk density tests are presented in Figure 4-3 and Figure 4-4 respectively.

Table 4-2. ***Pairwise correlation between sediment parameters for different classes of sediment size***

Percent Fines		**All**	**PF ≤ 40**	**40<PF<60**	**PF ≥ 60**
Number of Observations	**n**	**69**	**16**	**18**	**35**
ρ_{bulk} , W	ρ[5]	0.51	-0.34	0.59	0.11
	P[6]	0.000	0.196	0.0104	0.532
ρ_{bulk} , O	ρ	-0.79	-0.42	-0.71	-0.16
	P	0.000	0.106	0.001	0.349
ρ_{bulk} , PF	ρ	-0.78	0.00	0.78	0.15
	P	0.000	0.992	0.0001	0.401
ρ_{bulk} , D	ρ	-0.06	-0.07	-0.14	0.33
	P	0.607	0.797	0.5856	0.054
W, O	ρ	-0.59	0.77	-0.59	-0.29
	P	0.000	0.000	0.0098	0.092
W, PF	ρ	-0.46	0.66	0.43	-0.14
	P	0.000	0.005	0.072	0.411
W, D	ρ	-0.2	-0.14	-0.08	-0.29
	P	0.108	0.598	0.7576	0.085
O , PF	ρ	0.67	0.43	-0.72	-0.04

[5] Pearson correlation
[6] P-value for correlation

O , D	P	0.000	0.093	0.0007	0.806
	ρ	0.21	0.32	0.24	0.11
PF , D	P	0.079	0.228	0.3444	0.519
	ρ	0.06	-0.17	-0.12	0.06
	P	0.625	0.52	0.6239	0.732

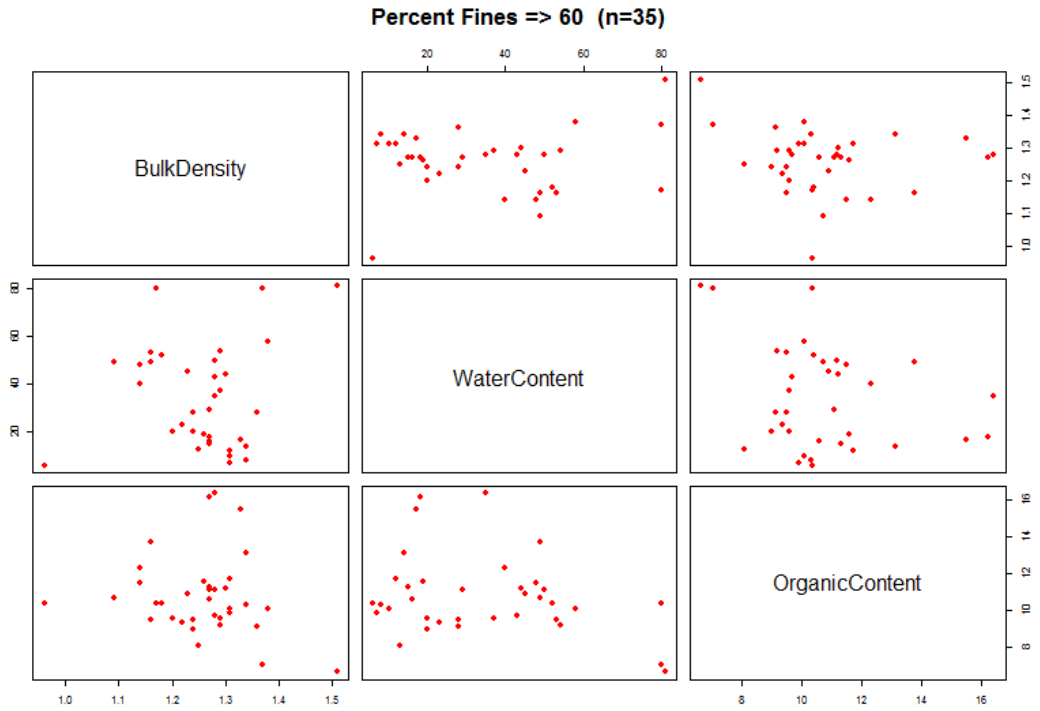

Figure 4-1. **Scatterplot matrix of sediment properties - PF ≥ 60**

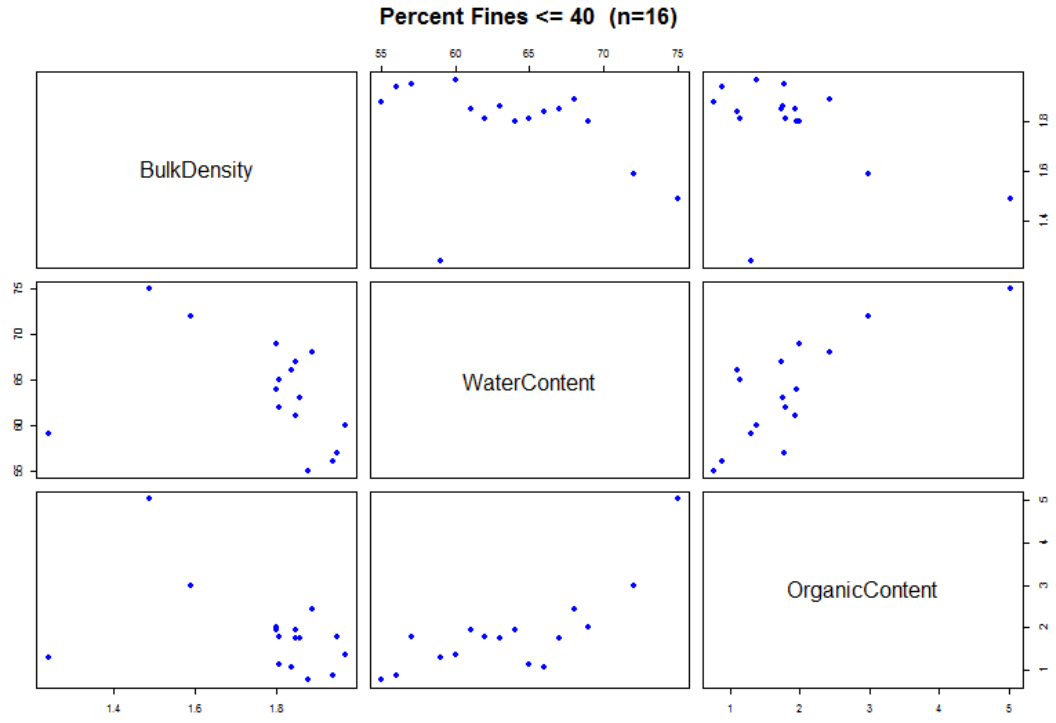

Figure 4-2. **Scatterplot matrix of sediment properties - PF ≤ 40**

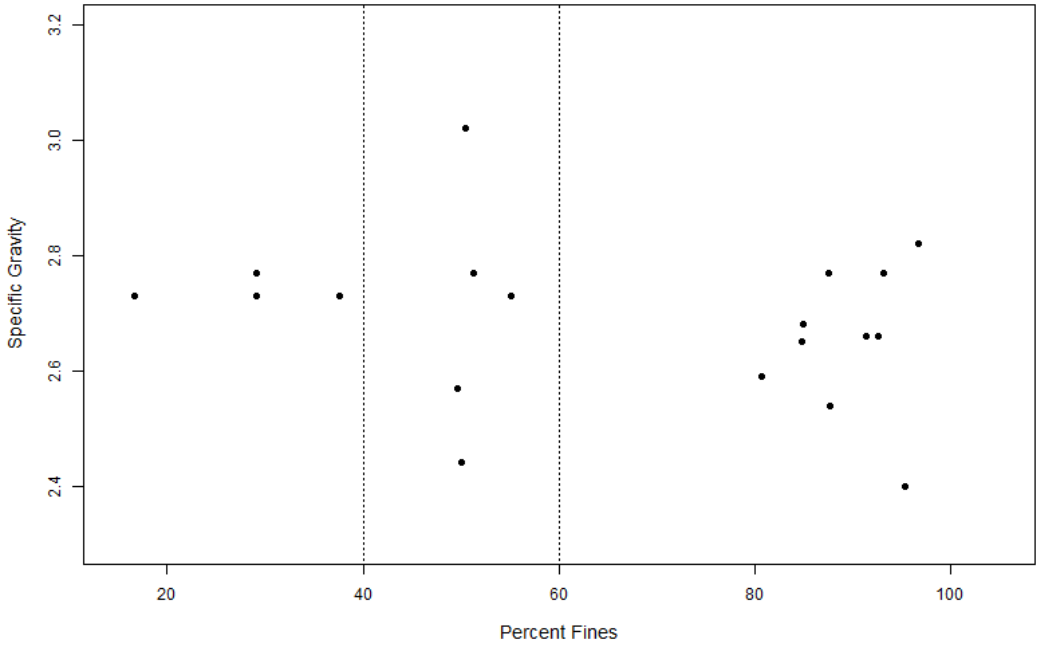

Figure 4-3. **Specific gravity versus percent fines for all samples**

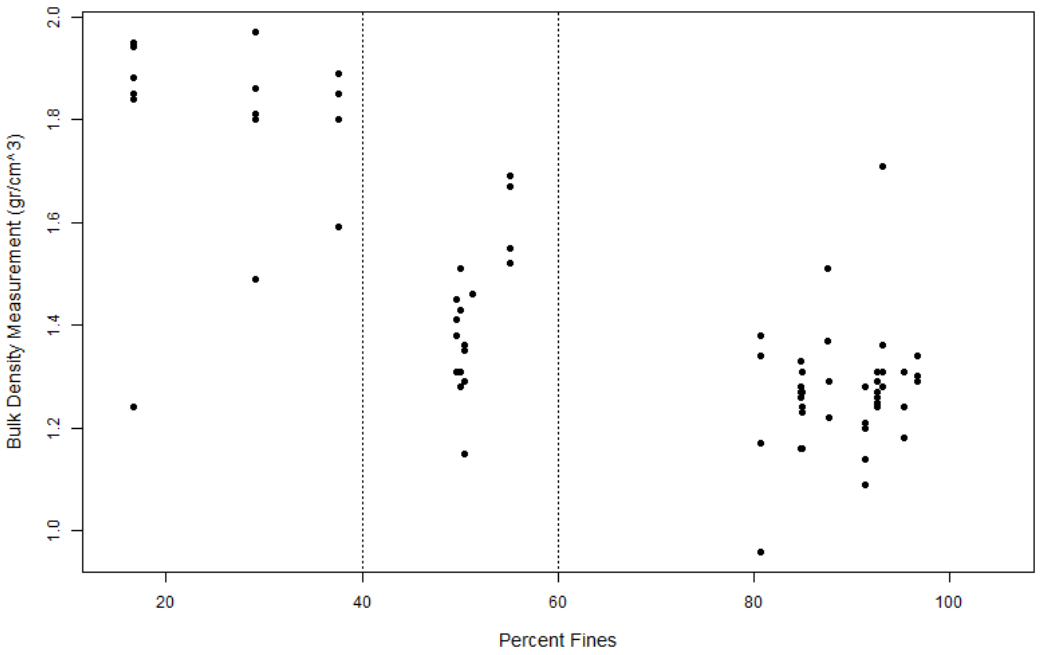

***Figure 4-4*. Bulk density versus percent fines for all samples**

4.2. Erosion Tests

Figure 4-5 and Figure 4-6 show the box plots of observed erosion rates and average velocities for different classes of sediment size, respectively. Figure 4-7 and Figure 4-8 display the distribution of average velocities and theoretical shear stresses used in the tests. The erosion rate measurements are plotted against theoretical shear stress values in Figure 4-9 and Figure 4-10 shows the frequency distribution of erosion rates. Table 4-3 includes correlation values between erosion rate and sediment parameters for different classes of sediment size.

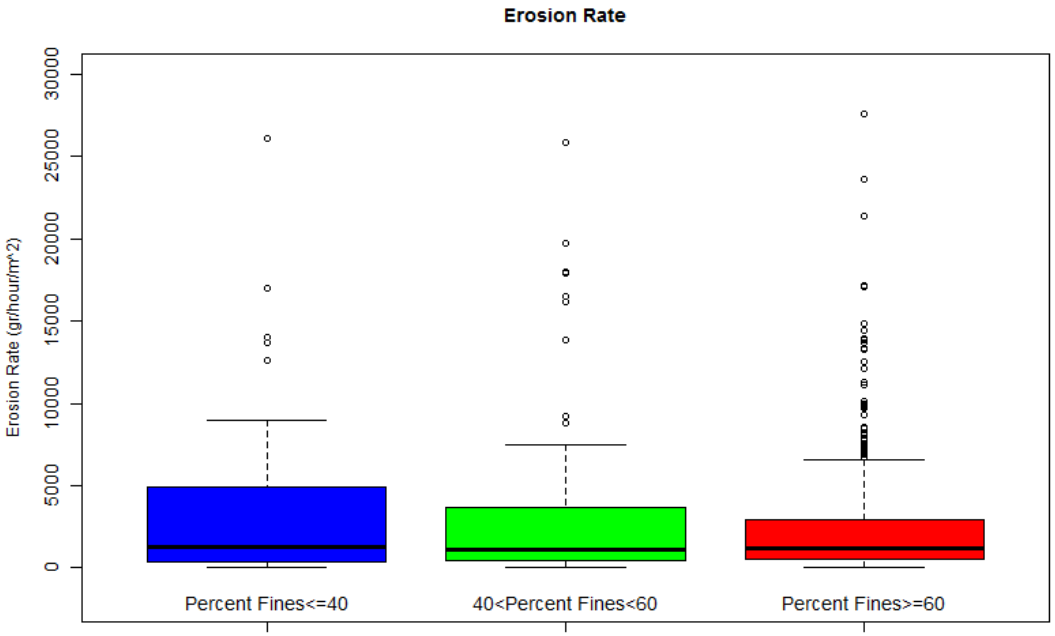

Figure 4-5. **Observed erosion rates for different classes of sediment size**

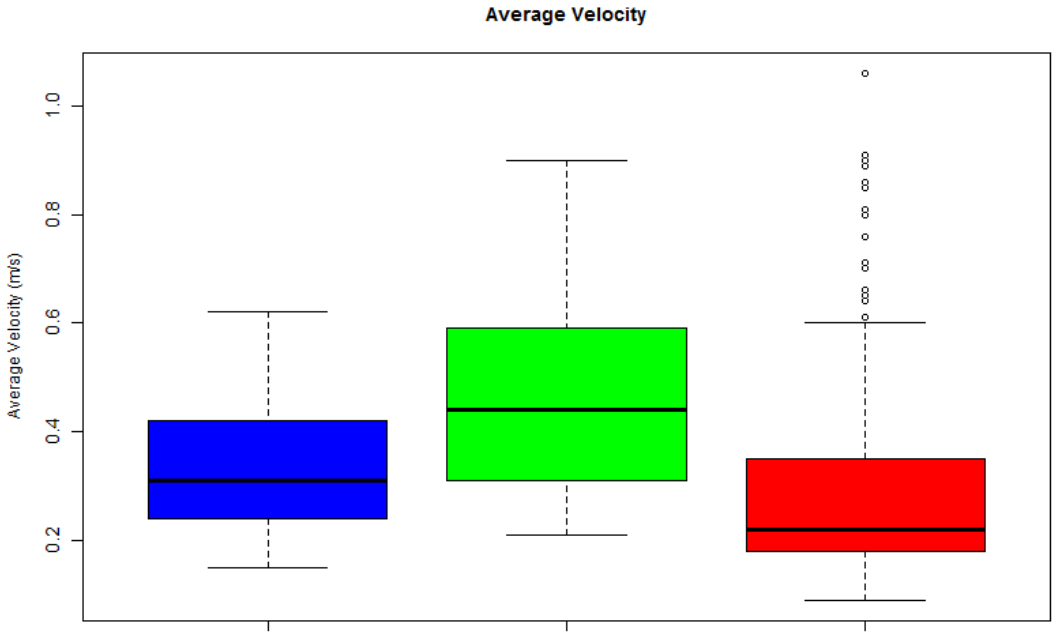

Figure 4-6. **Average velocities used for testing different classes of sediment size**

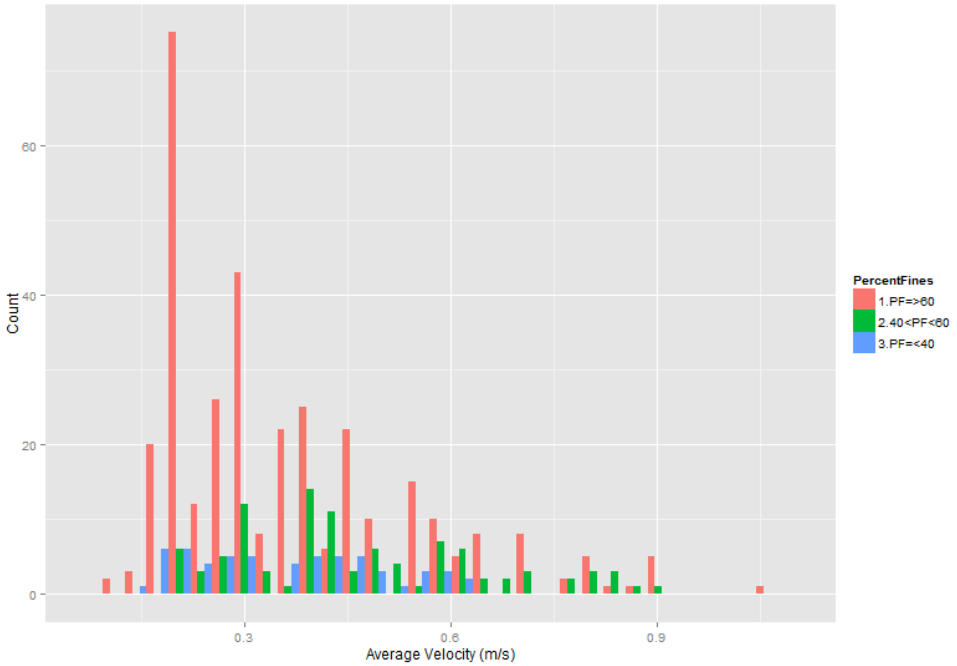

Figure 4-7. **Average velocities used for testing different classes of sediment size**

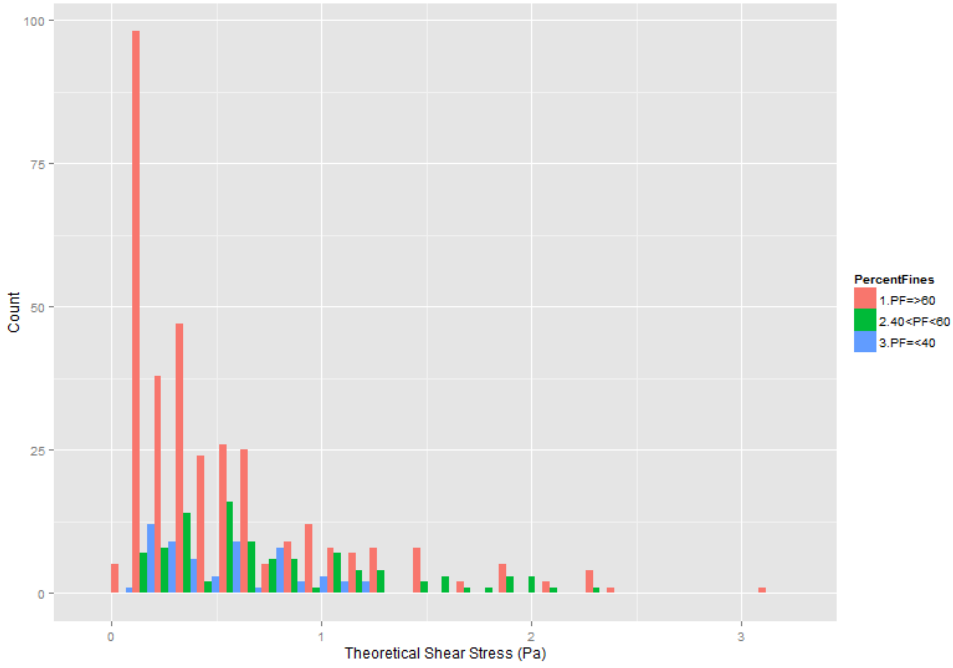

Figure 4-8. **Theoretical shear stresses used for testing different classes of sediment size**

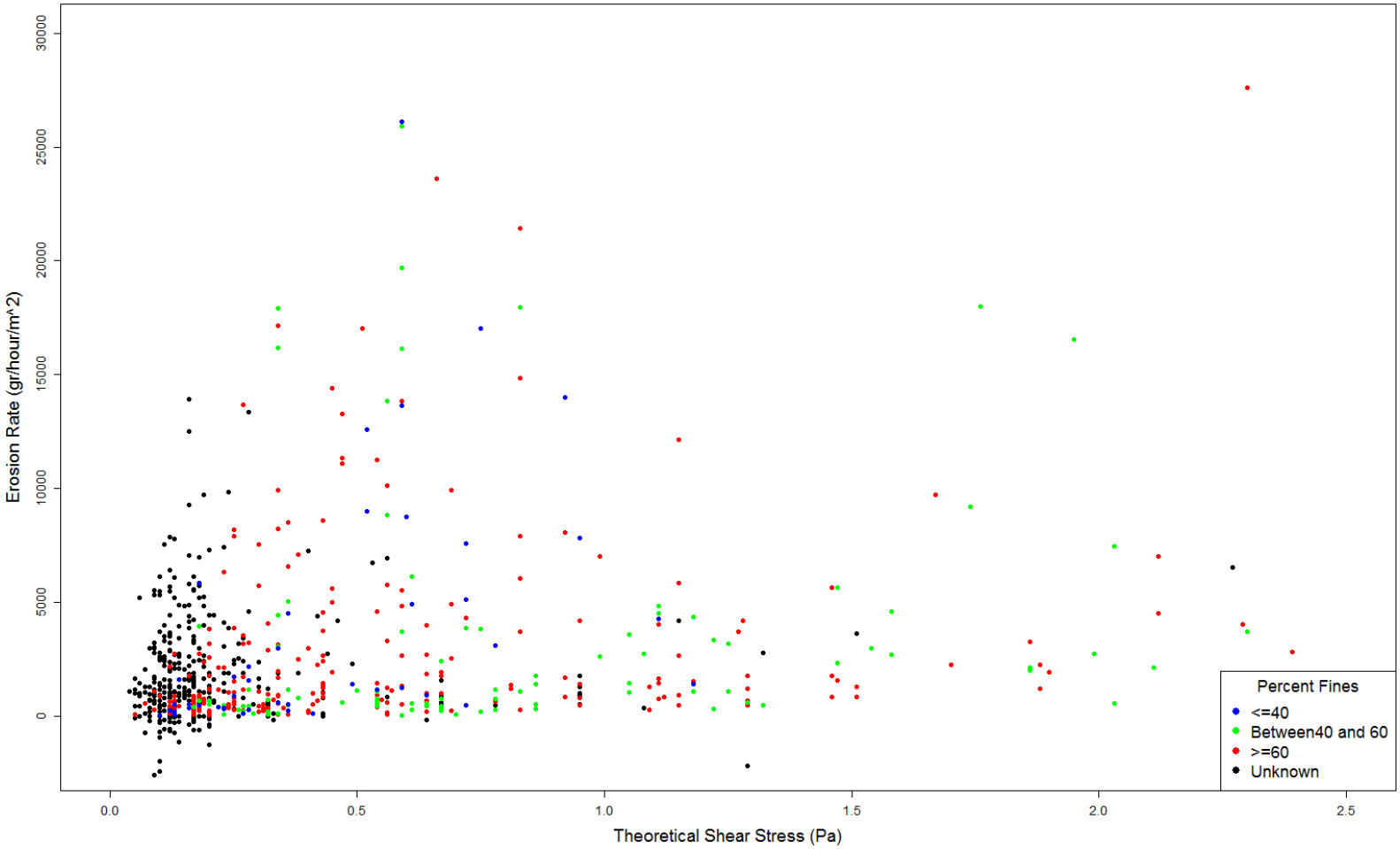

Figure 4-9. **Observed erosion rates at different shear stress levels**

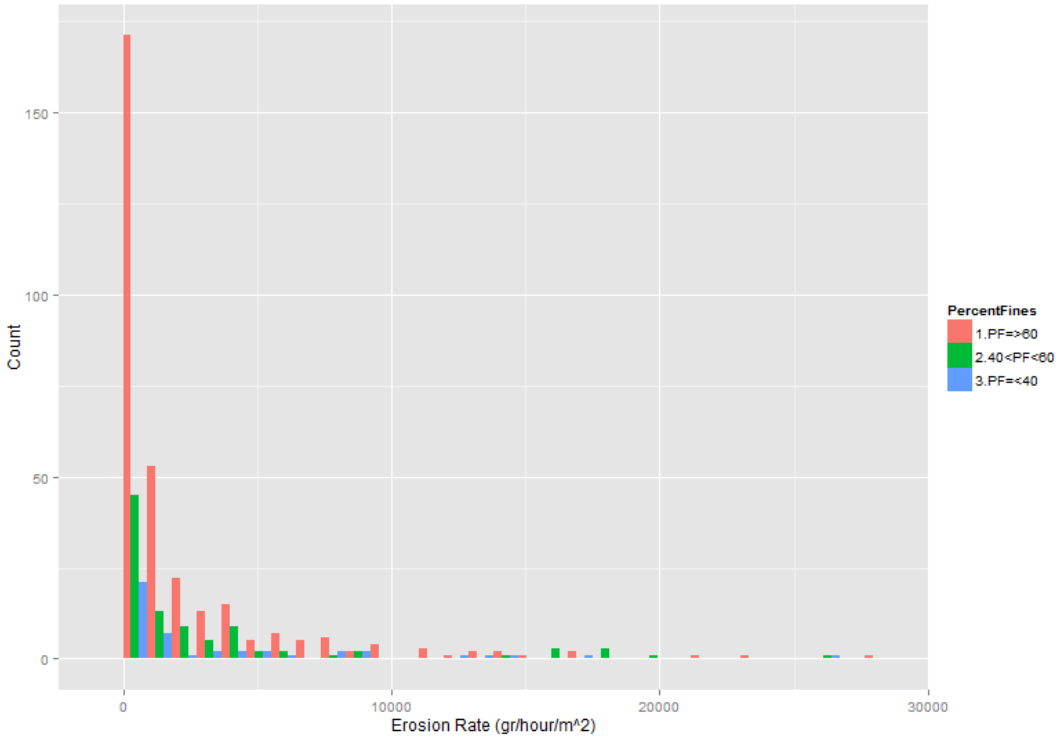

Figure 4-10. **Erosion rates observed for testing different classes of sediment size**

Table 4-3. ***Correlation between erosion rate and sediment parameters for different classes of sediment size***

Percent Fines		All	PF ≤ 40	40<PF<60	PF ≥ 60
ER , V	ρ	0.22	0.47	0.16	0.20
	P	0.0000	0.001	0.1179	0.0000
	n	703	45	97	561
ER , ρ_{bulk}	ρ	-0.01	-0.13	0.08	-0.27
	P	0.8282	0.398	0.4254	0.0000
	n	703	45	97	561
ER , W	ρ	0.20	0.03	0.08	0.29
	P	0.00	0.8412	0.4351	0.0000
	n	453	45	97	311
ER , O	ρ	-0.05	-0.13	-0.13	0.13
	P	0.34	0.3840	0.2069	0.0340
	n	408	45	97	266
ER , D	ρ	-0.24	-0.28	-0.38	-0.25
	P	0.0000	0.0611	0.0001	0.0000
	n	703	45	97	561

5. DATA ANALYSIS

5.1. Introduction

The research framework used in this study consists of the following four main components: (1) device assessment, (2) experimental tests, (3) regression analysis of the experimental data, and (4) stochastic analysis. Figure 5-1 shows the flow chart of the main research activities accomplished in this study. Chapter 5 is on data analysis and explains the analytical methodology used in this research in two sections: regression analysis and stochastic analysis. Section 5.2 describes the regression analysis used to develop two models for erosion rate of both fine and coarse sediments in the Newark Bay. Section 5.3, describes the methodology developed to build upon these models and conduct stochastic simulations for cohesive sediment erosion. The main conclusions have been discussed at the end of each section.

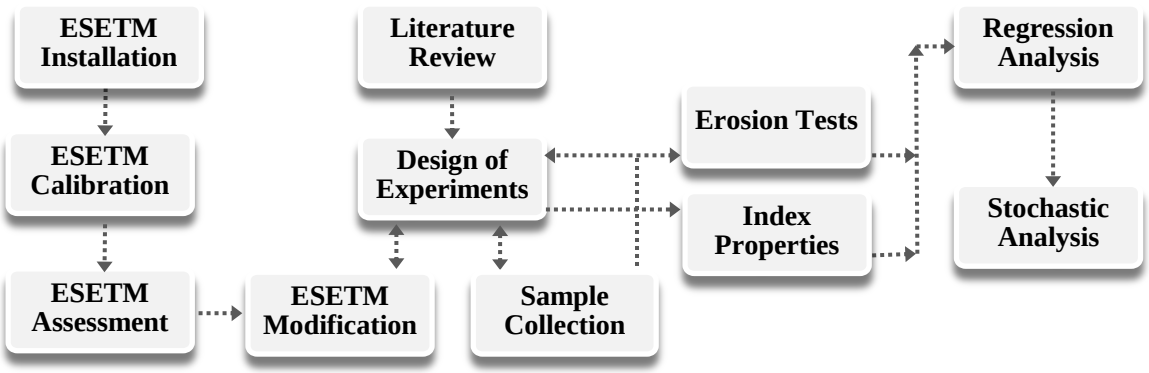

Figure 5-1. **The research methodology framework for the current study**

5.2. Regression Analysis

5.2.1. Introduction

Researchers have used many different forms of equations, some of which have been described in Chapter 2, to fit empirical models to their observed erosion measurements. Considering the lack of any physical theory behind the complex forms of some empirical erosion models, it can be concluded that the simplicity of models does not necessarily impair their effectiveness. As multiple linear regression models have not been widely used in the literature to construct erosion models based on sediment index properties, this technique was used in the current study.

Section 5.2.2 explains how the data was clustered prior to analysis. In section 5.2.3, the model development procedure is explained. The two models finally selected in this section (Newark Bay Fine Model[7] and Newark Bay Coarse Model[8]) are validated in section 5.2.4. A comparative analysis was performed in section 5.2.5 to further evaluate the performance of NBFM and NBCM. In section 5.2.6 the main conclusions of regression analysis are discussed.

5.2.2. Clustering the Dataset

Cluster analysis (Figure 5-2 - Figure 5-5) of the observed data revealed two breaks in the percentage of fines (at 40 and 60 percent) that were used to categorize the samples into three groups: below 40 percent (fine), between 40 and 60 percent, and above 60 percent (coarse). Separate models were developed for each of these groups of sediments. It is interesting to

[7] NBFM
[8] NBCM

compare the ranges of observed water and organic contents in Figure 5-3 and Figure 5-4. While finer sediments had lower water contents, coarser sediments had lower organic contents.

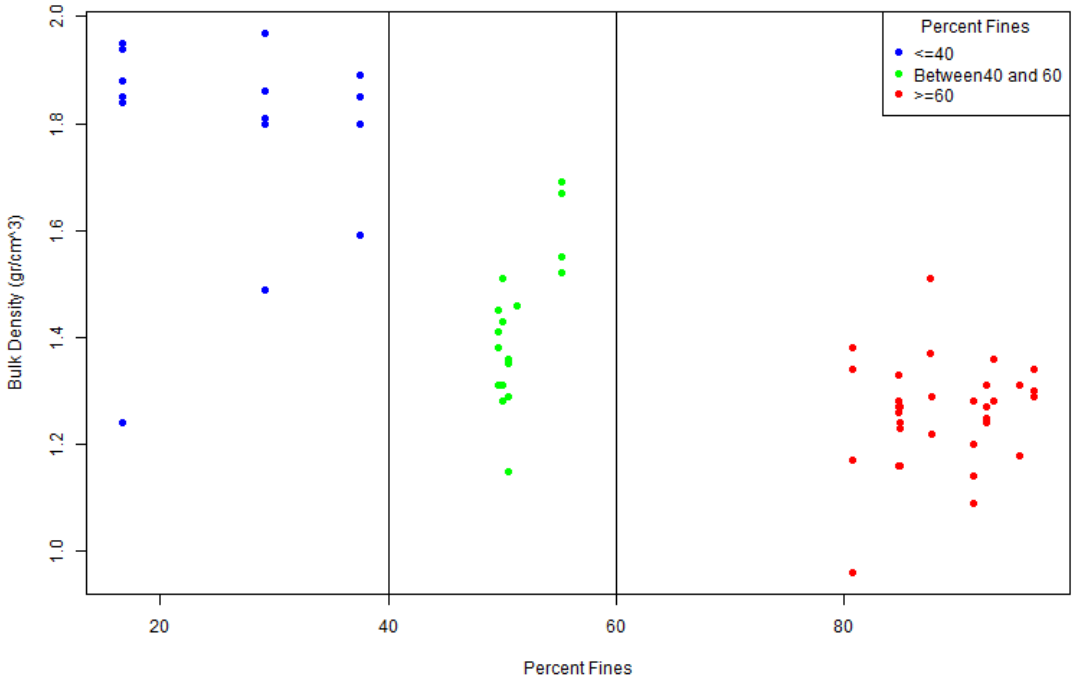

***Figure 5-2*. Bulk density versus percentage of fines for all the samples**

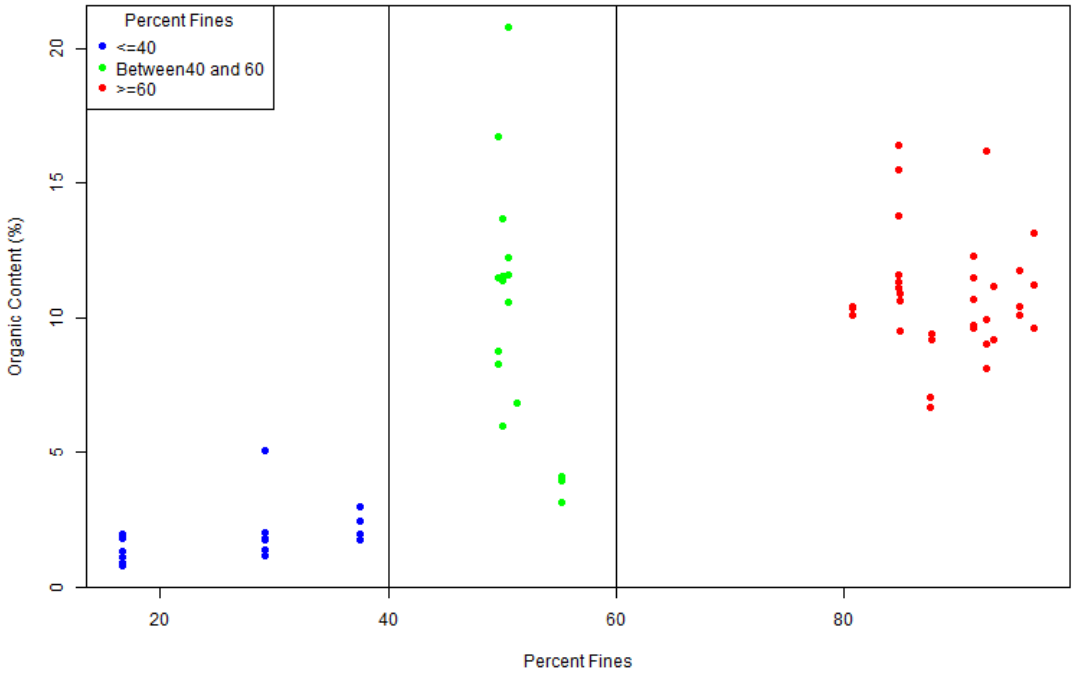

Figure 5-3. **Organic content versus percentage of fines for all the samples**

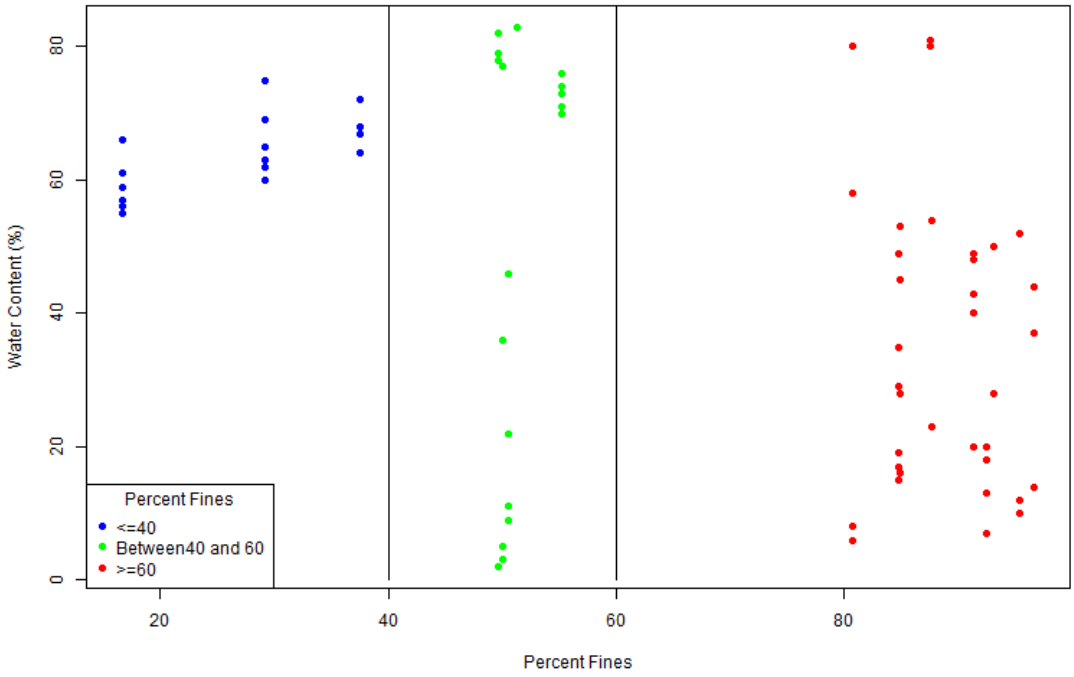

Figure 5-4. **Water content versus percentage of fines for all the samples**

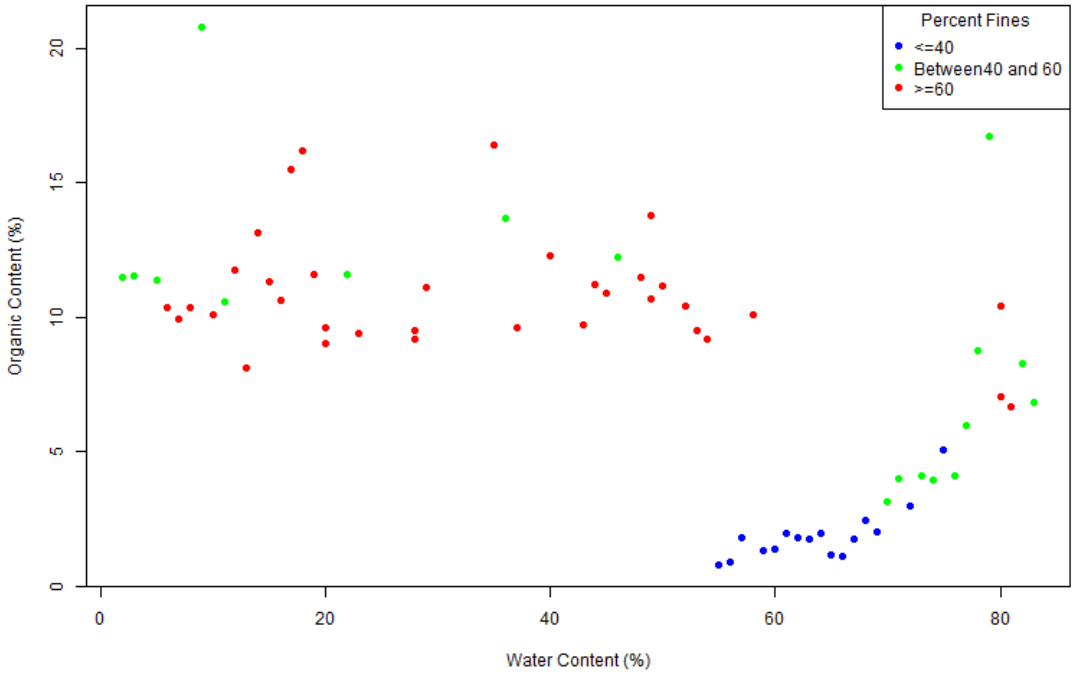

Figure 5-5. **Organic content versus water content for different classes of sediment size**

5.2.3. Model Development

A full simple linear regression model was initially fitted to the data including all the measured index properties (bulk density, water content, organic content, and depth), as well as the average velocity. Both forward selection and backward elimination methods were applied to select the best fit among all possible models, resulting in the selection of the following (full) model. This model was not adequate according to Box A. 28 and Figure A. 29.

The observed residuals' patterns in Figure A. 29 revealed obvious problems with this model and suggested applying a transformation on the response values for an improved model. Several transformation options were considered to linearize the model and stabilize its residuals'

variance. Figure 5-6 suggested that the lognormal distribution is a good fit for the erosion rate data: the plotted points almost follow a straight line and the p-value for the goodness of fit is 0.149, which is greater than 0.05, thus making it significant[9]. FigureA. 30 compares the histogram of ln(Erosion Rate) with the normal distribution. However, it should be noted that the distribution of Erosion Rate as the response variable also depends on the patterns of variation in the regressors. Therefore, we cannot treat it as a univariate and fit a distribution to it.

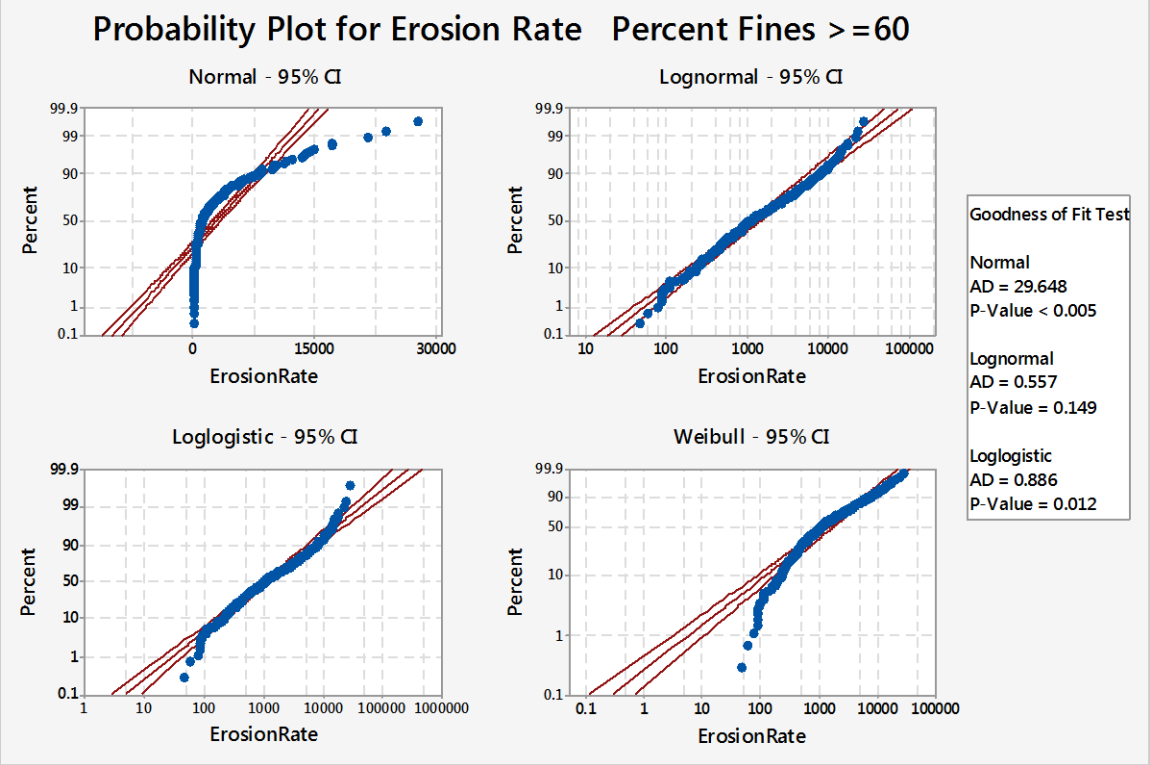

Figure 5-6. **Multiple distributions fitted erosion rate measurements - PF ≥ 60**

[9] This is the p-value for a chi-square-goodness-of-fit test and should not be confused with the p-value used in regression analysis.

A logarithmic transformation on the average velocity proved to be helpful as well. The forward selection and backward elimination methods were applied again, which resulted in the selection of the following model. This model is to be called the Newark Bay Fine Model (NBFM).

$$\mathbf{ln(ER) = \beta_0 + \beta_1 . ln(V) + \beta_2 . \rho_{Bulk} + \beta_3 . W + \varepsilon \quad Percent\ Fines \geq 60 \qquad NBFM}$$

ER: erosion rate $(\frac{gr}{m^2 . hour})$

V: average velocity in the channel $(\frac{cm}{s})$

ρ_{Bulk}: bulk density $(\frac{gr}{cm^3})$

W: water content (%)

Box 5-1. ***Model summary for:*** $ln(ER) = \beta_0 + \beta_1 . ln(V) + \beta_2 . \rho_{Bulk} + \beta_3 . W + \varepsilon$ ***- PF*** ≥ 60

Lm(ln (Erosion Rate) ~ ln(AverageVelocity)+Bulk Density+Water Content)

Residuals:

Min	1Q	Median	3Q	Max
-2.4317	-0.6565	0.0756	0.6222	2.4221

Coefficients:

	Estimate	Std. Error	t value	Pr (>|t|)
(Intercept)	7.99318	1.21117	6.60	0.00000000024968 ***
ln(V)	1.94370	0.14123	13.76	< 0.0000000000000002 ***
ρ_{Bulk}	-7.10538	0.87328	-8.14	0.00000000000002 ***
W	0.03173	0.00358	8.85	< 0.0000000000000002 ***

Signif. codes: 0 '***' 0.001 '**' 0.01 '*' 0.05 '.' 0.1 ' ' 1

Residual standard error: 0.92 on 247 degrees of freedom

Multiple R-squared: 0.533, Adjusted R-squared: 0.527

F-statistic: 93.9 on 3 and 247 DF, p-value: <0.0000000000000002

In order to check the model adequacy, different plots of residuals were investigated as shown in Figure 5-7. The plots of the model's least-squared residuals versus the corresponding

fitted values (panels I and III) show no obvious model defects as the residuals can be contained within a horizontal band. The residuals in the normal Q-Q plot (panel II) almost lie along a straight line. According to panel IV, points 123, 126, and 125 have the largest leverage values, and a closer investigation of Cook's distances in Figure 5-8 reveals that these points have the largest Cook's distances as well. However, as these points have small residuals and were not detected to be influential in the model, they were not discarded from the dataset. Figure 5-9 presents the histogram of standardized residuals, which is closely comparable to normal distribution. Plots of the residuals versus the corresponding values of each regressor variable are presented in Figure 5-10. It can be seen that the distribution of residuals is desirably random and vastly improved compared to the results in FigureA. 30.

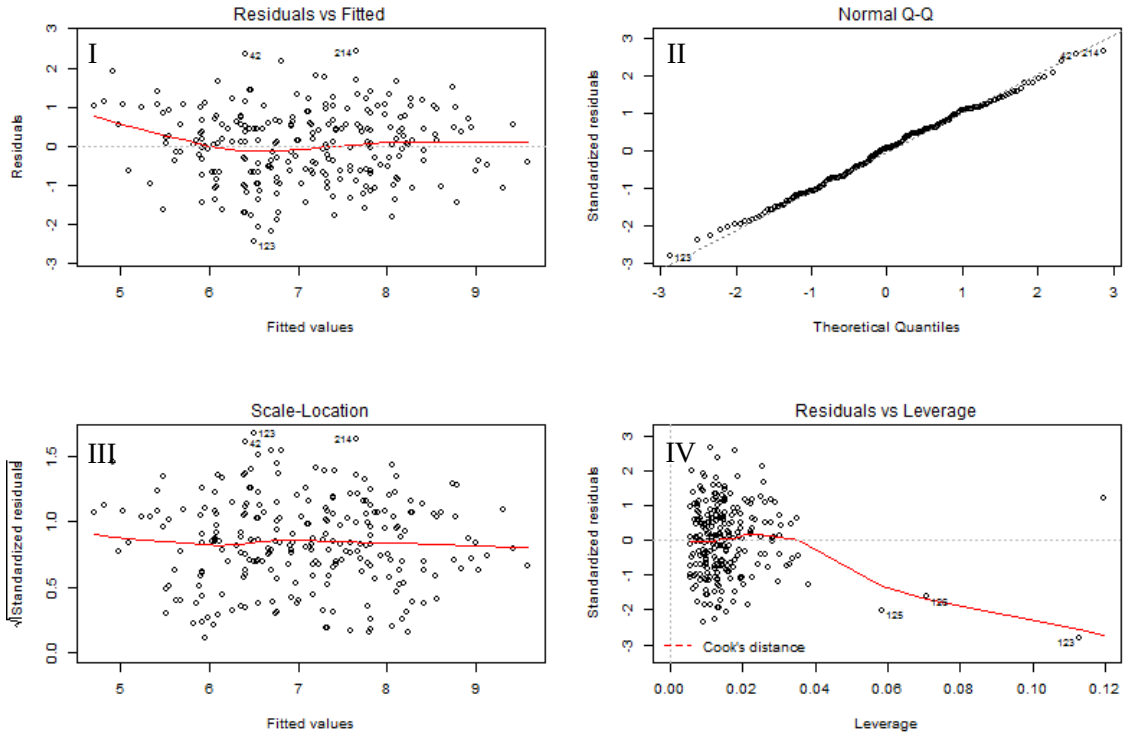

Figure 5-7. **Analysis of residuals for NBFM**

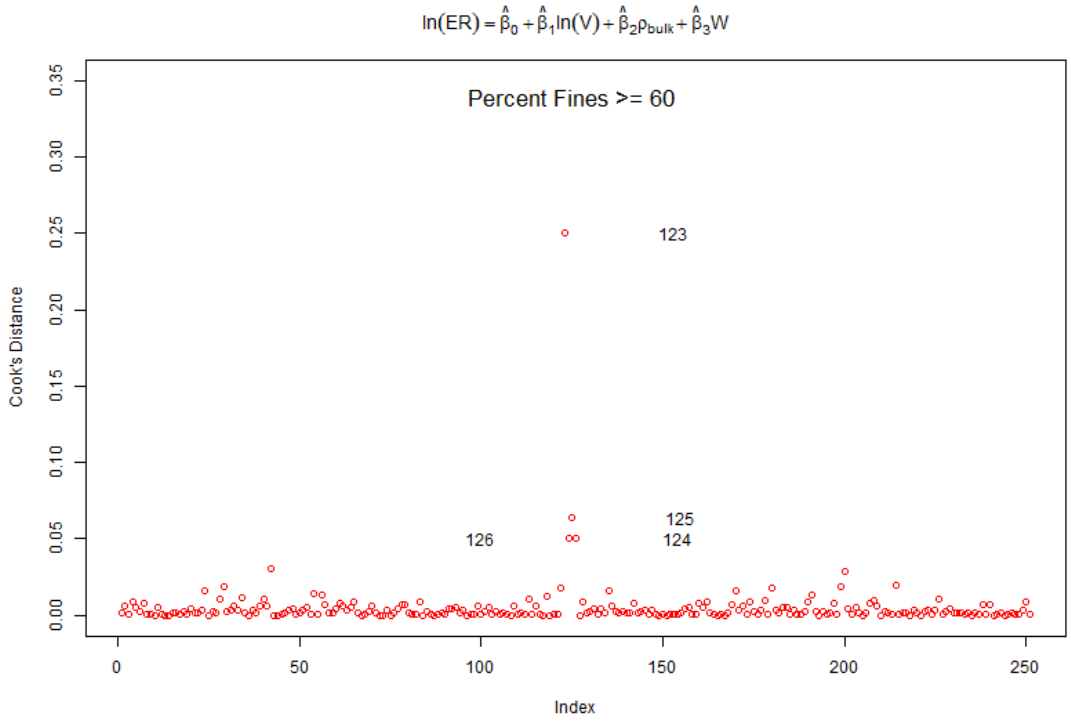

Figure 5-8. **Cook's distances for NBFM**

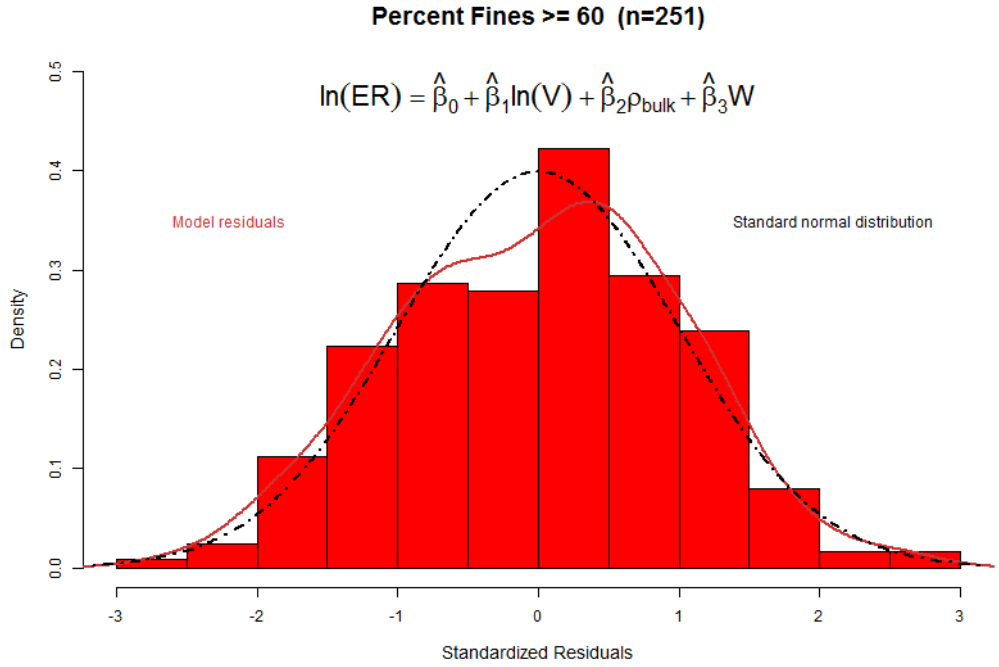

Figure 5-9. **Frequency distribution of standardized residuals for NBFM**

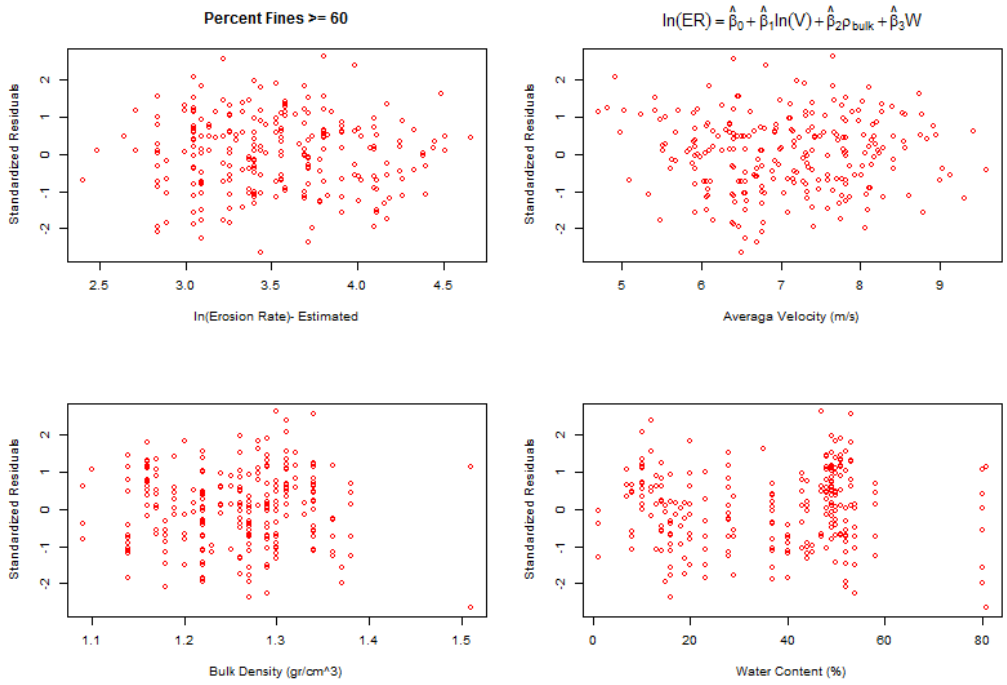

***Figure 5-10*. Plots of standardized residuals versus: fitted values (top left), Average Velocity (top tight), Bulk Density (bottom left), and Water Content (bottom right) - NBFM**

Figure 5-11 presents a plot of values predicted by this model versus the natural logarithm of observed erosion rates.

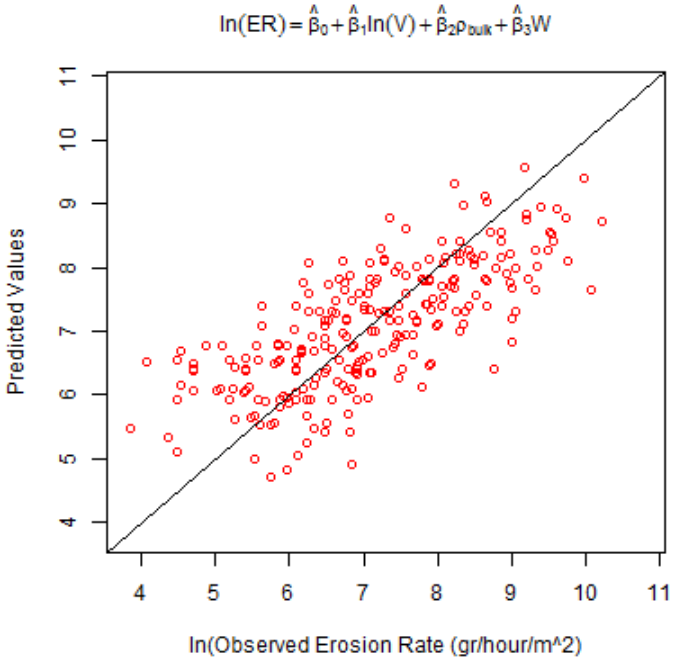

Figure 5-11. **Predicted versus observed erosion rates for NBFM**

In order to check the presence of multicollinearity, the regressors used in the model were investigated for possible correlations. According to Table 4-2 and Figure 4-1, there is no significant correlation between bulk density and water content in fine sediments.

Analysis of data with percent fines less than 40 percent (44 data points) resulted in the following model with an R-squared of 62 percent (Box 5-2 and Figure 5-12 - Figure 5-15). This model is to be called the Newark Bay Coarse Model (NBCM).

$$\mathbf{ln(ER) = \beta_0 + \beta_1 . V + \beta_2 . \rho_{Bulk} + \beta_3 . O + \varepsilon} \qquad \textbf{Percent Fines} \leq \textbf{40} \qquad \textbf{NBCM}$$

ER: erosion rate $(\frac{gr}{m^2 . hour})$

V: average velocity in the channel $(\frac{cm}{s})$

ρ_{Bulk}: bulk density $(\frac{gr}{cm^3})$

O: organic content (%)

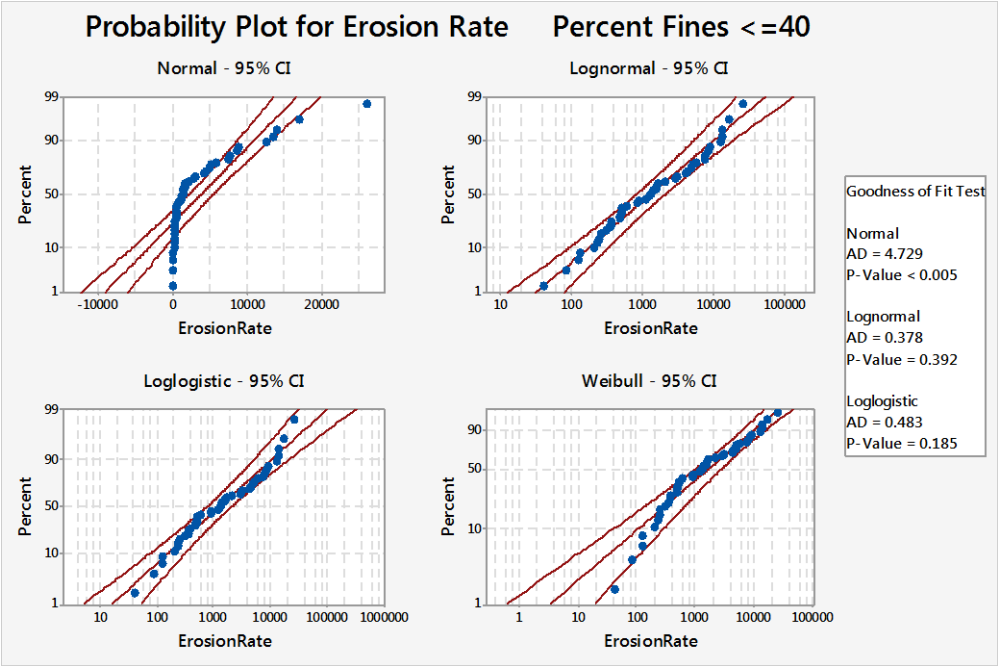

Figure 5-12. **Multiple distributions fitted to the erosion rate data**

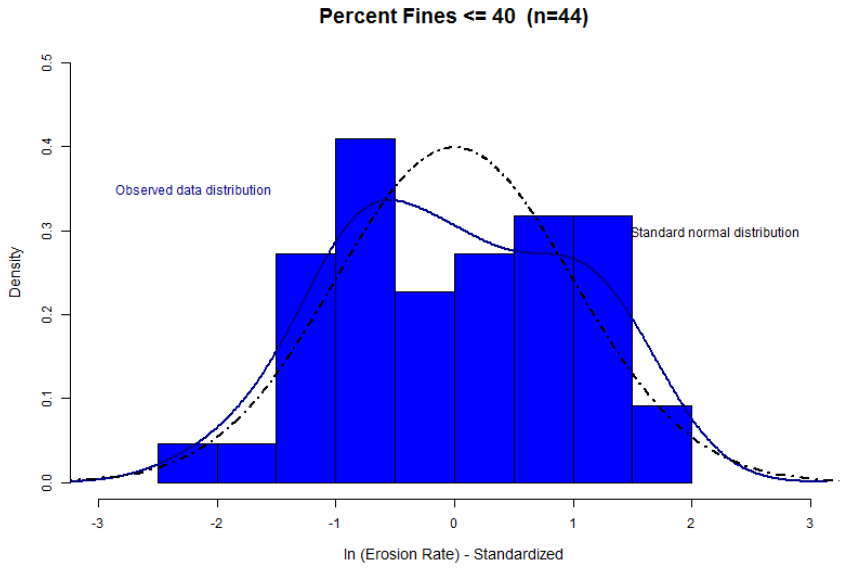

Figure 5-13. **Frequency distribution of the natural logarithm of observed erosion rates**

Box 5-2. ***Model summary for: NBCM - PF ≤ 40***

Lm (ln (Erosion Rate) ~ Average Velocity+Bulk Density+Organic Content

Residuals:

Min	1Q	Median	3Q	Max
-2.3669	-0.7214	0.0003	0.6353	2.1384

Coefficients:

	Estimate	Std. Error	t value	Pr(>|t|)
(Intercept)	9.9089	2.0885	4.74	0.000026625 ***
V	0.0987	0.0133	7.41	0.000000005 ***
ρ_{Bulk}	-2.3583	1.0330	-2.28	0.028 *
O	-0.9102	0.1878	-4.85	0.000019211 ***

Signif. codes: 0 '***' 0.001 '**' 0.01 '*' 0.05 '.' 0.1 ' ' 1

Residual standard error: 1.02 on 40 degrees of freedom

Multiple R-squared: 0.622, Adjusted R-squared: 0.594

F-statistic: 22 on 3 and 40 DF, p-value: 0.0000000145

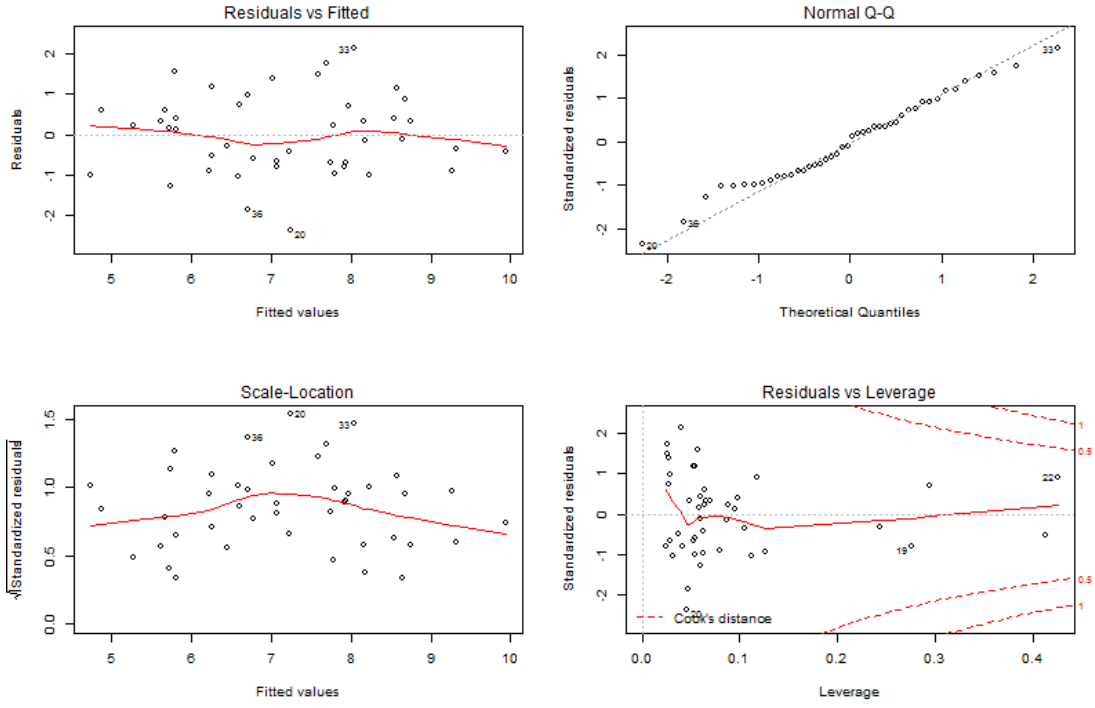

Figure 5-14. **Analysis of residuals for NBCM**

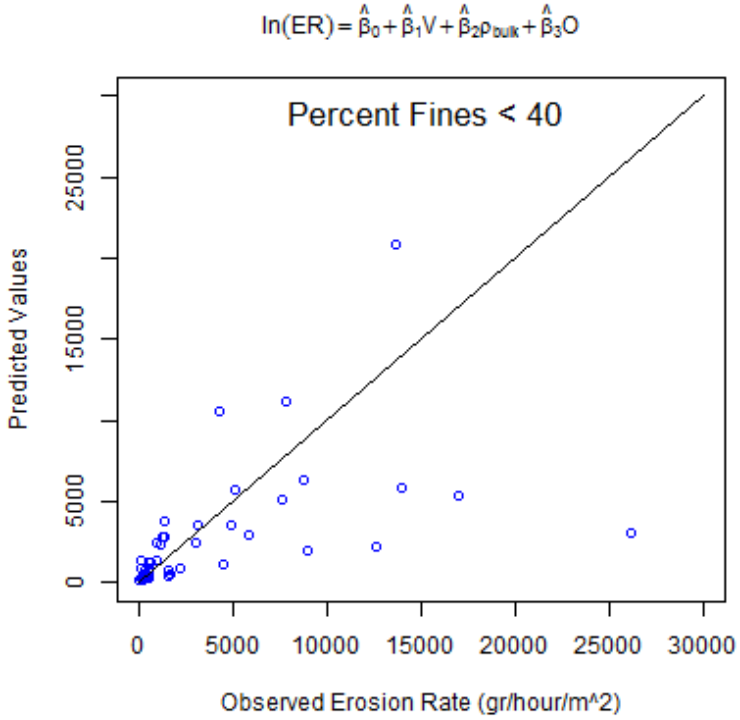

Figure 5-15. **Predicted versus observed erosion rates for NBCM**

In order to check the presence of multicollinearity, the regressors used in the model were investigated for possible correlations. According to Table 4-2 and Figure 4-2, there is no significant correlation between bulk density and organic content in coarse sediments.

The same procedure was applied for sediments with percent fines between 40 and 60 and the following model with an R-squared of 0.27 was found to fit the data (96 data points) the best. Box A. 31 and Figure A. 32 present the model summary and plots of residuals. The non-normal distribution of residuals and low R^2 value suggest that this model is not valid.

$$\mathbf{ER = \beta_0 + \beta_1 . V + \beta_2 . D + \varepsilon} \qquad \mathbf{40 < Percent\ Fines < 60}$$

ER: erosion rate $(\frac{\text{gr}}{\text{m}^2 . \text{hour}})$

V: average velocity in the channel $(\frac{\text{cm}}{\text{s}})$

D: depth of the samp′esurface (mm)

5.2.4. Model Validation

One of the techniques widely used for model validation is cross-validation (Mosteller and Tukey, 1968). In order to protect a model against overfitting, this method evaluates the performance of a model for independent measurements without requiring the collection of new data. The available data is randomly split into K folds, one of which is removed as the test set; the remaining folds are used to refit a model to the data. The common division ratio of 90% train (10% test) was used in this study which corresponds to a ten-fold cross validation. Figure 5-16 and Figure 5-17 display the results of cross-validation for NBFM and NBCM respectively and Box A. 33 and BoxA. 34 provide the corresponding ANOVA tables.

The fitted lines (each representing one fold of data) in Figure 5-16 are almost on top of each other and indicate that outliers are not very influential in the model. Larger points are actual observations for each fold of data and smaller ones (plotted on the line) are the values predicted by the model when each fold of data is deleted. The distance between the large points and their corresponding small points is a measure of the model's prediction accuracy. It can be concluded that despite having a lower R-squared value, NBFM is more stable than NBCM in general. However, the difference in the size of the datasets used for developing each of these models should not be ignored.

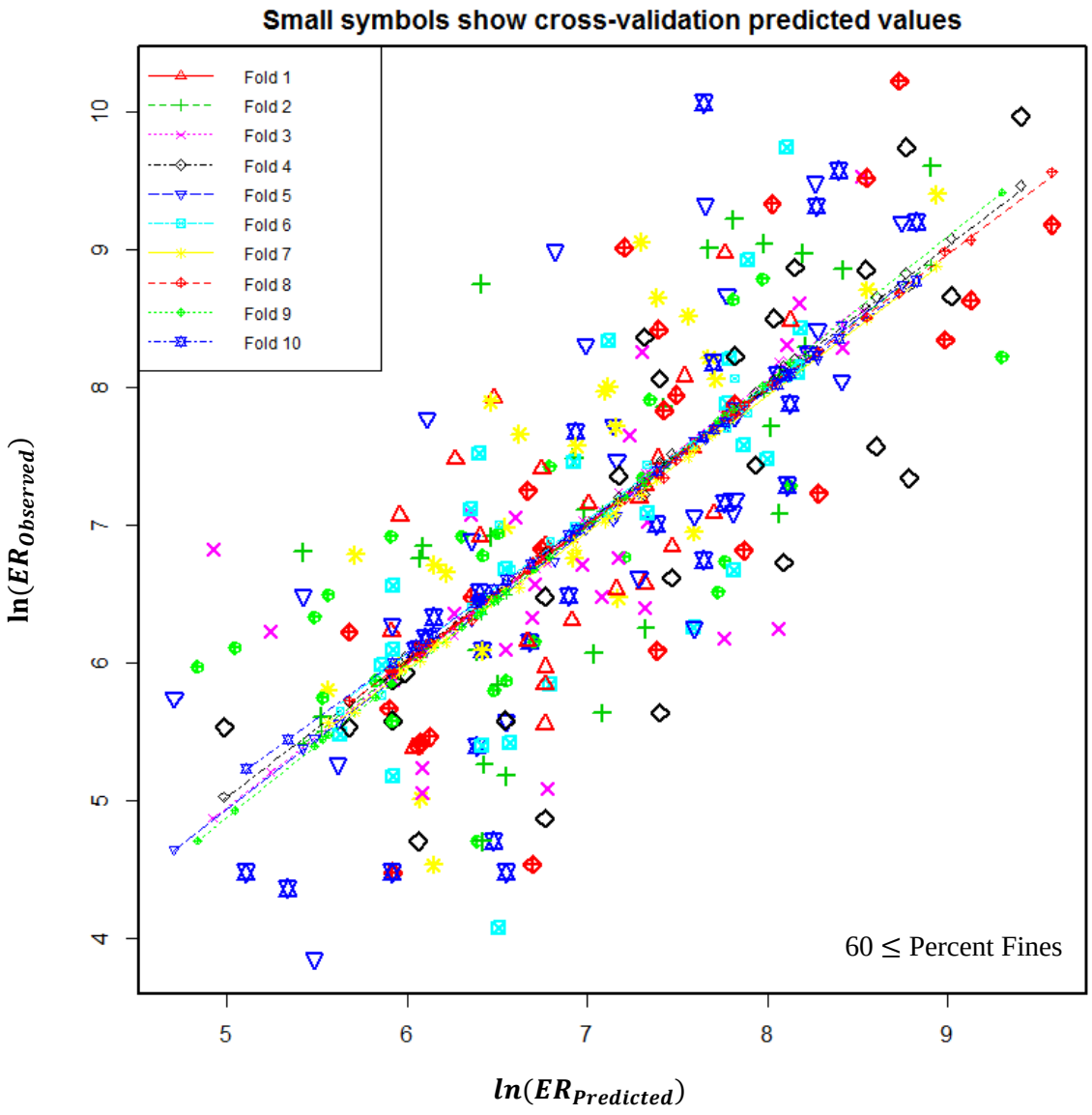

Figure 5-16. **Results of the ten-fold cross-validation analysis for NBCM**

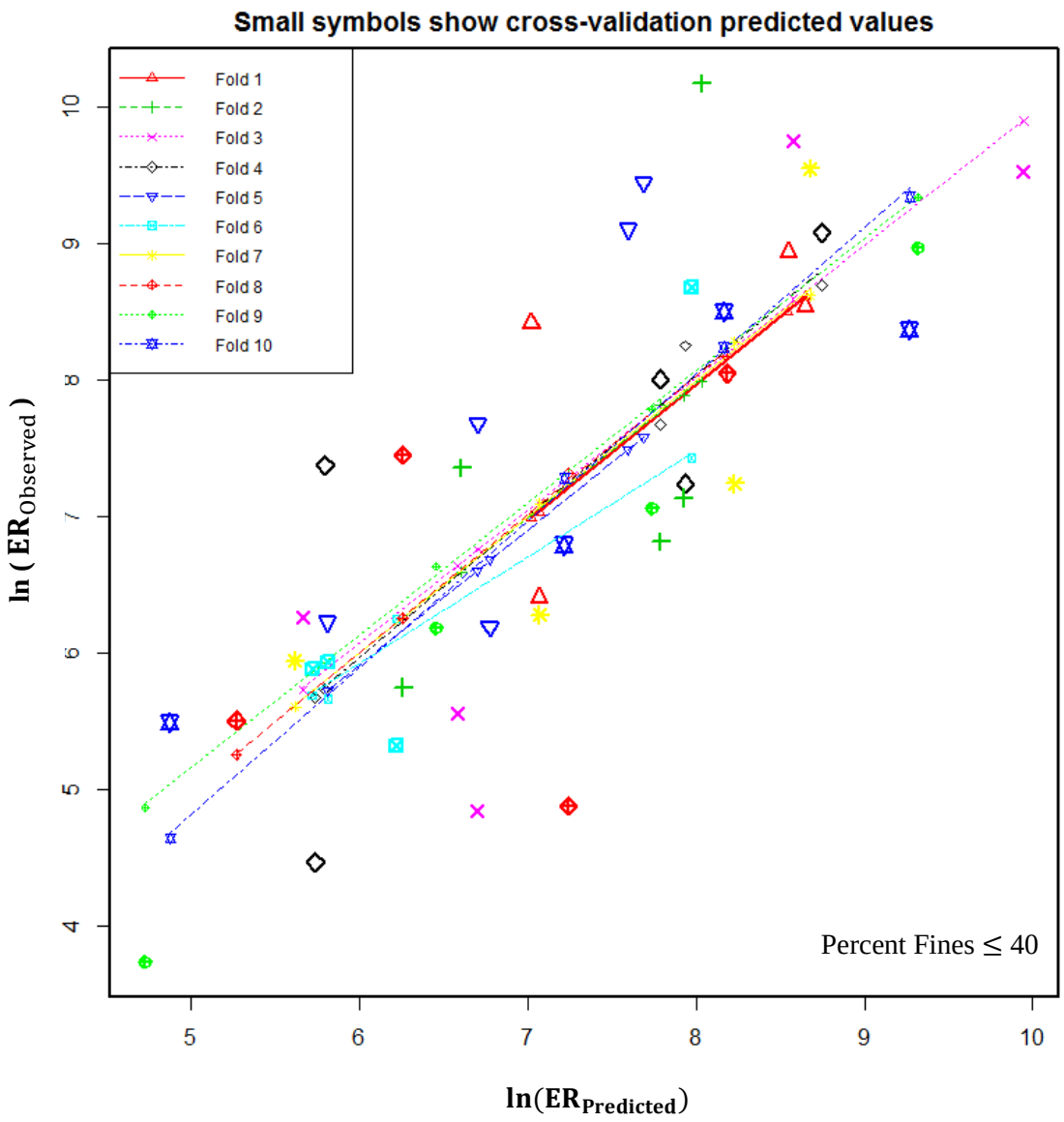

Figure 5-17. **Results of the ten-fold cross-validation analysis for NBCM**

In order to estimate the prediction power of NBFM and NBCM, R-squared was calculated for the models' predictions (for the test dataset) using PRESS statistic as defined below. According to Table 5-1, NBFM's prediction power reduced by three percentage points (from 0.53 to 0.50) when it is used for a new dataset. The corresponding decrease for NBCM was five percentage points (from 0.62 to 0.57). These low reductions in the two models' power indicate that none of the models are overfitted.

$$\mathbf{R_{CV}^2 = 1 - \frac{Press}{SS_T}}$$

$$\text{Press} = \sum_{i=1}^{n} [y_i - \hat{y}_{(i)}]^2$$

$$SS_T = \sum_{i=1}^{n} y_i{}^2 - n\bar{y}^2$$

y_i: the i_{th} observation

$\hat{y}_{(i)}$: the predicted value of y_i if the y^{th} observation is deleted

Table 5-1. ***Prediction power of the selected regression models measured by ten-fold cross-validation***

Model		R^2	$R^2_{Prediction}$	Overall MSE (CV)	PF
NBFM	$\mathbf{\ln(ER) = \beta_0 + \beta_1 . \ln(V) + \beta_2 . \rho_{Bulk} + \beta_3 . W}$ $\mathbf{ER = e^{\beta_0 + \beta_1 . \ln(V) + \beta_2 . \rho_{Bulk} + \beta_3 . W}}$	**0.533**	**0.506**	**0.879**	**≥ 60**
NBCM	$\mathbf{\ln(ER) = \beta_0 + \beta_1 . V + \beta_2 . \rho_{Bulk} + \beta_3 . O}$ $\mathbf{ER = e^{\beta_0 + \beta_1 . V + \beta_2 . \rho_{Bulk} + \beta_3 . O}}$	**0.622**	**0.578**	**1.050**	**≤ 40**

Another set of numerical experiments were conducted to study the effect of sample size. In each of these experiments random samples of different sizes were drawn from the observations for 1000 times and NBFM and NBCM was fitted to them. Figure 5-18 and Figure 5-19 show the distribution of model coefficients in these experiments. Figure 5-20 and Figure 5-21 Show the results of the same experiments for coarse sediments of the Newark Bay.

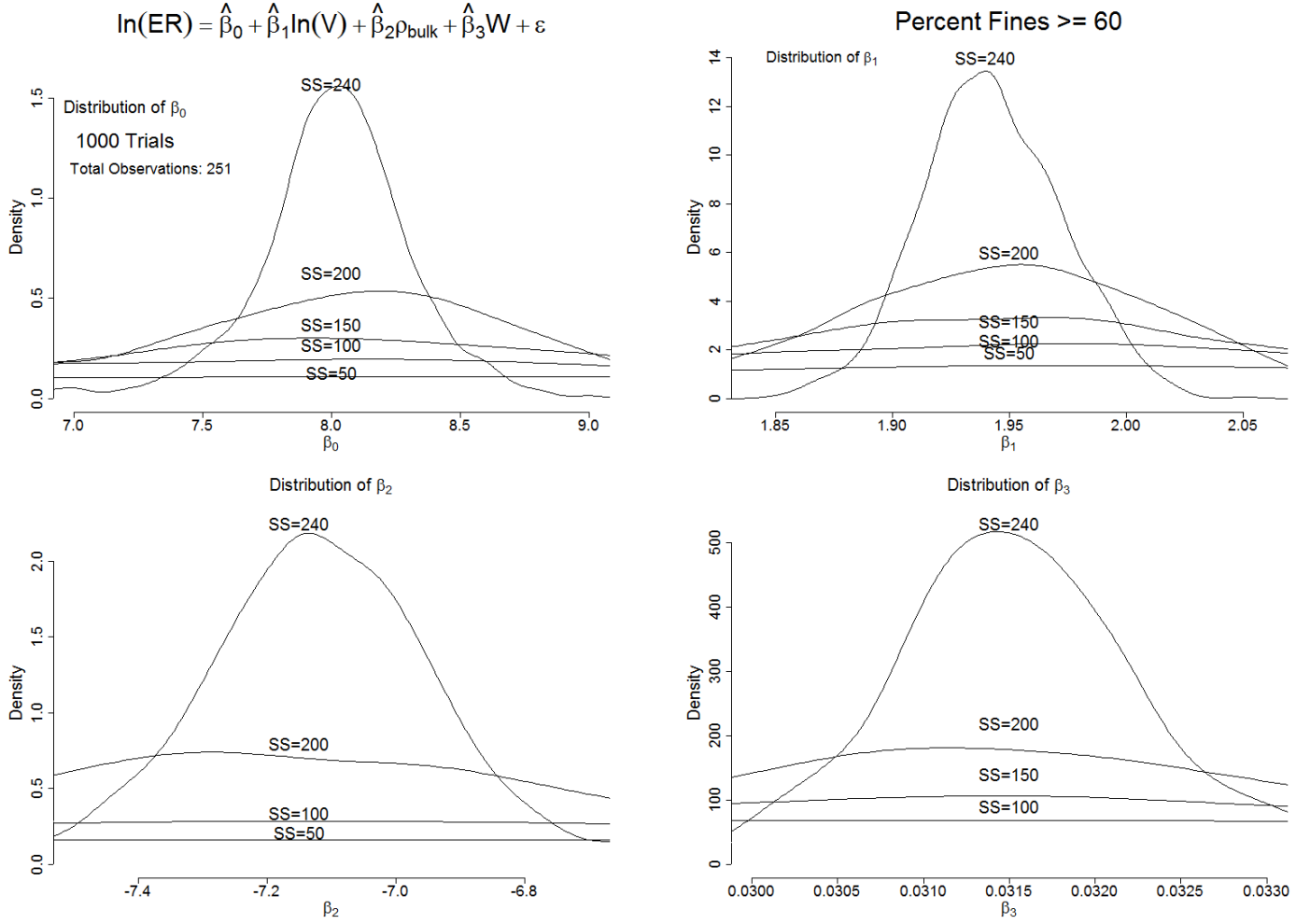

***Figure 5-18*. Distribution of regression model parameters estimated based on samples of different sizes (derived from original observations)–NBFM**

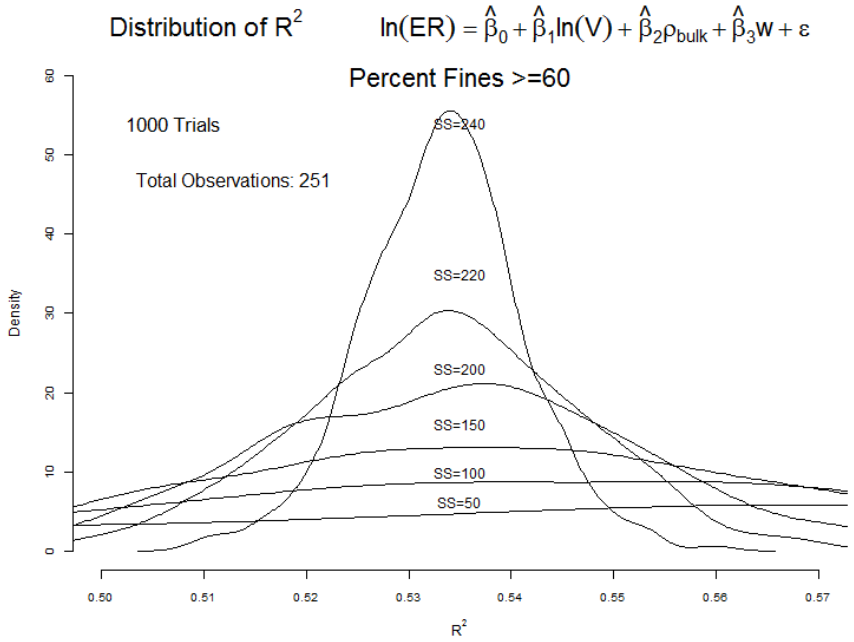

Figure 5-19. **Distribution of coefficients of distribution estimated based on samples of different sizes (derived from observations) –NBFM**

Table 5-2 compares the mean and standard deviation of model coefficients obtained from this experiment (for 150-point data sets) to the coefficients obtained from the complete dataset.

Table 5-2. ***NBFM coefficients estimated based on all the observations (251) compared to the ones based on 59% of them (150) averaged from 1000 trials***

Observations used	**Total (251)**[10]		**Partial (150)** [11]	
Indicator	**Value**	**SE**	**Mean**	**SD**
R^2	**0.533**	**-**	**0.533**	**0.007**
β_0	**7.993**	**1.211**	**7.900**	**1.43**
β_1	**1.940**	**0.141**	**1.950**	**0.121**
β_2	**-7.105**	**0.873**	**-7.070**	**0.967**
β_3	**0.031**	**0.003**	**0.032**	**0.003**

[10] From Box 5-1

[11] NBFM was fitted to samples of 150 data points that were randomly drawn from the 251-point observation dataset. The mean and standard deviation of estimated coefficients are presented here.

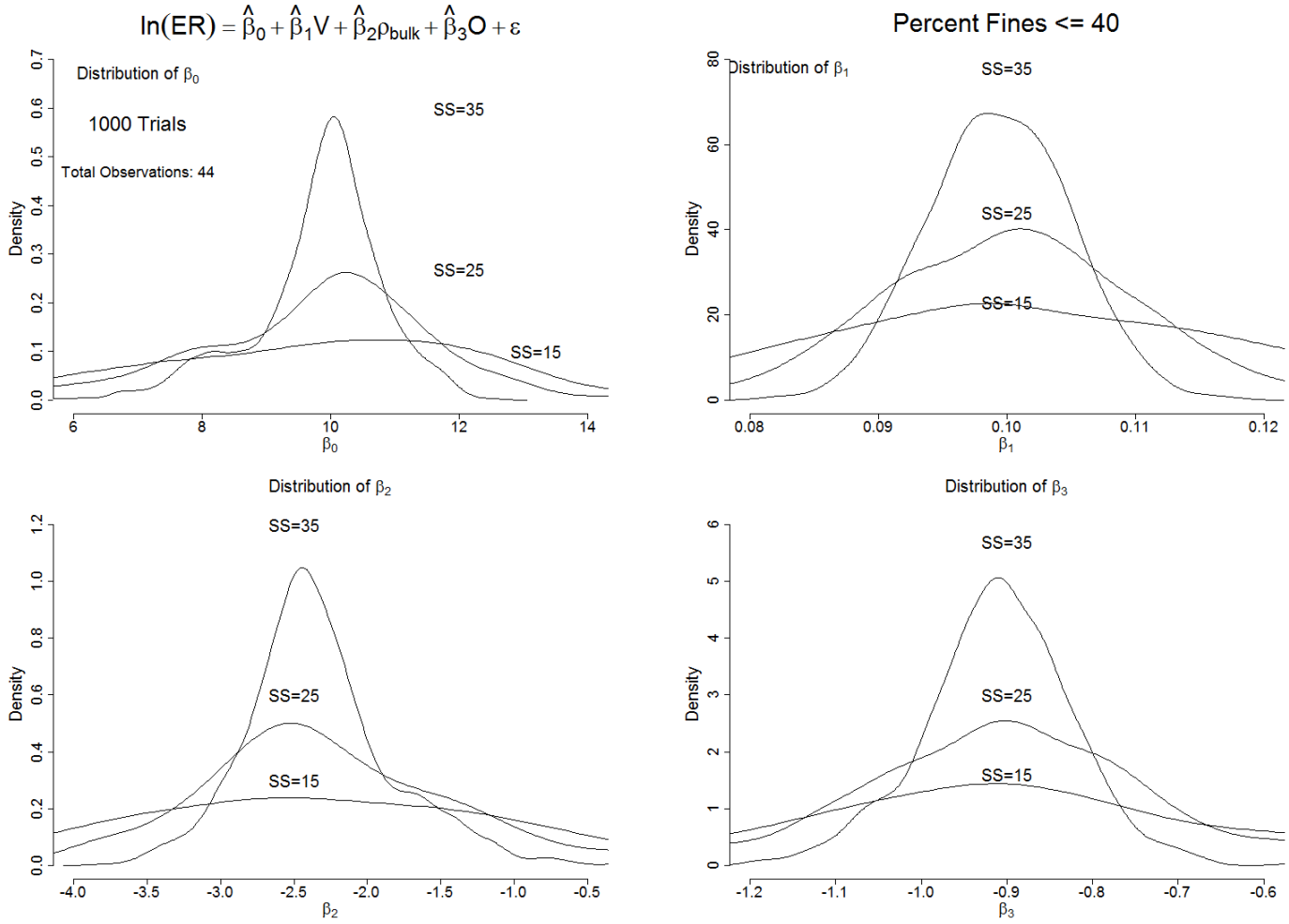

Figure 5-20. **Distribution of regression model parameters estimated based on samples of different sizes (derived from observations) – NBCM**

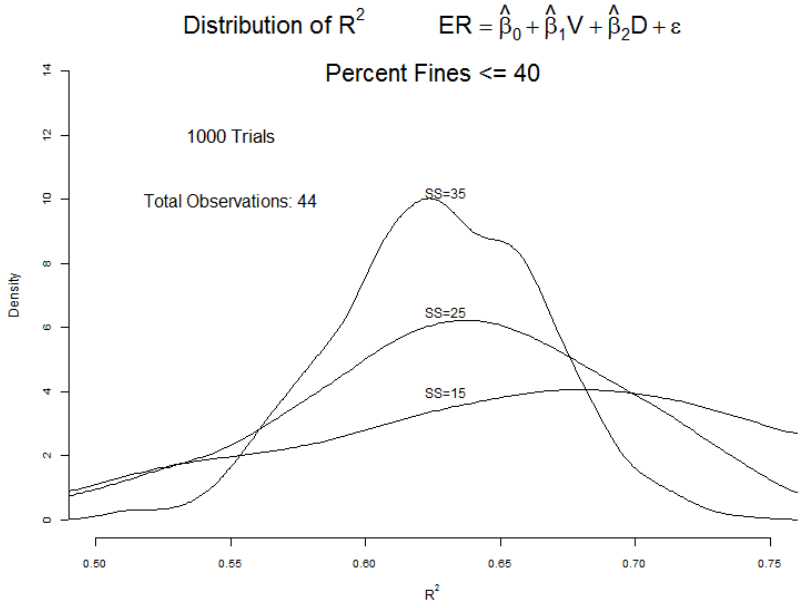

Figure 5-21. **Distribution of coefficients of distribution estimated based on samples of different sizes (derived from observations) – NBCM**

Table 5-3 compares the mean and standard deviation of model coefficients obtained from this experiment (for 25-point data sets) to the coefficients obtained from the complete dataset.

Table 5-3. ***NBCM coefficients estimated based on all the observations for coarse sediments (44) compared to the ones based on 56% of them (25) - averaged from 1000 trials***

Observations used	**Total (44)**[12]		**Partial (25)** [13]	
Indicator	**Value**	**SE**	**Mean**	**SD**

[12] Box 5-2

[13] NBCM was fitted to samples of 25 data points that were randomly drawn from the 44-point observation dataset. The mean and standard deviation of estimated coefficients are presented here.

R^2	0.622		0.633	0.065
β_0	9.908	2.088	9.500	2.220
β_1	0.098	0.013	0.101	0.010
β_2	-2.358	1.030	-2.200	1.090
β_3	-0.912	0.187	-0.886	0.179

From the above analysis, it can be concluded that a higher number of data points will result in more robust models.

5.2.5. Comparative Analysis

This section compares the results of this study with other experimental flume studies (section 5.2.5.1), as well as other empirical models (section 5.2.5.2).

5.2.5.1. Comparison with Other Experimental Flume Studies

In this section, the results of four erosion studies have been compared to the findings of this study (ESETM). As Ex-Situ Erosion Testing Machine had originally been designed to address the shortcomings of Sedflume, the first three studies selected for comparison either used Sedflume or had an erosion mechanism close to it. Of these three studies, the first study (Borrowman et al., 2006) is the most important as it was conducted in the Lower Passaic River, which is very close to the current study's sampling sites in the Newark Bay. The fourth study compared in this section (Ravens, 1997) was conducted in the Boston Harbor. The study was selected because Ravens used an in-situ straight flume to measure suspended solids concentrations. Although the site of Ravens' study – and hence the material - was different from the current study (ESETM), the fact that it was conducted in-situ and that the results were

independent of the instructor's subjective decision (for extruding the samples), made it a good candidate for comparison. Table 5-4 summarizes the key information about the studies compared in this section.

Table 5-4. ***Key information on the studies compared in Section 5.2.5.1***

	Study	Device	Study Site	Sample Type	Erosion measurement	Range of ER measurements
	Current study	ESETM	Newark Bay	Undisturbed samples	Weight loss (direct measurement)	0- 30,000
1	**(Borrowman et al., 2006)**	Sedflume[14]	Lower Passaic	Undisturbed cores	The core's extrusion rate	4,680-4,680,000
2	**(Witt & Westrich, 2003)**	SETEG[15]	Marckolsheim Reservoir, Germany	Homogenized and manufactured cores	Volume loss (laser measurements)	42,000-220,000
3	**(Robert et al., 1998)**	Sedflume	Quartz particles	Manufactured	Core's upward movement	1,800-3,200,000
4	**Ravens (1997)**	In-situ flume	Boston Harbor	In-situ	Measurement of SSC	0-6,000

[14] Sedflume was designed by McNeil et al. (1996) to measure sediment erosion with depth under high shear stresses.
[15] SETEG was designed by Witt and Westrich (2003) based on Sedflume.

Study1: Borrowman et al. (2006) conducted an erodibility study for the Lower Passaic River sediments. The Passaic is the main river flowing into the Newark Bay, and its lower region is close to the sampling sites of the ESETM study. Figure 5-22 displays a sample of erosion rate graphs published by Borrowman et al. (2006).The erosion rates in this graph are reported in $\frac{cm}{s}$. In order to compare these values to the findings of this study, which are reported in ($\frac{gr}{m^2.hour}$), the conversion factor has been calculated as follows (assuming an average bulk density of 1.3 $\frac{gr}{cm^3}$ according to their study):

$$\mathbf{1\,\frac{cm}{s} = \frac{1 \times 10^4 \times 1.3}{\frac{1}{3600}}\,\frac{\frac{gr}{m^2}}{hour} = 46,800,000\,\frac{gr}{m^2.hour}}$$

The converted units are provided on the top axis of Figure 5-22. It is interesting to note that all the erosion rate values indicated in Borrowman et al.'s report are larger than 4680 $\frac{gr}{m^2.hour}$.

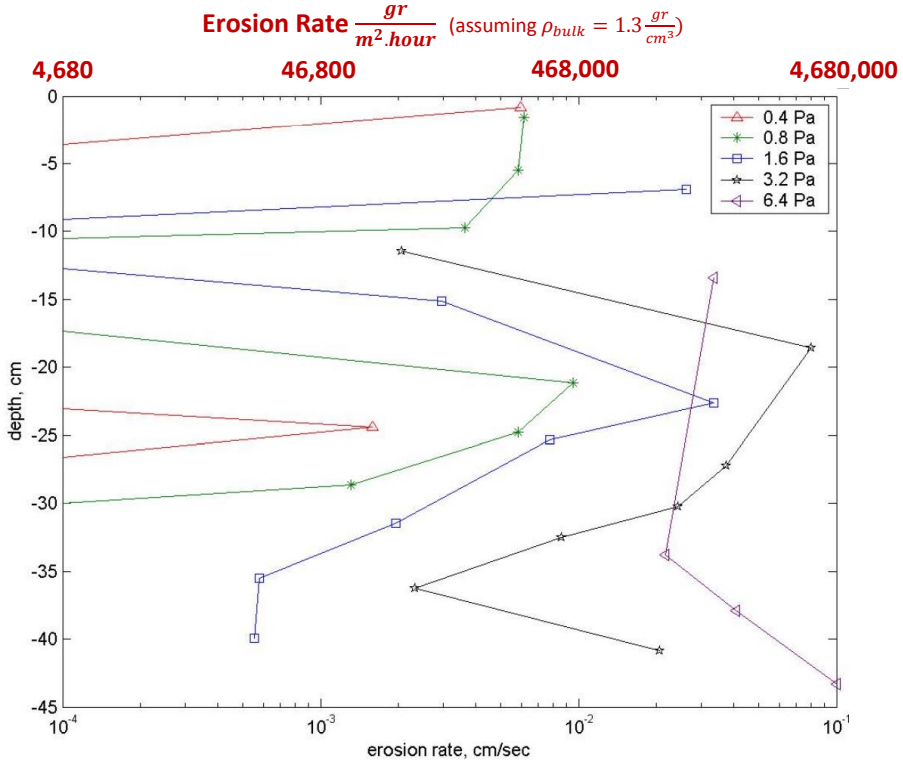

Figure 5-22. **A typical erosion rate graph republished from "Erodibility Study Of Passaic River Sediments Using USACE Sedflume" by T. D. Borrowman et al. (2006)**

Figure 5-23 compares the minimum erosion rate values reported in (Borrowman et al., 2006) with the values obtained in this study. Figure A. 35 and Figure A. 36 also show the observed erosion rates in the units of $\frac{cm}{s}$ and $\frac{mm}{hour}$ respectively. As can be seen in this figure, the current study has been a lot more successful in measuring lower erosion rates. However, it should be noted that such a comparison is only valid when erosion rates obtained by ESETM and Sedflume are compared for tests with similar shear stress levels. Table 5-5 compares the values used in these two studies. Sedflume tests, in general, had higher shear stress levels (0.2-8.0 Pa) compared to ESETM tests (0.1-2.5 Pa as shown in Figure 4-8).

Table 5-5. ***Comparison of average shear stresses of erosion tests in this study with those used in the Sedflume study conducted by Borrowman et al., 2006***

Study	Average Shear Stress	Average Velocity
ESETM (current study)	0.1 – 2.5 Pa	$5 - 80\ \frac{cm}{s}$
Sedflume (Borrowman et al., 2006)	0.2 – 8.0 Pa	$18 - 175\ \frac{cm}{s}$

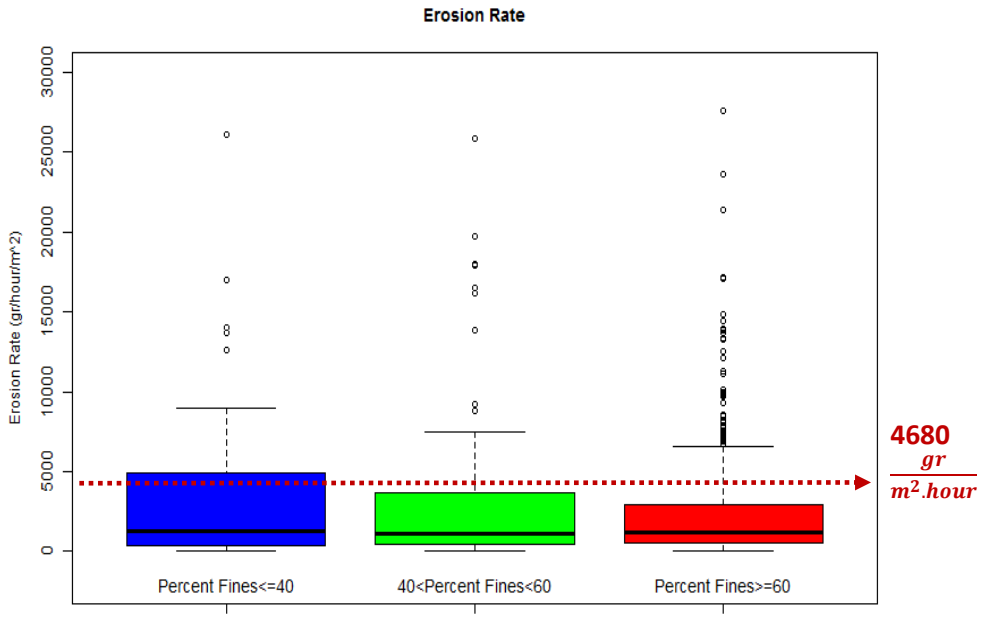

Figure 5-23. **Observed erosion rates for different classes of sediment size (ESETM). The minimum erosion rate value reported in the Sedflume study by Borrowman et al., (2006) is marked by the red arrow**

Wilson (2006) conducted a study to monitor flow velocities at the bottom of the Lower Passaic River in December 2005. He found the average velocity in the Lower Passaic to be 0.4 and 0.2 $\frac{m}{s}$ in the downriver and upriver directions, respectively. Figure 5-24 displays the bottom velocities measured at the Lower Passaic River in blue. By comparing the average velocities in Table 5-5 with the average velocities observed in the Lower Passaic River, we can conclude that

although the shear stresses used in this study are lower than the ones in the Sedflume study, they represent natural conditions more realistically.

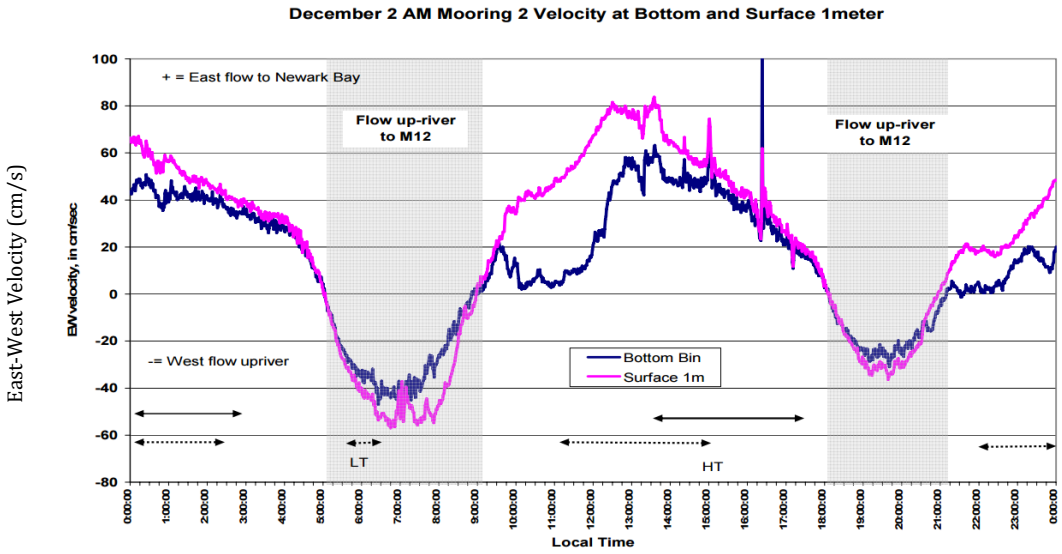

Figure 5-24. **East-west velocity measurements at mooring 2, Lower Passaic River, New Jersey, December 5, 2005. Republished from "Results of Cross-Channel Monitoring During the Lower Passaic River Environmental Dredging Pilot Program on the Lower Passaic River, December 1 to 12" by T. P. Wilson (2006)**

Study 2: The second study (Witt & Westrich, 2003) tested homogenized manufactured sediment cores in a device that was designed based on Sedflume (SETEG). Using laser technology, the researchers in this study measured samples' rate of volume loss as an indicator of erosion rate. Figure 5-25 shows their published results for shear stress levels in the range of 2-4 Pa.

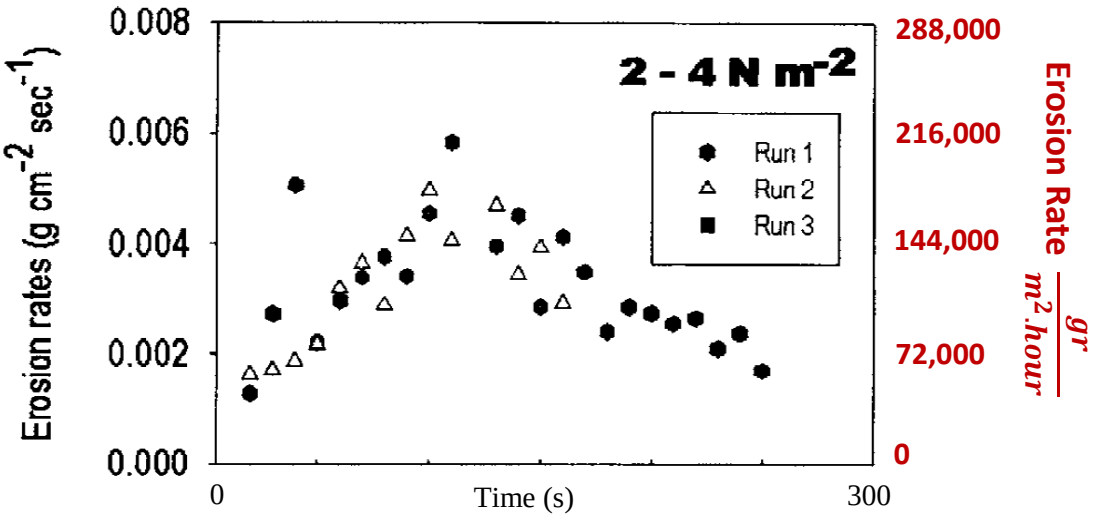

Figure 5-25. **Erosion rates measured by Witt and Westrich (2003) for manually homogenized sediment cores tested at shear stress levels in the range of 2-4 Pa. Republished from "Quantification of erosion rates for undisturbed contaminated cohesive sediment cores by image analysis" by O. Witt and B. Westrich (2003)**

Study 3: Robert et al., (1998) also used Sedflume to study the erosion of manufactured samples made of fine quartz particles. Figure 5-26 shows one of their published graphs.

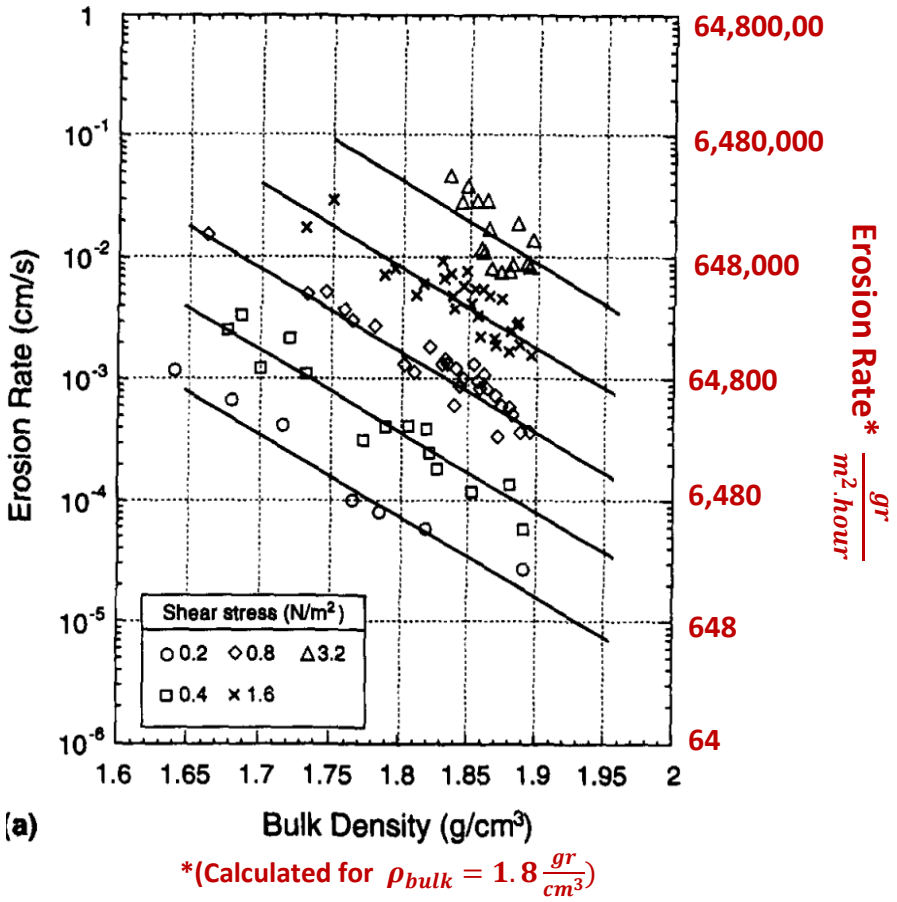

Figure 5-26. **Erosion rate as a function of bulk density for samples made of 14.8-micron quartz particles and tested under different shear stresses. Republished from "Effects of particle size and bulk density on erosion of quartz particles" by J. Robert et al. (1998)**

Study 4: Ravens (1997) conducted in-situ flume experiments to study the resuspension of sediments in the Boston Harbor. He evaluated the shear stress at the bottom of the Harbor comprehensively by taking current, low frequency waves, ocean swell, local wind waves, and boat waves into account. He evaluated the maximum shear stress values to be 0.071, 0.093, 0.092, and 0.17 Pa for low frequency, middle frequency, wind, and boat waves, respectively and his measured shear stresses were in the ranges of $0.076 \pm 0.031\ Pa$ and $0.080 \pm 0.023\ Pa$ at the two study sites. In order to evaluate the erosion rate, he measured the concentration of suspended solids. Figure 5-27 shows the measured erosion rates at one of these sites. Comparison of his

measurements with ESETM's measurements reveals a close match between them. This is a significant achievement for this study as Ravens (1997) found his findings to be consistent with the results of some other in-situ studies at similar sites in other estuaries. The fact that this ex-situ study has been as successful as in-situ studies is quite an achievement.

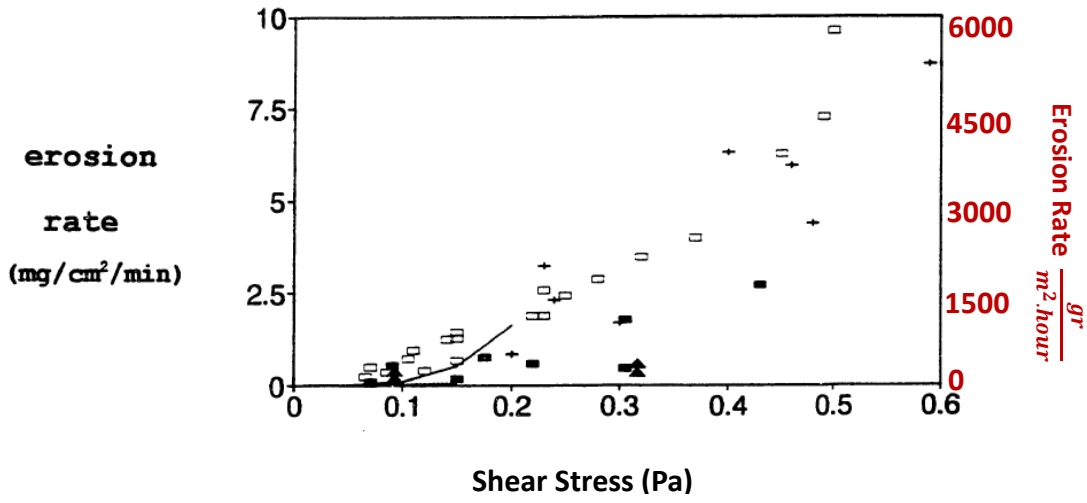

Figure 5-27. **Erosion rates measured by (Ravens, 1997) in the Boston Harbor through six flume experiments in 1995. Republished from "Sediment resuspension in Boston Harbor" by T. M. Ravens (1997). Massachusetts Institute of Technology**

5.2.5.2. Comparison with Other Empirical Models

Among the various forms of empirical models provided in Table 2-6, models 1 and 2 do not depend on critical shear stress. These models were fitted to the fine sediments dataset and the results are summarized in Box 5-3 and Box 5-4.

Model 1 (Table 2-6):

$$\mathbf{ER = \alpha\,|\tau|^{\eta}}\ ^{16} \quad \rightarrow \quad \mathbf{\ln(ER) = \ln(\alpha) + \eta.\ln(\tau)}$$

τ: shear stress

α, η: $\alpha\ \left(\frac{\text{mass}}{\text{Area}\,.\,\text{Time}}\right)$, η is non − dimensional

The model obtained based on this power law equation has an R-squared of 0.17 (Box 5-3) which is much lower than NBFM.

Box 5-3. ***Model summary for:*** $\boldsymbol{ln(ER) = \beta_0 + \beta_1 . ln\,(\tau_{th}) + \varepsilon}$ ***- PF ≥ 60***

lm(formula = ln (Erosion Rate) ~ ln (τ_{th}))

Residuals:

Min	1Q	Median	3Q	Max
-2.895	-0.866	-0.167	0.888	2.817

Coefficients:

	Estimate	Std. Error	t value	Pr (>|t|)
(Intercept)	7.6988	0.1181	65.18	< 0.0000000000000002 ***
ln (τ_{th})	0.7105	0.0978	7.27	0.0000000000048 ***

Signif. codes: 0 '***' 0.001 '**' 0.01 '*' 0.05 '.' 0.1 ' ' 1

Residual standard error: 1.22 on 249 degrees of freedom

Multiple R-squared: 0.175, Adjusted R-squared: 0.172

F-statistic: 52.8 on 1 and 249 DF, p-value: 0.00000000000478

Model 2 (Table 2-6):

$$\mathbf{ER = A\tau^{n}\rho_{Bulk}^{m}}\ ^{17} \quad \rightarrow \quad \mathbf{\ln(ER) = \ln(\alpha) + \eta.\ln(\tau) + m.\ln(\rho_{Bulk})}$$

---

[16] (Lavelle et al., 1984) and others

τ: shear stress

ρ: bulk density

n, m: constants

The results of fitting this model to the data are provided in Box 5-4. The R-squared value for this model is 0.43.

Box 5-4. ***Model summary for: ln(ER)=β0+β1.ln(τ_{th})+ β2.ln(ρ_{Bulk})+ϵ - PF ≥ 60***

lm(formula = ln (Erosion Rate) ~ ln (τ_{th})+ ln (ρ_{Bulk}))

Residuals:

Min	1Q	Median	3Q	Max
-2.6633	-0.7262	-0.0533	0.7326	2.9944

Coefficients:

	Estimate	Std. Error	t value	Pr (>|t|)	
(Intercept)	10.4115	0.3053	34.11	<0.0000000000000002	***
ln (τ_{th})	0.8719	0.0858	10.16	<0.0000000000000002	***
ln (ρ_{Bulk})	-11.3382	1.2033	-9.42	<0.0000000000000002	***

Signif. codes: 0 '***' 0.001 '**' 0.01 '*' 0.05 '.' 0.1 ' ' 1

Residual standard error: 1.05 on 248 degrees of freedom

Multiple R-squared: 0.392, Adjusted R-squared: 0.388

F-statistic: 80.1 on 2 and 248 DF, p-value: <0.0000000000000002

If this model is compared to the previous model (Box 5-3), it can concluded that bulk density is a significant contributor for the determination of erosion rates as it increased the R-

[17] (Roberts et al., 1998), (Jepsen et al., 1997), and others

squared from 0.17 to 0.43. Comparison of this model with NBFM reveals that adding water content to regressors also increased the R-squared (from 0.43 to 0.53).

5.2.6. Conclusion and Discussion

Earlier in this chapter, NBFM and NBCM (models) were developed (5.2.3) and validated (5.2.4) and their performance was evaluated and compared with models developed by other researchers (5.2.5). The data used for developing these models was obtained from erosion tests on undisturbed samples (taken from the Newark Bay, NJ in 2012) using the Ex-Situ Erosion Testing Machine (ESETM).

(1) Newark Bay Fine Model (NBFM) based on 251 observations - PF $\geq$ 60

$$\mathbf{ln(ER) = \beta_0 + \beta_1 . ln(V) + \beta_2 . \rho_{Bulk} + \beta_3 . W + \varepsilon}$$

$$\mathbf{ER = e^{\beta_0 + \beta_1 . ln(V) + \beta_2 . \rho_{Bulk} + \beta_3 . W + \varepsilon}}$$

(2) Newark Bay Coarse Model (NBCM) based on 44 observations - PF $\leq$ 40

$$\mathbf{ln(ER) = \beta_0 + \beta_1 . V + \beta_2 . \rho_{Bulk} + \beta_3 . O + \varepsilon}$$

$$\mathbf{ER = e^{\beta_0 + \beta_1 . V + \beta_2 . \rho_{Bulk} + \beta_3 . O + \varepsilon}}$$

The main points regarding this analysis are as follows:

1- Both NBFM and NBCM were valid models with significant P-values. Their R-squared values were 0.53 and 0.63 respectively. Since R-squared values for experimental erosion studies are not frequently reported in the literature, it is difficult to compare the prediction power of different tests. One of the very few studies that measured R-squared was conducted by Hamilton and Mitchell (1996). They reported R-squared values ranging from 0.47-0.73 for their empirical model developed based on samples taken from seven lakes in New Zealand.

2- Even though this study focused mainly on the erosion behavior of cohesive sediments, a model was also developed for non-cohesive samples. Thus, the linear regression approach adds further value to research on sediment erosion by providing a practical and robust framework that can be used to study both fine and granular sediments. However, no sufficient linear model could be created for samples with the percentage of fines between 40 and 60. This could be caused by an inherently different erosion behavior for mixtures of fine and coarse sediments or could be attributed to inaccuracies in the measurements of percentages of fines for the samples. It is critical to note that in this study, percentages-of-fines tests were performed on a mixture of subsamples taken from all the tested subsections of each core. Consequently, it is hypothesized that the cores with percentages of fines between 40 and 60 were actually composed of both cohesive and granular subsections. In order to avoid such inaccuracies in the future, measurements should be taken from each section of the core to obtain more representative percentage-of-fines values for individual samples.

3- One of the main conclusions drawn from the literature review was that erosion of natural sediments has not been well studied at low shear stress levels. This is in part because most of the techniques used for the measurement of erosion rates are incapable of detecting low rates of erosion. Prevalent use of the poorly defined concept of critical shear stress is also a major contributor to the present confusion in erosion behavior of cohesive sediments at low shear stresses. Another factor hindering erosion tests at low shear stresses is the limitations of some of the shear stress measurement techniques. The current study has successfully addressed this shortcoming in the literature by providing empirical insight into the behavior of cohesive sediments at low shear stresses.

4- The considerable size of the dataset used for fine sediments (251) gives this research an advantage when compared to similar studies with relatively small sizes of the datasets. For example, the sample size used by Hamilton and Mitchell (1996) – one of the only

studies that had reported R-squared values – was in the range of 13-55 for each of the lakes they studied.

5- It should be noted that the datasets corresponding to fine and coarse sediments did not have comparable sizes. While the fine dataset included 251 observations, there were only 44 observations in the coarse dataset.

6- The form of the relationship between erosion rate and flow velocity varies between NBCM and NBFM. While average velocity is one of the regressors in the former, its natural logarithm is among the regressors in the latter. Some other studies in the literature (including (Roberts et al., 2000) and (Jepsen et al., 1997)) also found the same type of relationship for cohesive sediments.

7- Both NBFM and NBCM indicate the presence of a negative correlation between bulk density and erodibility. In addition to flow velocity and bulk density, NBFM and NBCM depended on water content and organic content respectively. While the water-content parameter is 0.03 in NBFM, the organic-content parameter is -0.91 in NBCM. This indicates that in coarse sediments of the Newark Bay, a higher organic content will result in a lower erodibility. This might be in part explained by the correlation between bulk density and organic content.

8- Although many researchers have studied the impact of depth on erosion, this study did not find any significant relationship between depth and erosion rate in either NBFM or NBCM.

9- Negative weight losses were measured in almost 8% of erosion tests (67 out of 755) indicating that the sample actually gained weight during the erosion test. Given the high level of confidence in the accuracy of weight measurements, this phenomenon is attributed to the presence of gas in the samples. Flow of water into air voids can replace the gas, which results in negative weight losses. This hypothesis was validated by the fact

that most negative values were observed in the initial test steps when the sample had just been exposed to air for preparation.

In order to mitigate this problem, all the observations with negative values (67 out of 755) were removed from the dataset. However, this did not completely address the possibility of such an error in the remaining measurements. Thirteen observations that had erosion rates larger than 30,000 $\frac{gr}{hour.m^2}$ were considered as outliers and removed before fitting the models.

10- All the techniques and methods used for measuring average velocity, bulk density, weight loss, and water and organic content were very accurate and reliable, especially when compared to most other erosion studies. Consequently, the observed error can be mainly attributed to model prediction. However, the observed negative weight losses increase the uncertainty in weight loss measurements not because of the measurement technique but because they added a physical factor that could not be controlled or measured.

5.3. Stochastic Analysis

This section introduction is devoted to stochastic analysis of the results and includes four sections on introduction, analysis, model evaluation, and discussion.

5.3.1. Introduction

In Section 5.2.3, two linear regression models were developed for the Newark Bay samples tested in ESETM and it was concluded that both models have acceptable prediction power. Figure 5-28 and Figure 5-29 compare the density distribution of observed erosion rates with predicted rates for NBFM and NBCM respectively. However, it should be noted that the distributions displayed in these two figures completely depend on the experimental design of the

study. This means that if more tests were conducted at higher velocities, higher erosion rates would push the curves upward.

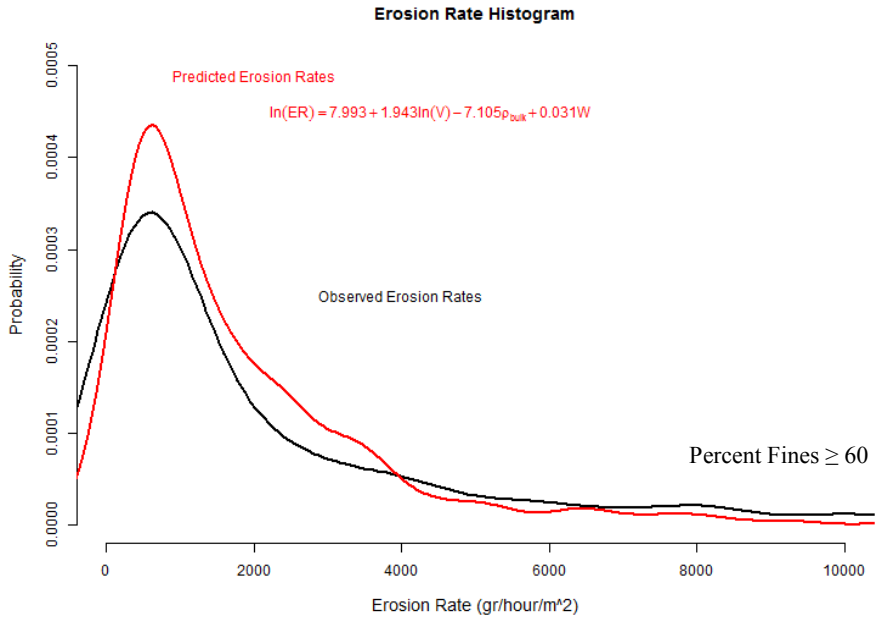

Figure 5-28. **Density distribution of observed and predicted erosion rates (NBFM)**

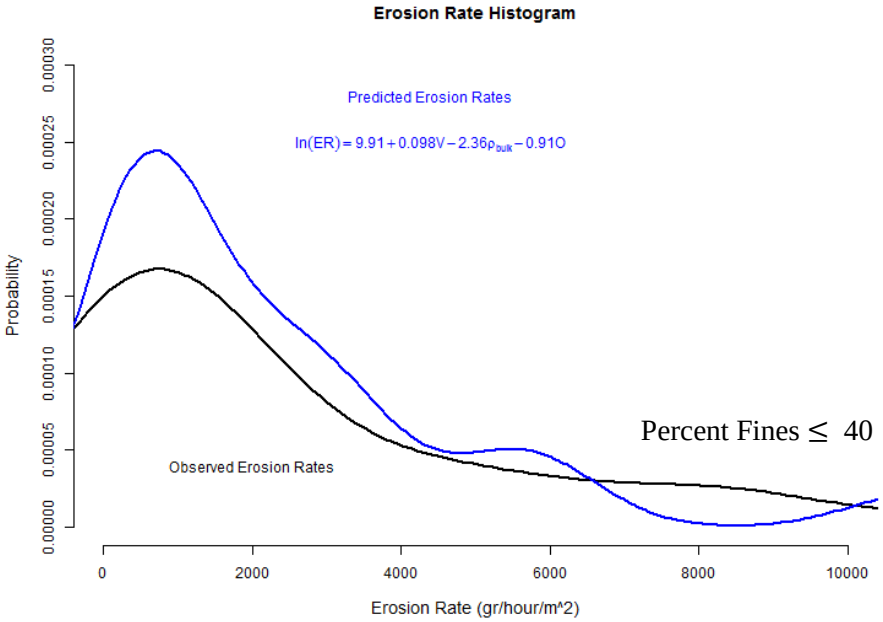

Figure 5-29. **Density distribution of observed and predicted erosion rates (NBCM)**

In such cases, stochastic simulation can be used to simulate random natural scenarios and build confidence intervals for predictions. Although stochastic analysis has been previously used for sediment erosion (Section 2.3.6.3), to the best of the author's knowledge, the approach used in this study has not been previously used in any cohesive sediment erosion studies. Section 5.3.2 explains the analysis process and provides the results. In Section 5.3.3, the Newark Bay Fine Model was interestingly evaluated using an independent dataset that was not used for developing the model. The main conclusions from the stochastic analysis are provided in section 5.3.4.

5.3.2. Analysis

Stochastic simulation is the use of stochastic processes to generate various realizations of a variable with statistical characteristics similar to those of the observed data. On one hand, the complexity of sediment transport processes precludes the application of purely analytical methods. On the other hand, limited access to experimental data makes it challenging to take randomness into account, apply a model to different situations (combinations of input values), and compare model predictions for different scenarios. As simulation techniques provide a potential solution to these challenges, the Monte Carlo simulation method was applied in this study. This method simulates multiple experiments by using sets of artificially generated input

variables, resulting in the distribution of possible model predictions.

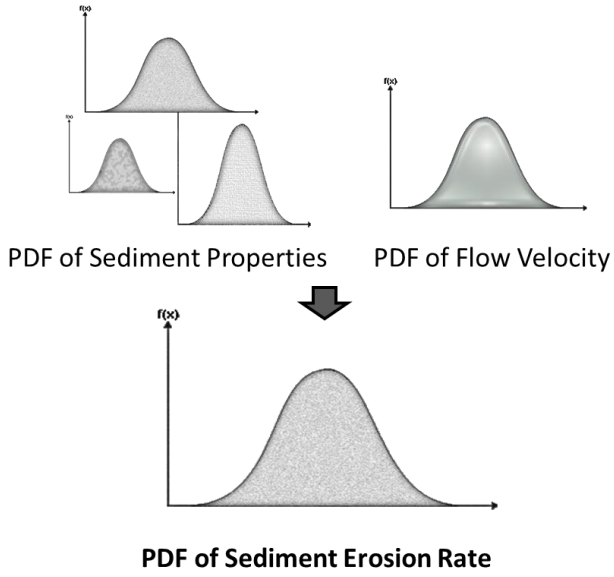

Figure 5-30 presents the main idea involved in applying the Monte Carlo method to the results of this erosion study.

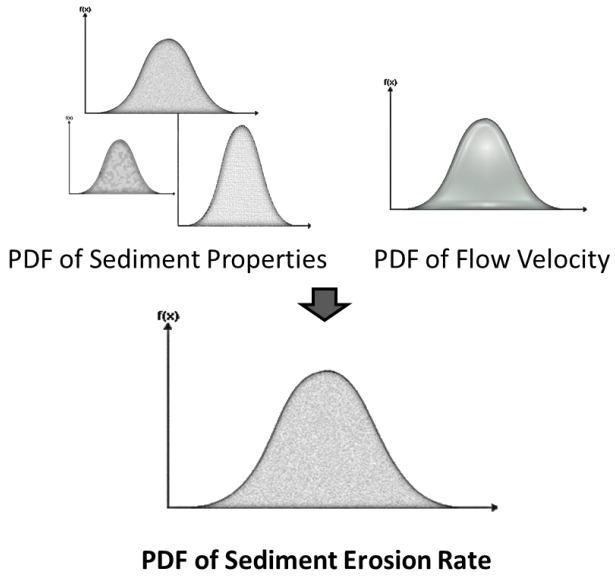

***Figure 5-30*. Steps involved in stochastic simulation of erosion**

In this study, pseudo-populations of input factors were created by drawing random samples from the observed dataset. The model's output is the Monte Carlo estimate of the sampling distribution of the weight of eroded material per hour and per unit area of the surface when exposed to the assumed velocity distribution.

Figure 5-31 shows the cumulative frequency distribution of erosion rates simulated for different velocities using the original (observed) sediment parameters and velocities of 10, 20, 30, and 40 $\frac{cm}{s}$ and Figure 5-32 compares the empirical cumulative frequency distribution of the observed, predicted and simulated data. Both these figures are based on NBFM and the corresponding results for NBCM are presented in Figure 5-33 and Figure 5-34.

The information gained with the help of stochastic analysis provides a deep insight on erosion risk analysis. This is very helpful for both researchers and policy makers to predict and decide more realistically. Another advantage of stochastic models is that they provide a feasible platform for the comparison of the confidence interval of predictions made by different models for any specific scenario.

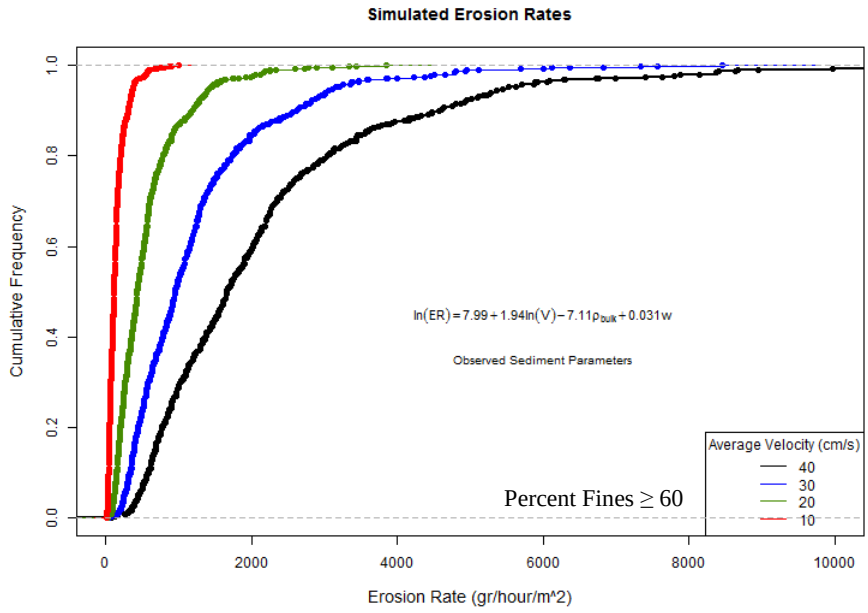

Figure 5-31. **Cumulative frequency distribution of erosion rates simulated for different velocities using the original (observed) sediment parameters and four velocity levels– Simulations are based on NBFM**

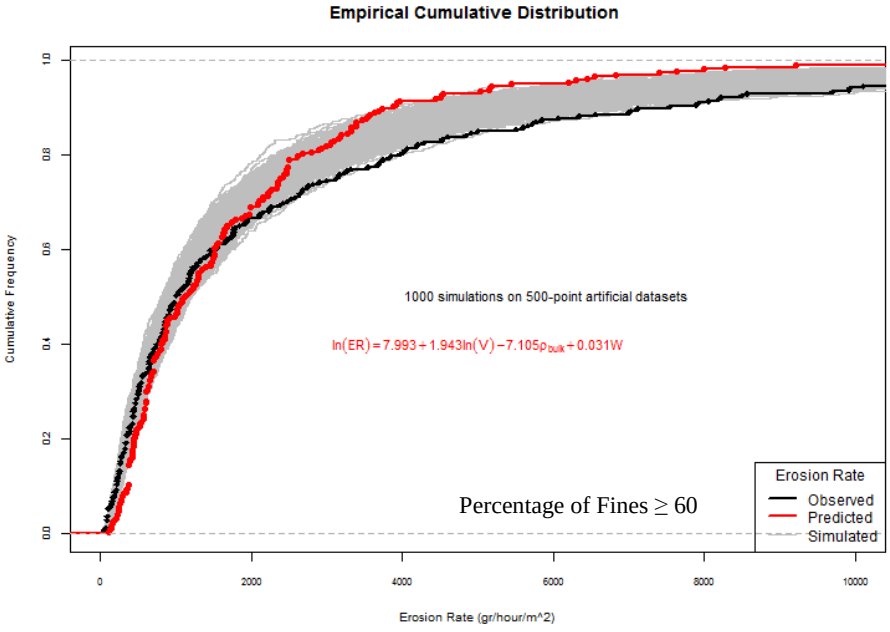

Figure 5-32. **Empirical cumulative frequency distribution of the observed, predicted and simulated data – Simulations are based on NBFM**

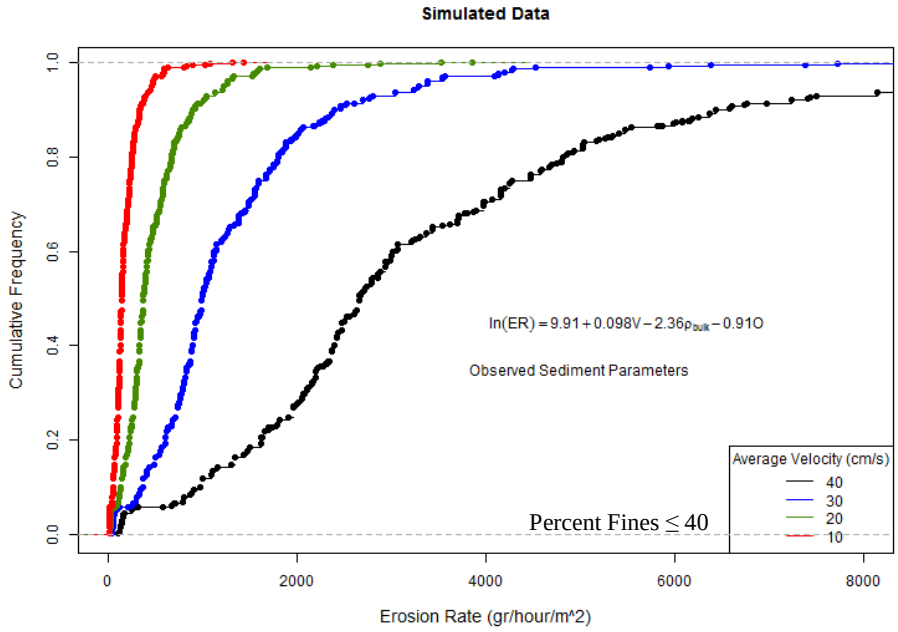

Figure 5-33. **Cumulative frequency distribution of erosion rates simulated for different velocities using the observed sediment parameters (at four velocity levels) – Simulations are based on NBCM**

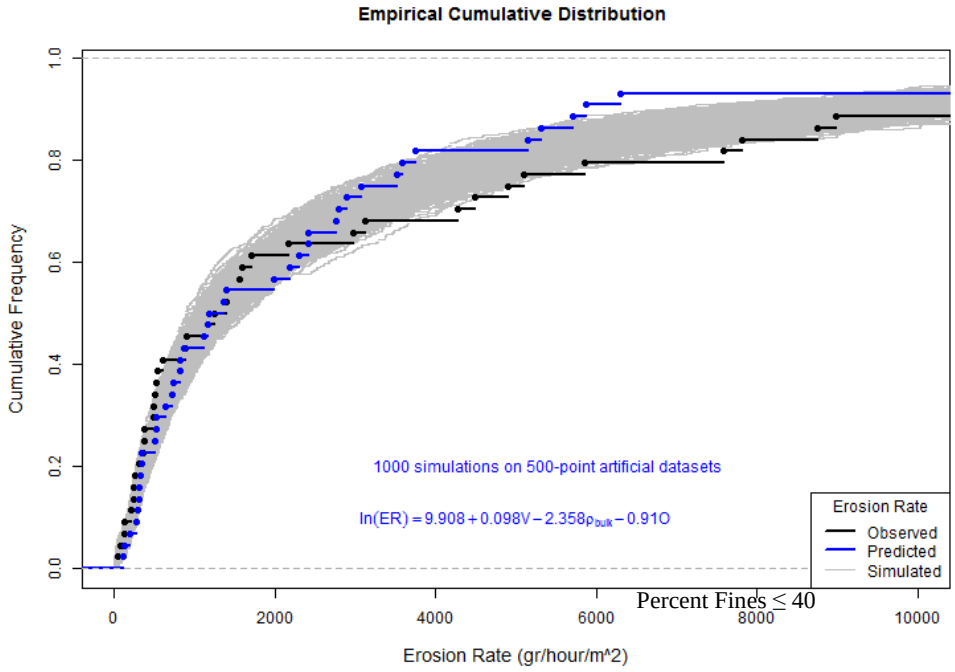

Figure 5-34. **Empirical Cumulative frequency distribution of the observed, predicted and simulated data - Simulations are based on NBCM**

5.3.3. Model Evaluation

Finally, the stochastic analysis methodology developed in Section 5.3.2 was validated using a set of partially new data that was not used for model development (training). This data came from samples obtained from the Newark Bay in the first two days of sample collection. Two hundred and sixty-three erosion tests were conducted on thirty-one samples taken from eight cores. Only erosion rate (ER) and average velocity (V) were measured in these tests and hence, index properties were not available. Figure 5-35 shows the cumulative frequency distribution of erosion rates measured in these tests. The gray curves represent the results of 1000 simulations using the average velocities used for the actual tests combined with bulk density and water content values simulated based on the measurements obtained from other samples. Although data was not available on the percentage of fines for these samples, it was assumed that all the samples had more than 60% of fines and hence NBFM was used for them.

According to Figure 5-35, the stochastic approach is fairly successful in predicting the erosion rates for an independent dataset. The stochastic simulation results overestimate the erosion rates in the range below 4000 $\frac{gr}{m^2.hour}$. However, it is much more successful in higher erosion rates.

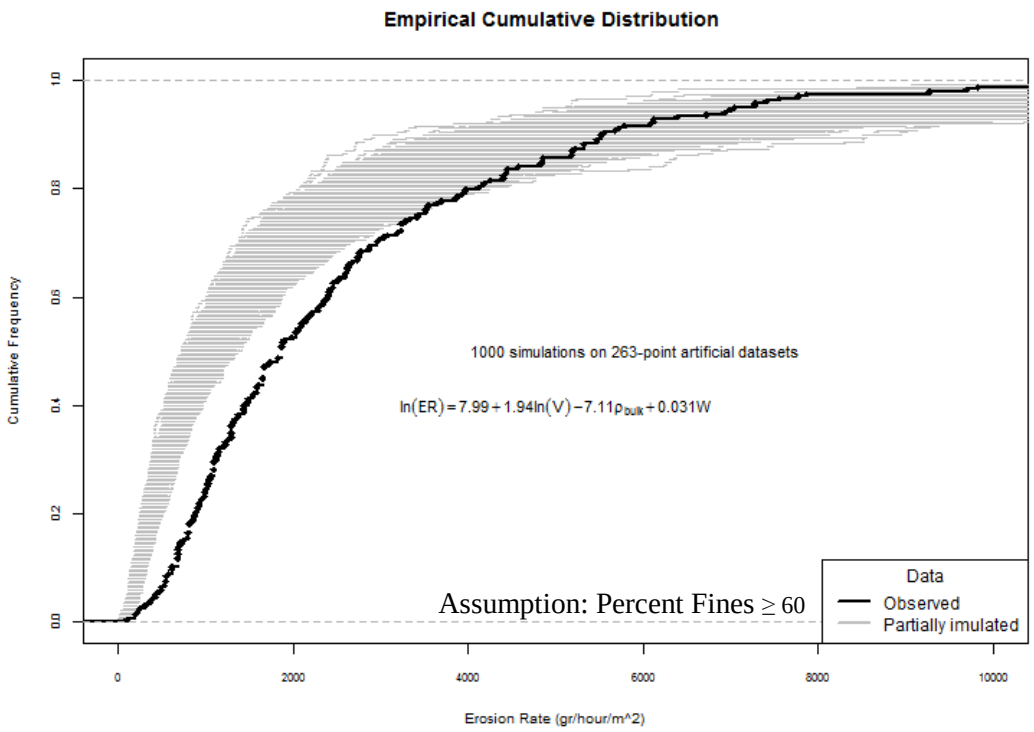

Figure 5-35. **Empirical cumulative frequency distribution of new observations compared with simulated data. The erosion rate values and average velocity values used to generate this graph (238 points) were not used for training the regression model and hence can be considered as a new validation set. However, as index properties were not determined for this validation set, it has been assumed that all the samples contained more than 60% of fines and artificial bulk density and water content values were used based on the rest of the tests.**

5.3.4. Discussion

1- In Section 5.3, the regression model developed in Section 5.2 was used to perform the stochastic analysis. To the best of the author's knowledge, such an approach to stochastic analysis has not been previously conducted in the literature of cohesive sediment transport.

2- The information gained with the help of stochastic analysis provides a deep insight on erosion risk analysis. This is very helpful for both researchers and policy makers to predict and decide more realistically. Another advantage of stochastic models is that they offer a feasible platform for the comparison of the confidence interval of the predictions made by different models for any specific scenario.

3- The Monte Carlo simulation method was applied to the selected regression models to stochastically predict erosion rates for synthetically generated input parameters. To the best of the author's knowledge, this technique has not been used previously in the study of sediment erosion.

4- A partially new dataset (including erosion rate and average velocity measurements only) which was not used for model development was used to validate the stochastic analysis methodology and it was concluded that the stochastic analysis conducted in Section 5.3 is meaningful and helpful.

6. CONCLUSION

"The eventual goal of understanding and predicting fine sediment erodibility on the basis of more readily measured sediment properties remains a very important one."[18]

This study aimed to predict the erosion behavior of cohesive sediments at flow velocities below 1 $\frac{m}{s}$ based on their index properties. In summary, the main outcomes of this study are as follows: (1) Two fairly valid erosion models were developed for fine- and coarse-grained sediments of the Newark Bay. (2) A framework was developed for stochastic analysis of erosion test results. (3) An experimental methodology was designed for comparatively less subjective measurement of erosion rates at low shear stress levels. (4) A probabilistic modeling platform was developed to explore the impact of experimental design on interpretation of erosion test results. (5) A comprehensive review of the literature on scale-related issues in cohesive sediment transport was conducted. (6) A novel erosion testing flume – Ex-Situ Erosion Testing Machine (ESETM) – was assessed for its potential to be used in sediment erosion studies. (7) A comprehensive literature review was conducted on cohesive sediment transport with emphasis on erosion.

The discussion of the major results and contributions of this study is organized into three parts: (1) literature review, (2) methodology, and (3) analysis.

[18] Larry Sanford (Sanford, 2006)

Literature Review

1- A main conclusion drawn from the literature review is that erosion of natural sediments has not been well studied at low shear stress levels. This is in part because most of the techniques used for the measurement of erosion rates are incapable of detecting low rates of erosion. Prevalent use of the poorly defined concept of critical shear stress is also a major contributor to the present confusion in the erosion behavior of cohesive sediments at low shear stress levels.

2- The experimental methodology and data interpretation scheme in this research were devised based on the critical analysis of previous literature and aimed to reduce uncertainty, subjectivity, and arbitrariness.

3- In conducting empirical studies on erosion, spatial heterogeneity and temporal variation in properties of natural cohesive sediments, together with the lack of physical modeling of erosion pose significant challenges to predict sediment erosion.

4- Physics-based models might fit a limited set of experimental data well but are only applicable to the particular material tested and under conditions similar to the testing conditions. This is due to both the complex nature of sediment erosion and the extensive input parameters required by such models. Contrarily, a purely empirical erosion model that concentrates on the most significant factors can be generalized to a wider variety of materials and conditions. There is a great need for such models, as complex physics-based models demand extensive accurate inputs that cannot be realistically measured in large-scale real-world situations.

5- Another important aspect explored in this study is the concept of scale. The concept of scale in the sediment transport field, if not completely ignored, has generally been used in an unclear or inaccurate manner. Presently, there is no clear indication of the different scales associated with most sediment transport studies especially in the case of modeling scales. This is a serious barrier to comparing the results from different studies. There is a need for a

framework that guides researchers through dealing with the issue of scale in their erosion studies. This study investigates various scale-related aspects in cohesive sediment transport based on the current literature, and is the first step toward developing a holistic framework.

6- A final point worth mentioning is that researchers in the field of cohesive sediment erosion should weigh a model's complexity and comprehensiveness on one hand with its accuracy and reliability on the other hand. A legitimate question that arose in this context is: which model is better? A more complex model with poorly measured input variables (e.g. critical shear stress) or a simpler model with fewer well-defined parameters measured more accurately and less subjectively?

Methodology

1- In this study, 755 erosion rate tests were conducted on 142 fairly undisturbed samples taken from 24 cores extracted from the Newark Bay. The considerable size of the dataset used for fine sediments (251) gives this research an advantage when compared to similar studies with relatively small sizes of the datasets.

2- Comparison of erosion measurements made in this study with the results of some in-situ studies reveals a strong consistency between them. The fact that this ex-situ study has been as successful as in-situ studies is quite an achievement.

3- The success of the devised experimental methodology is also highlighted when the results are compared to similar ex-situ studies as the range of erosion rates measured in this study are well beyond the capability of many other methods.

4- After the Ex-Situ Erosion Testing Machine was assembled, installed, and calibrated, extensive research was conducted to evaluate its performance. Significant effort was made in implementing a scientific methodology to identify the strengths and weaknesses of ESETM and evaluate the accuracy and reliability of its measurements. Subsequently, the research

objective was transformed into "prediction of erosion rate for cohesive sediments of the Newark Bay at flow velocities below 1 $\frac{m}{s}$ and based on index properties."

5- To further ensure that the samples represented natural sediments, preservation and preparation methods were chosen after testing several techniques to minimize sample disturbance. One of the limitations found in the experimental phase of this study was the geometric constraint imposed by the edge of the ring confining the sample during erosion tests. Although the device's elevator provided the required flexibility to push the sample upward, the decision of when to move the sample was left to the technician's discretion. In order to minimize the level of subjectivity, shorter tests were performed on more samples and long tests were avoided. In general, it can be concluded that the field and laboratory protocols established for this study were followed thoroughly and generated consistent data.

6- An observation worth mentioning again is the presence of a significant amount of gas in the tested samples. In order to determine whether this occurred only due to the penetration of air into the samples during sample preparation, a few undisturbed samples taken from the bay were kept entirely submerged until they were placed in a vacuum chamber. The noticeable amount of gas observed in these samples was not an unexpected result due to the presence of organic material in natural sediments. However, it drew attention to the unrealistic saturation assumption made by many erosion researchers (including McNeil et al., 1996; Jepsen et al., 1997; Roberts et al., 2000; and Borrowman et al., 2006 among others) when determining a sample's bulk density based on its water content and specific gravity (to observe this illustration, refer back to Figure 3-8).

7- All the techniques and methods used for measuring average velocity, bulk density, weight loss, and water and organic content were very accurate and reliable, especially when compared to most other erosion studies. Consequently, the observed errors were primarily attributed to model's predictive power. However, the presence of negative weight losses

increases the uncertainty in weight loss measurements not because of the measurement technique but because of adding a physical factor that is not measurable or controllable.

Analysis

Regression Analysis

1- Regression analysis of the data resulted in the development of two fairly valid models for fine- and coarse-grained sediments of the Newark Bay: NBFM and NBCM.

(1) Newark Bay Fine Model (NBFM) based on 251 observations - PF ≥ 60

$$\mathbf{ln(ER) = \beta_0 + \beta_1 . ln(V) + \beta_2 . \rho_{Bulk} + \beta_3 . + \varepsilon}$$

$$\mathbf{ER = e^{\beta_0 + \beta_1 . ln(V) + \beta_2 . \rho_{Bulk} + \beta_3 . W + \varepsilon}}$$

(2) Newark Bay Cine Model (NBCM) based on 44 observations - PF ≤ 40

$$\mathbf{ln(ER) = \beta_0 + \beta_1 . V + \beta_2 . \rho_{Bulk} + \beta_3 . O + \varepsilon}$$

$$\mathbf{ER = e^{\beta_0 + \beta_1 . V + \beta_2 . \rho_{Bulk} + \beta_3 . O + \varepsilon}}$$

2- In order to validate NBFM and NBCM, the models were cross-validated, compared to other models in the literature, and validated by using a new (independent) dataset.

3- Both NBFM and NBCM were relatively valid models with significant P-values. Their R-squared values were 0.53 and 0.63 respectively. The fact that R-squared values for experimental erosion studies are not frequently reported in the literature makes it difficult to compare the prediction power of different tests. One of the very few studies that measured R-squared was conducted by Hamilton and Mitchell (1996) who reported R-squared values ranging from 0.47-0.73 for their empirical model developed based on samples taken from seven lakes in New Zealand.

4- To enhance the accuracy of the model, only those variables that could be determined by persistent processes were included. Consequently, critical shear stress, which is the most important factor in many empirical erosion models, has not been used in the proposed model because of the numerous discrepancies between different researchers in the definition and

measurement of this factor. Additionally, the literature reveals that there is a high chance of erosion even at shear stress levels well below the average critical shear stress (Lopez & Garcia, 2001), thus calling into question the very validity of this concept. Another source of discrepancy in the findings of different studies is the methodology used for the estimation of shear stress giving rise to inconsistent shear stress values. Since there is no universal method to obtain shear stress values, the proposed model avoided the inclusion of this factor. Instead, this model includes flow velocity, which is a commonly used indicator of shear stress.

5- The suggested modeling framework avoids dependency on too many parameters. This might yield a poorer fit to the observed data (than more complex models) in the calibration phase but eliminates over-parameterization, which can result in a more robust performance in the verification phase (Merritt et al., 2003). Given the high spatial variability of the factors used in erosion models, complicated models that include numerous factors or suggest complex forms cannot be generalized to any domain other than the ones for which they have been obtained. With a simpler model on the other hand, the level of uncertainty can be reduced through the acquisition of more samples representing the domain.

6- Even though this study focused mainly on the erosion behavior of cohesive sediments, a model was also developed for non-cohesive samples. Thus, the linear regression approach adds further value to the research on sediment erosion by providing a practical and robust framework that can be used to study both fine and granular sediments. However, no sufficient linear model could be created for samples with percentage of fines between 40 and 60. This could be caused by an inherently different erosion behavior for mixtures of fine and coarse sediments, or otherwise attributed to inaccuracies in determination of percentage of fines. It is critical to note that in this study, *percentage of fines* tests were performed on a mixture of subsamples taken from all the tested subsections of each core. Consequently, it can be hypothesized that the cores with percentages of fines between 40 and 60 were actually composed of both cohesive and granular subsections. In order to avoid such inaccuracies in

the future, measurements should be taken from each section of the core to get percentage of fines values that are more representative of individual samples.

It should be noted that the datasets corresponding to fine and coarse sediments did not have similar sizes. While the fine dataset included 251 observations, there were only 44 coarse data points available.

Stochastic Analysis

1- A new methodology was developed for the stochastic analysis of erosion by applying the Monte Carlo simulation technique to NBFM and NBCM. To the best of the author's knowledge, this technique has not been used previously in the study of sediment erosion. The availability of such a robust stochastic process makes it possible to study the erosion behavior of sediments over many artificially generated samples (in lieu of measured data), resulting in higher levels of confidence in predictions.

2- The information gained with the help of stochastic analysis provides a deep insight on erosion risk analysis. This is very helpful for both researchers and policy makers to predict and decide more realistically.

3- A partially new dataset (including erosion rate and average velocity measurements only), which was not used for model development, was used to validate the stochastic analysis methodology and it was concluded that the stochastic analysis conducted in Section 5.3 is meaningful and helpful.

Probabilistic Analysis

1- The framework developed in section 3.5.2 for the probabilistic analysis of erosion data offers a standardized methodology for data analysis that paves the way for the comparison of different studies. The main takeaways from this analysis are: (1) Classification of sediments to uniform clusters, which was initially conducted by Van Prooijen and Winterwerp (2010), is an effective method to capture the time-dependent erosion behavior of sediments. (2) As

clearly indicated in Figure 3-37, design of the experiment has a significant role in the results of erosion tests and this should be considered in the analysis and interpretation phases. (3) The results obtained by this new methodology are not dependent on any particular testing arrangement. (4) This framework can be considered as an initial step toward comparing the results obtained in different studies. (5) Although the optimization problem is ill-posed (as is typical for inverse problems) and has no unique optimal solution, modifications in the design of experiments can help select the most interpretable result from the set of possible solutions.

2- The probabilistic analysis conducted in this study clearly indicated the significant impact of the design of erosion experiments – specifically the length and order of different shear stress levels applied to sediments – on experimental outcomes.

3- The probabilistic analysis clearly demonstrated that the validity of measurements decreases as more tests are conducted on one sample because of the impact of shear history. It can be concluded that for the purpose of this study, the number of shear stress steps to which a sample is exposed should be limited to avoid unrealistic results.

Future Research

1- The erosion behavior of sediments with percent fines between 40 and 60 needs more research.

2- The predictions made by the Newark Bay Corse Model can be compared with available models for prediction of granular sediments.

3- If models similar to NBFM and NBCM are further validated, the next important step will be to develop practical techniques for extensive measurement of the index properties required by these models (bulk density, percent fines, and water and organic content).

4- The probabilistic framework developed in this study for the analysis of erosion rate data is independent of the experimental design, which opens the way for the comparison of different studies.

APPENDIX A.

Other graphs, tables and boxes

Richard N. Weeks

Soil Sediment Managemant Laboratory

Core Acquisition Data						
Date						
Core#	ID	Time	Sampling method	Depth	Thick.	Photos
	Sample Description/comment					
	Sampling Coordination	X		Y		
	Location Description					
	Sample Description/comment					
	Sampling Coordination	X		Y		
	Location Description					
	Sample Description/comment					
	Sampling Coordination	X		Y		
	Location Description					

RUTGERS Center for Advanced Infrastructure and Transportation

Science beneath the surface

Form Number 1- 1

Figure A. 1. Core Acquisition Data (Form 1)

Richard N. Weeks

Soil and Sediment Managemant Laboratory

Ring Identification Data

	Thickness	R#	Date	Time		Thickness	R#	Date	Time		Thickness	R#	Date	Time
Core ID					Core ID					Core ID				
C01					**C02**					**C03**				
Thickness					Thickness					Initial Thickness				
Core ID					Core ID					Core ID				
C04					**C05**					**C06**				
itial Thickne					tial Thickn					itial Thickne				

RUTGERS
Center for Advanced Infrastructure and Transportation

Form Number 2- 1

Science beneath the surface

Figure A. 2. Ring Identification Data (Form 2)

Richard N. Weeks

Soil and Sediment Managemant Laboratory

Undisturbed Sample Identification Form

Count	Coring Date	Sampling Date	Core #	Ring #	Sample #	Top dep.	Bot. dep.	Testing Date	Age	Sample ID	Test ID
1											
2											
3											
4											
5											
6											
7											
8											
9											
10											
11											
12											
13											
14											
15											
16											
17											
18											

RUTGERS
Center for Advanced Infrastructure and Transportation

Form Number: 3-1

Science beneath the surface

Figure A. 3. Undisturbed Sample Identification Form (Form 3)

Table A. 4. Parameters used in simulations 1 and 2 presented in *Figure 3-40* (10-minute long test steps)

	Simulation 1			**Simulation 2**			
	Material cluster			Material cluster			
	I	II	III	I	II	III	IV
	Weight proportion			**Weight proportion**			
	0.12	0.11	0.77	0.11	0.00	0.26	0.60
Level	**Probability of erosion**			**Probability of erosion**			
1	0.98	0.02	0.00	0.97	0.009	0.00	0.00
2	0.99	0.06	0.00	1.00	0.076	0.02	0.00
3	1.00	0.23	0.00	1.00	0.336	0.03	0.00
4	1.00	0.23	0.00	1.00	0.342	0.03	0.00
5	1.00	0.76	0.02	1.00	0.512	0.07	0.00
6	1.00	0.76	0.03	1.00	0.743	0.52	0.02
7	1.00	0.76	0.03	1.00	0.957	0.70	0.02
8	1.00	0.76	0.32	1.00	0.957	0.79	0.02

Table A. 5. Parameters used in simulations 1 and 2 presented in Figure 3-41 (20-minute long test steps)

	Simulation 1			**Simulation 2**			
	Material cluster			Material cluster			
	I	II	III	I	II	III	IV
	Weight proportion			**Weight proportion**			
	0.12	0.16	0.72	0.03	0.30	0.177	0.50
Level	**Probability of erosion**			**Probability of erosion**			
1	0.73	0.00	0.00	0.82	0.12	0.00	0.00
2	0.75	0.10	0.00	0.82	0.12	0.00	0.00
3	0.95	0.53	0.00	0.82	0.16	0.03	0.02
4	0.98	0.66	0.09	0.92	0.92	0.08	0.02
5	1.00	0.72	0.20	1.00	0.97	0.87	0.14
6	1.00	0.85	0.82	1.00	1.00	0.97	0.82

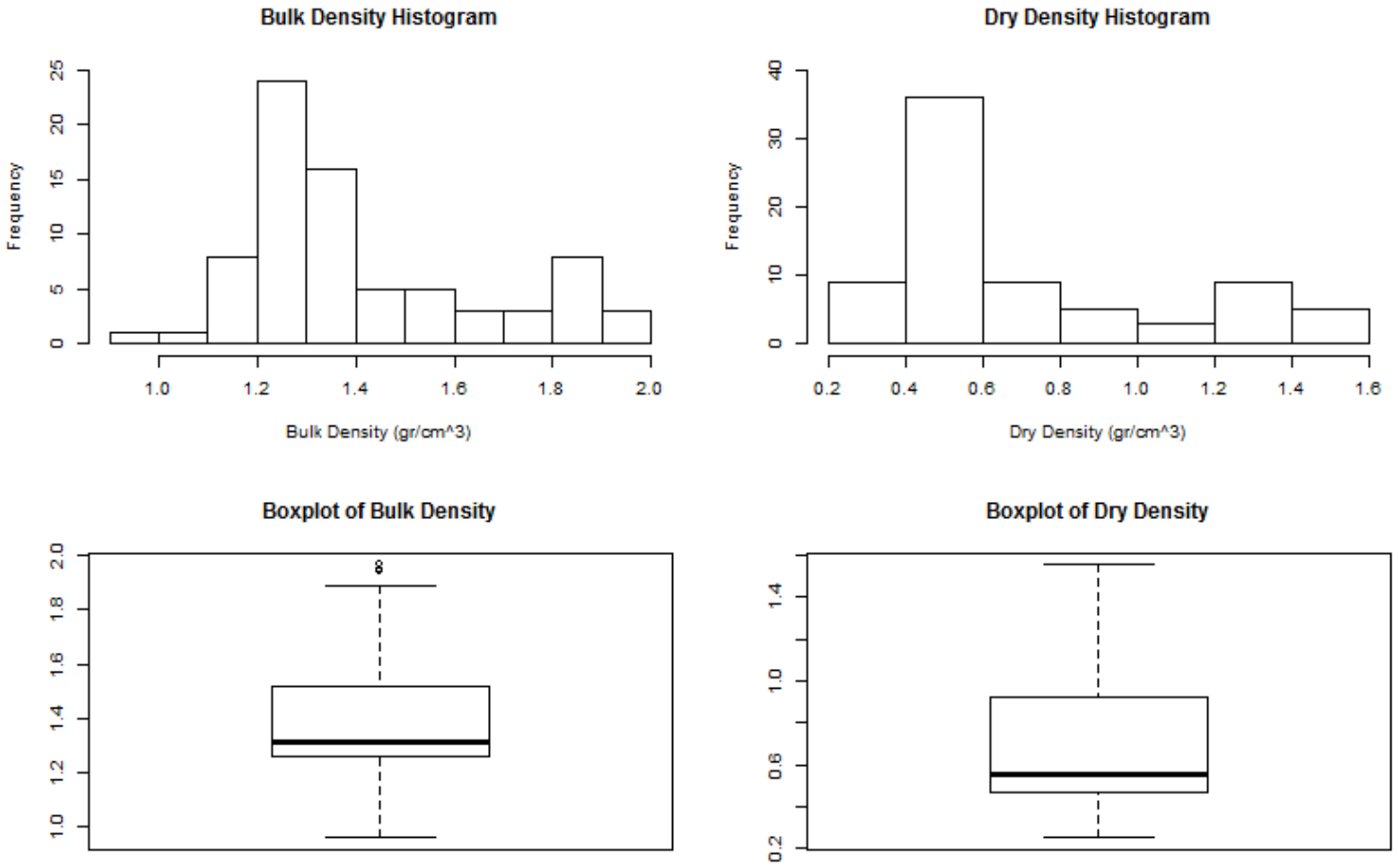

Figure A. 6. Histograms and boxplots of bulk density for all the samples

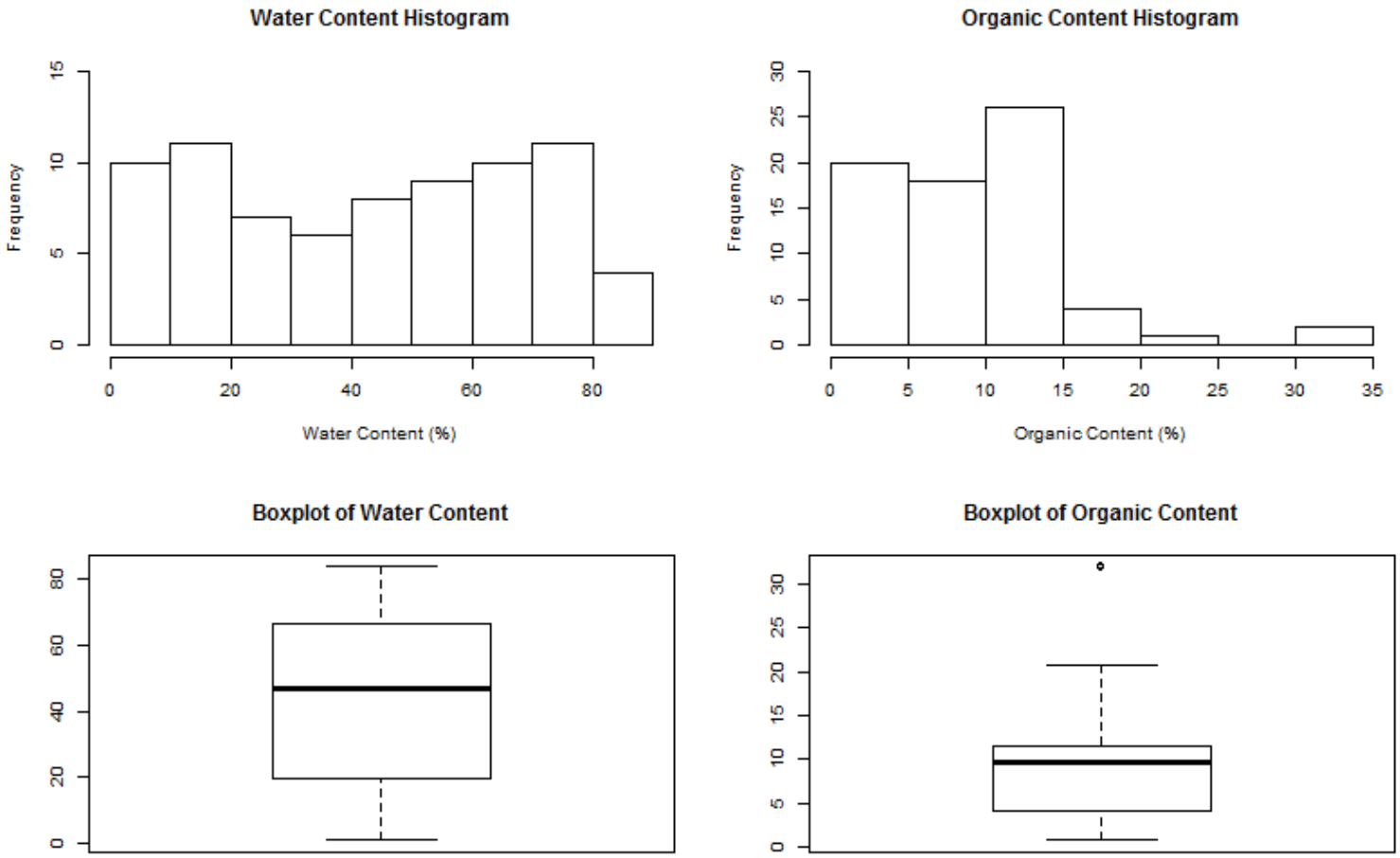

Figure A. 7. Histograms and boxplots of water content and organic content for all the samples

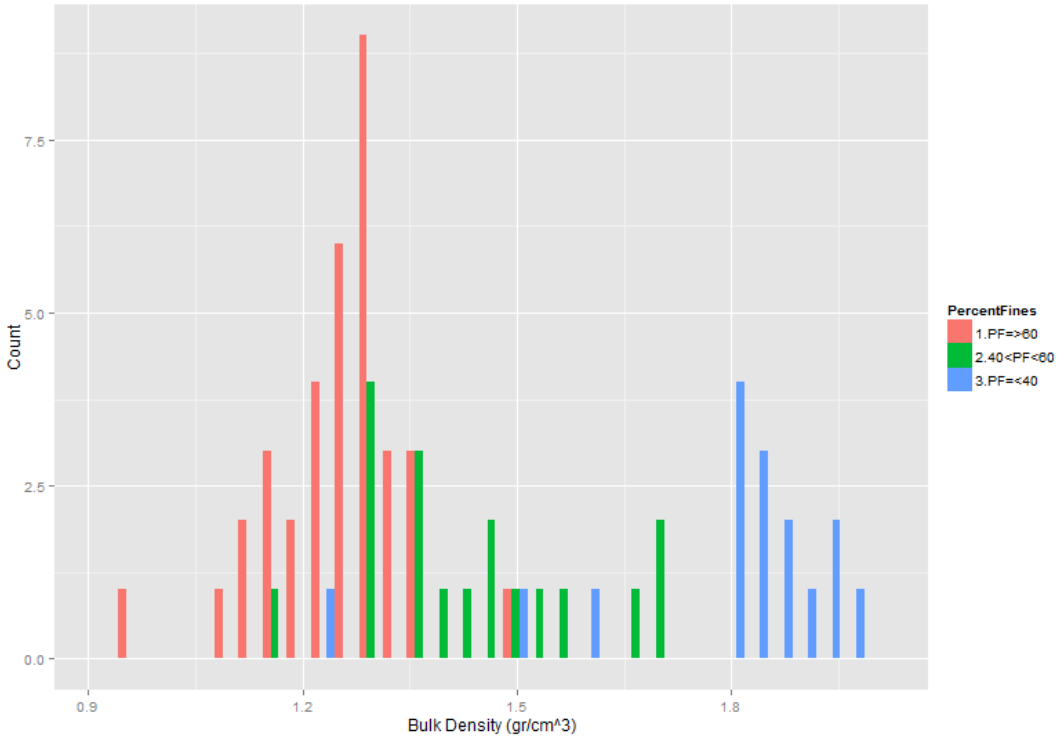

Figure A. 8. Frequency distribution of bulk density for different classes of sediment size

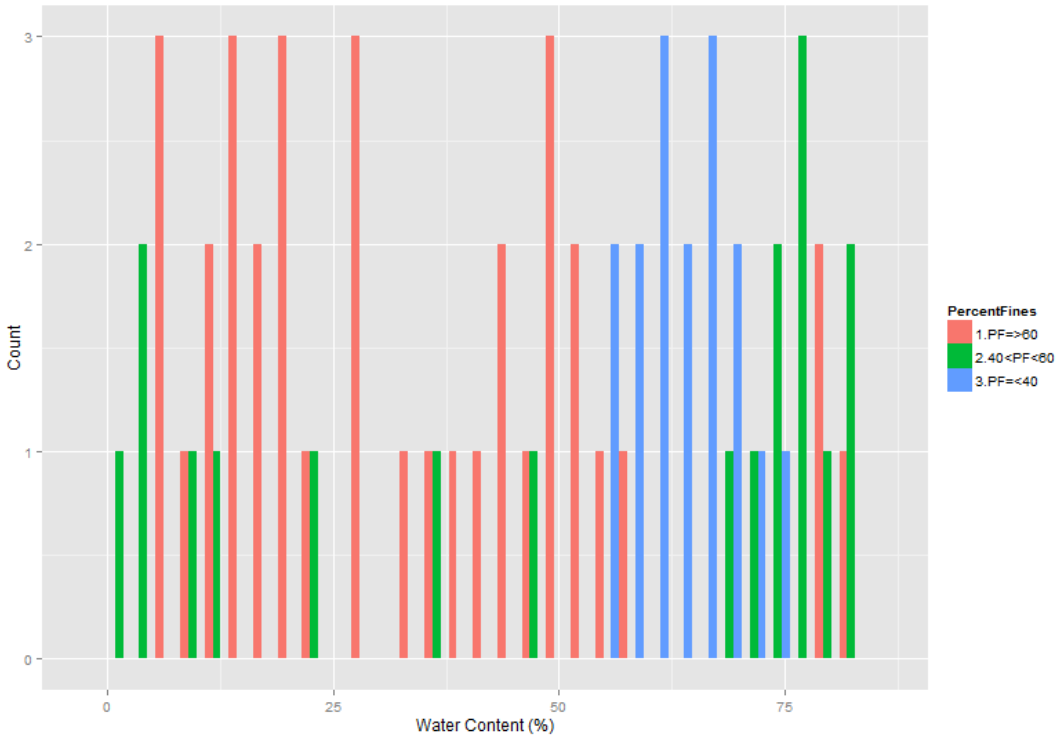

Figure A. 9. Frequency distribution of water content for different classes of sediment size

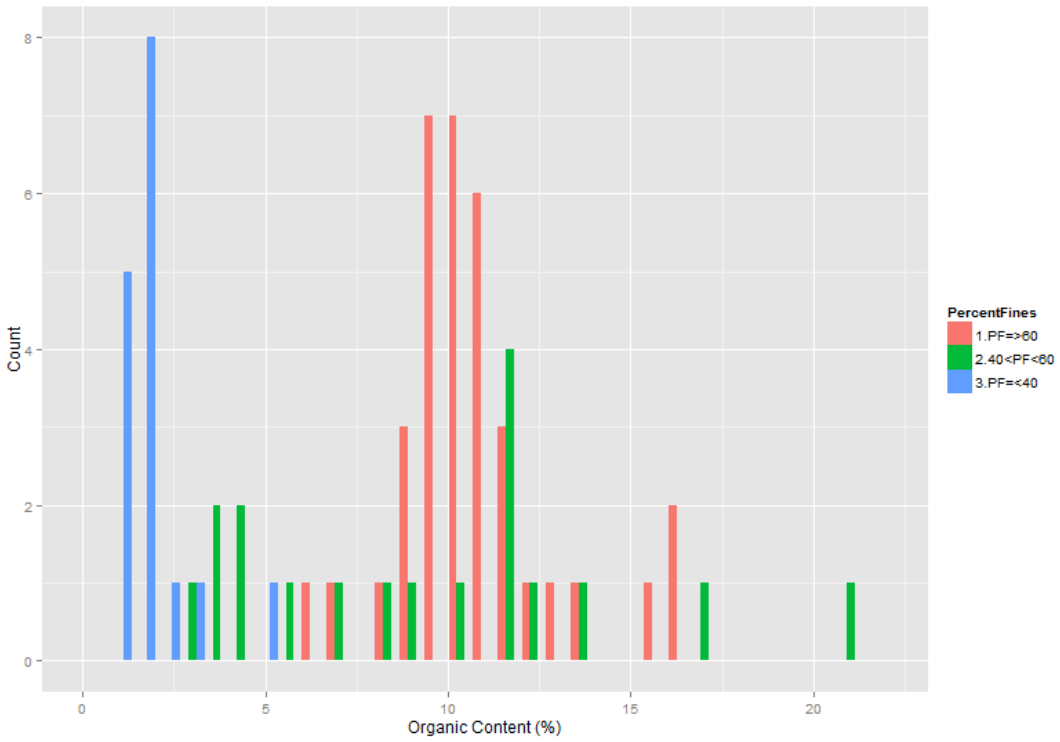

Figure A. 10. Frequency distribution of organic content for different classes of sediment size

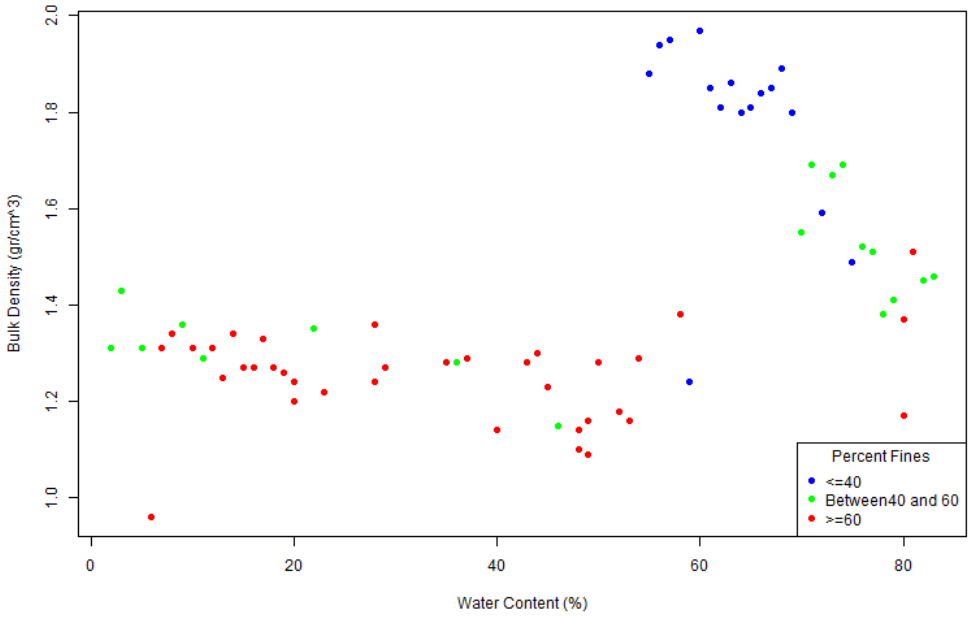

Figure A. 11. Bulk density versus water content for different classes of sediment size

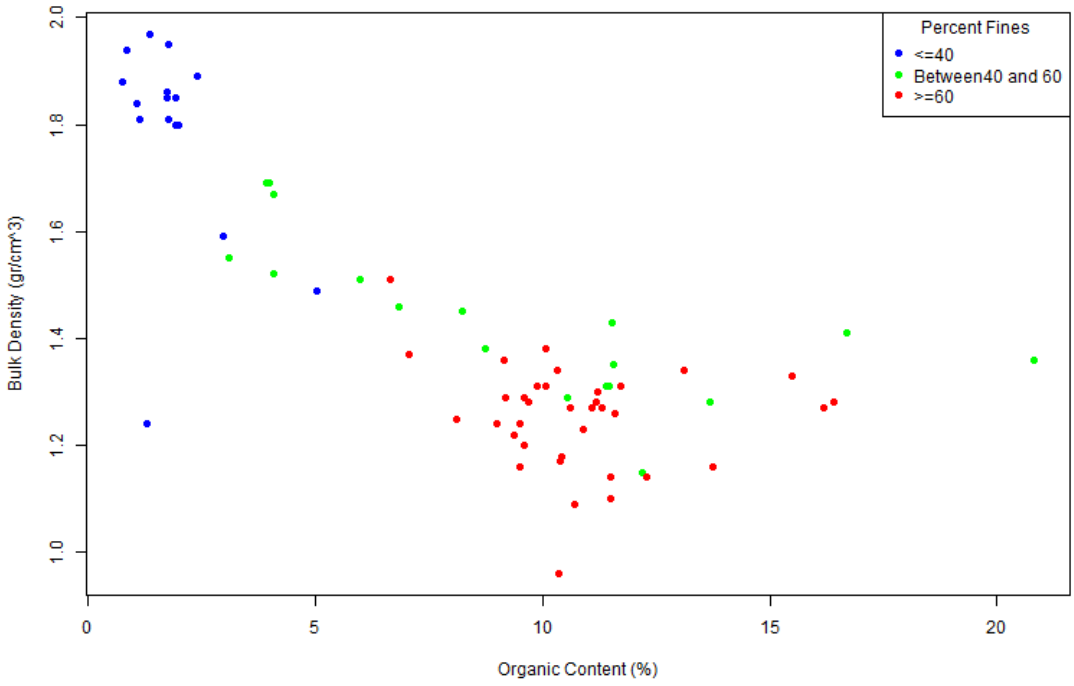

Figure A. 12. Bulk density versus organic content for different classes of sediment size

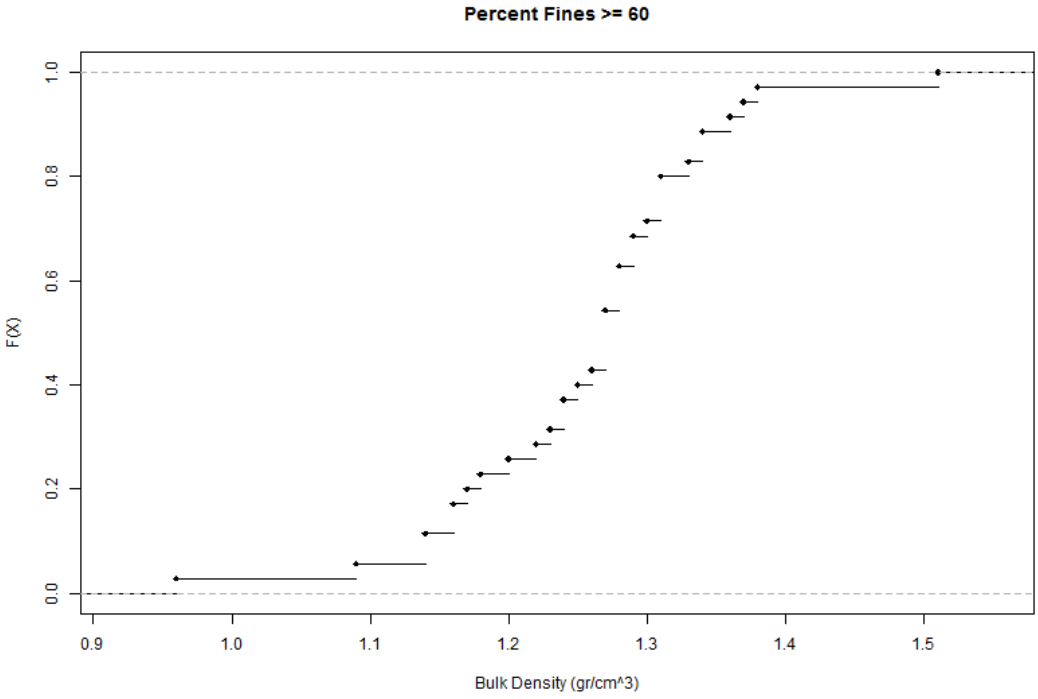

Figure A. 13. Empirical cumulative distribution of bulk density - PF ≥ 60

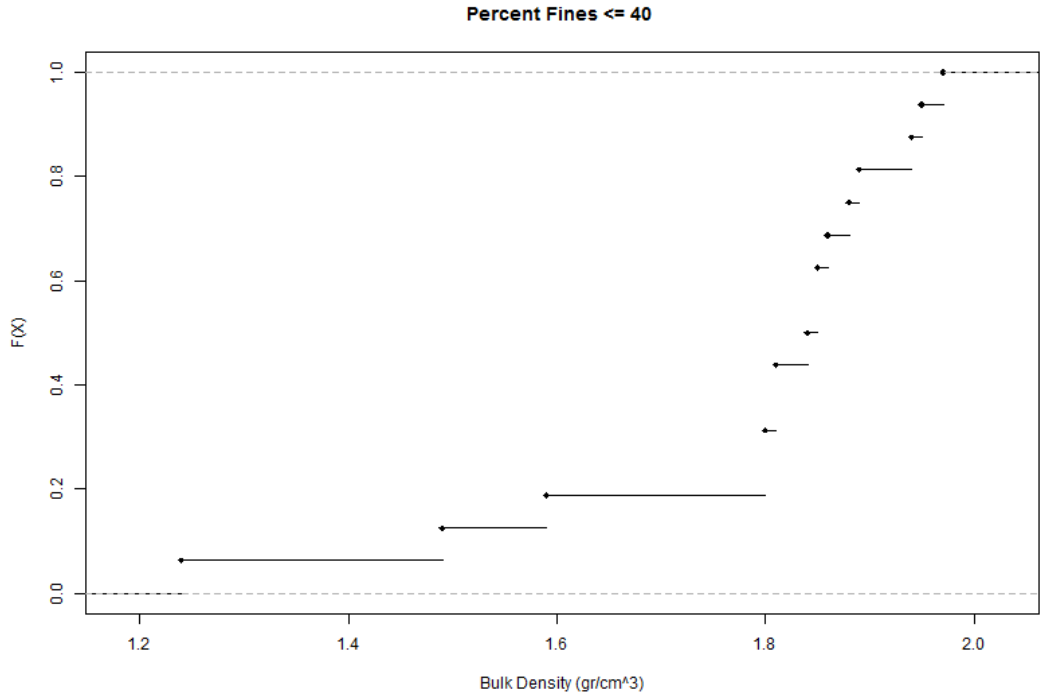

Figure A. 14. Empirical cumulative distribution of bulk density - PF ≤ 40

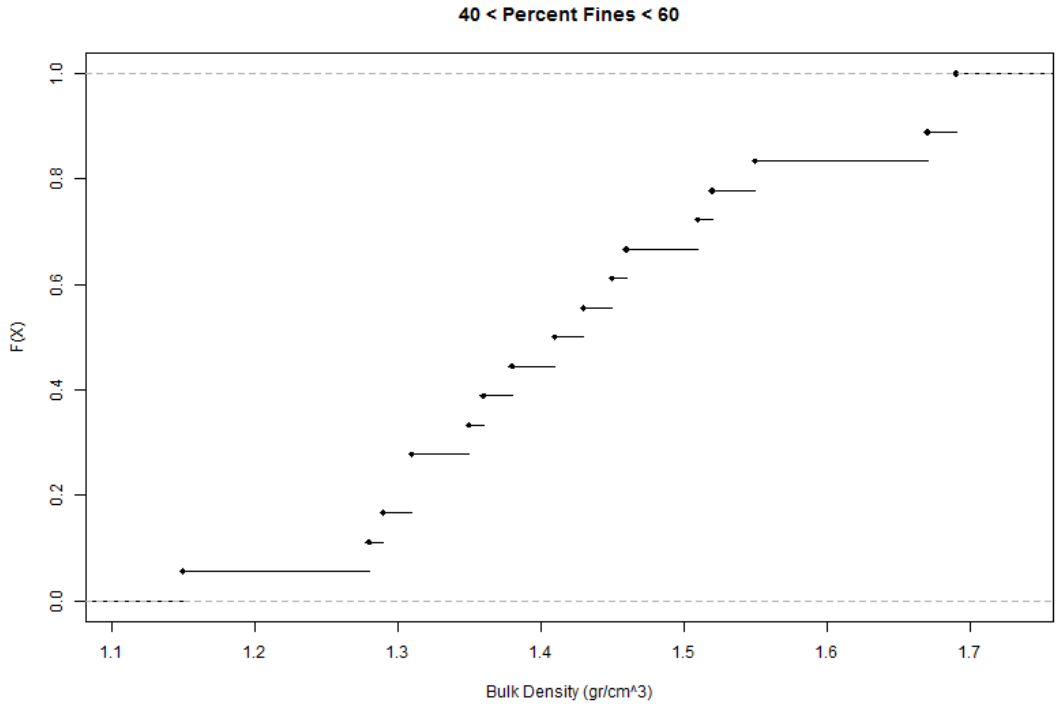

Figure A. 15. Empirical cumulative distribution of bulk density - 40 < PF < 60

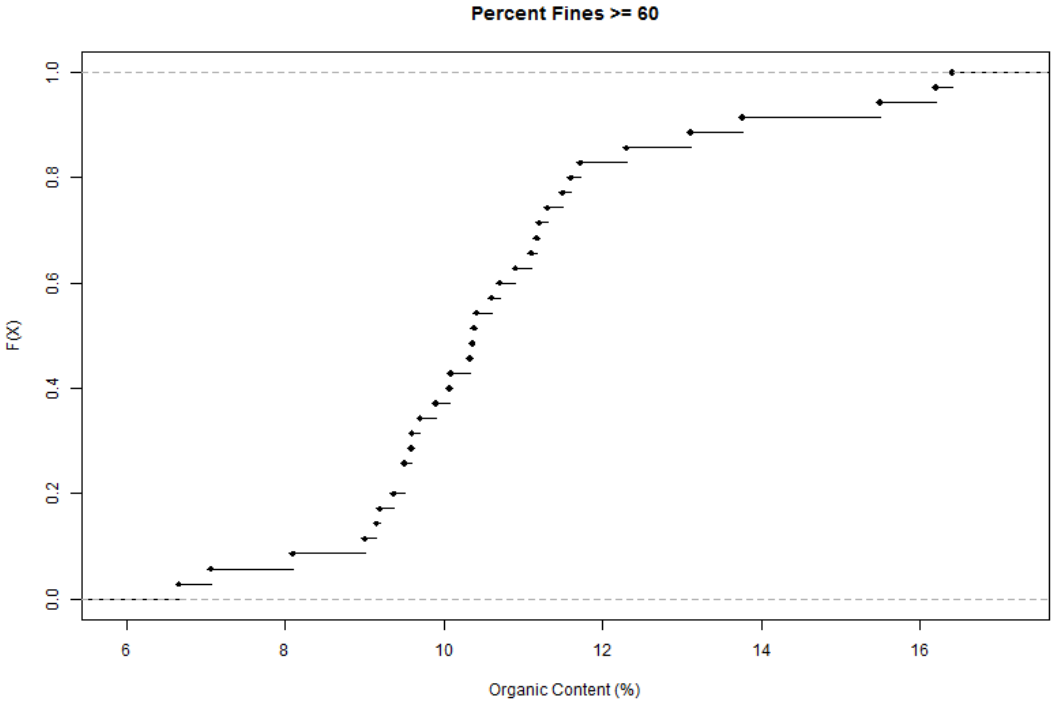

Figure A. 16. Empirical cumulative distribution of organic content - PF ≥ 60

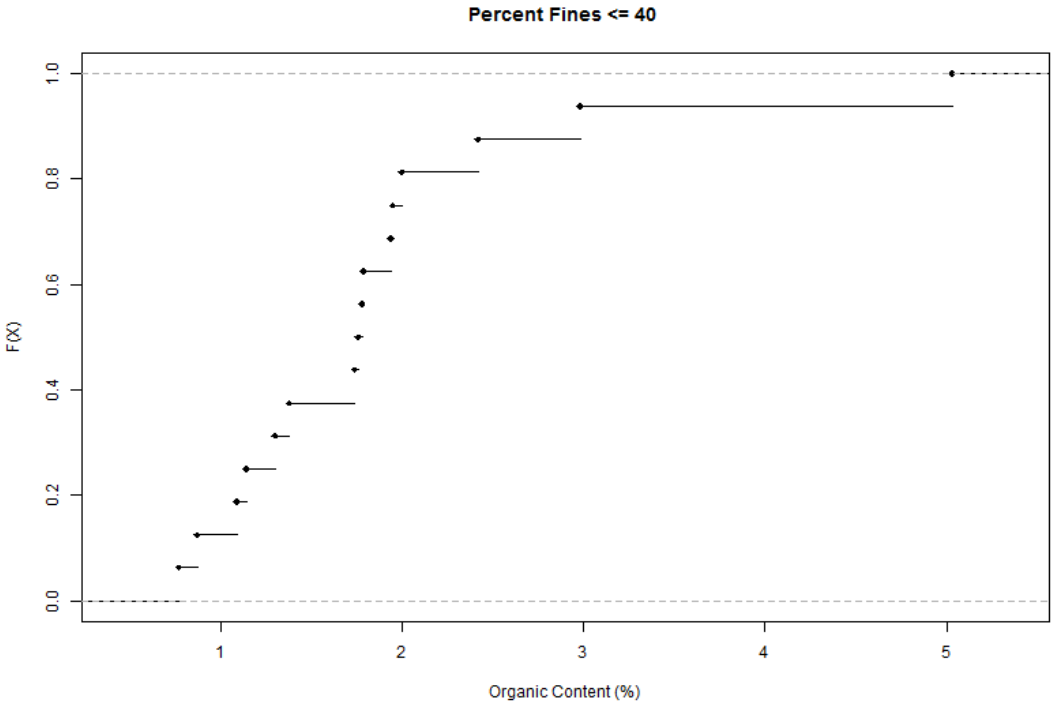

Figure A. 17. Empirical cumulative distribution of organic content - PF ≤ 40

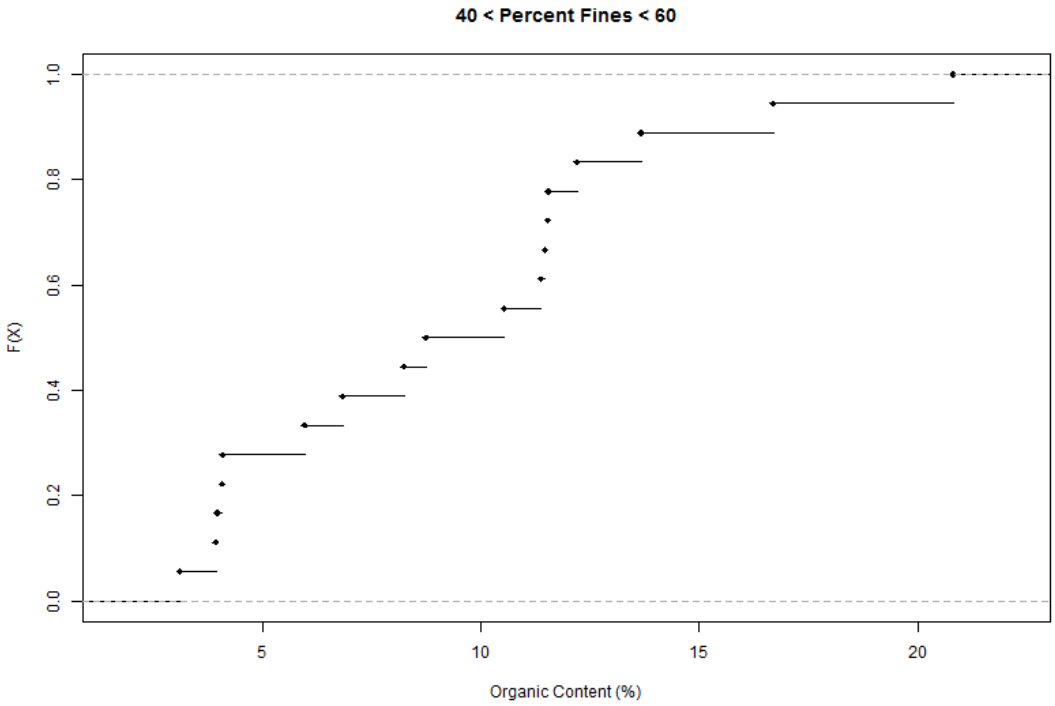

Figure A. 18. Empirical cumulative distribution of organic content - 40 < PF < 60

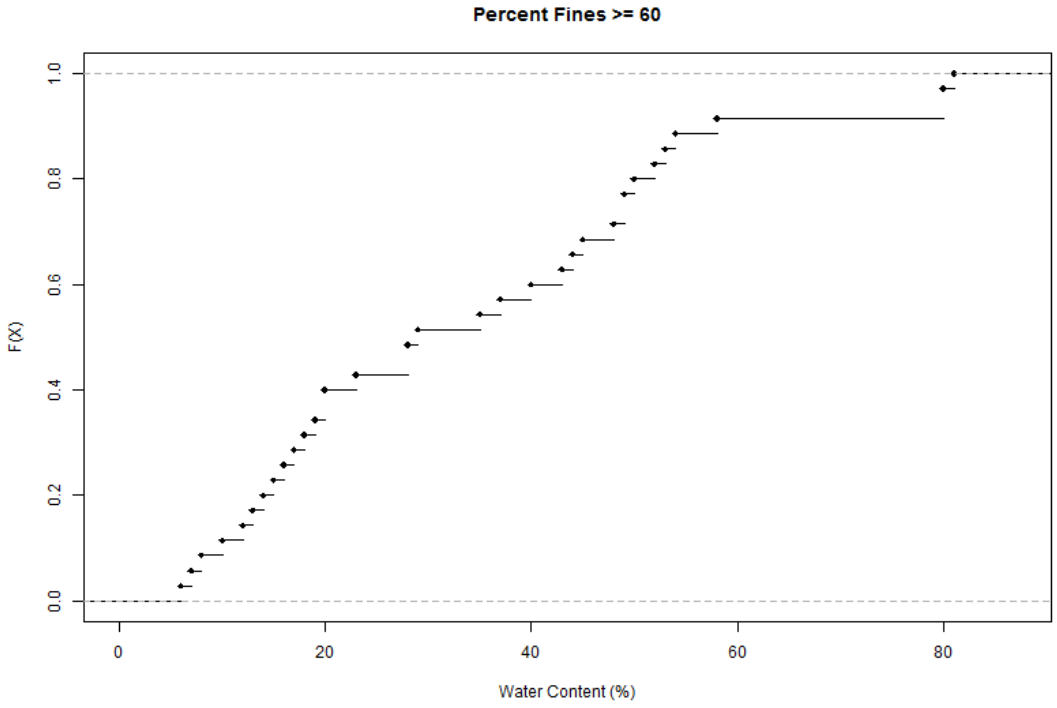

Figure A. 19. Empirical cumulative distribution of water content - PF ≥ 60

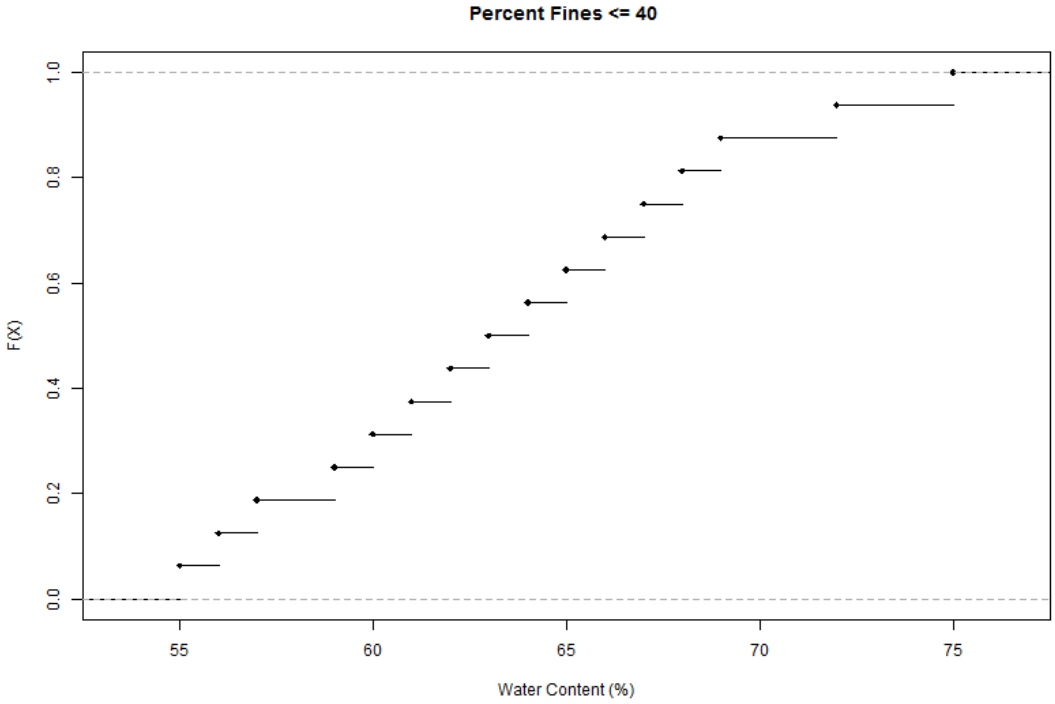

Figure A. 20. Empirical cumulative distribution of water content - PF ≤ 40

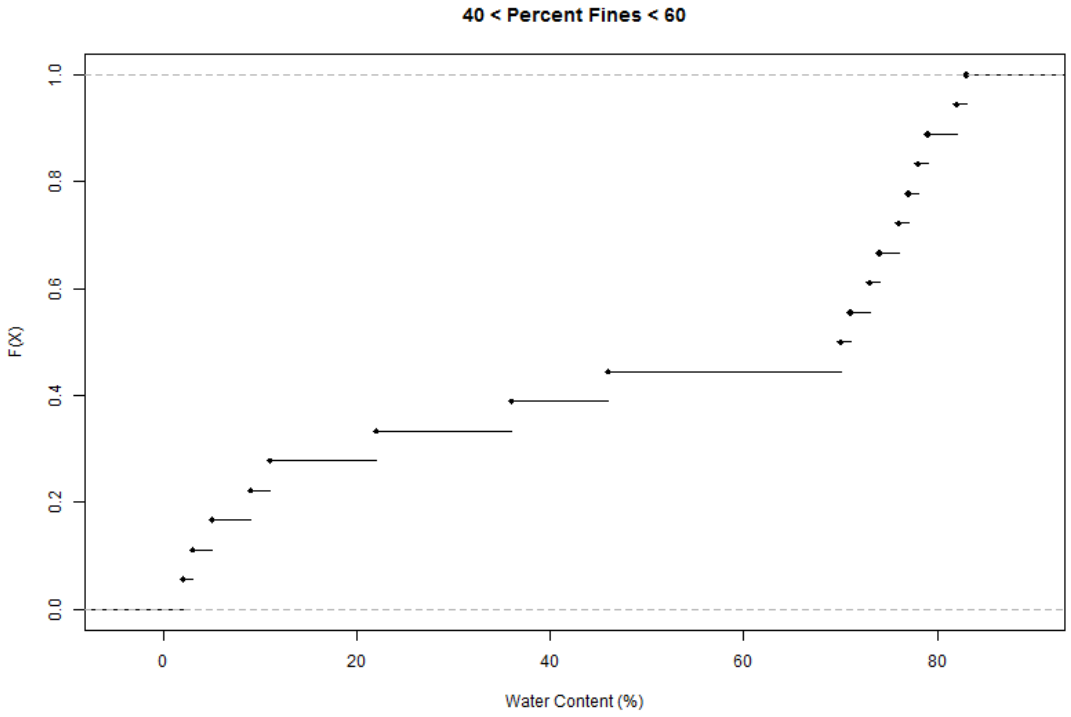

Figure A. 21. Empirical cumulative distribution of water content - 40 < PF < 60

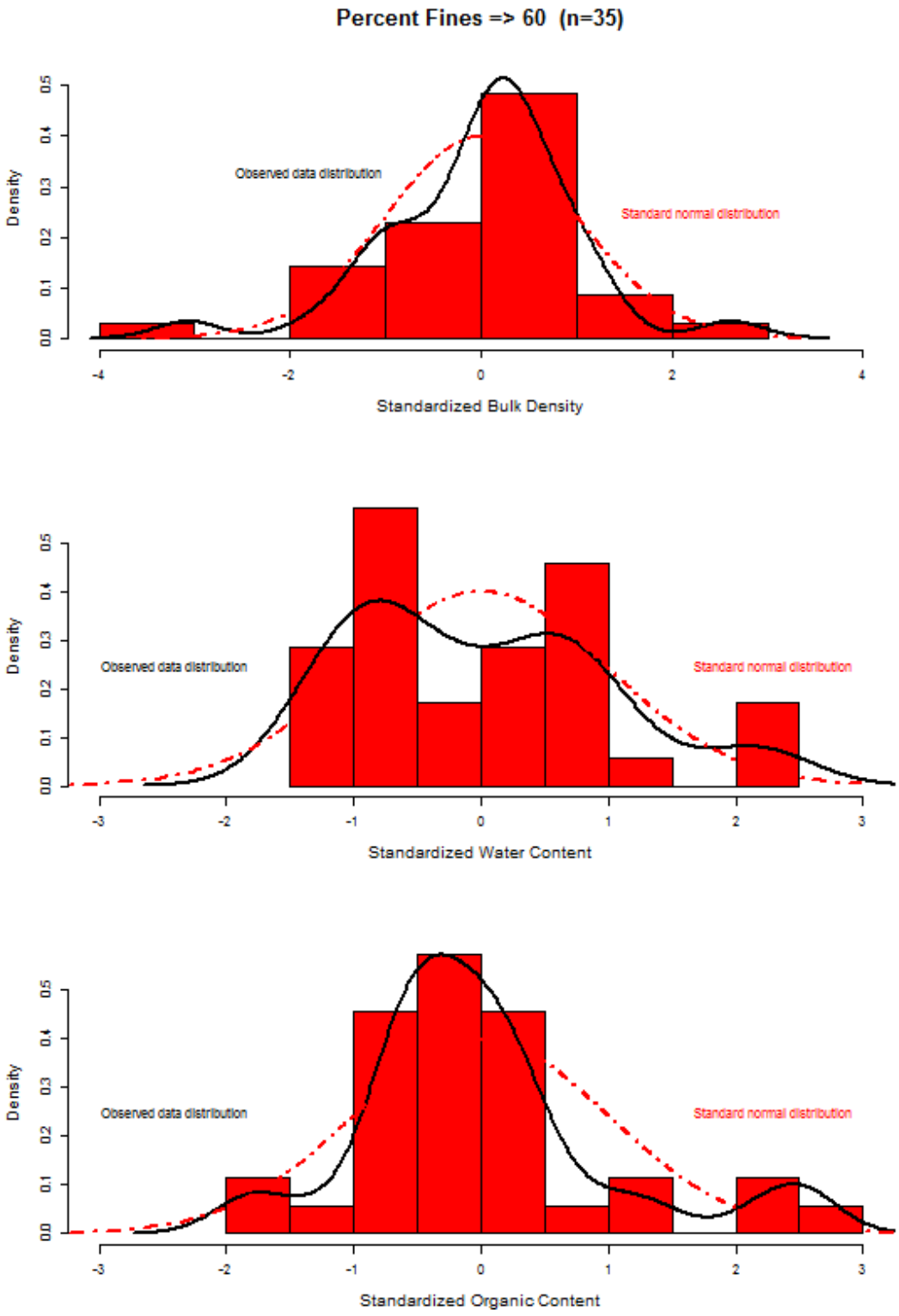

Figure A. 22. Distribution density of standardized sediment properties – PF ≥ 60

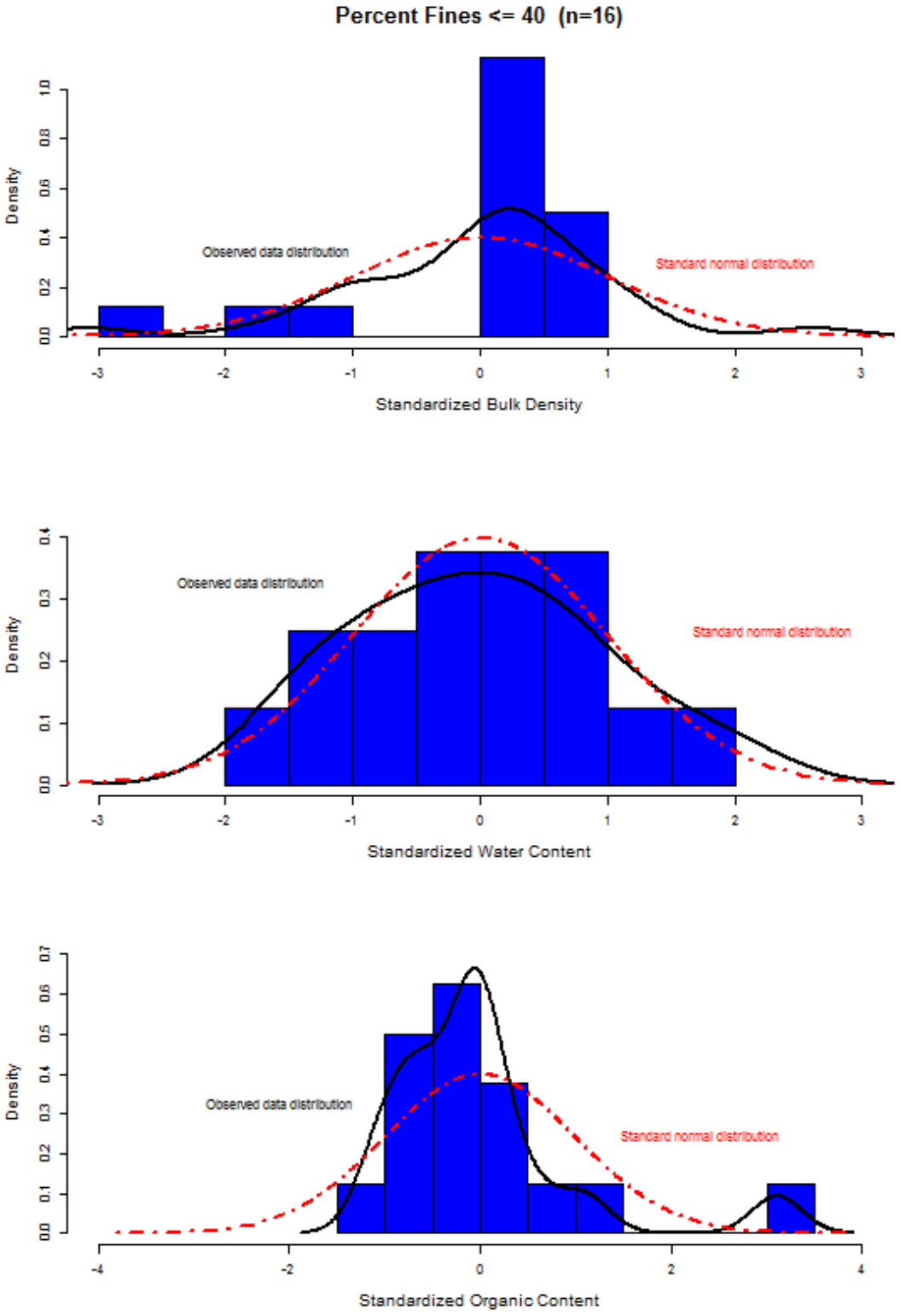

Figure A. 23. Distribution density of standardized sediment properties – PF ≤ 40

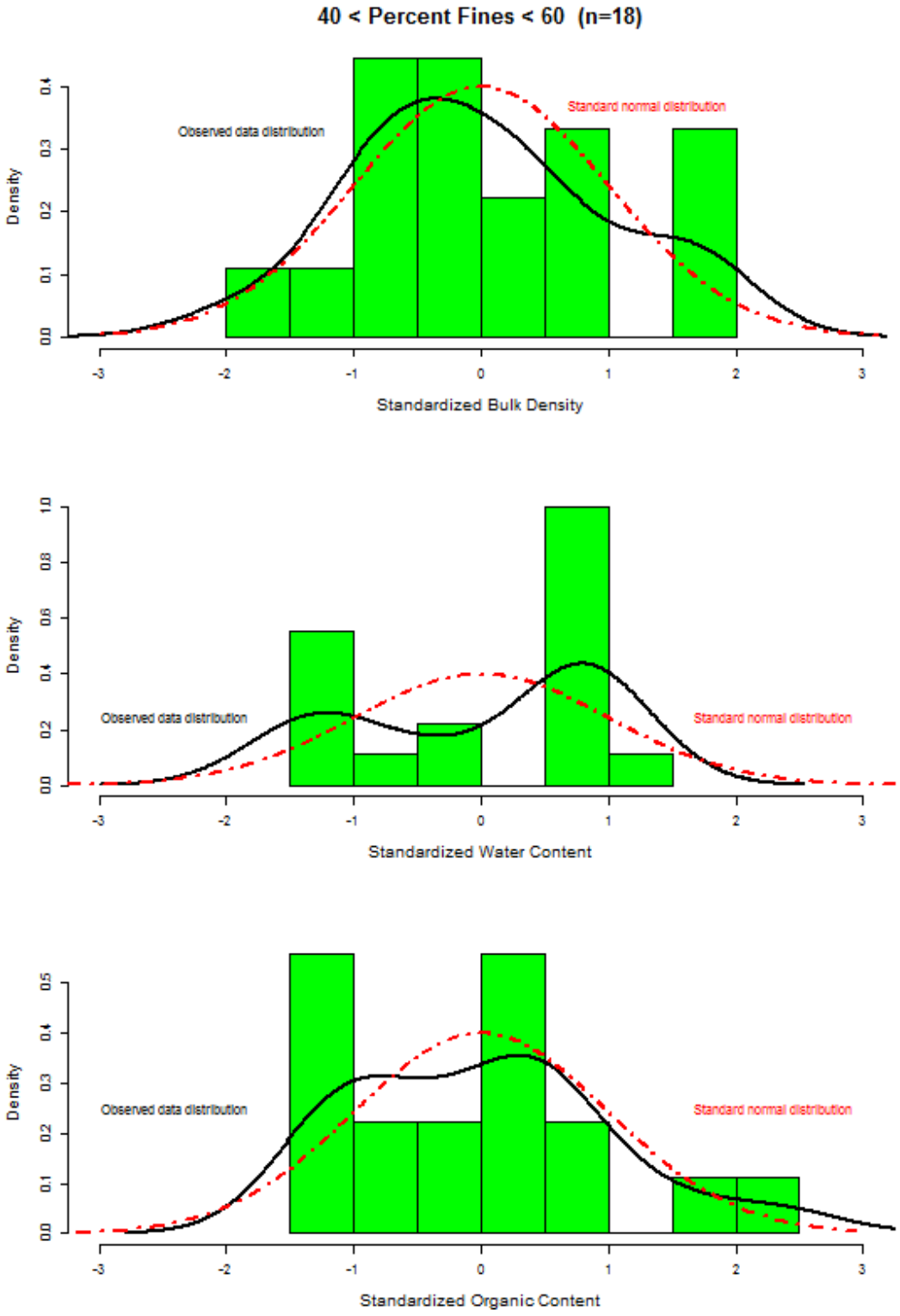

Figure A. 24. Distribution density of standardized sediment properties – 40 < PF < 60

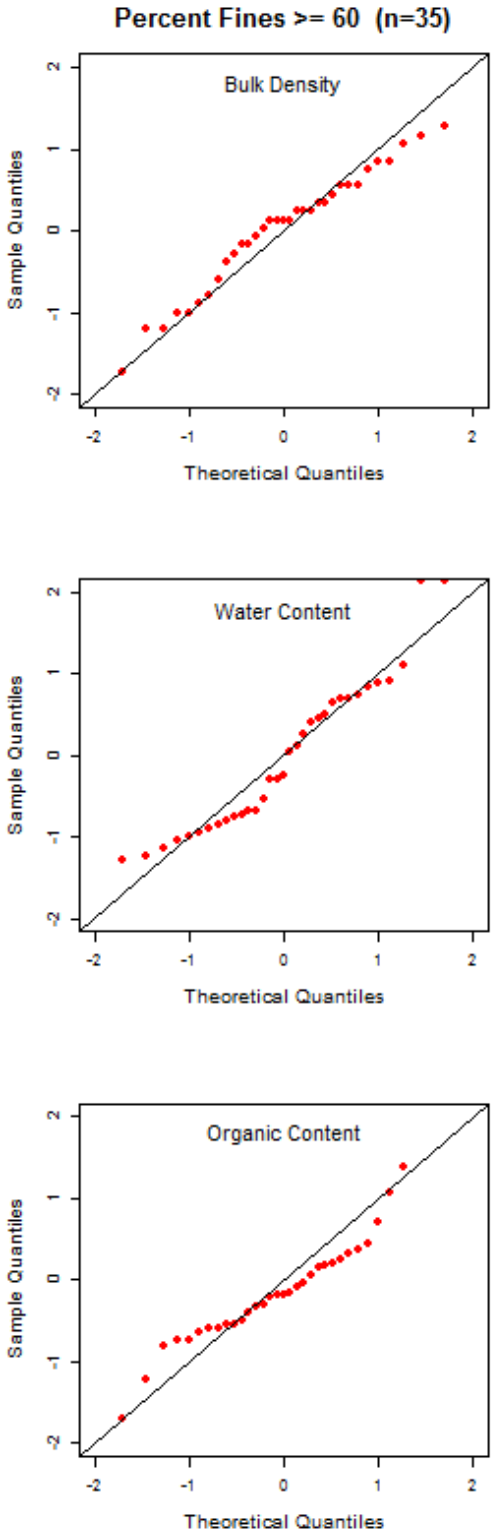

Figure A. 25. Q-Q plot of sediment properties – PF ≥ 60

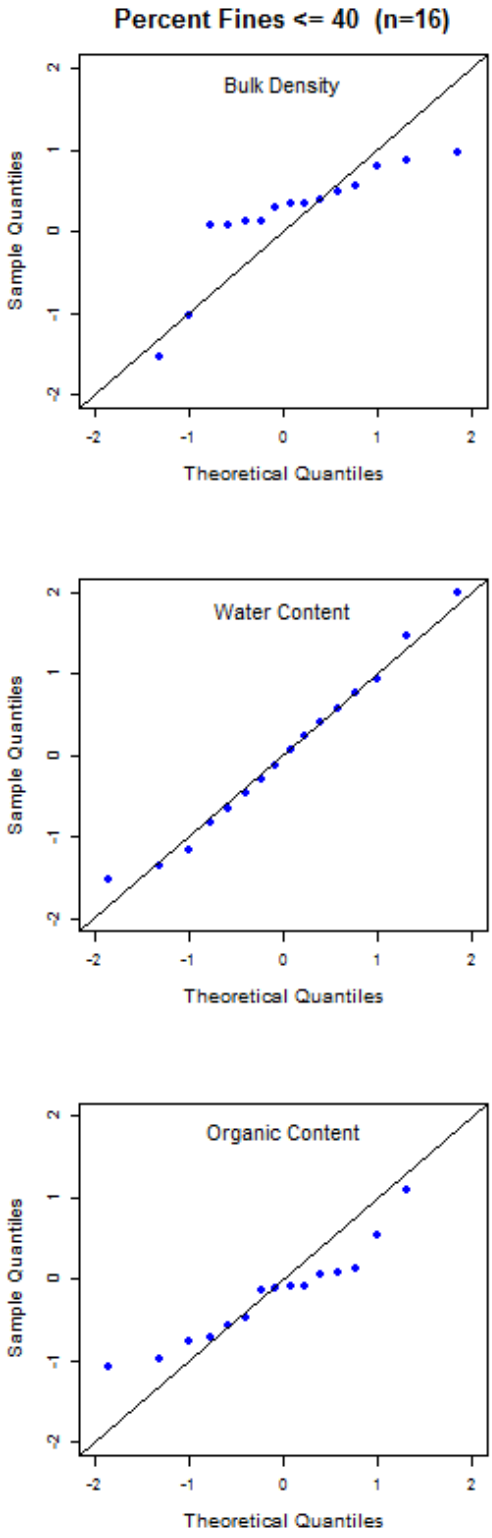

Figure A. 26. Q-Q plot of sediment properties – PF ≤ 40

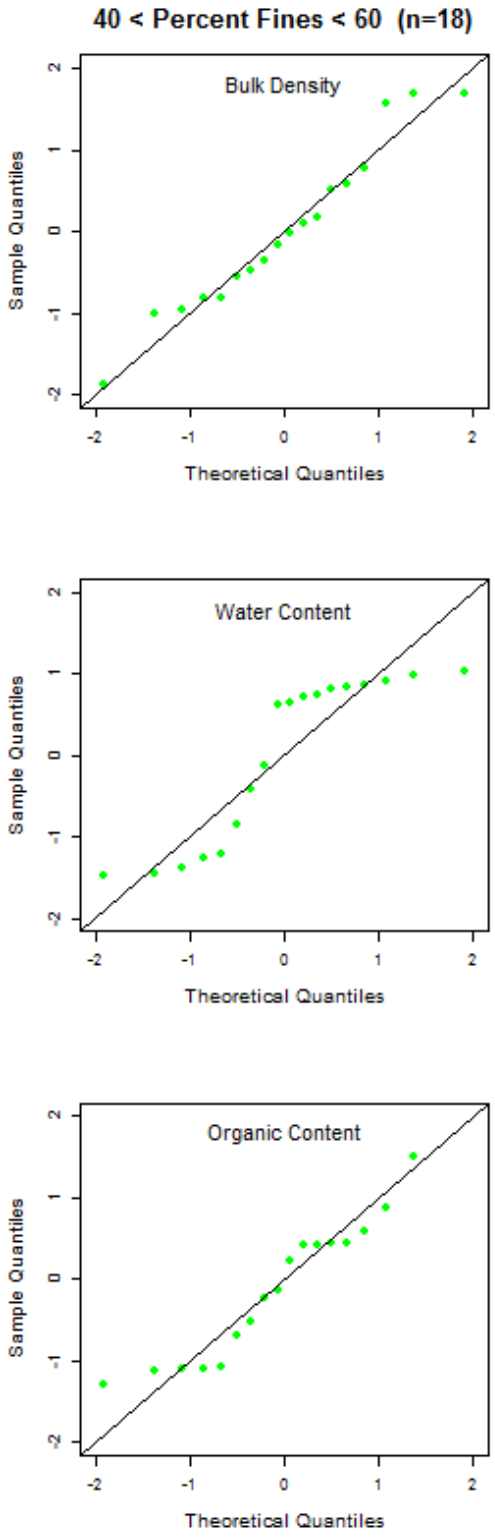

Figure A. 27. Q-Q plot of sediment properties – 40 < PF < 60

Box A. 28. ***Model summary for: ER=β0+β1.V+β2. ρ_{Bulk}+β3.W+β4.O+ β5.D +ϵ - PF ≥ 60***

lm(ErosionRate ~ Average Velocity+Bulk Density+Water Content+Organic Content +Depth)

Residuals:

Min	1Q	Median	3Q	Max
-4133	-2070	-492	1014	19899

Coefficients:

	Estimate	Std. Error	t value	Pr (>|t|)
(Intercept)	13035.08	4592.86	2.84	0.0049 **
V	105.52	12.99	8.12	0.000000000000023 ***
ρ_{Bulk}	-14310.81	3463.55	-4.13	0.000049425331031 ***
W	76.22	14.64	5.21	0.000000406487841 ***
O	139.00	77.91	1.78	0.0756 .
D	-10.86	5.08	-2.14	0.0335 *

Signif. codes: 0 '***' 0.001 '**' 0.01 '*' 0.05 '.' 0.1 ' ' 1

Residual standard error: 3290 on 245 degrees of freedom

Multiple R-squared: 0.354, Adjusted R-squared: 0.341

F-statistic: 26.9 on 5 and 245 DF, p-value: <0.0000000000000002

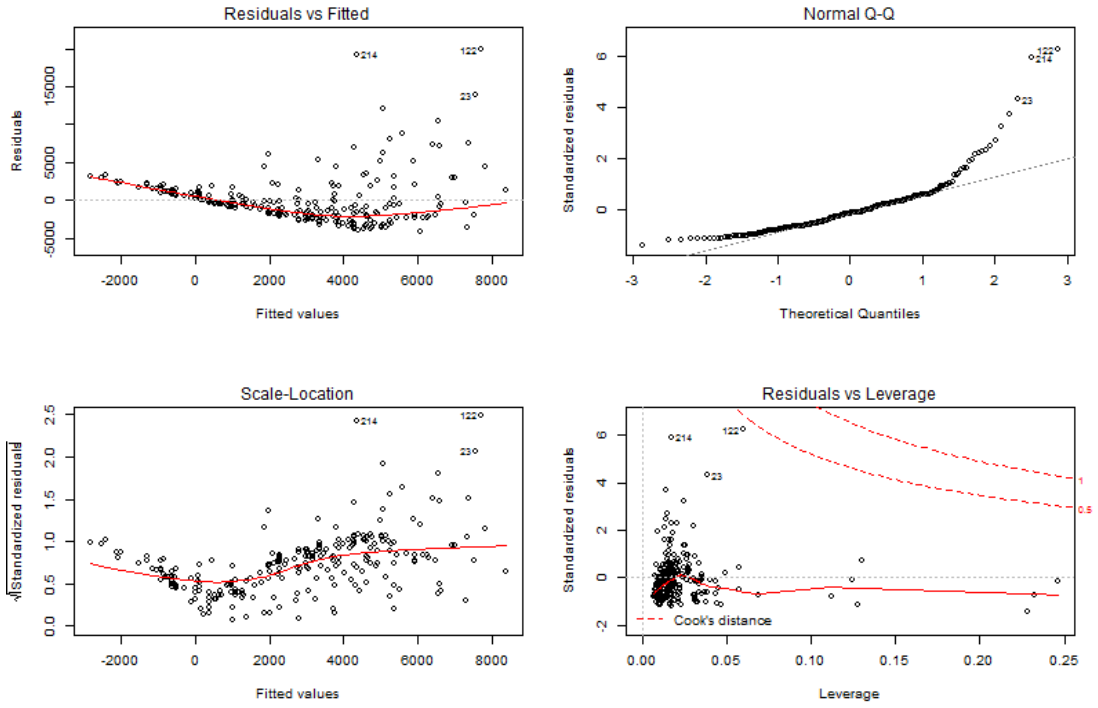

Figure **A. 29. Analysis of residuals for ER=β0+β1.V+β2. ρ_{Bulk}+β3.W+β4.O+ β5.D +ϵ - PF ≥ 60**

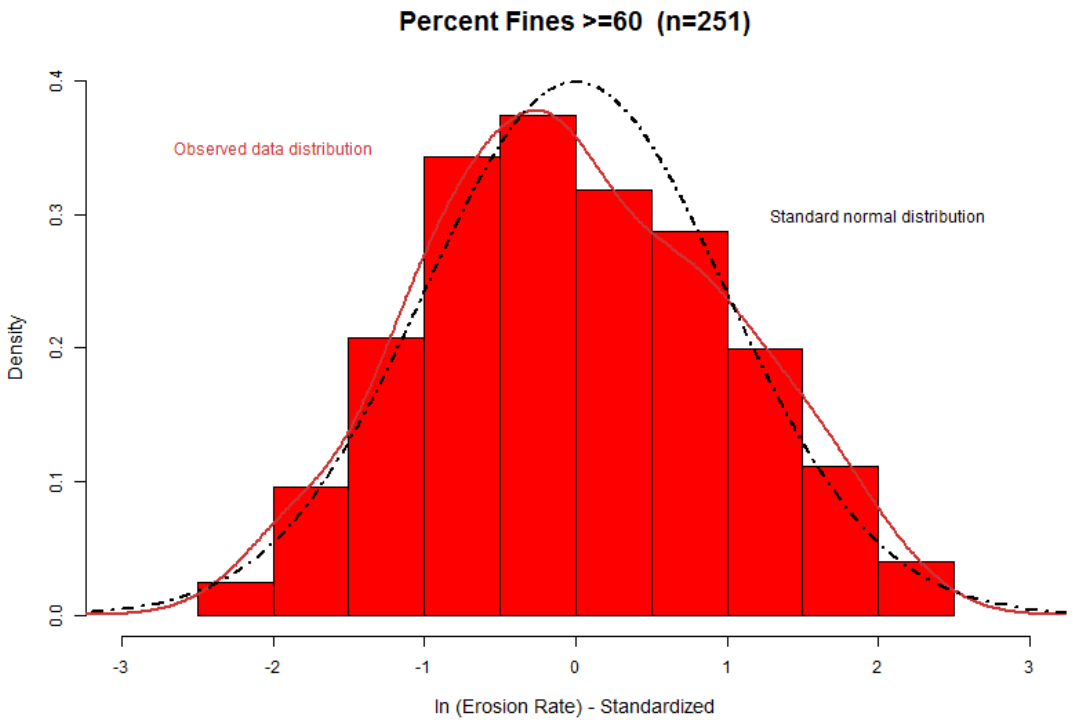

***Figure*A. 30. Frequency distribution of the predicted erosion rates with log-normal distribution for: ER=β0+β1.V+β2. ρ_{Bulk}+β3.W+β4.O+ β5.D +ϵ - PF ≥ 60**

Box A. 31. *Model summary for: $ER = \beta_0 + \beta_1.V + \beta_2.D + \varepsilon$ - $40 < PF < 60$*

lm(Erosion Rate ~ AverageVelocity+Depth)

Residuals:

Min	1Q	Median	3Q	Max
-5416	-2781	-1447	1612	19068

Coefficients:

	Estimate	Std. Error	t value	Pr (>|t|)
(Intercept)	1965.72	1314.12	1.50	0.14
V	118.70	28.83	4.12	0.00008299 ***
D	-45.39	7.99	-5.68	0.00000015 ***

Signif. codes: 0 '***' 0.001 '**' 0.01 '*' 0.05 '.' 0.1 ' ' 1

Residual standard error: 4490 on 93 degrees of freedom

Multiple R-squared: 0.275, Adjusted R-squared: 0.26

F-statistic: 17.7 on 2 and 93 DF, p-value: 0.000000316

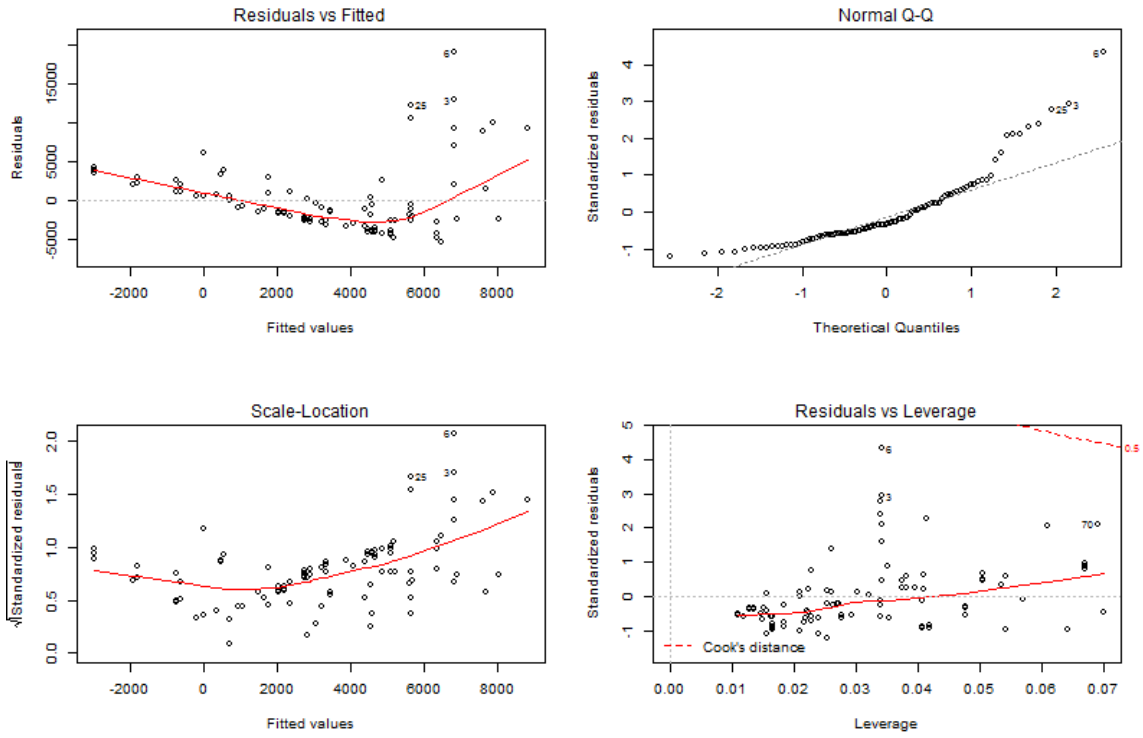

Figure **A. 32. Analysis of residuals for: $ER = \beta_0 + \beta_1 . V + \beta_2 . D + \varepsilon$ $-40 < PF < 60$**

Box A. 33 . ***Analysis of Variance for the 10-fold cross-validation – NBFM - $PF \geq 60$***

Response: log(ErosionRate)

	Df	Sum Sq	Mean Sq	F value	Pr(>F)
ln(V)	1	75.8	75.8	89.6	<0.0000000000000002 ***
ρ_{Bulk}	1	96.2	96.2	113.7	<0.0000000000000002 ***
W	1	66.3	66.3	78.4	<0.0000000000000002 ***
Residuals	247	208.9	0.8		

Signif. codes: 0 '***' 0.001 '**' 0.01 '*' 0.05 '.' 0.1 ' ' 1

BoxA. 34. ***Analysis of Variance for the 10-fold cross-validation - NBCM - PF ≤ 40***

Response: log(ErosionRate)

	Df	Sum Sq	Mean Sq	F value	Pr(>F)
V	1	43.9	43.9	42.3	0.000000093 ***
ρ_{Bulk}	1	0.1	0.1	0.1	0.76
O	1	24.4	24.4	23.5	0.000019211 ***
Residuals	40	41.5	1.0		

Signif. codes: 0 '***' 0.001 '**' 0.01 '*' 0.05 '.' 0.1 ' ' 1

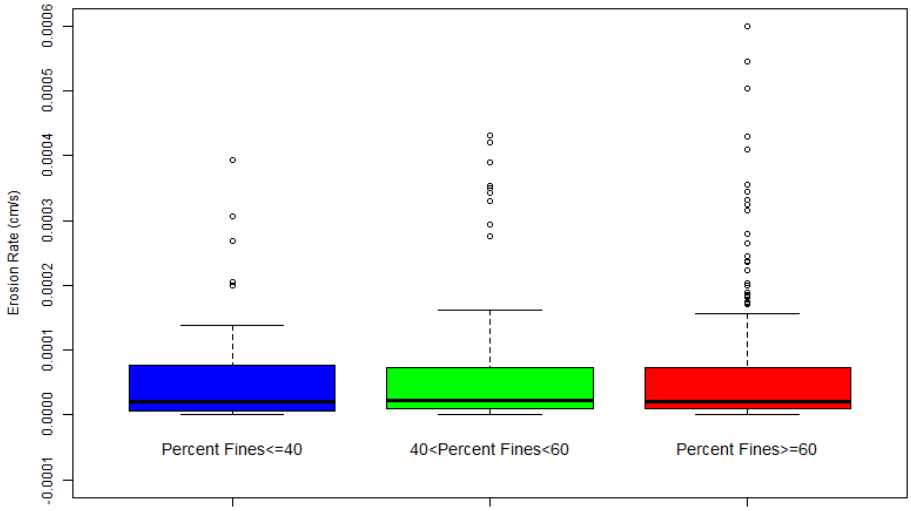

Figure A. 35. **Observed erosion rates (cm/s) for different classes of sediment size (ESETM). The minimum erosion rate values reported by Borrowman et al. (2006)**

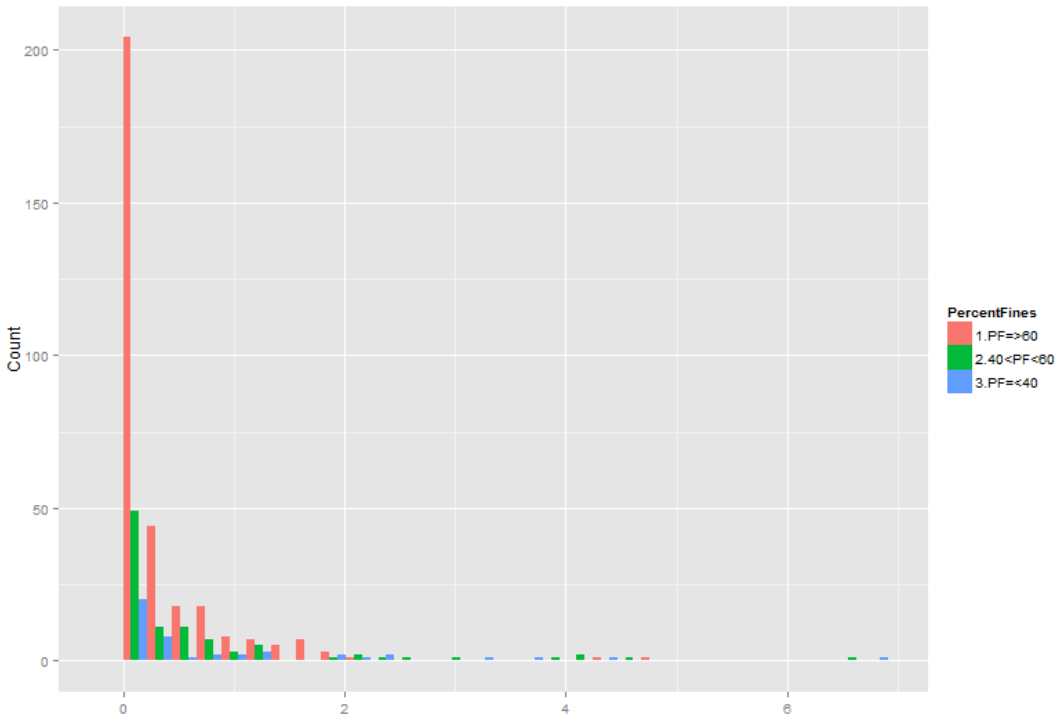

***Figure A. 36*. Frequency distribution of Erosion Rate (mm/hour) for different classes of sediment size**

APPENDIX B

Test results

					Test Specifications			Erosion Test Results		Properties										
#	Day	Core	Test	Test ID	Step	V $(\frac{cm}{s})$	Duration (min)	WL (gr)	ER $\frac{gr}{m^2.hour}$	Depth (mm)	ρ_{Bulk} $(\frac{gr}{cm^3})$	W (%)	O (%)	τ_{th} (Pa)	Gs	% Fines	LL (%)	PL (%)	PI
1	1	1	1	021612-020112-C1-R1-S1	1	16.74	5	0.08	2057	0	1.19	NA	NA	0.12	NA	NA	NA	NA	NA
2	1	1	1	021612-020112-C1-R1-S1	2	16.42	5	0.13	3236	0	1.19	NA	NA	0.12	NA	NA	NA	NA	NA
3	1	1	1	021612-020112-C1-R1-S1	3	16.40	10	0.05	622	0	1.19	NA	NA	0.12	NA	NA	NA	NA	NA
4	1	1	2	021612-020112-C1-R1-S2	1	16.39	5	0.1	2385	0	1.2	NA	NA	0.12	NA	NA	NA	NA	NA
5	1	1	2	021612-020112-C1-R1-S2	2	16.59	5	0.09	2146	0	1.2	NA	NA	0.12	NA	NA	NA	NA	NA
6	1	1	2	021612-020112-C1-R1-S2	3	16.56	10	0.306	3649	0	1.2	NA	NA	0.12	NA	NA	NA	NA	NA
7	1	1	2	021612-020112-C1-R1-S2	4	16.29	10	0.07	835	0	1.2	NA	NA	0.12	NA	NA	NA	NA	NA
8	1	1	2	021612-020112-C1-R1-S2	5	19.33	10	0.37	4412	0	1.2	NA	NA	0.16	NA	NA	NA	NA	NA
9	1	1	2	021612-020112-C1-R1-S2	6	19.65	10	0.35	4173	0	1.2	NA	NA	0.16	NA	NA	NA	NA	NA
10	1	1	2	021612-020112-C1-R1-S2	7	19.59	10	0.13	1550	0	1.2	NA	NA	0.16	NA	NA	NA	NA	NA
11	1	1	3	021712-020112-C1-R2-S1	1	16.41	5	0.2	5471	18	1.17	NA	NA	0.12	NA	NA	NA	NA	NA
12	1	1	3	021712-020112-C1-R2-S1	2	16.38	5	0.13	3556	18	1.17	NA	NA	0.12	NA	NA	NA	NA	NA
13	1	1	3	021712-020112-C1-R2-S1	3	16.10	10	0.09	1231	18	1.17	NA	NA	0.12	NA	NA	NA	NA	NA
14	1	1	4	021712-020112-C1-R2-S2	1	16.28	5	0.06	2073	18	1.13	NA	NA	0.12	NA	NA	NA	NA	NA
15	1	1	4	021712-020112-C1-R2-S2	2	16.09	5	0.04	1382	18	1.13	NA	NA	0.12	NA	NA	NA	NA	NA
16	1	1	4	021712-020112-C1-R2-S2	3	15.90	10	0.04	691	18	1.13	NA	NA	0.1	NA	NA	NA	NA	NA
17	1	1	5	022012-020112-C1-R3-S1	1	15.88	5	0.16	3983	38	1.19	NA	NA	0.11	NA	NA	NA	NA	NA
18	1	1	5	022012-020112-C1-R3-S1	2	15.90	5	0.01	249	38	1.19	NA	NA	0.11	NA	NA	NA	NA	NA
19	1	1	5	022012-020112-C1-R3-S1	3	15.86	10	0.02	249	38	1.19	NA	NA	0.11	NA	NA	NA	NA	NA
20	1	1	5	022012-020112-C1-R3-S1	4	21.20	5	0.39	9709	38	1.19	NA	NA	0.19	NA	NA	NA	NA	NA
21	1	1	5	022012-020112-C1-R3-S1	5	21.31	5	0.16	3983	38	1.19	NA	NA	0.19	NA	NA	NA	NA	NA
22	1	1	5	022012-020112-C1-R3-S1	6	21.18	5	0.21	5228	38	1.19	NA	NA	0.19	NA	NA	NA	NA	NA
23	1	1	6	022012-020112-C1-R4-S1	1	15.96	5	0.11	2425	55	1.22	NA	NA	0.11	NA	NA	NA	NA	NA
24	1	1	6	022012-020112-C1-R4-S1	2	15.89	5	0.1	2204	55	1.22	NA	NA	0.11	NA	NA	NA	NA	NA
25	1	1	6	022012-020112-C1-R4-S1	3	15.61	10	-0.05	-551	55	1.22	NA	NA	0.11	NA	NA	NA	NA	NA
26	1	1	6	022012-020112-C1-R4-S1	4	21.21	5	0.22	4849	55	1.22	NA	NA	0.19	NA	NA	NA	NA	NA
27	1	1	6	022012-020112-C1-R4-S1	5	21.39	5	0.12	2645	55	1.22	NA	NA	0.19	NA	NA	NA	NA	NA
28	1	1	6	022012-020112-C1-R4-S1	6	21.43	10	0.15	1653	55	1.22	NA	NA	0.19	NA	NA	NA	NA	NA
29	1	1	7	022112-020112-C1-R4-S2	1	15.68	5	-0.08	-1992	55	1.19	NA	NA	0.1	NA	NA	NA	NA	NA
30	1	1	7	022112-020112-C1-R4-S2	2	15.72	5	0.22	5477	55	1.19	NA	NA	0.1	NA	NA	NA	NA	NA

					Test Specifications			Erosion Test Results		Properties										
#	Day	Core	Test	Test ID	Step	V $(\frac{cm}{s})$	Duration (min)	WL (gr)	ER $\frac{gr}{m^2.hour}$	Depth (mm)	ρ_{Bulk} $(\frac{gr}{cm^3})$	W (%)	O (%)	τ_{th} (Pa)	Gs	% Fines	LL (%)	PL (%)	PI
31	1	1	7	022112-020112-C1-R4-S2	3	15.46	10	0.04	498	55	1.19	NA	NA	0.1	NA	NA	NA	NA	NA
32	1	1	7	022112-020112-C1-R4-S2	4	21.34	5	0.23	5726	55	1.19	NA	NA	0.18	NA	NA	NA	NA	NA
33	1	1	7	022112-020112-C1-R4-S2	5	21.14	5	0.03	747	55	1.19	NA	NA	0.18	NA	NA	NA	NA	NA
34	1	1	7	022112-020112-C1-R4-S2	6	21.01	10	0.24	2987	55	1.19	NA	NA	0.18	NA	NA	NA	NA	NA
35	1	1	8	022112-020112-C1-R5-S1	1	15.54	5	0.06	1156	119	1.26	NA	NA	0.1	NA	NA	NA	NA	NA
36	1	1	8	022112-020112-C1-R5-S1	2	15.28	5	0.07	1348	119	1.26	NA	NA	0.1	NA	NA	NA	NA	NA
37	1	1	8	022112-020112-C1-R5-S1	3	15.33	10	0.15	1445	119	1.26	NA	NA	0.1	NA	NA	NA	NA	NA
38	1	1	8	022112-020112-C1-R5-S1	4	20.47	5	0.318	6125	119	1.26	NA	NA	0.17	NA	NA	NA	NA	NA
39	1	1	8	022112-020112-C1-R5-S1	5	21.09	5	0.03	578	119	1.26	NA	NA	0.18	NA	NA	NA	NA	NA
40	1	1	8	022112-020112-C1-R5-S1	6	20.88	10	0.18	1734	119	1.26	NA	NA	0.17	NA	NA	NA	NA	NA
41	1	1	9	022112-020112-C1-R6-S1	1	14.99	5	0.02	547	188	1.17	NA	NA	0.09	NA	NA	NA	NA	NA
42	1	1	9	022112-020112-C1-R6-S1	2	15.18	5	-0.01	-274	188	1.17	NA	NA	0.1	NA	NA	NA	NA	NA
43	1	1	9	022112-020112-C1-R6-S1	3	15.04	10	0	0	188	1.17	NA	NA	0.1	NA	NA	NA	NA	NA
44	1	1	9	022112-020112-C1-R6-S1	4	20.41	5	0.05	1368	188	1.17	NA	NA	0.17	NA	NA	NA	NA	NA
45	1	1	9	022112-020112-C1-R6-S1	5	20.56	5	0.03	821	188	1.17	NA	NA	0.17	NA	NA	NA	NA	NA
46	1	1	9	022112-020112-C1-R6-S1	6	20.65	10	-0.01	-137	188	1.17	NA	NA	0.17	NA	NA	NA	NA	NA
47	1	2	1	022212-020112-C2-R1-S1	1	14.74	5	0.16	5528	0	1.13	NA	NA	0.09	NA	NA	NA	NA	NA
48	1	2	1	022212-020112-C2-R1-S1	2	15.00	5	-0.02	-691	0	1.13	NA	NA	0.1	NA	NA	NA	NA	NA
49	1	2	1	022212-020112-C2-R1-S1	3	14.48	10	0.04	691	0	1.13	NA	NA	0.09	NA	NA	NA	NA	NA
50	1	2	1	022212-020112-C2-R1-S1	4	20.17	5	0.16	5528	0	1.13	NA	NA	0.17	NA	NA	NA	NA	NA
51	1	2	1	022212-020112-C2-R1-S1	5	20.14	5	0.07	2418	0	1.13	NA	NA	0.17	NA	NA	NA	NA	NA
52	1	2	1	022212-020112-C2-R1-S1	6	20.28	10	0.11	1900	0	1.13	NA	NA	0.17	NA	NA	NA	NA	NA
53	1	2	2	022212-020112-C2-R1-S2	1	14.57	5	0.1	3237	0	1.14	NA	NA	0.09	NA	NA	NA	NA	NA
54	1	2	2	022212-020112-C2-R1-S2	2	14.68	5	0.1	3237	0	1.14	NA	NA	0.09	NA	NA	NA	NA	NA
55	1	2	2	022212-020112-C2-R1-S2	3	14.32	10	0.07	1133	0	1.14	NA	NA	0.09	NA	NA	NA	NA	NA
56	1	2	2	022212-020112-C2-R1-S2	4	19.80	5	0.43	13917	0	1.14	NA	NA	0.16	NA	NA	NA	NA	NA
57	1	2	2	022212-020112-C2-R1-S2	5	19.99	5	0.12	3884	0	1.14	NA	NA	0.16	NA	NA	NA	NA	NA
58	1	2	2	022212-020112-C2-R1-S2	6	20.16	10	0.2	3237	0	1.14	NA	NA	0.17	NA	NA	NA	NA	NA
59	1	2	2	022212-020112-C2-R1-S2	7	20.13	10	0.08	1295	0	1.14	NA	NA	0.17	NA	NA	NA	NA	NA
60	1	2	2	022212-020112-C2-R1-S2	8	22.93	10	-1.56	-25245	0	1.14	NA	NA	0.2	NA	NA	NA	NA	NA

					Test Specifications			Erosion Test Results		Properties										
#	Day	Core	Test	Test ID	Step	V $(\frac{cm}{s})$	Duration (min)	WL (gr)	ER $\frac{gr}{m^2.hour}$	Depth (mm)	ρ_{Bulk} $(\frac{gr}{cm^3})$	W (%)	O (%)	τ_{th} (Pa)	Gs	% Fines	LL (%)	PL (%)	PI
61	1	2	3	022412-020112-C2-R2-S1	1	14.31	5	0.08	2968	13	1.12	NA	NA	0.09	NA	NA	NA	NA	NA
62	1	2	3	022412-020112-C2-R2-S1	2	14.55	5	0.03	1113	13	1.12	NA	NA	0.09	NA	NA	NA	NA	NA
63	1	2	3	022412-020112-C2-R2-S1	3	14.15	10	0.03	556	13	1.12	NA	NA	0.09	NA	NA	NA	NA	NA
64	1	2	3	022412-020112-C2-R2-S1	4	19.59	5	0.25	9274	13	1.12	NA	NA	0.16	NA	NA	NA	NA	NA
65	1	2	3	022412-020112-C2-R2-S1	5	19.39	5	0.19	7049	13	1.12	NA	NA	0.16	NA	NA	NA	NA	NA
66	1	2	3	022412-020112-C2-R2-S1	6	19.79	10	0.09	1669	13	1.12	NA	NA	0.16	NA	NA	NA	NA	NA
67	1	2	4	022412-020112-C2-R2-S2	1	16.91	5	0.21	6399	13	1.15	NA	NA	0.12	NA	NA	NA	NA	NA
68	1	2	4	022412-020112-C2-R2-S2	2	17.21	5	0.2	6095	13	1.15	NA	NA	0.13	NA	NA	NA	NA	NA
69	1	2	4	022412-020112-C2-R2-S2	3	16.91	10	0.06	914	13	1.15	NA	NA	0.12	NA	NA	NA	NA	NA
70	1	2	4	022412-020112-C2-R2-S2	4	19.98	5	0.19	5790	13	1.15	NA	NA	0.16	NA	NA	NA	NA	NA
71	1	2	4	022412-020112-C2-R2-S2	5	19.57	5	0.41	12494	13	1.15	NA	NA	0.16	NA	NA	NA	NA	NA
72	1	2	4	022412-020112-C2-R2-S2	6	19.61	10	0.06	914	13	1.15	NA	NA	0.16	NA	NA	NA	NA	NA
73	1	2	5	022712-020112-C2-R3-S1	1	16.47	5	0.17	4430	33	1.18	NA	NA	0.12	NA	NA	NA	NA	NA
74	1	2	5	022712-020112-C2-R3-S1	2	16.61	5	0.04	1042	33	1.18	NA	NA	0.12	NA	NA	NA	NA	NA
75	1	2	5	022712-020112-C2-R3-S1	3	16.40	10	0.27	3518	33	1.18	NA	NA	0.12	NA	NA	NA	NA	NA
76	1	2	5	022712-020112-C2-R3-S1	4	18.90	5	0.1	2606	33	1.18	NA	NA	0.14	NA	NA	NA	NA	NA
77	1	2	5	022712-020112-C2-R3-S1	5	18.98	5	0.05	1303	33	1.18	NA	NA	0.14	NA	NA	NA	NA	NA
78	1	2	5	022712-020112-C2-R3-S1	6	18.86	10	0.18	2345	33	1.18	NA	NA	0.14	NA	NA	NA	NA	NA
79	1	2	6	022712-020112-C2-R4-S1	1	15.95	5	0.33	7558	85	1.21	NA	NA	0.11	NA	NA	NA	NA	NA
80	1	2	6	022712-020112-C2-R4-S1	2	15.94	5	0.11	2519	85	1.21	NA	NA	0.11	NA	NA	NA	NA	NA
81	1	2	6	022712-020112-C2-R4-S1	3	15.95	10	0.09	1031	85	1.21	NA	NA	0.11	NA	NA	NA	NA	NA
82	1	2	6	022712-020112-C2-R4-S1	4	18.59	5	-0.05	-1145	85	1.21	NA	NA	0.14	NA	NA	NA	NA	NA
83	1	2	6	022712-020112-C2-R4-S1	5	18.60	5	0.12	2748	85	1.21	NA	NA	0.14	NA	NA	NA	NA	NA
84	1	2	6	022712-020112-C2-R4-S1	6	18.49	10	-0.02	-229	85	1.21	NA	NA	0.14	NA	NA	NA	NA	NA
85	1	2	7	022812-020112-C2-R5-S1	1	16.21	5	0.18	7870	125	1.1	NA	NA	0.12	NA	NA	NA	NA	NA
86	1	2	7	022812-020112-C2-R5-S1	2	16.28	5	0.13	5684	125	1.1	NA	NA	0.12	NA	NA	NA	NA	NA
87	1	2	7	022812-020112-C2-R5-S1	3	15.83	10	0.12	2623	125	1.1	NA	NA	0.1	NA	NA	NA	NA	NA
88	1	2	7	022812-020112-C2-R5-S1	4	18.43	5	0.09	3935	125	1.1	NA	NA	0.14	NA	NA	NA	NA	NA
89	1	2	7	022812-020112-C2-R5-S1	5	18.16	5	0.02	874	125	1.1	NA	NA	0.14	NA	NA	NA	NA	NA
90	1	2	7	022812-020112-C2-R5-S1	6	18.30	10	0	0	125	1.1	NA	NA	0.14	NA	NA	NA	NA	NA

					Test Specifications			Erosion Test Results		Properties										
#	Day	Core	Test	Test ID	Step	V $(\frac{cm}{s})$	Duration (min)	WL (gr)	ER $\frac{gr}{m^2.hour}$	Depth (mm)	ρ_{Bulk} $(\frac{gr}{cm^3})$	W (%)	O (%)	τ_{th} (Pa)	Gs	% Fines	LL (%)	PL (%)	PI
91	1	2	7	022812-020112-C2-R5-S1	7	21.02	5	0.16	6996	125	1.1	NA	NA	0.18	NA	NA	NA	NA	NA
92	1	2	7	022812-020112-C2-R5-S1	8	19.86	5	0.06	2623	125	1.1	NA	NA	0.16	NA	NA	NA	NA	NA
93	1	3	1	022912-020112-C3-R1-S1	1	11.99	5	0.18	5187	0	1.16	NA	NA	0.06	NA	NA	NA	NA	NA
94	1	3	1	022912-020112-C3-R1-S1	2	11.71	5	0.05	1441	0	1.16	NA	NA	0.06	NA	NA	NA	NA	NA
95	1	3	1	022912-020112-C3-R1-S1	3	11.82	10	0.06	865	0	1.16	NA	NA	0.06	NA	NA	NA	NA	NA
96	1	3	1	022912-020112-C3-R1-S1	4	13.71	10	0.05	720	0	1.16	NA	NA	0.08	NA	NA	NA	NA	NA
97	1	3	1	022912-020112-C3-R1-S1	5	15.03	10	0.37	5331	0	1.16	NA	NA	0.1	NA	NA	NA	NA	NA
98	1	3	1	022912-020112-C3-R1-S1	6	14.67	10	0.08	1153	0	1.16	NA	NA	0.09	NA	NA	NA	NA	NA
99	1	3	1	022912-020112-C3-R1-S1	7	15.67	5	0.09	2594	0	1.16	NA	NA	0.1	NA	NA	NA	NA	NA
100	1	3	1	022912-020112-C3-R1-S1	8	17.25	5	0.27	7781	0	1.16	NA	NA	0.13	NA	NA	NA	NA	NA
101	1	3	2	022912-020112-C3-R1-S2	1	10.89	10	0.09	1669	0	1.12	NA	NA	0.05	NA	NA	NA	NA	NA
102	1	3	2	022912-020112-C3-R1-S2	2	12.49	10	0.07	1298	0	1.12	NA	NA	0.07	NA	NA	NA	NA	NA
103	1	3	2	022912-020112-C3-R1-S2	3	13.54	10	0.16	2968	0	1.12	NA	NA	0.08	NA	NA	NA	NA	NA
104	1	3	2	022912-020112-C3-R1-S2	4	14.63	10	-0.14	-2597	0	1.12	NA	NA	0.09	NA	NA	NA	NA	NA
105	1	3	2	022912-020112-C3-R1-S2	5	15.98	10	0.33	6121	0	1.12	NA	NA	0.1	NA	NA	NA	NA	NA
106	1	3	3	030112-020112-C3-R1-S2-1	1	14.82	10	0.09	1669	0	1.12	NA	NA	0.09	NA	NA	NA	NA	NA
107	1	3	3	030112-020112-C3-R1-S2-1	2	16.32	10	-0.03	-556	0	1.12	NA	NA	0.12	NA	NA	NA	NA	NA
108	1	3	3	030112-020112-C3-R1-S2-1	3	17.51	10	0.03	556	0	1.12	NA	NA	0.13	NA	NA	NA	NA	NA
109	1	3	3	030112-020112-C3-R1-S2-1	4	17.43	10	-0.04	-742	0	1.12	NA	NA	0.13	NA	NA	NA	NA	NA
110	1	3	3	030112-020112-C3-R1-S2-1	5	19.21	10	0.12	2226	0	1.12	NA	NA	0.16	NA	NA	NA	NA	NA
111	1	3	3	030112-020112-C3-R1-S2-1	6	19.04	10	0.09	1669	0	1.12	NA	NA	0.16	NA	NA	NA	NA	NA
112	1	3	3	030112-020112-C3-R1-S2-1	7	19.11	10	0.09	1669	0	1.12	NA	NA	0.16	NA	NA	NA	NA	NA
113	1	3	3	030112-020112-C3-R1-S2-1	8	20.77	10	0.3	5565	0	1.12	NA	NA	0.17	NA	NA	NA	NA	NA
114	1	3	3	030112-020112-C3-R1-S2-1	9	20.77	10	0.19	3524	0	1.12	NA	NA	0.17	NA	NA	NA	NA	NA
115	1	3	3	030112-020112-C3-R1-S2-	10	20.48	10	0.18	3339	0	1.12	NA	NA	0.17	NA	NA	NA	NA	NA

					Test Specifications			Erosion Test Results		Properties										
#	Day	Core	Test	Test ID	Step	V $(\frac{cm}{s})$	Duration (min)	WL (gr)	ER $\frac{gr}{m^2.hour}$	Depth (mm)	ρ_{Bulk} $(\frac{gr}{cm^3})$	W (%)	O (%)	τ_{th} (Pa)	Gs	% Fines	LL (%)	PL (%)	PI
				1																
116	1	3	3	030112-020112-C3-R1-S2-1	11	20.31	10	0.07	1298	0	1.12	NA	NA	0.17	NA	NA	NA	NA	NA	
117	1	3	3	030112-020112-C3-R1-S2-1	12	21.46	10	0.13	2411	0	1.12	NA	NA	0.19	NA	NA	NA	NA	NA	
118	1	3	4	0305012-020112-C3-R1-S2-2	1	15.52	10	0.1	3511	0	1.06	NA	NA	0.11	NA	NA	NA	NA	NA	
119	1	3	4	0305012-020112-C3-R1-S2-2	2	18.17	10	0.06	2107	0	1.06	NA	NA	0.14	NA	NA	NA	NA	NA	
120	1	3	4	0305012-020112-C3-R1-S2-2	3	21.44	10	0.03	1053	0	1.06	NA	NA	0.19	NA	NA	NA	NA	NA	
121	1	3	4	0305012-020112-C3-R1-S2-2	4	24.07	10	0.28	9831	0	1.06	NA	NA	0.24	NA	NA	NA	NA	NA	
122	1	3	4	0305012-020112-C3-R1-S2-2	5	24.21	10	0.11	3862	0	1.06	NA	NA	0.24	NA	NA	NA	NA	NA	
123	1	3	4	0305012-020112-C3-R1-S2-2	6	25.35	10	0.07	2458	0	1.06	NA	NA	0.25	NA	NA	NA	NA	NA	
124	1	3	5	0305012-020112-C3-R2-S1	1	10.34	10	0.07	1009	10	1.16	NA	NA	0.05	NA	NA	NA	NA	NA	
125	1	3	5	0305012-020112-C3-R2-S1	2	10.41	10	0.03	432	10	1.16	NA	NA	0.05	NA	NA	NA	NA	NA	
126	1	3	5	0305012-020112-C3-R2-S1	3	12.50	10	-0.05	-720	10	1.16	NA	NA	0.07	NA	NA	NA	NA	NA	
127	1	3	5	0305012-020112-C3-R2-S1	4	13.45	10	0.09	1297	10	1.16	NA	NA	0.08	NA	NA	NA	NA	NA	
128	1	3	5	0305012-020112-C3-R2-S1	5	14.14	10	0.37	5331	10	1.16	NA	NA	0.09	NA	NA	NA	NA	NA	
129	1	3	5	0305012-020112-C3-R2-S1	6	15.28	10	0.09	1297	10	1.16	NA	NA	0.11	NA	NA	NA	NA	NA	
130	1	3	5	0305012-020112-C3-R2-S1	7	16.22	10	0.2	2882	10	1.16	NA	NA	0.12	NA	NA	NA	NA	NA	
131	1	3	5	0305012-020112-C3-R2-S1	8	16.61	10	0.11	1585	10	1.16	NA	NA	0.12	NA	NA	NA	NA	NA	
132	1	3	6	030612-020112-C3-R3-S1	1	10.11	10	0.1	1145	25	1.21	NA	NA	0.05	NA	NA	NA	NA	NA	
133	1	3	6	030612-020112-C3-R3-S1	2	11.69	10	0	0	25	1.21	NA	NA	0.06	NA	NA	NA	NA	NA	
134	1	3	6	030612-020112-C3-R3-S1	3	12.75	10	0.01	115	25	1.21	NA	NA	0.07	NA	NA	NA	NA	NA	
135	1	3	6	030612-020112-C3-R3-S1	4	13.48	10	0	0	25	1.21	NA	NA	0.08	NA	NA	NA	NA	NA	
136	1	3	6	030612-020112-C3-R3-S1	5	14.71	10	0.15	1718	25	1.21	NA	NA	0.09	NA	NA	NA	NA	NA	
137	1	3	6	030612-020112-C3-R3-S1	6	16.21	10	0.07	802	25	1.21	NA	NA	0.12	NA	NA	NA	NA	NA	
138	1	3	6	030612-020112-C3-R3-S1	7	17.39	10	0.2	2290	25	1.21	NA	NA	0.13	NA	NA	NA	NA	NA	
139	1	3	6	030612-020112-C3-R3-S1	8	18.82	10	0.07	802	25	1.21	NA	NA	0.15	NA	NA	NA	NA	NA	

					Test Specifications			Erosion Test Results		Properties										
#	Day	Core	Test	Test ID	Step	V $(\frac{cm}{s})$	Duration (min)	WL (gr)	ER $\frac{gr}{m^2.hour}$	Depth (mm)	ρ_{Bulk} $(\frac{gr}{cm^3})$	W (%)	O (%)	τ_{th} (Pa)	Gs	% Fines	LL (%)	PL (%)	PI
140	1	3	6	030612-020112-C3-R3-S1	9	19.73	10	0.06	687	25	1.21	NA	NA	0.16	NA	NA	NA	NA	NA
141	1	3	6	030612-020112-C3-R3-S1	10	19.84	10	0.16	1832	25	1.21	NA	NA	0.16	NA	NA	NA	NA	NA
142	1	3	7	030612-020112-C3-R3-S2	1	11.94	10	0.04	425	25	1.23	NA	NA	0.06	NA	NA	NA	NA	NA
143	1	3	7	030612-020112-C3-R3-S2	2	12.73	10	0.1	1063	25	1.23	NA	NA	0.07	NA	NA	NA	NA	NA
144	1	3	7	030612-020112-C3-R3-S2	3	14.30	10	0.26	2763	25	1.23	NA	NA	0.09	NA	NA	NA	NA	NA
145	1	3	7	030612-020112-C3-R3-S2	4	15.36	10	0.05	531	25	1.23	NA	NA	0.11	NA	NA	NA	NA	NA
146	1	3	7	030612-020112-C3-R3-S2	5	16.66	10	0.27	2870	25	1.23	NA	NA	0.12	NA	NA	NA	NA	NA
147	1	3	8	030712-020112-C3-R4-S1	1	9.13	10	0.11	1093	55	1.25	NA	NA	0.04	NA	NA	NA	NA	NA
148	1	3	8	030712-020112-C3-R4-S1	2	11.58	10	0.1	994	55	1.25	NA	NA	0.06	NA	NA	NA	NA	NA
149	1	3	8	030712-020112-C3-R4-S1	3	13.85	10	0.02	199	55	1.25	NA	NA	0.08	NA	NA	NA	NA	NA
150	1	3	8	030712-020112-C3-R4-S1	4	15.11	10	0.16	1590	55	1.25	NA	NA	0.11	NA	NA	NA	NA	NA
151	1	3	8	030712-020112-C3-R4-S1	5	16.59	10	0.2	1987	55	1.25	NA	NA	0.12	NA	NA	NA	NA	NA
152	1	3	8	030712-020112-C3-R4-S1	6	17.91	10	0.27	2683	55	1.25	NA	NA	0.13	NA	NA	NA	NA	NA
153	1	3	8	030712-020112-C3-R4-S1	7	18.93	10	0.16	1590	55	1.25	NA	NA	0.15	NA	NA	NA	NA	NA
154	1	3	8	030712-020112-C3-R4-S1	8	19.86	10	0.11	1093	55	1.25	NA	NA	0.16	NA	NA	NA	NA	NA
155	1	3	8	030712-020112-C3-R4-S1	9	21.87	10	0.22	2186	55	1.25	NA	NA	0.19	NA	NA	NA	NA	NA
156	1	3	9	030712-020112-C3-R5-S1	2	10.75	10	-0.01	-103	87	1.24	NA	NA	0.05	NA	NA	NA	NA	NA
157	1	3	9	030712-020112-C3-R5-S1	3	13.23	10	-0.02	-205	87	1.24	NA	NA	0.08	NA	NA	NA	NA	NA
158	1	3	9	030712-020112-C3-R5-S1	4	14.22	10	0.06	616	87	1.24	NA	NA	0.09	NA	NA	NA	NA	NA
159	1	3	9	030712-020112-C3-R5-S1	5	15.72	10	0.08	821	87	1.24	NA	NA	0.11	NA	NA	NA	NA	NA
160	1	3	9	030712-020112-C3-R5-S1	6	17.13	10	-0.03	-308	87	1.24	NA	NA	0.13	NA	NA	NA	NA	NA
161	1	3	9	030712-020112-C3-R5-S1	7	19.51	10	0.11	1129	87	1.24	NA	NA	0.16	NA	NA	NA	NA	NA
162	1	3	9	030712-020112-C3-R5-S1	8	20.17	10	0.07	719	87	1.24	NA	NA	0.17	NA	NA	NA	NA	NA
163	1	3	9	030712-020112-C3-R5-S1	9	22.52	10	0.1	1027	87	1.24	NA	NA	0.2	NA	NA	NA	NA	NA
164	2	1	1	032012-031912-C1-R1-S1	1	15.17	10	0.36	3697	0	1.24	NA	NA	0.1	NA	NA	NA	NA	NA
165	2	1	1	032012-031912-C1-R1-S1	2	15.52	10	-0.09	-924	0	1.24	NA	NA	0.1	NA	NA	NA	NA	NA
166	2	1	1	032012-031912-C1-R1-S1	3	16.70	10	0.32	3286	0	1.24	NA	NA	0.11	NA	NA	NA	NA	NA
167	2	1	1	032012-031912-C1-R1-S1	4	17.64	10	0.1	1027	0	1.24	NA	NA	0.13	NA	NA	NA	NA	NA
168	2	1	1	032012-031912-C1-R1-S1	5	19.18	10	0.09	924	0	1.24	NA	NA	0.15	NA	NA	NA	NA	NA
169	2	1	1	032012-031912-C1-R1-S1	6	20.28	10	0.08	821	0	1.24	NA	NA	0.17	NA	NA	NA	NA	NA

					Test Specifications			Erosion Test Results		Properties									
#	Day	Core	Test	Test ID	Step	V $(\frac{cm}{s})$	Duration (min)	WL (gr)	ER $\frac{gr}{m^2.hour}$	Depth (mm)	ρ_{Bulk} $(\frac{gr}{cm^3})$	W (%)	O (%)	τ_{th} (Pa)	Gs	% Fines	LL (%)	PL (%)	PI
170	2	1	1	032012-031912-C1-R1-S1	7	20.51	10	0.15	1540	0	1.24	NA	NA	0.17	NA	NA	NA	NA	NA
171	2	1	1	032012-031912-C1-R1-S1	8	22.81	10	0.12	1232	0	1.24	NA	NA	0.2	NA	NA	NA	NA	NA
172	2	1	1	032012-031912-C1-R1-S1	9	23.90	10	0.06	616	0	1.24	NA	NA	0.21	NA	NA	NA	NA	NA
173	2	1	1	032012-031912-C1-R1-S1	10	24.71	10	0.14	1438	0	1.24	NA	NA	0.23	NA	NA	NA	NA	NA
174	2	1	1	032012-031912-C1-R1-S1	11	26.29	10	0.08	821	0	1.24	NA	NA	0.27	NA	NA	NA	NA	NA
175	2	1	1	032012-031912-C1-R1-S1	12	27.70	10	0.21	2156	0	1.24	NA	NA	0.28	NA	NA	NA	NA	NA
176	2	1	1	032012-031912-C1-R1-S1	13	28.66	10	0.23	2362	0	1.24	NA	NA	0.3	NA	NA	NA	NA	NA
177	2	1	2	032112-031912-C1-R1-S1-1	1	26.89	10	0.29	3196	0	1.22	NA	NA	0.26	NA	NA	NA	NA	NA
178	2	1	2	032112-031912-C1-R1-S1-1	2	28.19	10	0.15	1653	0	1.22	NA	NA	0.3	NA	NA	NA	NA	NA
179	2	1	2	032112-031912-C1-R1-S1-1	3	29.47	10	0.11	1212	0	1.22	NA	NA	0.32	NA	NA	NA	NA	NA
180	2	1	2	032112-031912-C1-R1-S1-1	4	30.57	10	0.17	1874	0	1.22	NA	NA	0.34	NA	NA	NA	NA	NA
181	2	1	2	032112-031912-C1-R1-S1-1	5	32.19	10	0.17	1874	0	1.22	NA	NA	0.38	NA	NA	NA	NA	NA
182	2	1	2	032112-031912-C1-R1-S1-1	6	33.48	10	0.66	7274	0	1.22	NA	NA	0.4	NA	NA	NA	NA	NA
183	2	1	2	032112-031912-C1-R1-S1-1	7	34.78	10	0.4	4408	0	1.22	NA	NA	0.42	NA	NA	NA	NA	NA
184	2	1	2	032112-031912-C1-R1-S1-1	8	35.31	10	0.25	2755	0	1.22	NA	NA	0.44	NA	NA	NA	NA	NA
185	2	1	2	032112-031912-C1-R1-S1-1	9	36.35	10	0.38	4188	0	1.22	NA	NA	0.46	NA	NA	NA	NA	NA
186	2	1	2	032112-031912-C1-R1-S1-1	10	37.73	10	0.21	2314	0	1.22	NA	NA	0.49	NA	NA	NA	NA	NA
187	2	1	2	032112-031912-C1-R1-S1-1	11	39.76	10	0.61	6723	0	1.22	NA	NA	0.53	NA	NA	NA	NA	NA
188	2	1	2	032112-031912-C1-R1-S1-1	12	40.96	10	0.63	6943	0	1.22	NA	NA	0.56	NA	NA	NA	NA	NA
189	2	1	3	032212-031912-C1-R1-S2	1	15.10	10	0.05	927	0	1.12	NA	NA	0.1	NA	NA	NA	NA	NA
190	2	1	3	032212-031912-C1-R1-S2	2	15.42	10	0.15	2782	0	1.12	NA	NA	0.1	NA	NA	NA	NA	NA
191	2	1	3	032212-031912-C1-R1-S2	3	16.61	10	-0.01	-185	0	1.12	NA	NA	0.11	NA	NA	NA	NA	NA
192	2	1	3	032212-031912-C1-R1-S2	4	17.48	10	0.28	5194	0	1.12	NA	NA	0.13	NA	NA	NA	NA	NA

					Test Specifications			Erosion Test Results		Properties										
#	Day	Core	Test	Test ID	Step	V $(\frac{cm}{s})$	Duration (min)	WL (gr)	ER $\frac{gr}{m^2.hour}$	Depth (mm)	ρ_{Bulk} $(\frac{gr}{cm^3})$	W (%)	O (%)	τ_{th} (Pa)	Gs	% Fines	LL (%)	PL (%)	PI
193	2	1	3	032212-031912-C1-R1-S2	5	19.28	10	0.26	4823	0	1.12	NA	NA	0.15	NA	NA	NA	NA	NA
194	2	1	3	032212-031912-C1-R1-S2	6	19.99	10	0.11	2040	0	1.12	NA	NA	0.15	NA	NA	NA	NA	NA
195	2	1	3	032212-031912-C1-R1-S2	7	21.26	10	0.28	5194	0	1.12	NA	NA	0.18	NA	NA	NA	NA	NA
196	2	1	3	032212-031912-C1-R1-S2	8	22.54	10	0.24	4452	0	1.12	NA	NA	0.2	NA	NA	NA	NA	NA
197	2	1	3	032212-031912-C1-R1-S2	9	23.72	10	0.24	4452	0	1.12	NA	NA	0.21	NA	NA	NA	NA	NA
198	2	1	3	032212-031912-C1-R1-S2	10	24.43	10	0.4	7420	0	1.12	NA	NA	0.23	NA	NA	NA	NA	NA
199	2	1	3	032212-031912-C1-R1-S2	11	26.19	10	0	0	0	1.12	NA	NA	0.26	NA	NA	NA	NA	NA
200	2	1	3	032212-031912-C1-R1-S2	12	27.20	10	0.72	13355	0	1.12	NA	NA	0.28	NA	NA	NA	NA	NA
201	2	1	3	032212-031912-C1-R1-S2	13	28.50	10	0.07	1298	0	1.12	NA	NA	0.3	NA	NA	NA	NA	NA
202	2	2	1	032312-031912-C2-R1-S1	1	14.64	10	0.1	3038	0	1.07	NA	NA	0.09	NA	NA	NA	NA	NA
203	2	2	1	032312-031912-C2-R1-S1	2	15.25	10	-0.08	-2430	0	1.07	NA	NA	0.1	NA	NA	NA	NA	NA
204	2	2	1	032312-031912-C2-R1-S1	3	16.02	10	0.01	304	0	1.07	NA	NA	0.12	NA	NA	NA	NA	NA
205	2	2	1	032312-031912-C2-R1-S1	4	17.05	10	0.09	2734	0	1.07	NA	NA	0.13	NA	NA	NA	NA	NA
206	2	2	1	032312-031912-C2-R1-S1	5	18.74	10	0.16	4861	0	1.07	NA	NA	0.14	NA	NA	NA	NA	NA
207	2	2	1	032312-031912-C2-R1-S1	6	19.92	10	0.16	4861	0	1.07	NA	NA	0.16	NA	NA	NA	NA	NA
208	2	2	1	032312-031912-C2-R1-S1	7	20.79	10	0.14	4253	0	1.07	NA	NA	0.17	NA	NA	NA	NA	NA
209	2	2	1	032312-031912-C2-R1-S1	8	22.07	10	0.24	7291	0	1.07	NA	NA	0.2	NA	NA	NA	NA	NA
210	2	2	2	032612-031912-C2-R1-S2	1	14.10	10	0.13	1489	0	1.21	NA	NA	0.09	NA	NA	NA	NA	NA
211	2	2	2	032612-031912-C2-R1-S2	2	14.66	10	0.06	687	0	1.21	NA	NA	0.09	NA	NA	NA	NA	NA
212	2	2	2	032612-031912-C2-R1-S2	3	15.78	10	0.03	344	0	1.21	NA	NA	0.1	NA	NA	NA	NA	NA
213	2	2	2	032612-031912-C2-R1-S2	4	16.41	10	0.23	2634	0	1.21	NA	NA	0.11	NA	NA	NA	NA	NA
214	2	2	2	032612-031912-C2-R1-S2	5	18.01	10	0.3	3435	0	1.21	NA	NA	0.14	NA	NA	NA	NA	NA
215	2	2	2	032612-031912-C2-R1-S2	6	19.26	10	0.11	1260	0	1.21	NA	NA	0.15	NA	NA	NA	NA	NA
216	2	2	2	032612-031912-C2-R1-S2	7	20.35	10	0.13	1489	0	1.21	NA	NA	0.17	NA	NA	NA	NA	NA
217	2	2	2	032612-031912-C2-R1-S2	8	21.58	10	0.04	458	0	1.21	NA	NA	0.18	NA	NA	NA	NA	NA
218	2	2	2	032612-031912-C2-R1-S2	9	22.74	10	0.16	1832	0	1.21	NA	NA	0.2	NA	NA	NA	NA	NA
219	2	2	2	032612-031912-C2-R1-S2	10	23.38	10	0.14	1603	0	1.21	NA	NA	0.21	NA	NA	NA	NA	NA
220	2	2	2	032612-031912-C2-R1-S2	11	24.94	10	0.36	4122	0	1.21	NA	NA	0.23	NA	NA	NA	NA	NA
221	2	2	2	032612-031912-C2-R1-S2	12	26.14	10	0.21	2405	0	1.21	NA	NA	0.27	NA	NA	NA	NA	NA
222	2	2	2	032612-031912-C2-R1-S2	13	27.29	10	0.4	4580	0	1.21	NA	NA	0.28	NA	NA	NA	NA	NA

					Test Specifications			Erosion Test Results		Properties										
#	Day	Core	Test	Test ID	Step	V $(\frac{cm}{s})$	Duration (min)	WL (gr)	ER $\frac{gr}{m^2.hour}$	Depth (mm)	ρ_{Bulk} $(\frac{gr}{cm^3})$	W (%)	O (%)	τ_{th} (Pa)	Gs	% Fines	LL (%)	PL (%)	PI
223	2	3	1	032712-031912-C3-R1-S1	1	14.09	10	0.15	1491	0	1.25	NA	NA	0.09	NA	NA	NA	NA	NA
224	2	3	1	032712-031912-C3-R1-S1	2	14.38	10	0.09	894	0	1.25	NA	NA	0.09	NA	NA	NA	NA	NA
225	2	3	1	032712-031912-C3-R1-S1	3	15.61	10	0.02	199	0	1.25	NA	NA	0.1	NA	NA	NA	NA	NA
226	2	3	1	032712-031912-C3-R1-S1	4	16.30	10	0.05	497	0	1.25	NA	NA	0.11	NA	NA	NA	NA	NA
227	2	3	1	032712-031912-C3-R1-S1	5	17.97	10	0.04	397	0	1.25	NA	NA	0.13	NA	NA	NA	NA	NA
228	2	3	1	032712-031912-C3-R1-S1	6	19.06	10	0.1	994	0	1.25	NA	NA	0.15	NA	NA	NA	NA	NA
229	2	3	1	032712-031912-C3-R1-S1	7	20.20	10	0.07	696	0	1.25	NA	NA	0.17	NA	NA	NA	NA	NA
230	2	3	1	032712-031912-C3-R1-S1	8	21.42	10	0.11	1093	0	1.25	NA	NA	0.18	NA	NA	NA	NA	NA
231	2	3	1	032712-031912-C3-R1-S1	9	22.49	10	0.19	1888	0	1.25	NA	NA	0.2	NA	NA	NA	NA	NA
232	2	3	1	032712-031912-C3-R1-S1	10	22.70	10	0.08	795	0	1.25	NA	NA	0.2	NA	NA	NA	NA	NA
233	2	3	1	032712-031912-C3-R1-S1	11	24.62	10	0.31	3080	0	1.25	NA	NA	0.23	NA	NA	NA	NA	NA
234	2	3	1	032712-031912-C3-R1-S1	12	25.95	10	0.23	2285	0	1.25	NA	NA	0.25	NA	NA	NA	NA	NA
235	2	3	1	032712-031912-C3-R1-S1	13	26.97	10	0.19	1888	0	1.25	NA	NA	0.27	NA	NA	NA	NA	NA
236	2	3	2	032812-031912-C3-R1-S2	1	13.67	10	0	0	0	1.22	NA	NA	0.08	NA	NA	NA	NA	NA
237	2	3	2	032812-031912-C3-R1-S2	2	14.03	10	0.08	882	0	1.22	NA	NA	0.09	NA	NA	NA	NA	NA
238	2	3	2	032812-031912-C3-R1-S2	3	15.10	10	-0.02	-220	0	1.22	NA	NA	0.1	NA	NA	NA	NA	NA
239	2	3	2	032812-031912-C3-R1-S2	4	15.91	10	0.13	1433	0	1.22	NA	NA	0.1	NA	NA	NA	NA	NA
240	2	3	2	032812-031912-C3-R1-S2	5	17.70	10	0.19	2094	0	1.22	NA	NA	0.13	NA	NA	NA	NA	NA
241	2	3	2	032812-031912-C3-R1-S2	6	18.70	10	0.09	992	0	1.22	NA	NA	0.14	NA	NA	NA	NA	NA
242	2	3	2	032812-031912-C3-R1-S2	7	20.04	10	0.15	1653	0	1.22	NA	NA	0.17	NA	NA	NA	NA	NA
243	2	3	2	032812-031912-C3-R1-S2	8	21.08	10	0.02	220	0	1.22	NA	NA	0.18	NA	NA	NA	NA	NA
244	2	3	2	032812-031912-C3-R1-S2	9	22.20	10	0.17	1874	0	1.22	NA	NA	0.2	NA	NA	NA	NA	NA
245	2	3	2	032812-031912-C3-R1-S2	10	22.69	10	0.12	1323	0	1.22	NA	NA	0.2	NA	NA	NA	NA	NA
246	2	3	2	032812-031912-C3-R1-S2	11	24.49	10	0.17	1874	0	1.22	NA	NA	0.23	NA	NA	NA	NA	NA
247	2	3	2	032812-031912-C3-R1-S2	12	25.84	10	0.17	1874	0	1.22	NA	NA	0.24	NA	NA	NA	NA	NA
248	2	3	2	032812-031912-C3-R1-S2	13	26.58	10	0.23	2535	0	1.22	NA	NA	0.26	NA	NA	NA	NA	NA
249	2	4	1	032912-031912-C4-R1-S1	1	13.00	10	0.05	684	0	1.17	NA	NA	0.08	NA	NA	NA	NA	NA
250	2	4	1	032912-031912-C4-R1-S1	2	13.11	10	0.07	957	0	1.17	NA	NA	0.08	NA	NA	NA	NA	NA
251	2	4	1	032912-031912-C4-R1-S1	3	14.42	10	0.07	957	0	1.17	NA	NA	0.09	NA	NA	NA	NA	NA
252	2	4	1	032912-031912-C4-R1-S1	4	15.37	10	0.18	2462	0	1.17	NA	NA	0.1	NA	NA	NA	NA	NA

					Test Specifications			Erosion Test Results		Properties									
#	Day	Core	Test	Test ID	Step	V $(\frac{cm}{s})$	Duration (min)	WL (gr)	ER $\frac{gr}{m^2.hour}$	Depth (mm)	ρ_{Bulk} $(\frac{gr}{cm^3})$	W (%)	O (%)	τ_{th} (Pa)	Gs	% Fines	LL (%)	PL (%)	PI
253	2	4	1	032912-031912-C4-R1-S1	5	17.11	10	0.08	1094	0	1.17	NA	NA	0.13	NA	NA	NA	NA	NA
254	2	4	1	032912-031912-C4-R1-S1	6	18.21	10	0.05	684	0	1.17	NA	NA	0.14	NA	NA	NA	NA	NA
255	2	4	1	032912-031912-C4-R1-S1	7	19.36	10	0.08	1094	0	1.17	NA	NA	0.15	NA	NA	NA	NA	NA
256	2	4	1	032912-031912-C4-R1-S1	8	20.48	10	0.04	547	0	1.17	NA	NA	0.17	NA	NA	NA	NA	NA
257	2	4	1	032912-031912-C4-R1-S1	9	21.59	10	0.18	2462	0	1.17	NA	NA	0.18	NA	NA	NA	NA	NA
258	2	4	1	032912-031912-C4-R1-S1	10	22.23	10	0.05	684	0	1.17	NA	NA	0.2	NA	NA	NA	NA	NA
259	2	4	1	032912-031912-C4-R1-S1	11	23.89	10	0.05	684	0	1.17	NA	NA	0.21	NA	NA	NA	NA	NA
260	2	4	1	032912-031912-C4-R1-S1	12	24.90	10	0.08	1094	0	1.17	NA	NA	0.23	NA	NA	NA	NA	NA
261	2	4	1	032912-031912-C4-R1-S1	13	26.14	10	0.25	3419	0	1.17	NA	NA	0.27	NA	NA	NA	NA	NA
262	2	4	2	033012-031912-C4-R1-S2	1	12.70	10	0.11	2040	0	1.12	NA	NA	0.07	NA	NA	NA	NA	NA
263	2	4	2	033012-031912-C4-R1-S2	2	13.09	10	0.02	371	0	1.12	NA	NA	0.08	NA	NA	NA	NA	NA
264	3	1	1	060412-060112-C1-R1-S1-F1	1	14.00	15	0.1	1079	0	1.14	192	11.50	0.09	2.66	91	198	87	111
265	3	1	1	060412-060112-C1-R1-S1-F1	2	18.00	15	0.04	432	0	1.14	192	11.50	0.14	2.66	91	198	87	111
266	3	1	1	060412-060112-C1-R1-S1-F1	3	22.00	15	0.24	2589	0	1.14	192	11.50	0.2	2.66	91	198	87	111
267	3	1	1	060412-060112-C1-R1-S1-F1	4	25.00	15	0.76	8199	0	1.14	192	11.50	0.25	2.66	91	198	87	111
268	3	1	1	060412-060112-C1-R1-S1-F1	5	28.00	15	0.7	7552	0	1.14	192	11.50	0.3	2.66	91	198	87	111
269	3	1	1	060412-060112-C1-R1-S1-F1	6	32.00	15	0.66	7120	0	1.14	192	11.50	0.38	2.66	91	198	87	111
270	3	1	1	060412-060112-C1-R1-S1-F2	1	38.25	15	1.17	17052	0	1.1	192	11.50	0.51	2.66	91	198	87	111
271	3	1	2	060512-060112-C1-R1-S2	1	24.14	10	0.17	2116	0	1.19	192	11.50	0.23	2.66	91	198	87	111
272	3	1	2	060512-060112-C1-R1-S2	2	27.85	10	0.26	3236	0	1.19	192	11.50	0.28	2.66	91	198	87	111
273	3	1	2	060512-060112-C1-R1-S2	3	32.03	10	0.2	2489	0	1.19	192	11.50	0.38	2.66	91	198	87	111
274	3	1	2	060512-060112-C1-R1-S2	4	36.40	10	0.91	11327	0	1.19	192	11.50	0.47	2.66	91	198	87	111
275	3	1	2	060512-060112-C1-R1-S2	5	39.47	10	0.37	4605	0	1.19	192	11.50	0.54	2.66	91	198	87	111
276	3	1	2	060512-060112-C1-R1-S2	6	43.87	10	0.32	3983	0	1.19	192	11.50	0.64	2.66	91	198	87	111
277	3	1	3	060612-060112-C1-R2-S1	1	14.55	10	0.03	273	20	1.28	182	9.70	0.09	2.66	91	198	87	111
278	3	1	3	060612-060112-C1-R2-S1	2	23.27	10	0.13	1181	20	1.28	182	9.70	0.22	2.66	91	198	87	111

					Test Specifications			Erosion Test Results		Properties									
#	Day	Core	Test	Test ID	Step	V $(\frac{cm}{s})$	Duration (min)	WL (gr)	ER $\frac{gr}{m^2.hour}$	Depth (mm)	ρ_{Bulk} $(\frac{gr}{cm^3})$	W (%)	O (%)	τ_{th} (Pa)	Gs	% Fines	LL (%)	PL (%)	PI
279	3	1	3	060612-060112-C1-R2-S1	3	33.83	10	0.33	2998	20	1.28	182	9.70	0.4	2.66	91	198	87	111
280	3	1	4	060812-060112-C1-R2-S1-1	1	22.52	10	0.09	775	20	1.3	182	9.70	0.19	2.66	91	198	87	111
281	3	1	4	060812-060112-C1-R2-S1-1	2	31.06	10	0.04	344	20	1.3	182	9.70	0.35	2.66	91	198	87	111
282	3	1	4	060812-060112-C1-R2-S1-1	3	41.21	10	0.13	1120	20	1.3	182	9.70	0.57	2.66	91	198	87	111
283	3	1	5	061212-060112-C1-R3-S1	1	22.07	10	0.05	1203	36	1.09	203	10.70	0.2	2.66	91	198	87	111
284	3	1	5	061212-060112-C1-R3-S1	2	30.41	10	0.13	3129	36	1.09	203	10.70	0.34	2.66	91	198	87	111
285	3	1	5	061212-060112-C1-R3-S1	3	40.70	10	0.24	5777	36	1.09	203	10.70	0.56	2.66	91	198	87	111
286	3	1	5	061212-060112-C1-R3-S1	4	50.03	10	0.89	21422	36	1.09	203	10.70	0.83	2.66	91	198	87	111
287	3	1	6	061212-060112-C1-R4-S1	1	22.10	10	0.2	2385	56	1.2	162	9.60	0.19	2.66	91	198	87	111
288	3	1	6	061212-060112-C1-R4-S1	2	30.45	10	0.06	715	56	1.2	162	9.60	0.33	2.66	91	198	87	111
289	3	1	6	061212-060112-C1-R4-S1	3	40.91	10	0.06	715	56	1.2	162	9.60	0.55	2.66	91	198	87	111
290	3	1	6	061212-060112-C1-R4-S1	4	50.06	10	0.1	1192	56	1.2	162	9.60	0.81	2.66	91	198	87	111
291	3	1	6	061212-060112-C1-R4-S1	5	60.84	10	0.07	835	56	1.2	162	9.60	1.12	2.66	91	198	87	111
292	3	1	7	061212-060112-C1-R5-S1	1	22.01	10	-0.11	-1260	75	1.21	NA	NA	0.2	2.66	91	198	87	111
293	3	1	7	061212-060112-C1-R5-S1	2	22.33	10	-0.04	-458	75	1.21	NA	NA	0.2	2.66	91	198	87	111
294	3	1	8	061312-060112-C1-R5-S1-1	1	17.75	10	-0.05	-651	75	1.18	NA	NA	0.12	2.66	91	198	87	111
295	3	1	8	061312-060112-C1-R5-S1-1	2	22.35	10	0.05	651	75	1.18	NA	NA	0.19	2.66	91	198	87	111
296	3	1	8	061312-060112-C1-R5-S1-1	3	26.18	10	0.02	261	75	1.18	NA	NA	0.26	2.66	91	198	87	111
297	3	1	8	061312-060112-C1-R5-S1-1	4	30.66	10	0.01	130	75	1.18	NA	NA	0.33	2.66	91	198	87	111
298	3	1	8	061312-060112-C1-R5-S1-1	5	35.80	10	0.08	1042	75	1.18	NA	NA	0.43	2.66	91	198	87	111
299	3	1	8	061312-060112-C1-R5-S1-1	6	40.77	10	0.05	651	75	1.18	NA	NA	0.54	2.66	91	198	87	111

					Test Specifications			Erosion Test Results		Properties									
#	Day	Core	Test	Test ID	Step	V $(\frac{cm}{s})$	Duration (min)	WL (gr)	ER $\frac{gr}{m^2.hour}$	Depth (mm)	ρ_{Bulk} $(\frac{gr}{cm^3})$	W (%)	O (%)	τ_{th} (Pa)	Gs	% Fines	LL (%)	PL (%)	PI
300	3	1	8	061312-060112-C1-R5-S1-1	7	45.71	10	0.12	1563	75	1.18	NA	NA	0.67	2.66	91	198	87	111
301	3	1	9	061312-060112-C1-R6-S1	1	17.63	10	0.01	162	102	1.14	180	12.30	0.12	2.66	91	198	87	111
302	3	1	9	061312-060112-C1-R6-S1	2	22.28	10	0.04	647	102	1.14	180	12.30	0.19	2.66	91	198	87	111
303	3	1	9	061312-060112-C1-R6-S1	3	26.32	10	0	0	102	1.14	180	12.30	0.26	2.66	91	198	87	111
304	3	1	9	061312-060112-C1-R6-S1	4	35.94	10	0.09	1456	102	1.14	180	12.30	0.43	2.66	91	198	87	111
305	3	1	9	061312-060112-C1-R6-S1	5	45.70	10	0.12	1942	102	1.14	180	12.30	0.67	2.66	91	198	87	111
306	3	1	9	061312-060112-C1-R6-S1	6	55.68	10	0.26	4208	102	1.14	180	12.30	0.95	2.66	91	198	87	111
307	3	1	9	061312-060112-C1-R6-S1	7	65.85	10	0.23	3722	102	1.14	180	12.30	1.27	2.66	91	198	87	111
308	3	1	9	061312-060112-C1-R6-S1	8	76.45	10	0.6	9710	102	1.14	180	12.30	1.67	2.66	91	198	87	111
309	3	2	1	060512-060112-C2-R1-S1	1	12.17	10	0.04	576	0	1.16	215	9.50	0.07	2.68	85	145	114	31
310	3	2	1	060512-060112-C2-R1-S1	2	16.83	10	0.15	2161	0	1.16	215	9.50	0.12	2.68	85	145	114	31

					Test Specifications			Erosion Test Results		Properties									
#	Day	Core	Test	Test ID	Step	V $(\frac{cm}{s})$	Duration (min)	WL (gr)	ER $\frac{gr}{m^2.hour}$	Depth (mm)	ρ_{Bulk} $(\frac{gr}{cm^3})$	W (%)	O (%)	τ_{th} (Pa)	Gs	% Fines	LL (%)	PL (%)	PI
311	3	2	1	060512-060112-C2-R1-S1	3	21.12	10	0.19	2738	0	1.16	215	9.50	0.18	2.68	85	145	114	31
312	3	2	1	060512-060112-C2-R1-S1	4	25.82	10	0.55	7925	0	1.16	215	9.50	0.25	2.68	85	145	114	31
313	3	2	1	060512-060112-C2-R1-S1	5	30.96	10	1.19	17146	0	1.16	215	9.50	0.34	2.68	85	145	114	31
314	3	2	1	060512-060112-C2-R1-S1	6	35.94	10	1	14408	0	1.16	215	9.50	0.45	2.68	85	145	114	31
315	3	2	2	060612-060112-C2-R1-S2	1	24.68	10	0.81	6344	0	1.34	215	9.50	0.23	2.68	85	145	114	31
316	3	2	3	061112-060112-C2-R2-S1	1	22.40	10	0	0	22	1.24	168	9.50	0.2	2.68	85	145	114	31
317	3	2	3	061112-060112-C2-R2-S1	2	30.66	10	0.09	924	22	1.24	168	9.50	0.34	2.68	85	145	114	31
318	3	2	3	061112-060112-C2-R2-S1	3	41.02	10	0.13	1335	22	1.24	168	9.50	0.59	2.68	85	145	114	31
319	3	2	3	061112-060112-C2-R2-S1	4	50.24	10	0.36	3697	22	1.24	168	9.50	0.83	2.68	85	145	114	31
320	3	2	4	061412-060112-C2-R3-S1	1	17.37	10	-0.01	-106	59	1.23	187	10.90	0.12	2.68	85	145	114	31
321	3	2	4	061412-060112-C2-R3-S1	2	22.08	10	0	0	59	1.23	187	10.90	0.19	2.68	85	145	114	31

					Test Specifications			Erosion Test Results		Properties									
#	Day	Core	Test	Test ID	Step	V $(\frac{cm}{s})$	Duration (min)	WL (gr)	ER $\frac{gr}{m^2.hour}$	Depth (mm)	ρ_{Bulk} $(\frac{gr}{cm^3})$	W (%)	O (%)	τ_{th} (Pa)	Gs	% Fines	LL (%)	PL (%)	PI
322	3	2	4	061412-060112-C2-R3-S1	3	35.93	10	0.08	850	59	1.23	187	10.90	0.43	2.68	85	145	114	31
323	3	2	4	061412-060112-C2-R3-S1	4	50.10	10	0.13	1382	59	1.23	187	10.90	0.81	2.68	85	145	114	31
324	3	2	5	061412-060112-C2-R4-S1	1	22.10	10	0.06	561	74	1.27	157	10.60	0.19	2.68	85	145	114	31
325	3	2	5	061412-060112-C2-R4-S1	2	30.43	10	-0.02	-187	74	1.27	157	10.60	0.33	2.68	85	145	114	31
326	3	2	5	061412-060112-C2-R4-S1	3	40.92	10	0.06	561	74	1.27	157	10.60	0.54	2.68	85	145	114	31
327	3	2	5	061412-060112-C2-R4-S1	4	49.92	10	0.07	654	74	1.27	157	10.60	0.78	2.68	85	145	114	31
328	3	2	5	061412-060112-C2-R4-S1	5	60.69	10	0.08	748	74	1.27	157	10.60	1.11	2.68	85	145	114	31
329	3	2	5	061412-060112-C2-R4-S1	6	70.88	10	0.09	841	74	1.27	157	10.60	1.46	2.68	85	145	114	31
330	3	2	5	061412-060112-C2-R4-S1	7	81.46	10	0.24	2244	74	1.27	157	10.60	1.88	2.68	85	145	114	31
331	3	2	6	061412-060112-C2-R4-S1-1	1	22.16	20	0.01	47	74	1.27	157	10.60	0.2	2.68	85	145	114	31
332	3	2	6	061412-060112-C2-R4-S1-1	2	30.58	10	0.06	561	74	1.27	157	10.60	0.34	2.68	85	145	114	31

					Test Specifications			Erosion Test Results		Properties									
#	Day	Core	Test	Test ID	Step	V $(\frac{cm}{s})$	Duration (min)	WL (gr)	ER $\frac{gr}{m^2.hour}$	Depth (mm)	ρ_{Bulk} $(\frac{gr}{cm^3})$	W (%)	O (%)	τ_{th} (Pa)	Gs	% Fines	LL (%)	PL (%)	PI
333	3	2	6	061412-060112-C2-R4-S1-1	3	40.78	10	0.01	93	74	1.27	157	10.60	0.56	2.68	85	145	114	31
334	3	2	6	061412-060112-C2-R4-S1-1	4	50.09	10	0.03	280	74	1.27	157	10.60	0.83	2.68	85	145	114	31
335	3	2	6	061412-060112-C2-R4-S1-1	5	60.53	10	0.1	935	74	1.27	157	10.60	1.15	2.68	85	145	114	31
336	3	2	6	061412-060112-C2-R4-S1-1	6	70.92	8	0.11	1285	74	1.27	157	10.60	1.51	2.68	85	145	114	31
337	3	2	7	061512-060112-C2-R5-S1	1	25.85	10	0.04	336	123	1.31	179	NA	0.25	2.68	85	145	114	31
338	3	2	7	061512-060112-C2-R5-S1	2	40.55	10	0.1	840	123	1.31	180	NA	0.56	2.68	85	145	114	31
339	3	2	7	061512-060112-C2-R5-S1	3	60.13	10	0.5	4199	123	1.31	181	NA	1.15	2.68	85	145	114	31
340	3	2	7	061512-060112-C2-R5-S1	4	70.66	10	0.43	3611	123	1.31	182	NA	1.51	2.68	85	145	114	31
341	3	3	1	060612-06012-C3-R1-S1 (F1, F2)	1	10.54	10	0.01	88	0	1.29	210	9.20	0.05	2.66	93	145	96	49
342	3	3	1	060612-06012-C3-R1-S1 (F1, F2)	2	15.36	10	0.1	884	0	1.29	210	9.20	0.1	2.66	93	145	96	49
343	3	3	1	060612-06012-C3-R1-S1 (F1, F2)	3	19.52	10	0.2	1768	0	1.29	210	9.20	0.16	2.66	93	145	96	49

					Test Specifications			Erosion Test Results		Properties									
#	Day	Core	Test	Test ID	Step	V ($\frac{cm}{s}$)	Duration (min)	WL (gr)	ER $\frac{gr}{m^2.hour}$	Depth (mm)	ρ_{Bulk} ($\frac{gr}{cm^3}$)	W (%)	O (%)	τ_{th} (Pa)	Gs	% Fines	LL (%)	PL (%)	PI
344	3	3	1	060612-06012-C3-R1-S1 (F1, F2)	4	23.88	10	0.24	2122	0	1.29	210	9.20	0.22	2.66	93	145	96	49
345	3	3	1	060612-06012-C3-R1-S1 (F1, F2)	5	29.46	10	0.46	4067	0	1.29	210	9.20	0.32	2.66	93	145	96	49
346	3	3	1	060612-06012-C3-R1-S1 (F1, F2)	6	34.36	10	0.97	8575	0	1.29	210	9.20	0.43	2.66	93	145	96	49
347	3	3	2	060712-06012-C3-R1-S2	1	17.86	10	0.04	547	0	1.17	210	9.20	0.13	2.66	93	145	96	49
348	3	3	2	060712-06012-C3-R1-S2	2	22.68	10	0.13	1778	0	1.17	210	9.20	0.2	2.66	93	145	96	49
349	3	3	2	060712-06012-C3-R1-S2	3	26.63	10	0.26	3556	0	1.17	210	9.20	0.27	2.66	93	145	96	49
350	3	3	2	060712-06012-C3-R1-S2	4	31.14	10	0.48	6565	0	1.17	210	9.20	0.36	2.66	93	145	96	49
351	3	3	2	060712-06012-C3-R1-S2	5	36.35	10	0.97	13267	0	1.17	210	9.20	0.47	2.66	93	145	96	49
352	3	3	3	061512-06012-C3-R3-S1	1	25.77	10	0.08	821	65	1.24	162	9.00	0.25	2.66	93	145	96	49
353	3	3	3	061512-06012-C3-R3-S1	2	40.48	10	0.12	1232	65	1.24	162	9.00	0.56	2.66	93	145	96	49
354	3	3	3	061512-06012-C3-R3-S1	3	60.18	10	0.26	2670	65	1.24	162	9.00	1.15	2.66	93	145	96	49

					Test Specifications			Erosion Test Results		Properties									
#	Day	Core	Test	Test ID	Step	V $(\frac{cm}{s})$	Duration (min)	WL (gr)	ER $\frac{gr}{m^2.hour}$	Depth (mm)	ρ_{Bulk} $(\frac{gr}{cm^3})$	W (%)	O (%)	τ_{th} (Pa)	Gs	% Fines	LL (%)	PL (%)	PI
355	3	3	3	061512-06012-C3-R3-S1	4	60.01	10	0.57	5853	65	1.24	162	9.00	1.15	2.66	93	145	96	49
356	3	3	4	061512-06012-C3-R4-S1	1	25.80	10	0.04	397	95	1.25	153	8.10	0.24	2.66	93	145	96	49
357	3	3	4	061512-06012-C3-R4-S1	2	45.12	10	0.18	1789	95	1.25	153	8.10	0.67	2.66	93	145	96	49
358	3	3	4	061512-06012-C3-R4-S1	3	70.59	10	0.57	5664	95	1.25	153	8.10	1.46	2.66	93	145	96	49
359	3	3	4	061512-06012-C3-R4-S1	4	81.13	10	0.12	1192	95	1.25	153	8.10	1.88	2.66	93	145	96	49
360	3	3	5	061512-06012-C3-R5-S1	1	25.64	10	0.06	504	134	1.31	144	9.90	0.24	2.66	93	145	96	49
361	3	3	5	061512-06012-C3-R5-S1	2	45.22	10	0.12	1008	134	1.31	144	9.90	0.67	2.66	93	145	96	49
362	3	3	5	061512-06012-C3-R5-S1	3	70.42	10	0.21	1764	134	1.31	144	9.90	1.46	2.66	93	145	96	49
363	3	3	6	061912-06012-C3-R6-S1	1	28.76	10	0.02	193	172	1.26	106	31.70	0.3	2.66	93	145	96	49
364	3	3	6	061912-06012-C3-R6-S1	2	43.88	10	0.02	193	172	1.26	106	31.70	0.64	2.66	93	145	96	49
365	3	3	6	061912-06012-C3-R6-S1	3	80.13	10	0.2	1926	172	1.26	106	31.70	1.9	2.66	93	145	96	49

					Test Specifications			Erosion Test Results		Properties										
#	Day	Core	Test	Test ID	Step	V $(\frac{cm}{s})$	Duration (min)	WL (gr)	ER $\frac{gr}{m^2.hour}$	Depth (mm)	ρ_{Bulk} $(\frac{gr}{cm^3})$	W (%)	O (%)	τ_{th} (Pa)	Gs	% Fines	LL (%)	PL (%)	PI
366	3	3	7	061912-06012-C3-R7-S1	1	28.74	10	0.02	187	189	1.27	159	16.20	0.3	2.66	93	145	96	49
367	3	3	7	061912-06012-C3-R7-S1	2	43.86	10	0.07	654	189	1.27	159	16.20	0.64	2.66	93	145	96	49
368	3	3	7	061912-06012-C3-R7-S1	3	79.98	10	0.35	3272	189	1.27	159	16.20	1.86	2.66	93	145	96	49
369	3	3	8	061912-06012-C3-R8-S1	1	28.90	10	0.06	530	211	1.29	N/A	NA	0.29	2.66	93	145	96	49
370	3	3	8	061912-06012-C3-R8-S1	2	59.33	10	0.04	354	211	1.29	N/A	NA	1.08	2.66	93	145	96	49
371	3	3	8	061912-06012-C3-R8-S1	3	90.18	10	0.74	6542	211	1.29	N/A	NA	2.27	2.66	93	145	96	49
372	3	4	1	060812-06012-C4-R1-S1	1	17.99	10	0.06	865	0	1.16	203	13.76	0.13	2.65	85	134	78	56
373	3	4	1	060812-06012-C4-R1-S1	2	22.69	10	0.22	3170	0	1.16	203	13.76	0.2	2.65	85	134	78	56
374	3	4	1	060812-06012-C4-R1-S1	3	26.65	10	0.22	3170	0	1.16	203	13.76	0.27	2.65	85	134	78	56
375	3	4	1	060812-06012-C4-R1-S1	4	31.08	10	0.59	8501	0	1.16	203	13.76	0.36	2.65	85	134	78	56
376	3	4	1	060812-06012-C4-R1-S1	5	36.35	10	0.77	11094	0	1.16	203	13.76	0.47	2.65	85	134	78	56

					Test Specifications			Erosion Test Results		Properties									
#	Day	Core	Test	Test ID	Step	V $(\frac{cm}{s})$	Duration (min)	WL (gr)	ER $\frac{gr}{m^2.hour}$	Depth (mm)	ρ_{Bulk} $(\frac{gr}{cm^3})$	W (%)	O (%)	τ_{th} (Pa)	Gs	% Fines	LL (%)	PL (%)	PI
377	3	4	1	060812-06012-C4-R1-S1	6	41.09	10	0.96	13832	0	1.16	203	13.76	0.59	2.65	85	134	78	56
378	3	4	1	060812-06012-C4-R1-S1	7	45.91	10	0.69	9942	0	1.16	203	13.76	0.69	2.65	85	134	78	56
379	3	4	1	060812-06012-C4-R1-S1	8	50.15	10	1.03	14841	0	1.16	203	13.76	0.83	2.65	85	134	78	56
380	3	4	2	061112-060112-C4-R1-S2-F1 and F2	1	17.48	10	0.05	482	0	1.26	203	13.76	0.13	2.65	85	134	78	56
381	3	4	2	061112-060112-C4-R1-S2-F1 and F2	2	22.22	10	0.12	1156	0	1.26	203	13.76	0.2	2.65	85	134	78	56
382	3	4	2	061112-060112-C4-R1-S2-F1 and F2	3	26.30	10	0.18	1734	0	1.26	203	13.76	0.27	2.65	85	134	78	56
383	3	4	2	061112-060112-C4-R1-S2-F1 and F2	4	30.41	4.1	0.35	8222	0	1.26	203	13.76	0.34	2.65	85	134	78	56
384	3	4	2	061112-060112-C4-R1-S2-F1 and F2	5	30.50	10	0.09	867	0	1.26	203	13.76	0.34	2.65	85	134	78	56
385	3	4	2	061112-060112-C4-R1-S2-F1 and F2	6	35.76	10	0.52	5008	0	1.26	203	13.76	0.45	2.65	85	134	78	56
386	3	4	2	061112-060112-C4-R1-S2-F1 and F2	7	40.57	8	0.84	10113	0	1.26	203	13.76	0.56	2.65	85	134	78	56
387	3	4	2	061112-060112-C4-R1-S2-F1 and F2	8	45.55	10	0.51	4912	0	1.26	203	13.76	0.69	2.65	85	134	78	56

					Test Specifications			Erosion Test Results		Properties									
#	Day	Core	Test	Test ID	Step	V $(\frac{cm}{s})$	Duration (min)	WL (gr)	ER $\frac{gr}{m^2.hour}$	Depth (mm)	ρ_{Bulk} $(\frac{gr}{cm^3})$	W (%)	O (%)	τ_{th} (Pa)	Gs	% Fines	LL (%)	PL (%)	PI
388	3	4	2	061112-060112-C4-R1-S2-F1 and F2	9	50.14	10	0.82	7897	0	1.26	203	13.76	0.83	2.65	85	134	78	56
389	3	4	2	061112-060112-C4-R1-S2-F1 and F2	10	55.59	10	0.73	7031	0	1.26	203	13.76	0.99	2.65	85	134	78	56
390	3	4	3	061112-060112-C4-R1-S2-1	1	60.60	10	1.06	12138	0	1.21	203	13.76	1.15	2.65	85	134	78	56
391	3	4	3	061112-060112-C4-R1-S2-1	2	50.16	10	0.53	6069	0	1.21	203	13.76	0.83	2.65	85	134	78	56
392	3	4	3	061112-060112-C4-R1-S2-1	3	40.97	10	0.29	3321	0	1.21	203	13.76	0.56	2.65	85	134	78	56
393	3	4	4	061812-060112-C4-R2-S1	1	24.78	10	0.01	93	36	1.27	168	11.10	0.23	2.65	85	134	78	56
394	3	4	4	061812-060112-C4-R2-S1	2	44.73	10	0.08	748	36	1.27	168	11.10	0.67	2.65	85	134	78	56
395	3	4	4	061812-060112-C4-R2-S1	3	64.68	10	0.19	1776	36	1.27	168	11.10	1.29	2.65	85	134	78	56
396	3	4	4	061812-060112-C4-R2-S1	4	85.60	10	0.75	7011	36	1.27	168	11.10	2.12	2.65	85	134	78	56
397	3	4	5	061812-060112-C4-R3-S1	1	64.57	10	0.05	482	50	1.26	159	11.60	1.29	2.65	85	134	78	56
398	3	4	5	061812-060112-C4-R3-S1	2	85.34	10	0.47	4527	50	1.26	159	11.60	2.12	2.65	85	134	78	56

					Test Specifications			Erosion Test Results		Properties									
#	Day	Core	Test	Test ID	Step	V $(\frac{cm}{s})$	Duration (min)	WL (gr)	ER $\frac{gr}{m^2.hour}$	Depth (mm)	ρ_{Bulk} $(\frac{gr}{cm^3})$	W (%)	O (%)	τ_{th} (Pa)	Gs	% Fines	LL (%)	PL (%)	PI
399	3	4	5	061812-060112-C4-R3-S1	3	64.49	10	0.07	674	50	1.26	159	11.60	1.29	2.65	85	134	78	56
400	3	4	5	061812-060112-C4-R3-S1	4	25.00	10	0.03	289	50	1.26	159	11.60	0.25	2.65	85	134	78	56
401	3	4	6	061812-060112-C4-R4-S1	1	90.77	10	0.43	4020	84	1.27	156	11.30	2.29	2.65	85	134	78	56
402	3	4	6	061812-060112-C4-R4-S1	2	59.55	10	0.03	280	84	1.27	156	11.30	1.09	2.65	85	134	78	56
403	3	4	6	061812-060112-C4-R4-S1	3	29.18	10	0.04	374	84	1.27	156	11.30	0.31	2.65	85	134	78	56
404	3	4	7	061812-060112-C4-R5-S1	1	29.09	10	0.03	240	123	1.33	158	15.50	0.31	2.65	85	134	78	56
405	3	4	7	061812-060112-C4-R5-S1	2	59.33	10	0.16	1282	123	1.33	158	15.50	1.09	2.65	85	134	78	56
406	3	4	7	061812-060112-C4-R6-S1	1	89.37	2.5	0.76	27619	123	1.28	174	16.40	2.3	2.65	85	134	78	56
407	4	1	1	062012-061912-C1-R1-S1	1	19.25	10	0.08	358	0	1.8	45	2.00	0.16	2.73	29	74	55	18
408	4	1	1	062012-061912-C1-R1-S1	2	27.96	10	0.35	1565	0	1.8	45	2.00	0.28	2.73	29	74	55	18
409	4	1	1	062012-061912-C1-R1-S1	3	38.11	10	2.01	8988	0	1.8	45	2.00	0.52	2.73	29	74	55	18

					Test Specifications			Erosion Test Results		Properties									
#	Day	Core	Test	Test ID	Step	V $(\frac{cm}{s})$	Duration (min)	WL (gr)	ER $\frac{gr}{m^2.hour}$	Depth (mm)	ρ_{Bulk} $(\frac{gr}{cm^3})$	W (%)	O (%)	τ_{th} (Pa)	Gs	% Fines	LL (%)	PL (%)	PI
410	4	1	1	062012-061912-C1-R1-S1	4	47.81	10	8.01	35817	0	1.8	45	2.00	0.75	2.73	29	74	55	18
411	4	1	2	062012-061912-C1-R1-S2	1	19.20	10	0.11	506	0	1.76	45	2.00	0.16	2.73	29	74	55	18
412	4	1	2	062012-061912-C1-R1-S2	2	27.66	10	0.47	2163	0	1.76	45	2.00	0.28	2.73	29	74	55	18
413	4	1	2	062012-061912-C1-R1-S2	3	38.19	10	2.74	12610	0	1.76	45	2.00	0.52	2.73	29	74	55	18
414	4	1	2	062012-061912-C1-R1-S2	4	47.29	10	3.7	17029	0	1.76	45	2.00	0.75	2.73	29	74	55	18
415	4	1	3	062012-061912-C1-R2-S1	1	18.64	10	0.37	1590	15	1.86	35	1.76	0.14	2.73	29	74	55	18
416	4	1	3	062012-061912-C1-R2-S1	2	27.23	10	0.06	258	15	1.86	35	1.76	0.28	2.73	29	74	55	18
417	4	1	3	062012-061912-C1-R2-S1	3	42.59	10	1.14	4900	15	1.86	35	1.76	0.61	2.73	29	74	55	18
418	4	1	3	062012-061912-C1-R2-S1	4	57.80	10	8.79	37782	15	1.86	35	1.76	1.05	2.73	29	74	55	18
419	4	1	4	062112-061912-C1-R3-S1	1	21.86	10	0.11	488	52	1.81	37	1.14	0.18	2.73	29	74	55	18
420	4	1	4	062112-061912-C1-R3-S1	2	42.05	10	1.97	8749	52	1.81	37	1.14	0.6	2.73	29	74	55	18

					Test Specifications			Erosion Test Results		Properties									
#	Day	Core	Test	Test ID	Step	V $(\frac{cm}{s})$	Duration (min)	WL (gr)	ER $\frac{gr}{m^2.hour}$	Depth (mm)	ρ_{Bulk} $(\frac{gr}{cm^3})$	W (%)	O (%)	τ_{th} (Pa)	Gs	% Fines	LL (%)	PL (%)	PI
421	4	1	4	062112-061912-C1-R3-S1	3	57.08	10	9.9	43965	52	1.81	37	1.14	1.02	2.73	29	74	55	18
422	4	1	5	062712-061912-C1-R4-S1	1	30.93	10	0.15	605	67	1.97	32	1.38	0.34	2.73	29	74	55	18
423	4	1	5	062712-061912-C1-R4-S1	2	46.11	10	1.88	7588	67	1.97	32	1.38	0.72	2.73	29	74	55	18
424	4	1	6	062712-061912-C1-R5-S1	1	31.27	10	0.12	533	103	1.81	34	1.79	0.36	2.73	29	74	55	18
425	4	1	6	062712-061912-C1-R5-S1	2	46.61	10	1.15	5107	103	1.81	34	1.79	0.72	2.73	29	74	55	18
426	4	1	6	062712-061912-C1-R5-S1	3	56.33	1	6.51	289103	103	1.81	34	1.79	1.02	2.73	29	74	55	18
427	4	1	7	062812-061912-C1-R6-S1	1	31.41	10	0.04	242	144	1.49	70	5.03	0.36	2.77	29	74	55	18
428	4	1	7	062812-061912-C1-R6-S1	2	46.62	10	0.08	483	144	1.49	70	5.03	0.72	2.77	29	74	55	18
429	4	1	7	062812-061912-C1-R6-S1	3	61.50	10	0.23	1390	144	1.49	70	5.03	1.18	2.77	29	74	55	18
430	4	2	1	062212-061912-C2-R1-S1	1	20.97	10	0.07	392	0	1.55	51	3.12	0.17	2.73	55	94	57	37
431	4	2	1	062212-061912-C2-R1-S1	2	31.09	10	0.9	5041	0	1.55	51	3.12	0.36	2.73	55	94	57	37

					Test Specifications			Erosion Test Results		Properties									
#	Day	Core	Test	Test ID	Step	V $(\frac{cm}{s})$	Duration (min)	WL (gr)	ER $\frac{gr}{m^2.hour}$	Depth (mm)	ρ_{Bulk} $(\frac{gr}{cm^3})$	W (%)	O (%)	τ_{th} (Pa)	Gs	% Fines	LL (%)	PL (%)	PI
432	4	2	1	062212-061912-C2-R1-S1	3	41.08	10	3.52	19715	0	1.55	51	3.12	0.59	2.73	55	94	57	37
433	4	2	2	062212-061912-C2-R1-S2	1	21.22	10	0.14	670	0	1.71	51	3.12	0.18	2.73	55	94	57	37
434	4	2	2	062212-061912-C2-R1-S2	2	30.82	10	0.93	4451	0	1.71	51	3.12	0.34	2.73	55	94	57	37
435	4	2	2	062212-061912-C2-R1-S2	3	41.16	9	4.87	25900	0	1.71	51	3.12	0.59	2.73	55	94	57	37
436	4	2	3	062212-061912-C2-R2-S1	1	20.94	10	0.08	389	27	1.69	51	3.99	0.17	2.73	55	94	57	37
437	4	2	3	062212-061912-C2-R2-S1	2	41.14	10	0.76	3699	27	1.69	51	3.99	0.59	2.73	55	94	57	37
438	4	2	5	062912-061912-C2-R4-S1	1	26.44	10	0.09	438	75	1.69	69	3.94	0.27	2.73	55	94	57	37
439	4	2	5	062912-061912-C2-R4-S1	2	36.16	10	0.12	584	75	1.69	69	3.94	0.47	2.73	55	94	57	37
440	4	2	5	062912-061912-C2-R4-S1	3	55.86	10	0.54	2629	75	1.69	69	3.94	0.99	2.73	55	94	57	37
441	4	2	5	062912-061912-C2-R4-S1	4	76.57	10	1.89	9200	75	1.69	69	3.94	1.74	2.73	55	94	57	37
442	4	2	6	062912-061912-C2-R5-S1	1	26.61	10	0.04	198	90	1.67	67	4.10	0.27	2.73	55	94	57	37

					Test Specifications			Erosion Test Results		Properties									
#	Day	Core	Test	Test ID	Step	V ($\frac{cm}{s}$)	Duration (min)	WL (gr)	ER $\frac{gr}{m^2.hour}$	Depth (mm)	ρ_{Bulk} ($\frac{gr}{cm^3}$)	W (%)	O (%)	τ_{th} (Pa)	Gs	% Fines	LL (%)	PL (%)	PI
443	4	2	6	062912-061912-C2-R5-S1	2	41.38	10	0.01	50	90	1.67	67	4.10	0.59	2.73	55	94	57	37
444	4	2	6	062912-061912-C2-R5-S1	3	61.18	10	0.22	1090	90	1.67	67	4.10	1.18	2.73	55	94	57	37
445	4	2	6	062912-061912-C2-R5-S1	4	81.66	10	3.34	16545	90	1.67	67	4.10	1.95	2.73	55	94	57	37
446	4	2	7	062912-061912-C2-R6-S1	1	26.70	10	0.05	290	130	1.52	73	4.09	0.26	2.73	55	94	57	37
447	4	2	7	062912-061912-C2-R6-S1	2	46.23	10	0.01	58	130	1.52	73	4.09	0.7	2.73	55	94	57	37
448	4	2	7	062912-061912-C2-R6-S1	3	66.06	10	0.08	465	130	1.52	73	4.09	1.32	2.73	55	94	57	37
449	4	2	7	062912-061912-C2-R6-S1	4	86.87	10	0.37	2149	130	1.52	73	4.09	2.11	2.73	55	94	57	37
450	4	2	8	070212-061912-C2-R7-S1	1	30.68	10	0.02	126	167	1.46	94	6.84	0.34	2.77	51	94	57	37
451	4	2	8	070212-061912-C2-R7-S1	2	50.32	10	0.17	1072	167	1.46	94	6.84	0.83	2.77	51	94	57	37
452	4	2	8	070212-061912-C2-R7-S1	3	71.04	10	0.47	2965	167	1.46	94	6.84	1.54	2.77	51	94	57	37
453	4	3	1	062112-061912-C3-R1-S1	1	17.87	10	-0.01	-44	0	1.84	38	1.09	0.13	2.73	17			0

					Test Specifications			Erosion Test Results		Properties									
#	Day	Core	Test	Test ID	Step	V $(\frac{cm}{s})$	Duration (min)	WL (gr)	ER $\frac{gr}{m^2.hour}$	Depth (mm)	ρ_{Bulk} $(\frac{gr}{cm^3})$	W (%)	O (%)	τ_{th} (Pa)	Gs	% Fines	LL (%)	PL (%)	PI
454	4	3	1	062112-061912-C3-R1-S1	2	26.57	10	0.03	131	0	1.84	38	1.09	0.27	2.73	17			0
455	4	3	1	062112-061912-C3-R1-S1	3	37.01	10	0.32	1393	0	1.84	38	1.09	0.49	2.73	17			0
456	4	3	1	062112-061912-C3-R1-S1	4	46.90	10	13.32	57986	0	1.84	38	1.09	0.72	2.73	17			0
457	4	3	2	062112-061912-C3-R2-S1	1	21.87	10	0.57	5853	27	1.24	30	1.30	0.18	2.73	17			0
458	4	3	2	062112-061912-C3-R2-S1	2	41.83	10	1.33	13657	27	1.24	30	1.30	0.59	2.73	17			0
459	4	3	3	062112-061912-C3-R3-S1	1	21.68	10	0	0	41	1.85	33	1.94	0.18	2.73	17			0
460	4	3	3	062112-061912-C3-R3-S1	2	41.83	10	0.29	1254	41	1.85	33	1.94	0.59	2.73	17			0
461	4	3	3	062112-061912-C3-R3-S1	3	61.52	10	9.6	41524	41	1.85	33	1.94	1.18	2.73	17			0
462	4	3	4	062212-061912-C3-R4-S1	1	16.24	10	0.06	245	71	1.95	28	1.78	0.12	2.73	17			0
463	4	3	4	062212-061912-C3-R4-S1	2	25.58	10	0.42	1713	71	1.95	28	1.78	0.25	2.73	17			0
464	4	3	5	062512-061912-C3-R5-S1	1	17.00	10	0.05	205	104	1.94	28	0.87	0.13	2.73	17			0

					Test Specifications			Erosion Test Results		Properties									
#	Day	Core	Test	Test ID	Step	V $(\frac{cm}{s})$	Duration (min)	WL (gr)	ER $\frac{gr}{m^2.hour}$	Depth (mm)	ρ_{Bulk} $(\frac{gr}{cm^3})$	W (%)	O (%)	τ_{th} (Pa)	Gs	% Fines	LL (%)	PL (%)	PI
465	4	3	5	062512-061912-C3-R5-S1	2	36.09	10	8.52	34946	104	1.94	28	0.87	0.47	2.73	17			0
466	4	3	5	062512-061912-C3-R5-S1	3	53.00	0.5	5.81	476604	104	1.94	28	0.87	0.89	2.73	17			0
467	4	3	6	062512-061912-C3-R6-S1	1	16.73	10	-0.01	-42	121	1.88	26	0.77	0.12	2.73	17			0
468	4	3	6	062512-061912-C3-R6-S1	2	25.48	10	0.21	886	121	1.89	26	0.77	0.25	2.73	17			0
469	4	3	6	062512-061912-C3-R6-S1	3	30.59	10	0.71	2979	121	1.90	26	0.77	0.34	2.73	17			0
470	4	3	6	062512-061912-C3-R6-S1	4	35.63	4	11.65	121489	121	1.91	26	0.77	0.45	2.73	17			0
471	4	4	1	062512-061912-C4-R1-S1	1	17.65	10	0.02	87	0	1.85	39	1.74	0.13	2.73	38	73	63	10
472	4	4	1	062512-061912-C4-R1-S1	2	31.32	10	1.04	4498	0	1.85	39	1.74	0.36	2.73	38	73	63	10
473	4	4	1	062512-061912-C4-R1-S1	3	41.38	10	7.49	32398	0	1.85	39	1.74	0.59	2.73	38	73	63	10
474	4	4	2	062512-061912-C4-R1-S2	1	17.29	10	0.12	522	0	1.84	39	1.74	0.13	2.73	38	73	63	10
475	4	4	2	062512-061912-C4-R1-S2	2	41.19	10	6	26120	0	1.84	39	1.74	0.59	2.73	38	73	63	10

					Test Specifications			Erosion Test Results		Properties									
#	Day	Core	Test	Test ID	Step	V ($\frac{cm}{s}$)	Duration (min)	WL (gr)	ER $\frac{gr}{m^2.hour}$	Depth (mm)	ρ_{Bulk} ($\frac{gr}{cm^3}$)	W (%)	O (%)	τ_{th} (Pa)	Gs	% Fines	LL (%)	PL (%)	PI
476	4	4	2	062512-061912-C4-R1-S2	3	49.89	1	1.34	58334	0	1.84	39	1.74	0.8	2.73	38	73	63	10
477	4	4	3	062612-061912-C4-R2-S1	1	15.46	10	0.01	42	28	1.89	42	2.42	0.1	2.73	38	73	63	10
478	4	4	3	062612-061912-C4-R2-S1	2	24.32	10	0.09	380	28	1.89	42	2.42	0.22	2.73	38	73	63	10
479	4	4	3	062612-061912-C4-R2-S1	3	34.84	10	0.03	127	28	1.89	42	2.42	0.41	2.73	38	73	63	10
480	4	4	3	062612-061912-C4-R2-S1	4	49.96	10	0.74	3123	28	1.89	42	2.42	0.78	2.73	38	73	63	10
481	4	4	3	062612-061912-C4-R2-S1	5	54.97	10	3.32	14012	28	1.89	42	2.42	0.92	2.73	38	73	63	10
482	4	4	4	062612-061912-C4-R3-S1	1	24.44	10	0.07	313	45	1.8	37	1.95	0.23	2.73	38	73	63	10
483	4	4	4	062612-061912-C4-R3-S1	2	39.40	10	0.26	1163	45	1.8	37	1.95	0.54	2.73	38	73	63	10
484	4	4	4	062612-061912-C4-R3-S1	3	54.53	10	1.75	7825	45	1.8	37	1.95	0.95	2.73	38	73	63	10
485	4	4	5	062612-061912-C4-R4-S1	1	24.13	10	0.07	375	73	1.59	64	2.98	0.23	2.73	38	73	63	10
486	4	4	5	062612-061912-C4-R4-S1	2	43.81	10	0.17	910	73	1.59	64	2.98	0.64	2.73	38	73	63	10

					Test Specifications			Erosion Test Results		Properties									
#	Day	Core	Test	Test ID	Step	V ($\frac{cm}{s}$)	Duration (min)	WL (gr)	ER $\frac{gr}{m^2.hour}$	Depth (mm)	ρ_{Bulk} ($\frac{gr}{cm^3}$)	W (%)	O (%)	τ_{th} (Pa)	Gs	% Fines	LL (%)	PL (%)	PI
487	4	4	5	062612-061912-C4-R4-S1	3	59.44	10	0.8	4285	73	1.59	64	2.98	1.11	2.73	38	73	63	10
488	4	4	6	062712-061912-C4-R5-S1	1	31.35	10	0.01	59	129	1.51	94	6.66	0.36	2.77	88	73	63	10
489	4	4	6	062712-061912-C4-R5-S1	2	46.62	10	0.73	4295	129	1.51	94	6.66	0.72	2.77	88	73	63	10
490	4	4	7	062712-061912-C4-R6-S1	1	41.63	10	0.07	515	176	1.37	93	7.06	0.59	2.77	88	73	63	10
491	4	4	7	062712-061912-C4-R6-S1	2	61.32	10	0.21	1545	176	1.37	93	7.06	1.18	2.77	88	73	63	10
492	4	4	7	062712-061912-C4-R6-S1	3	81.91	1	0.64	47095	176	1.37	93	7.06	1.95	2.77	88	73	63	10
493	5	1	1	070512-070212-C1-R1-S1	1	22.03	10	0.28	3830	0	1.17	93	10.38	0.2	2.59	81	137	72	65
494	5	1	1	070512-070212-C1-R1-S1	2	26.29	4	0.4	13678	0	1.17	93	10.38	0.27	2.59	81	137	72	65
495	5	1	1	070512-070212-C1-R1-S1	3	30.38	4	0.29	9916	0	1.17	93	10.38	0.34	2.59	81	137	72	65
496	5	1	1	070512-070212-C1-R1-S1	4	35.22	10	0.41	5608	0	1.17	93	10.38	0.45	2.59	81	137	72	65
497	5	1	2	070612-070212-C1-R2-S1	1	21.56	10	0.03	217	72	1.38	285	10.09	0.18	2.59	81	137	72	65

					Test Specifications			Erosion Test Results		Properties									
#	Day	Core	Test	Test ID	Step	V ($\frac{cm}{s}$)	Duration (min)	WL (gr)	ER $\frac{gr}{m^2.hour}$	Depth (mm)	ρ_{Bulk} ($\frac{gr}{cm^3}$)	W (%)	O (%)	τ_{th} (Pa)	Gs	% Fines	LL (%)	PL (%)	PI
498	5	1	2	070612-070212-C1-R2-S1	2	25.87	10	0.09	650	72	1.38	285	10.09	0.25	2.59	81	137	72	65
499	5	1	2	070612-070212-C1-R2-S1	3	35.30	10	0.27	1949	72	1.38	285	10.09	0.45	2.59	81	137	72	65
500	5	1	2	070612-070212-C1-R2-S1	4	45.16	10	0.35	2526	72	1.38	285	10.09	0.69	2.59	81	137	72	65
501	5	1	2	070612-070212-C1-R2-S1	5	54.88	10	0.11	794	72	1.38	285	10.09	0.95	2.59	81	137	72	65
502	5	1	3	070612-070212-C1-R3-S1	1	30.33	10	0.01	78	107	1.34	144	10.33	0.34	2.59	81	137	72	65
503	5	1	3	070612-070212-C1-R3-S1	2	45.35	10	0.03	235	107	1.34	144	10.33	0.69	2.59	81	137	72	65
504	5	1	3	070612-070212-C1-R3-S1	3	60.25	10	0.06	470	107	1.34	144	10.33	1.15	2.59	81	137	72	65
505	5	1	3	070612-070212-C1-R3-S1	4	75.51	10	0.29	2271	107	1.34	144	10.33	1.7	2.59	81	137	72	65
506	5	1	3	070612-070212-C1-R3-S1	5	91.13	10	0.36	2820	107	1.34	144	10.33	2.39	2.59	81	137	72	65
507	5	1	3	070612-070212-C1-R3-S1	6	106.43	10	0.47	3681	107	1.34	144	10.33	3.13	2.59	81	137	72	65
508	5	1	4	070612-070212-C1-R4-S1	1	40.37	10	0.21	-10016	145	0.96	139	10.36	0.56	2.59	81	137	72	65

					Test Specifications			Erosion Test Results		Properties									
#	Day	Core	Test	Test ID	Step	V $(\frac{cm}{s})$	Duration (min)	WL (gr)	ER $\frac{gr}{m^2.hour}$	Depth (mm)	ρ_{Bulk} $(\frac{gr}{cm^3})$	W (%)	O (%)	τ_{th} (Pa)	Gs	% Fines	LL (%)	PL (%)	PI
509	5	1	4	070612-070212-C1-R4-S1	2	90.12	1	0.9	-429271	145	0.96	139	10.36	2.34	2.59	81	137	72	65
510	5	1	4	070612-070212-C1-R4-S1	3	70.07	5	59.04	######	145	0.96	139	10.36	1.51	2.59	81	137	72	65
511	5	2	1	070512-070212-C2-R1-S1	1	21.80	10	0.26	3961	0	1.15	188	12.21	0.18	3.02	50	131	97	34
512	5	2	1	070512-070212-C2-R1-S1	2	30.54	4	0.47	17903	0	1.15	188	12.21	0.34	3.02	50	131	97	34
513	5	2	1	070512-070212-C2-R1-S1	3	41.02	10	1.06	16151	0	1.15	188	12.21	0.59	3.02	50	131	97	34
514	5	2	2	070912-070212-C2-R2-S1	1	24.71	10	0.06	460	45	1.35	164	11.56	0.23	3.02	50	131	97	34
515	5	2	2	070912-070212-C2-R2-S1	2	24.91	10	0.01	77	45	1.35	164	11.56	0.23	3.02	50	131	97	34
516	5	2	2	070912-070212-C2-R2-S1	3	39.84	10	0.14	1073	45	1.35	164	11.56	0.54	3.02	50	131	97	34
517	5	2	2	070912-070212-C2-R2-S1	4	39.64	10	0.06	460	45	1.35	164	11.56	0.54	3.02	50	131	97	34
518	5	2	2	070912-070212-C2-R2-S1	5	39.80	10	0.1	767	45	1.35	164	11.56	0.54	3.02	50	131	97	34
519	5	2	2	070912-070212-C2-R2-S1	6	59.45	10	0.59	4523	45	1.35	164	11.56	1.11	3.02	50	131	97	34

					Test Specifications			Erosion Test Results		Properties									
#	Day	Core	Test	Test ID	Step	V $(\frac{cm}{s})$	Duration (min)	WL (gr)	ER $\frac{gr}{m^2.hour}$	Depth (mm)	ρ_{Bulk} $(\frac{gr}{cm^3})$	W (%)	O (%)	τ_{th} (Pa)	Gs	% Fines	LL (%)	PL (%)	PI
520	5	2	3	070912-070212-C2-R3-S1	1	29.21	10	0.01	75	98	1.36	148	20.81	0.32	3.02	50	131	97	34
521	5	2	3	070912-070212-C2-R3-S1	2	44.35	10	0.05	375	98	1.36	148	20.81	0.67	3.02	50	131	97	34
522	5	2	3	070912-070212-C2-R3-S1	3	44.37	10	0.03	225	98	1.36	148	20.81	0.67	3.02	50	131	97	34
523	5	2	3	070912-070212-C2-R3-S1	4	44.28	10	0.06	450	98	1.36	148	20.81	0.67	3.02	50	131	97	34
524	5	2	3	070912-070212-C2-R3-S1	5	64.13	10	0.08	601	98	1.36	148	20.81	1.29	3.02	50	131	97	34
525	5	2	4	070912-070212-C2-R4-S1	1	29.29	10	0	0	176	1.29	151	10.54	0.32	3.02	50	131	97	34
526	5	2	4	070912-070212-C2-R4-S1	2	48.99	10	0.03	265	176	1.29	151	10.54	0.78	3.02	50	131	97	34
527	5	2	4	070912-070212-C2-R4-S1	3	79.97	10	0.24	2122	176	1.29	151	10.54	1.86	3.02	50	131	97	34
528	5	2	4	070912-070212-C2-R4-S1	4	79.88	10	0.23	2033	176	1.29	151	10.54	1.86	3.02	50	131	97	34
529	5	3	5	070512-070212-C3-R1-S1	1	22.13	10	0.08	672	0	1.31	115	11.48	0.2	2.57	50	88	65	23
530	5	3	5	070512-070212-C3-R1-S1	2	30.63	4	0.77	16167	0	1.31	115	11.48	0.34	2.57	50	88	65	23

					Test Specifications			Erosion Test Results		Properties									
#	Day	Core	Test	Test ID	Step	V $(\frac{cm}{s})$	Duration (min)	WL (gr)	ER $\frac{gr}{m^2.hour}$	Depth (mm)	ρ_{Bulk} $(\frac{gr}{cm^3})$	W (%)	O (%)	τ_{th} (Pa)	Gs	% Fines	LL (%)	PL (%)	PI
531	5	3	5	070512-070212-C3-R1-S1	3	40.55	4	0.66	13857	0	1.31	115	11.48	0.56	2.57	50	88	65	23
532	5	3	6	071012-070212-C3-R2-S1	1	29.15	10	0.11	704	46	1.45	94	8.25	0.32	2.57	50	88	65	23
533	5	3	6	071012-070212-C3-R2-S1	2	29.15	10	0.03	192	46	1.45	94	8.25	0.32	2.57	50	88	65	23
534	5	3	6	071012-070212-C3-R2-S1	3	29.03	10	0.01	64	46	1.45	94	8.25	0.32	2.57	50	88	65	23
535	5	3	6	071012-070212-C3-R2-S1	4	44.14	10	0.38	2433	46	1.45	94	8.25	0.67	2.57	50	88	65	23
536	5	3	6	071012-070212-C3-R2-S1	5	44.11	10	0.12	768	46	1.45	94	8.25	0.67	2.57	50	88	65	23
537	5	3	6	071012-070212-C3-R2-S1	6	69.18	10	0.88	5635	46	1.45	94	8.25	1.47	2.57	50	88	65	23
538	5	3	7	071012-070212-C3-R3-S1	1	39.25	10	0.09	650	97	1.38	78	8.76	0.54	2.57	50	88	65	23
539	5	3	7	071012-070212-C3-R3-S1	2	39.27	10	0.08	577	97	1.38	78	8.76	0.54	2.57	50	88	65	23
540	5	3	7	071012-070212-C3-R3-S1	3	39.15	10	0.06	433	97	1.38	78	8.76	0.54	2.57	50	88	65	23
541	5	3	7	071012-070212-C3-R3-S1	4	59.34	10	0.67	4836	97	1.38	78	8.76	1.11	2.57	50	88	65	23

					Test Specifications			Erosion Test Results		Properties									
#	Day	Core	Test	Test ID	Step	V $(\frac{cm}{s})$	Duration (min)	WL (gr)	ER $\frac{gr}{m^2.hour}$	Depth (mm)	ρ_{Bulk} $(\frac{gr}{cm^3})$	W (%)	O (%)	τ_{th} (Pa)	Gs	% Fines	LL (%)	PL (%)	PI
542	5	3	7	071012-070212-C3-R3-S1	5	58.62	10	0.38	2743	97	1.38	78	8.76	1.08	2.57	50	88	65	23
543	5	3	8	071012-070212-C3-R4-S1	1	48.37	10	0.17	1162	153	1.41	85	16.70	0.78	2.57	50	88	65	23
544	5	3	8	071012-070212-C3-R4-S1	2	48.42	10	0.11	752	153	1.41	85	16.70	0.78	2.57	50	88	65	23
545	5	3	8	071012-070212-C3-R4-S1	3	69.16	10	0.34	2324	153	1.41	85	16.70	1.47	2.57	50	88	65	23
546	5	3	8	071012-070212-C3-R4-S1	4	89.96	10	0.54	3691	153	1.41	85	16.70	2.3	2.57	50	88	65	23
547	5	4	1	070512-070212-C4-R1-S1	1	22.01	10	0.09	530	0	1.51	74	5.98	0.2	2.44	50	118	47	71
548	5	4	1	070512-070212-C4-R1-S1	2	30.60	10	0.52	3060	0	1.51	74	5.98	0.34	2.44	50	118	47	71
549	5	4	1	070512-070212-C4-R1-S1	3	40.93	10	1.5	8826	0	1.51	74	5.98	0.56	2.44	50	118	47	71
550	5	4	1	070512-070212-C4-R1-S1	4	50.42	10	3.05	17947	0	1.51	74	5.98	0.83	2.44	50	118	47	71
551	5	4	2	071112-070212-C4-R2-S1	1	28.70	10	0.02	132	55	1.43	122	11.54	0.29	2.44	50	118	47	71
552	5	4	2	071112-070212-C4-R2-S1	2	38.84	10	0.17	1124	55	1.43	122	11.54	0.5	2.44	50	118	47	71

					Test Specifications			Erosion Test Results		Properties									
#	Day	Core	Test	Test ID	Step	V $(\frac{cm}{s})$	Duration (min)	WL (gr)	ER $\frac{gr}{m^2.hour}$	Depth (mm)	ρ_{Bulk} $(\frac{gr}{cm^3})$	W (%)	O (%)	τ_{th} (Pa)	Gs	% Fines	LL (%)	PL (%)	PI
553	5	4	2	071112-070212-C4-R2-S1	3	48.01	10	0.03	198	55	1.43	122	11.54	0.75	2.44	50	118	47	71
554	5	4	2	071112-070212-C4-R2-S1	4	58.40	10	0.22	1454	55	1.43	122	11.54	1.05	2.44	50	118	47	71
555	5	4	2	071112-070212-C4-R2-S1	5	58.37	10	0.54	3569	55	1.43	122	11.54	1.05	2.44	50	118	47	71
556	5	4	2	071112-070212-C4-R2-S1	6	58.25	10	0.22	1454	55	1.43	122	11.54	1.05	2.44	50	118	47	71
557	5	4	2	071112-070212-C4-R2-S1	7	58.50	10	0.16	1057	55	1.43	122	11.54	1.05	2.44	50	118	47	71
558	5	4	2	071112-070212-C4-R2-S1	8	78.69	4	1.09	18010	55	1.43	122	11.54	1.76	2.44	50	118	47	71
559	5	4	3	071112-070212-C4-R3-S1	1	43.20	10	0.06	545	111	1.28	175	13.68	0.64	2.44	50	118	47	71
560	5	4	3	071112-070212-C4-R3-S1	2	42.89	10	0.03	273	111	1.28	175	13.68	0.61	2.44	50	118	47	71
561	5	4	3	071112-070212-C4-R3-S1	3	63.36	10	0.35	3180	111	1.28	175	13.68	1.25	2.44	50	118	47	71
562	5	4	3	071112-070212-C4-R3-S1	4	63.21	10	0.12	1090	111	1.28	175	13.68	1.25	2.44	50	118	47	71
563	5	4	3	071112-070212-C4-R3-S1	5	43.11	10	-0.02	-182	111	1.28	175	13.68	0.64	2.44	50	118	47	71

					Test Specifications			Erosion Test Results		Properties									
#	Day	Core	Test	Test ID	Step	V $(\frac{cm}{s})$	Duration (min)	WL (gr)	ER $\frac{gr}{m^2.hour}$	Depth (mm)	ρ_{Bulk} $(\frac{gr}{cm^3})$	W (%)	O (%)	τ_{th} (Pa)	Gs	% Fines	LL (%)	PL (%)	PI
564	5	4	3	071112-070212-C4-R3-S1	6	43.06	10	0.05	454	111	1.28	175	13.68	0.64	2.44	50	118	47	71
565	5	4	4	071212-070212-C4-R4-S1	1	42.87	10	0.06	545	156	1.28	128	32.06	0.61	2.44	50	118	47	71
566	5	4	4	071212-070212-C4-R4-S1	2	62.99	10	0.37	3361	156	1.28	128	32.06	1.22	2.44	50	118	47	71
567	5	4	4	071212-070212-C4-R4-S1	3	83.62	10	0.82	7450	156	1.28	128	32.06	2.03	2.44	50	118	47	71
568	5	4	4	071212-070212-C4-R4-S1	4	27.87	10	0.05	454	156	1.28	128	32.06	0.28	2.44	50	118	47	71
569	5	4	4	071212-070212-C4-R4-S1	5	47.08	10	0.42	3816	156	1.28	128	32.06	0.75	2.44	50	118	47	71
570	5	4	5	071212-070212-C4-R4-S2	1	42.66	10	0.75	6148	156	1.32	128	32.06	0.61	2.44	50	118	47	71
571	5	4	5	071212-070212-C4-R4-S2	2	62.55	10	0.04	328	156	1.32	128	32.06	1.22	2.44	50	118	47	71
572	5	4	5	071212-070212-C4-R4-S2	3	83.53	10	0.07	574	156	1.32	128	32.06	2.03	2.44	50	118	47	71
573	5	4	5	071212-070212-C4-R4-S2	4	27.57	10	0.14	1148	156	1.32	128	32.06	0.28	2.44	50	118	47	71
574	5	4	5	071212-070212-C4-R4-S2	5	46.86	10	0.47	3853	156	1.32	128	32.06	0.72	2.44	50	118	47	71

					Test Specifications			Erosion Test Results		Properties									
#	Day	Core	Test	Test ID	Step	V $(\frac{cm}{s})$	Duration (min)	WL (gr)	ER $\frac{gr}{m^2.hour}$	Depth (mm)	ρ_{Bulk} $(\frac{gr}{cm^3})$	W (%)	O (%)	τ_{th} (Pa)	Gs	% Fines	LL (%)	PL (%)	PI
575	5	4	6	071312-070212-C4-R5-S1	1	31.62	10	0.14	1176	193	1.31	129	11.39	0.36	2.44	50	118	47	71
576	5	4	6	071312-070212-C4-R5-S1	2	51.44	10	0.21	1764	193	1.31	129	11.39	0.86	2.44	50	118	47	71
577	5	4	6	071312-070212-C4-R5-S1	3	72.16	10	0.32	2687	193	1.31	129	11.39	1.58	2.44	50	118	47	71
578	5	4	6	071312-070212-C4-R5-S1	4	51.56	10	0.06	504	193	1.31	129	11.39	0.86	2.44	50	118	47	71
579	5	4	7	071312-070212-C4-R5-S2	1	31.90	10	0.06	492	193	1.32	129	11.39	0.36	2.44	50	118	47	71
580	5	4	7	071312-070212-C4-R5-S2	2	51.54	10	0.17	1394	193	1.32	129	11.39	0.86	2.44	50	118	47	71
581	5	4	7	071312-070212-C4-R5-S2	3	72.15	10	0.56	4591	193	1.32	129	11.39	1.58	2.44	50	118	47	71
582	5	4	7	071312-070212-C4-R5-S2	4	51.50	10	0.04	328	193	1.32	129	11.39	0.86	2.44	50	118	47	71
583	5	4	8	071312-070212-C4-R5-S1-1	1	22.52	10	-0.04	-363	193	1.28	128	32.06	0.2	2.44	50	118	47	71
584	5	4	8	071312-070212-C4-R5-S1-1	2	32.19	10	0.09	818	193	1.28	128	32.06	0.38	2.44	50	118	47	71
585	5	4	8	071312-070212-C4-R5-S1-1	3	61.62	10	0.48	4361	193	1.28	128	32.06	1.18	2.44	50	118	47	71

					Test Specifications			Erosion Test Results		Properties									
#	Day	Core	Test	Test ID	Step	V $(\frac{cm}{s})$	Duration (min)	WL (gr)	ER $\frac{gr}{m^2.hour}$	Depth (mm)	ρ_{Bulk} $(\frac{gr}{cm^3})$	W (%)	O (%)	τ_{th} (Pa)	Gs	% Fines	LL (%)	PL (%)	PI
586	5	4	8	071312-070212-C4-R5-S1-1	4	82.65	10	0.3	2726	193	1.28	128	32.06	1.99	2.44	50	118	47	71
587	6	1	1	072712-072412-C1-R1-S1	1	39.80	5	0.62	11266	0	1.28	205	11.17	0.54	2.77	93	73	63	10
588	6	1	1	072712-072412-C1-R1-S1	2	29.57	5	0.16	2907	0	1.28	205	11.17	0.32	2.77	93	73	63	10
589	6	1	1	072712-072412-C1-R1-S1	3	34.70	5	0.25	4543	0	1.28	205	11.17	0.43	2.77	93	73	63	10
590	6	1	2	072712-072412-C1-R1-S2	1	28.13	5	0.26	5731	0	1.22	205	11.17	0.3	2.77	93	73	63	10
591	6	1	2	072712-072412-C1-R1-S2	2	28.04	5	0.05	1102	0	1.22	205	11.17	0.3	2.77	93	73	63	10
592	6	1	2	072712-072412-C1-R1-S2	3	28.20	5	0.02	441	0	1.22	205	11.17	0.3	2.77	93	73	63	10
593	6	1	2	072712-072412-C1-R1-S2	4	34.90	5	0.17	3747	0	1.22	205	11.17	0.43	2.77	93	73	63	10
594	6	1	2	072712-072412-C1-R1-S2	5	34.64	5	0.12	2645	0	1.22	205	11.17	0.43	2.77	93	73	63	10
595	6	1	2	072712-072412-C1-R1-S2	6	34.82	5	0.06	1323	0	1.22	205	11.17	0.43	2.77	93	73	63	10
596	6	1	2	072712-072412-C1-R1-S2	7	34.75	5	0.11	2425	0	1.22	205	11.17	0.43	2.77	93	73	63	10

					Test Specifications			Erosion Test Results		Properties									
#	Day	Core	Test	Test ID	Step	V $(\frac{cm}{s})$	Duration (min)	WL (gr)	ER $\frac{gr}{m^2.hour}$	Depth (mm)	ρ_{Bulk} $(\frac{gr}{cm^3})$	W (%)	O (%)	τ_{th} (Pa)	Gs	% Fines	LL (%)	PL (%)	PI
597	6	1	2	072712-072412-C1-R1-S2	8	41.61	5	0.25	5510	0	1.22	205	11.17	0.59	2.77	93	73	63	10
598	6	1	2	072712-072412-C1-R1-S2	9	41.43	5	0.22	4849	0	1.22	205	11.17	0.59	2.77	93	73	63	10
599	6	1	2	072712-072412-C1-R1-S2	10	41.36	5	0.12	2645	0	1.22	205	11.17	0.59	2.77	93	73	63	10
600	6	1	3	080212-072412-C1-R2-S1	1	20.24	10	0.05	420	48	1.31	162	NA	0.17	2.77	93	73	63	10
601	6	1	3	080212-072412-C1-R2-S1	2	29.20	10	0.06	504	48	1.31	162	NA	0.32	2.77	93	73	63	10
602	6	1	3	080212-072412-C1-R2-S1	3	29.21	10	0.07	588	48	1.31	162	NA	0.32	2.77	93	73	63	10
603	6	1	3	080212-072412-C1-R2-S1	4	29.23	10	0	0	48	1.31	165	NA	0.32	2.77	93	73	63	10
604	6	1	3	080212-072412-C1-R2-S1	5	29.30	10	0.03	252	48	1.31	165	NA	0.32	2.77	93	73	63	10
605	6	1	3	080212-072412-C1-R2-S1	6	20.56	10	0.02	168	48	1.31	165	NA	0.17	2.77	93	73	63	10
606	6	1	3	080212-072412-C1-R2-S1	7	20.79	10	0.03	252	48	1.31	165	NA	0.17	2.77	93	73	63	10
607	6	1	3	080212-072412-C1-R2-S1	8	20.81	10	0	0	48	1.31	165	NA	0.17	2.77	93	73	63	10

					Test Specifications			Erosion Test Results		Properties									
#	Day	Core	Test	Test ID	Step	V $(\frac{cm}{s})$	Duration (min)	WL (gr)	ER $\frac{gr}{m^2.hour}$	Depth (mm)	ρ_{Bulk} $(\frac{gr}{cm^3})$	W (%)	O (%)	τ_{th} (Pa)	Gs	% Fines	LL (%)	PL (%)	PI
608	6	1	3	080212-072412-C1-R2-S1	9	20.91	10	0	0	48	1.31	165	NA	0.17	2.77	93	73	63	10
609	6	1	3	080212-072412-C1-R2-S1	10	29.34	10	0.05	420	48	1.31	165	NA	0.32	2.77	93	73	63	10
610	6	1	3	080212-072412-C1-R2-S1	11	20.76	10	0.03	252	48	1.31	165	NA	0.17	2.77	93	73	63	10
611	6	1	4	080212-072412-C1-R2-S2	1	20.70	10	0.02	153	48	1.35	165	NA	0.17	2.77	93	73	63	10
612	6	1	4	080212-072412-C1-R2-S2	2	29.21	10	0	0	48	1.35	165	NA	0.32	2.77	93	73	63	10
613	6	1	4	080212-072412-C1-R2-S2	3	29.34	10	0.01	77	48	1.35	165	NA	0.32	2.77	93	73	63	10
614	6	1	5	080312-072412-C1-R3-S1	1	19.95	10	-0.05	-375	99	1.36	168	9.15	0.16	2.77	93	73	63	10
615	6	1	5	080312-072412-C1-R3-S1	2	33.64	10	0.03	225	99	1.36	168	9.15	0.4	2.77	93	73	63	10
616	6	1	5	080312-072412-C1-R3-S1	3	33.83	10	0.02	150	99	1.36	168	9.15	0.4	2.77	93	73	63	10
617	6	1	5	080312-072412-C1-R3-S1	4	44.15	10	0.03	225	99	1.36	168	9.15	0.67	2.77	93	73	63	10
618	6	1	5	080312-072412-C1-R3-S1	5	53.56	10	0.11	826	99	1.36	168	9.15	0.92	2.77	93	73	63	10

					Test Specifications			Erosion Test Results		Properties									
#	Day	Core	Test	Test ID	Step	V $(\frac{cm}{s})$	Duration (min)	WL (gr)	ER $\frac{gr}{m^2.hour}$	Depth (mm)	ρ_{Bulk} $(\frac{gr}{cm^3})$	W (%)	O (%)	τ_{th} (Pa)	Gs	% Fines	LL (%)	PL (%)	PI
619	6	1	5	080312-072412-C1-R3-S1	6	64.60	10	0.16	1201	99	1.36	168	9.15	1.29	2.77	93	73	63	10
620	6	1	5	080312-072412-C1-R3-S1	7	64.23	10	-0.29	-2177	99	1.36	168	9.15	1.29	2.77	93	73	63	10
621	6	1	5	080312-072412-C1-R3-S1	8	20.32	10	0.06	450	99	1.36	168	9.15	0.17	2.77	93	73	63	10
622	6	1	5	080312-072412-C1-R3-S1	9	20.23	10	0	0	99	1.36	168	9.15	0.17	2.77	93	73	63	10
623	6	1	6	080312-072412-C1-R3-S2	1	20.52	10	0.08	656	99	1.32	168	9.15	0.17	2.77	93	73	63	10
624	6	1	6	080312-072412-C1-R3-S2	2	20.67	10	0.11	902	99	1.32	168	9.15	0.17	2.77	93	73	63	10
625	6	1	6	080312-072412-C1-R3-S2	3	20.77	10	0	0	99	1.32	168	9.15	0.17	2.77	93	73	63	10
626	6	1	6	080312-072412-C1-R3-S2	4	20.74	10	-0.03	-246	99	1.32	168	9.15	0.17	2.77	93	73	63	10
627	6	1	6	080312-072412-C1-R3-S2	5	34.30	10	0.15	1230	99	1.32	168	9.15	0.43	2.77	93	73	63	10
628	6	1	6	080312-072412-C1-R3-S2	6	34.37	10	0.12	984	99	1.32	168	9.15	0.43	2.77	93	73	63	10
629	6	1	6	080312-072412-C1-R3-S2	7	20.85	10	-0.03	-246	99	1.32	168	9.15	0.17	2.77	93	73	63	10

					Test Specifications			Erosion Test Results		Properties									
#	Day	Core	Test	Test ID	Step	V $(\frac{cm}{s})$	Duration (min)	WL (gr)	ER $\frac{gr}{m^2.hour}$	Depth (mm)	ρ_{Bulk} $(\frac{gr}{cm^3})$	W (%)	O (%)	τ_{th} (Pa)	Gs	% Fines	LL (%)	PL (%)	PI
630	6	1	7	080312-072412-C1-R4-S1	1	20.71	10	0.05	239	138	1.71	178	NA	0.17	2.77	93	73	63	10
631	6	1	7	080312-072412-C1-R4-S1	2	20.64	10	0.02	96	138	1.71	178	NA	0.17	2.77	93	73	63	10
632	6	1	7	080312-072412-C1-R4-S1	3	20.95	10	0	0	138	1.71	178	NA	0.17	2.77	93	73	63	10
633	6	1	7	080312-072412-C1-R4-S1	4	29.17	10	0.02	96	138	1.71	178	NA	0.32	2.77	93	73	63	10
634	6	1	7	080312-072412-C1-R4-S1	5	29.22	10	0.04	191	138	1.71	178	NA	0.32	2.77	93	73	63	10
635	6	1	7	080312-072412-C1-R4-S1	6	29.12	10	0.01	48	138	1.71	178	NA	0.32	2.77	93	73	63	10
636	6	1	7	080312-072412-C1-R4-S1	7	48.81	10	0.1	479	138	1.71	178	NA	0.78	2.77	93	73	63	10
637	6	2	1	072512-072412-C2-R1-S1	1	16.58	10	-0.03	-265	0	1.29	219	9.19	0.12	2.54	88	175	76	98
638	6	2	1	072512-072412-C2-R1-S1	2	16.82	10	0.05	442	0	1.29	219	9.19	0.12	2.54	88	175	76	98
639	6	2	1	072512-072412-C2-R1-S1	3	21.77	10	0.05	442	0	1.29	219	9.19	0.18	2.54	88	175	76	98
640	6	2	1	072512-072412-C2-R1-S1	4	21.95	10	0.09	796	0	1.29	219	9.19	0.18	2.54	88	175	76	98

					Test Specifications			Erosion Test Results		Properties									
#	Day	Core	Test	Test ID	Step	V $(\frac{cm}{s})$	Duration (min)	WL (gr)	ER $\frac{gr}{m^2.hour}$	Depth (mm)	ρ_{Bulk} $(\frac{gr}{cm^3})$	W (%)	O (%)	τ_{th} (Pa)	Gs	% Fines	LL (%)	PL (%)	PI
641	6	2	1	072512-072412-C2-R1-S1	5	21.89	10	-0.07	-619	0	1.29	219	9.19	0.18	2.54	88	175	76	98
642	6	2	1	072512-072412-C2-R1-S1	6	21.88	10	0.04	354	0	1.29	219	9.19	0.18	2.54	88	175	76	98
643	6	2	1	072512-072412-C2-R1-S1	7	22.09	10	0.02	177	0	1.29	219	9.19	0.2	2.54	88	175	76	98
644	6	2	1	072512-072412-C2-R1-S1	8	22.05	10	0.01	88	0	1.29	219	9.19	0.2	2.54	88	175	76	98
645	6	2	1	072512-072412-C2-R1-S1	9	21.91	10	0.03	265	0	1.29	219	9.19	0.18	2.54	88	175	76	98
646	6	2	1	072512-072412-C2-R1-S1	10	22.04	10	0	0	0	1.29	219	9.19	0.2	2.54	88	175	76	98
647	6	2	1	072512-072412-C2-R1-S1	11	22.13	10	61.73	545715	0	1.29	219	9.19	0.2	2.54	88	175	76	98
648	6	2	2	072512-072412-C2-R2-S1	1	17.30	10	0.06	661	38	1.22	165	9.37	0.13	2.54	88	175	76	98
649	6	2	2	072512-072412-C2-R2-S1	2	17.22	10	0.03	331	38	1.22	165	9.37	0.13	2.54	88	175	76	98
650	6	2	2	072512-072412-C2-R2-S1	3	22.02	10	-0.01	-110	38	1.22	165	9.37	0.2	2.54	88	175	76	98
651	6	2	2	072512-072412-C2-R2-S1	4	22.06	10	0.01	110	38	1.22	165	9.37	0.2	2.54	88	175	76	98

					Test Specifications			Erosion Test Results		Properties									
#	Day	Core	Test	Test ID	Step	V $(\frac{cm}{s})$	Duration (min)	WL (gr)	ER $\frac{gr}{m^2.hour}$	Depth (mm)	ρ_{Bulk} $(\frac{gr}{cm^3})$	W (%)	O (%)	τ_{th} (Pa)	Gs	% Fines	LL (%)	PL (%)	PI
652	6	2	2	072512-072412-C2-R2-S1	5	22.06	10	0.02	220	38	1.22	165	9.37	0.2	2.54	88	175	76	98
653	6	2	2	072512-072412-C2-R2-S1	6	26.01	10	0.04	441	38	1.22	165	9.37	0.27	2.54	88	175	76	98
654	6	2	2	072512-072412-C2-R2-S1	7	26.03	10	0.02	220	38	1.22	165	9.37	0.27	2.54	88	175	76	98
655	6	2	2	072512-072412-C2-R2-S1	8	26.11	10	0.01	110	38	1.22	165	9.37	0.27	2.54	88	175	76	98
656	6	3	1	072612-072412-C3-R1-S1	1	16.65	10	0.05	651	0	1.18	212	10.41	0.12	2.4	95	208	110	98
657	6	3	1	072612-072412-C3-R1-S1	2	16.74	10	0.01	130	0	1.18	212	10.41	0.12	2.4	95	208	110	98
658	6	3	1	072612-072412-C3-R1-S1	3	16.87	10	0	0	0	1.18	212	10.41	0.12	2.4	95	208	110	98
659	6	3	1	072612-072412-C3-R1-S1	4	16.94	10	0.03	391	0	1.18	212	10.41	0.12	2.4	95	208	110	98
660	6	3	1	072612-072412-C3-R1-S1	5	25.81	10	0.08	1042	0	1.18	212	10.41	0.25	2.4	95	208	110	98
661	6	3	1	072612-072412-C3-R1-S1	6	25.80	10	0.04	521	0	1.18	212	10.41	0.25	2.4	95	208	110	98
662	6	3	1	072612-072412-C3-R1-S1	7	25.82	10	0.04	521	0	1.18	212	10.41	0.25	2.4	95	208	110	98

					Test Specifications			Erosion Test Results		Properties									
#	Day	Core	Test	Test ID	Step	V ($\frac{cm}{s}$)	Duration (min)	WL (gr)	ER $\frac{gr}{m^2.hour}$	Depth (mm)	ρ_{Bulk} ($\frac{gr}{cm^3}$)	W (%)	O (%)	τ_{th} (Pa)	Gs	% Fines	LL (%)	PL (%)	PI
663	6	3	1	072612-072412-C3-R1-S1	8	26.02	10	0.09	1173	0	1.18	212	10.41	0.27	2.4	95	208	110	98
664	6	3	1	072612-072412-C3-R1-S1	9	30.35	10	0.07	912	0	1.18	212	10.41	0.34	2.4	95	208	110	98
665	6	3	1	072612-072412-C3-R1-S1	10	30.41	10	0.15	1954	0	1.18	212	10.41	0.34	2.4	95	208	110	98
666	6	3	1	072612-072412-C3-R1-S1	11	30.52	10	0.13	1694	0	1.18	212	10.41	0.34	2.4	95	208	110	98
667	6	3	2	072612-072412-C3-R1-S2	1	17.21	10	0	0	0	1.22	212	10.41	0.13	2.4	95	208	110	98
668	6	3	2	072612-072412-C3-R1-S2	2	17.14	10	0.03	331	0	1.22	212	10.41	0.13	2.4	95	208	110	98
669	6	3	2	072612-072412-C3-R1-S2	3	17.30	10	0.25	2755	0	1.22	212	10.41	0.13	2.4	95	208	110	98
670	6	3	2	072612-072412-C3-R1-S2	4	17.29	10	0.01	110	0	1.22	212	10.41	0.13	2.4	95	208	110	98
671	6	3	2	072612-072412-C3-R1-S2	5	26.00	10	0.35	3857	0	1.22	212	10.41	0.25	2.4	95	208	110	98
672	6	3	2	072612-072412-C3-R1-S2	6	25.93	10	0.14	1543	0	1.22	212	10.41	0.25	2.4	95	208	110	98
673	6	3	3	073012-072412-C3-R2-S1	1	21.02	10	0.03	252	51	1.31	153	11.72	0.18	2.4	95	208	110	98

					Test Specifications			Erosion Test Results		Properties									
#	Day	Core	Test	Test ID	Step	V $(\frac{cm}{s})$	Duration (min)	WL (gr)	ER $\frac{gr}{m^2.hour}$	Depth (mm)	ρ_{Bulk} $(\frac{gr}{cm^3})$	W (%)	O (%)	τ_{th} (Pa)	Gs	% Fines	LL (%)	PL (%)	PI
674	6	3	3	073012-072412-C3-R2-S1	2	29.82	10	0.03	252	51	1.31	153	11.72	0.31	2.4	95	208	110	98
675	6	3	3	073012-072412-C3-R2-S1	3	29.73	5	0.03	504	51	1.31	153	11.72	0.31	2.4	95	208	110	98
676	6	3	3	073012-072412-C3-R2-S1	4	44.96	5	0.16	2687	51	1.31	153	11.72	0.64	2.4	95	208	110	98
677	6	3	3	073012-072412-C3-R2-S1	5	44.87	5	0.06	1008	51	1.31	153	11.72	0.64	2.4	95	208	110	98
678	6	3	3	073012-072412-C3-R2-S1	6	54.42	5	0.48	8062	51	1.31	153	11.72	0.92	2.4	95	208	110	98
679	6	3	4	073012-072412-C3-R3-S1	1	21.31	10	0.11	924	99	1.31	150	10.07	0.18	2.4	95	208	110	98
680	6	3	4	073012-072412-C3-R3-S1	2	34.93	10	0.12	1008	99	1.31	150	10.07	0.41	2.4	95	208	110	98
681	6	3	4	073012-072412-C3-R3-S1	3	34.93	10	0.06	504	99	1.31	150	10.07	0.41	2.4	95	208	110	98
682	6	3	4	073012-072412-C3-R3-S1	4	35.09	10	0	0	99	1.31	150	10.07	0.43	2.4	95	208	110	98
683	6	3	4	073012-072412-C3-R3-S1	5	44.88	10	0.22	1848	99	1.31	150	10.07	0.64	2.4	95	208	110	98
684	6	3	4	073012-072412-C3-R3-S1	6	44.95	10	0.12	1008	99	1.31	150	10.07	0.64	2.4	95	208	110	98

					Test Specifications			Erosion Test Results		Properties									
#	Day	Core	Test	Test ID	Step	V $(\frac{cm}{s})$	Duration (min)	WL (gr)	ER $\frac{gr}{m^2.hour}$	Depth (mm)	ρ_{Bulk} $(\frac{gr}{cm^3})$	W (%)	O (%)	τ_{th} (Pa)	Gs	% Fines	LL (%)	PL (%)	PI
685	6	3	4	073012-072412-C3-R3-S1	7	44.95	10	0.08	672	99	1.31	150	10.07	0.64	2.4	95	208	110	98
686	6	3	4	073012-072412-C3-R3-S1	8	54.60	10	0.2	1680	99	1.31	150	10.07	0.92	2.4	95	208	110	98
687	6	3	4	073012-072412-C3-R3-S1	9	65.03	10	0.5	4199	99	1.31	150	10.07	1.28	2.4	95	208	110	98
688	6	3	5	073012-072412-C3-R3-S2	1	21.07	10	0.04	313	99	1.34	150	10.07	0.18	2.4	95	208	110	98
689	6	3	5	073012-072412-C3-R3-S2	2	39.91	10	0.15	1175	99	1.34	150	10.07	0.54	2.4	95	208	110	98
690	6	3	5	073012-072412-C3-R3-S2	3	39.99	10	0.05	392	99	1.34	150	10.07	0.54	2.4	95	208	110	98
691	6	3	5	073012-072412-C3-R3-S2	4	59.88	10	0.21	1645	99	1.34	150	10.07	1.11	2.4	95	208	110	98
692	6	3	6	073112-072412-C3-R4-S1	1	20.95	10	0.03	308	146	1.24	165	NA	0.17	2.4	95	208	110	98
693	6	3	6	073112-072412-C3-R4-S1	2	34.76	10	0.08	821	146	1.24	166	NA	0.43	2.4	95	208	110	98
694	6	3	6	073112-072412-C3-R4-S1	3	34.71	10	0.01	103	146	1.24	167	NA	0.43	2.4	95	208	110	98
695	6	3	6	073112-072412-C3-R4-S1	4	44.63	10	0.05	513	146	1.24	168	NA	0.67	2.4	95	208	110	98

					Test Specifications			Erosion Test Results		Properties									
#	Day	Core	Test	Test ID	Step	V $(\frac{cm}{s})$	Duration (min)	WL (gr)	ER $\frac{gr}{m^2.hour}$	Depth (mm)	ρ_{Bulk} $(\frac{gr}{cm^3})$	W (%)	O (%)	τ_{th} (Pa)	Gs	% Fines	LL (%)	PL (%)	PI
696	6	3	6	073112-072412-C3-R4-S1	5	44.80	10	0.09	924	146	1.24	169	NA	0.67	2.4	95	208	110	98
697	6	3	6	073112-072412-C3-R4-S1	6	44.69	10	0.04	411	146	1.24	170	NA	0.67	2.4	95	208	110	98
698	6	3	6	073112-072412-C3-R4-S1	7	54.39	10	0.05	513	146	1.24	171	NA	0.95	2.4	95	208	110	98
699	6	3	6	073112-072412-C3-R4-S1	8	54.61	10	0.09	924	146	1.24	172	NA	0.95	2.4	95	208	110	98
700	6	3	7	073112-072412-C3-R4-S2	1	21.22	10	0.05	497	146	1.25	165	NA	0.18	2.4	95	208	110	98
701	6	3	7	073112-072412-C3-R4-S2	2	44.81	10	0.09	894	146	1.25	166	NA	0.67	2.4	95	208	110	98
702	6	3	7	073112-072412-C3-R4-S2	3	54.61	10	0.18	1789	146	1.25	167	NA	0.95	2.4	95	208	110	98
703	6	3	7	073112-072412-C3-R4-S2	4	44.78	10	0.06	596	146	1.25	168	NA	0.67	2.4	95	208	110	98
704	6	3	7	073112-072412-C3-R4-S2	5	54.45	10	0.09	894	146	1.25	169	NA	0.95	2.4	95	208	110	98
705	6	3	7	073112-072412-C3-R4-S2	6	54.29	10	0.13	1292	146	1.25	170	NA	0.95	2.4	95	208	110	98
706	6	3	7	073112-072412-C3-R4-S2	7	44.76	10	0.05	497	146	1.25	171	NA	0.67	2.4	95	208	110	98

					Test Specifications			Erosion Test Results		Properties									
#	Day	Core	Test	Test ID	Step	V $(\frac{cm}{s})$	Duration (min)	WL (gr)	ER $\frac{gr}{m^2.hour}$	Depth (mm)	ρ_{Bulk} $(\frac{gr}{cm^3})$	W (%)	O (%)	τ_{th} (Pa)	Gs	% Fines	LL (%)	PL (%)	PI
707	6	3	7	073112-072412-C3-R4-S2	8	54.53	10	0.1	994	146	1.25	172	NA	0.95	2.4	95	208	110	98
708	6	3	7	073112-072412-C3-R4-S2	9	65.00	10	0.28	2782	146	1.25	173	NA	1.32	2.4	95	208	110	98
709	6	4	1	072712-072412-C4-R1-S2	1	34.51	5	0.04	689	0	1.3	190	11.38	0.42	2.82	97	174	107	67
710	6	4	1	072712-072412-C4-R1-S2	2	34.58	5	0.13	2239	0	1.3	190	11.38	0.42	2.82	97	174	107	67
711	6	4	1	072712-072412-C4-R1-S2	3	44.55	5	1.37	23597	0	1.3	190	11.38	0.66	2.82	97	174	107	67
712	6	4	1	072712-072412-C4-R1-S2	4	25.06	5	0.06	1033	0	1.3	190	11.38	0.24	2.82	97	174	107	67
713	6	4	1	072712-072412-C4-R1-S2	5	25.21	5	0.02	344	0	1.3	190	11.38	0.24	2.82	97	174	107	67
714	6	4	2	080112-072412-C4-R2-S1	1	20.99	10	0.1	861	49	1.3	185	11.20	0.17	2.82	97	174	107	67
715	6	4	2	080112-072412-C4-R2-S1	2	29.67	10	0.11	947	49	1.3	185	11.20	0.32	2.82	97	174	107	67
716	6	4	2	080112-072412-C4-R2-S1	3	29.74	10	0.03	258	49	1.3	185	11.20	0.32	2.82	97	174	107	67
717	6	4	2	080112-072412-C4-R2-S1	4	29.64	10	0.04	344	49	1.3	185	11.20	0.32	2.82	97	174	107	67

					Test Specifications			Erosion Test Results		Properties									
#	Day	Core	Test	Test ID	Step	V $(\frac{cm}{s})$	Duration (min)	WL (gr)	ER $\frac{gr}{m^2.hour}$	Depth (mm)	ρ_{Bulk} $(\frac{gr}{cm^3})$	W (%)	O (%)	τ_{th} (Pa)	Gs	% Fines	LL (%)	PL (%)	PI
718	6	4	2	080112-072412-C4-R2-S1	5	39.92	10	0.17	1464	49	1.3	185	11.20	0.54	2.82	97	174	107	67
719	6	4	2	080112-072412-C4-R2-S1	6	40.02	10	0.07	603	49	1.3	185	11.20	0.56	2.82	97	174	107	67
720	6	4	2	080112-072412-C4-R2-S1	7	39.84	10	0.06	517	49	1.3	185	11.20	0.54	2.82	97	174	107	67
721	6	4	2	080112-072412-C4-R2-S1	8	59.64	10	0.47	4048	49	1.3	185	11.20	1.11	2.82	97	174	107	67
722	6	4	2	080112-072412-C4-R2-S1	9	59.95	10	0.17	1464	49	1.3	185	11.20	1.11	2.82	97	174	107	67
723	6	4	3	080112-072412-C4-R3-S1	1	21.07	10	0.05	392	99	1.34	155	13.11	0.18	2.82	97	174	107	67
724	6	4	3	080112-072412-C4-R3-S1	2	29.80	10	0.04	313	99	1.34	155	13.11	0.32	2.82	97	174	107	67
725	6	4	3	080112-072412-C4-R3-S1	3	39.82	10	0.12	940	99	1.34	155	13.11	0.54	2.82	97	174	107	67
726	6	4	3	080112-072412-C4-R3-S1	4	40.02	10	0.02	157	99	1.34	155	13.11	0.56	2.82	97	174	107	67
727	6	4	3	080112-072412-C4-R3-S1	5	54.31	10	0.18	1410	99	1.34	155	13.11	0.95	2.82	97	174	107	67
728	6	4	3	080112-072412-C4-R3-S1	6	54.50	10	0.06	470	99	1.34	155	13.11	0.95	2.82	97	174	107	67

					Test Specifications			Erosion Test Results		Properties									
#	Day	Core	Test	Test ID	Step	V $(\frac{cm}{s})$	Duration (min)	WL (gr)	ER $\frac{gr}{m^2.hour}$	Depth (mm)	ρ_{Bulk} $(\frac{gr}{cm^3})$	W (%)	O (%)	τ_{th} (Pa)	Gs	% Fines	LL (%)	PL (%)	PI
729	6	4	3	080112-072412-C4-R3-S1	7	54.46	10	0.06	470	99	1.34	155	13.11	0.95	2.82	97	174	107	67
730	6	4	3	080112-072412-C4-R3-S1	8	69.99	10	0.2	1567	99	1.34	155	13.11	1.47	2.82	97	174	107	67
731	6	4	3	080112-072412-C4-R3-S1	9	70.07	10	0.11	862	99	1.34	155	13.11	1.51	2.82	97	174	107	67
732	6	4	4	080612-072412-C4-R4-S1	1	20.07	10	-0.07	-619	145	1.29	176	9.59	0.17	2.82	97	174	107	67
733	6	4	4	080612-072412-C4-R4-S1	2	20.31	10	0.04	354	145	1.29	176	9.59	0.17	2.82	97	174	107	67
734	6	4	4	080612-072412-C4-R4-S1	3	20.41	10	0	0	145	1.29	176	9.59	0.17	2.82	97	174	107	67
735	6	4	4	080612-072412-C4-R4-S1	4	20.64	10	0.02	177	145	1.29	176	9.59	0.17	2.82	97	174	107	67
736	6	4	4	080612-072412-C4-R4-S1	5	20.62	10	0.03	265	145	1.29	176	9.59	0.17	2.82	97	174	107	67
737	6	4	4	080612-072412-C4-R4-S1	6	20.57	10	0.01	88	145	1.29	176	9.59	0.17	2.82	97	174	107	67
738	6	4	4	080612-072412-C4-R4-S1	7	20.61	10	0	0	145	1.29	176	9.59	0.17	2.82	97	174	107	67
739	6	4	4	080612-072412-C4-R4-S1	8	20.72	10	0.06	530	145	1.29	176	9.59	0.17	2.82	97	174	107	67

					Test Specifications			Erosion Test Results		Properties									
#	Day	Core	Test	Test ID	Step	V $(\frac{cm}{s})$	Duration (min)	WL (gr)	ER $\frac{gr}{m^2.hour}$	Depth (mm)	ρ_{Bulk} $(\frac{gr}{cm^3})$	W (%)	O (%)	τ_{th} (Pa)	Gs	% Fines	LL (%)	PL (%)	PI
740	6	4	4	080612-072412-C4-R4-S1	9	20.57	10	0.01	88	145	1.29	176	9.59	0.17	2.82	97	174	107	67
741	6	4	4	080612-072412-C4-R4-S1	10	20.58	10	0	0	145	1.29	176	9.59	0.17	2.82	97	174	107	67
742	6	4	4	080612-072412-C4-R4-S1	11	20.80	10	0	0	145	1.29	176	9.59	0.17	2.82	97	174	107	67
743	6	4	4	080612-072412-C4-R4-S1	12	20.70	10	0.04	354	145	1.29	176	9.59	0.17	2.82	97	174	107	67
744	6	4	4	080612-072412-C4-R4-S1	13	20.78	10	0.05	442	145	1.29	176	9.59	0.17	2.82	97	174	107	67
745	6	4	4	080612-072412-C4-R4-S1	14	20.82	10	0.08	707	145	1.29	176	9.59	0.17	2.82	97	174	107	67
746	6	4	4	080612-072412-C4-R4-S1	15	20.67	10	0.04	354	145	1.29	176	9.59	0.17	2.82	97	174	107	67
747	6	4	4	080612-072412-C4-R4-S1	16	20.72	10	0.03	265	145	1.29	176	9.59	0.17	2.82	97	174	107	67
748	6	4	4	080612-072412-C4-R4-S1	17	29.16	10	0.03	265	145	1.29	176	9.59	0.32	2.82	97	174	107	67
749	6	4	4	080612-072412-C4-R4-S1	18	29.20	10	0	0	145	1.29	176	9.59	0.32	2.82	97	174	107	67
750	6	4	5	080612-072412-C4-R4-S2	1	20.53	10	0.08	882	145	1.22	176	9.59	0.17	2.82	97	174	107	67

					Test Specifications			Erosion Test Results		Properties									
#	Day	Core	Test	Test ID	Step	V ($\frac{cm}{s}$)	Duration (min)	WL (gr)	ER $\frac{gr}{m^2.hour}$	Depth (mm)	ρ_{Bulk} ($\frac{gr}{cm^3}$)	W (%)	O (%)	τ_{th} (Pa)	Gs	% Fines	LL (%)	PL (%)	PI
751	6	4	5	080612-072412-C4-R4-S2	2	20.62	10	0.04	441	145	1.22	176	9.59	0.17	2.82	97	174	107	67
752	6	4	5	080612-072412-C4-R4-S2	3	20.77	10	0.02	220	145	1.22	176	9.59	0.17	2.82	97	174	107	67
753	6	4	5	080612-072412-C4-R4-S2	4	20.90	10	0.01	110	145	1.22	176	9.59	0.17	2.82	97	174	107	67
754	6	4	5	080612-072412-C4-R4-S2	5	21.01	10	0.04	441	145	1.22	176	9.59	0.18	2.82	97	174	107	67
755	6	4	5	080612-072412-C4-R4-S2	6	20.93	10	0	0	145	1.22	176	9.59	0.17	2.82	97	174	107	67

BIBLIOGRAPHY

Aberle, J., Nikora, V., & Walters, R. (2004). Effects of bed material properties on cohesive sediment erosion. *Marine Geology, 207* (1), 83–93.

Aberle, J., Nikora, V., & Walters, R. (2006). Data interpretation for in situ measurements of cohesive sediment erosion. *Journal of Hydraulic Engineering, 132* (6), 581–588.

Amore, E., Modica, C., Nearing, M. A., & Santoro, V. C. (2004). Scale effect in USLE and WEPP application for soil erosion computation from three Sicilian basins. *Journal of Hydrology, 293* (1), 100–114.

Anderson, K. and Knight, D., (2012) “”CAIT Channel Calculation”,” Technical Report, Rutgers University, Center for Computational Design.

Angelaki, M. (2006). *Evaluation of bed shear stress under turbid flows through measures of flow deceleration* (Unpublished doctoral dissertation). University of Southampton.

Annandale, G. W. (2005). *Scour technology: mechanics and engineering practice*. McGraw Hill Professional.

Been, K. (1980). *Stress strain behaviour of a cohesive soil deposited under water*. (Unpublished doctoral dissertation). University of Oxford.

Beer, T. (1996). *Environmental oceanography* (Vol. 11). CRC Press.

Bergström, S. (1991). Principles and confidence in hydrological modelling. *Nord. Hydrol.*, 22 (2), 123–136.

Bergström, S., & Graham, L. (1998). On the scale problem in hydrological modelling. *Journal of Hydrology, 211* (1), 253–265.

Bierkens, M. F., Finke, P. A., & Willigen, P. d. (2000). Upscaling and downscaling methods for environmental research.

Blöschl, G., & Sivapalan, M. (1995). Scale issues in hydrological modelling: a review. *Hydrological processes, 9* (3-4), 251–290.

Borrowman, T. D., Smith, E. R., Gailani, J. Z., & Caviness, L. (2006).*Erodibility Study Of Passaic River Sediments Using USACE Sedflume* (No. ERDC-TR-06-7). ENGINEER RESEARCH AND DEVELOPMENT CENTER VICKSBURG MS ENVIRONMENTAL LAB.

Borsje, B. W., de Vries, M. B., Hulscher, S. J., & de Boer, G. J. (2008). Modeling large-scale cohesive sediment transport affected by small-scale biological activity. *Estuarine, Coastal and Shelf Science, 78* (3), 468–480.

Briaud, J. L., Ting, F. C. K., Chen, H. C., Cao, Y., Han, S. W., & Kwak, K. W. (2001). Erosion function apparatus for scour rate predictions. *Journal of geotechnical and geoenvironmental engineering*.

Burke, P., Bruno, M., Rankin, K., & Herrington, T. (2002). Sediment transport between deep navigation channels and shallow side banks under variable tidal and meteorological forcing. In *AGU Fall meeting abstracts* (Vol. 1, p. 0258).

Burt, N., Parker, R., & Watts, J. H. (1997). Cohesive sediments. John Wiley.

Chant, R. J. (2005). *Hydrodynamics of the Newark Bay/Kills system* (Tech.Rep.). New Jersey Department of Environmental Protection.

Cundy, A. B., Collins, P. E., Turner, S. D., Croudace, I. W., & Horne, D. (1998). 100 years of environmental change in a coastal wetland, Augusta Bay, southeast Sicily: evidence from geochemical and palaeoecological studies. *Geological Society, London, Special Publications, 139* (1), 243–254.

De Vriend, H. J. (1991a). Mathematical modelling and large-scale coastal behaviour: Part 2: Predictive models. *Journal of Hydraulic Research, 29* (6), 741–753.

De Vriend, H. J. (1991b). Mathematical modelling and large-scale coastal behaviour: Part 2: Predictive models. *Journal of Hydraulic Research, 29* (6), 741–753.

Dyer, K. (1998). Sedimentary processes in the intertidal zone. In K. S. Black,D. M. Paterson, & A. Cramp (Eds.), (p. 11-24). Geological Society of London.

Fenton, J., & Abbott, J. (1977). Initial movement of grains on a stream bed: The effect of relative protrusion. *Proceedings of the Royal Society of London*. A. Mathematical and Physical Sciences, 352 (1671), 523–537.

Freund, L. B., & Suresh, S. (2003). Thin film materials: *stress, defect formation and surface evolution*. Cambridge University Press.

Garcaia, M. H. (2008). *Sedimentation engineering: processes, measurements, modeling, and practice* (No. 110). ASCE Publications.

Geyer, W. R. (2010). Contemporary issues in estuarine physics. In A. ValleLevinson (Ed.), (p. 12-26). Cambridge University Press.

Goodchild, M. F., et al. (1997). Scale in remote sensing and GIS. CRC Press.

Grabowski, R. C., Droppo, I. G., & Wharton, G. (2011). Erodibility of cohesive sediment: The importance of sediment properties. *Earth-Science Reviews, 105* (3), 101–120.

Green, M. O., Black, K. P., & Amos, C. L. (1997). Control of estuarine sediment dynamics by interactions between currents and waves at several scales. *Marine Geology, 144* (1), 97–116.

Hamilton, D. P., & Mitchell, S. F. (1996). An empirical model for sediment resuspension in shallow lakes. *Hydrobiologia*, *317*(3), 209-220.

Halonen, J. (2011). Effects of historical morphologic change on sediment accumulation in Newark Bay, New Jersey (Unpublished doctoral dissertation). University of Delaware.

Herman, P. M., Middelburg, J. J., & Heip, C. H. (2001). Benthic community structure and sediment processes on an intertidal flat: results from the ECOFLAT project. *Continental Shelf Research, 21* (18), 2055–2071.

Heuvelink, G., & Webster, R. (2001). Modelling soil variation: past, present, and future. *Geoderma, 100* (3), 269–301.

Heuvelink, G. B. (1998). Uncertainty analysis in environmental modelling under a change of spatial scale. *Nutrient Cycling in Agroecosystems, 50* (1-3), 255–264.

Hickin, E. J. (1995). River geomorphology. John Wiley & Sons.

Jeng, D. S., Barry, D., & Li, L. (2000). Water wave-driven seepage in marine sediments. *Advances in water resources, 24* (1), 1–10.

Jepsen, R., Roberts, J., & Lick, W. (1997). Effects of bulk density on sediment erosion rates. *Water, Air, and Soil Pollution*, *99*(1-4), 21-31.

João, E. (2007). A research agenda for data and scale issues in strategic environmental assessment (SEA). *Environmental Impact Assessment Review, 27* (5), 479–491.

João, E. M. (2000). The importance of scale issues in environmental impact assessment and the need for scale guidelines.

Karstens, S. (2009). Bridging boundaries: *Making scale choices in multi-actor policy analysis on water management* (Vol. 4). IOS Press.

Kirby, R. (2000). Practical implications of tidal flat shape. *Continental Shelf Research, 20* , 1061 - 1077.

Kirchner, J. W., Dietrich, W. E., Iseya, F., & Ikeda, H. (1990). The variability of critical shear stress, friction angle, and grain protrusion in water-worked sediments. *Sedimentology, 37* (4), 647–672.

Kornman, B. A., & De Deckere, E. M. (1998). Temporal variation in sediment erodibility and suspended sediment dynamics in the Dollard estuary. *Geological Society, London, Special Publications, 139* (1), 231–241.

Kronvang, B., Faganeli, J., & Ogrinc, N. (2006). *The interactions between sediments and water*. Springer.

Lavelle, J. W., Mofjeld, H. O., & Baker, E. T. (1984). An in situ erosion rate for a fine-grained marine sediment. *Journal of Geophysical Research: Oceans (1978–2012), 89*(C4), 6543-6552.

Lee, D.-Y., Lick, W., & Kang, S. W. (1981). The entrainment and deposition of fine-grained sediments in Lake Erie. *Journal of Great Lakes Research, 7* (3), 224–233.

Lee, S. C., & Mehta, A. J. (1994). Cohesive sediment erosion. *Final report prepared for Dept. of the Army, U.S. Army Corps of Engineers*.

Leupi, C. (2005). *Numerical modeling of cohesive sediment transport and bed morphology in estuaries* (Unpublished doctoral dissertation). ÉCOLE POLYTECHNIQUE FÉDÉRALE DE LAUSANNE.

Lick, W. (2008). *Sediment and contaminant transport in surface waters*. CRC Press.

Lintern, D. G. (2003). *Influences of flocculation on bed properties for fine-grained cohesive sediment* (Unpublished doctoral dissertation). University of Oxford.

Lopez, F., & Garcia, M. H. (2001). Risk of sediment erosion and suspension in turbulent flows. *Journal of Hydraulic Engineering, 127* (3), 231–235.

Luettich, R. A., Harleman, D. R., & Somlyody, L. (1990). Dynamic behavior of suspended sediment concentrations in a shallow lake perturbed by episodic wind events. *Limnology and Oceanography, 35* (5), 1050–1067.

Lund-Hansen, L. C., Christiansen, C., Jensen, O., & Laima, M. (1999). The LABEREX chamber for studying the critical shear stress for fine-grained sediment. *Geografisk Tidsskrift-Danish Journal of Geography, 99* (1), 1–7.

Malcolm, D. B., S. J.; Sivyer. (1997). Biogeochemistry of intertidal sediments. In J. E. Jickells T. D.; Rae (Ed.), (p. 84-98). Cambridge University Press.

Mariotti, G., Valentine, K., & Fagherazzi, S. (2013). Time-dependent behavior of a placed bed of cohesive sediment subjected to erosion and deposition cycles. *Ocean Dynamics*, 1–8.

McBratney, A. B. (1998). Some considerations on methods for spatially aggregating and disaggregating soil information. *In Soil and water quality at different scales* (pp. 51–62). Springer.

McNeil, J., Taylor, C., & Lick, W. (1996). Measurements of erosion of undisturbed bottom sediments with depth. *Journal of Hydraulic Engineering, 122* (6), 316–324.

Meadows, A., Meadows, P. S., & McLaughlin, P. (1998). Spatial heterogeneity in an intertidal sedimentary environment and its macrobenthic community. Geological Society, London, *Special Publications, 139* (1), 367–388.

Meadows, P. S., Murray, J. M., Meadows, A., Wood, D. M., & West, F. J. (1998). Microscale biogeotechnical differences in intertidal sedimentary ecosystems. Geological Society, London, *Special Publications, 139* (1), 349–366.

Mehta, A. (1988). Laboratory studies on cohesive sediment deposition and erosion. In *Physical processes in estuaries* (pp. 427–445). Springer.

Merritt, W. S., Letcher, R. A., & Jakeman, A. J. (2003). A review of erosion and sediment transport models. *Environmental Modelling & Software, 18* (8), 761–799.

Meysman, F. J., Middelburg, J. J., Herman, P. M., & Heip, C. H. (2003). Reactive transport in surface sediments. II. media: an object-oriented problem-solving environment for early diagenesis. *Computers & Geosciences, 29* , 301 - 318.

Mikkelsen, O., & Pejrup, M. (1998). Comparison of flocculated and dispersed suspended sediment in the Dollard estuary. Geological Society, London, *Special Publications, 139* (1), 199–209.

Mosteller, F., & Tukey, J. W. (1968). *Data analysis, including statistics*.

Murphy, R., Tolhurst, T., Chapman, M., & Underwood, A. (2004). Estimation of surface chlorophyll on an exposed mudflat using digital colour-infrared (CIR) photography. Estuarine, *Coastal and Shelf Science, 59* (4), 625–638.

Neumann, A. C., & Land, L. S. (1975). Lime mud deposition and calcareous algae in the Bight of Abaco, Bahamas: a budget. *Journal of Sedimentary Research, 45* (4).

Nicholson, J., & O'Connor, B. A. (1986). Cohesive sediment transport model. *Journal of Hydraulic Engineering*, *112*(7), 621-640.

Paintal, A. (1971). Concept of critical shear stress in loose boundary open channels. *Journal of Hydraulic Research, 9* (1), 91–113.

Parchure, T. M., & Mehta, A. J. (1985). Erosion of soft cohesive sediment deposits. *Journal of Hydraulic Engineering, 111* (10), 1308–1326.

Partheniades, E. (1993). Turbulence, flocculation and cohesive sediment dynamics. *Nearshore and estuarine cohesive sediment transport*, 40–59.

Paterson, D., & Black, K. (1999). Water flow, sediment dynamics and benthic biology. *Advances in Ecological Research, 29*, 155–194.

Pritchard, D., Hogg, A., & Roberts, W. (2002). Morphological modelling of intertidal mudflats: the role of cross-shore tidal currents. *Continental Shelf Research, 22* (11), 1887–1895.

Quinton, J. N. (2005). Environmental modelling: Finding simplicity in complexity. In J. Wainwright & M. Mulligan (Eds.), (p. 187-196). John Wiley & Sons.

Ravens, T. M. (1997). Sediment resuspension in Boston Harbor (Unpublished doctoral dissertation). Massachusetts Institute of Technology.

Ravens, T. M. (2007). Comparison of two techniques to measure sediment erodibility in the Fox River, Wisconsin. *Journal of Hydraulic Engineering, 133* (1), 111–115.

Ravens, T. M., & Gschwend, P. M. (1999). Flume measurements of sediment erodibility in Boston Harbor. *Journal of Hydraulic Engineering, 125* (10), 998–1005.

Riethmüller, R., Hakvoort, J., Heineke, M., Heymann, K., Kuehl, H., & Witte, G. (1998). Relating erosion shear stress to tidal flat surface colour. Geological Society, London, *Special Publications*, 139 (1), 283–293.

Roberts, J., Jepsen, R., Bryan, C., and Chapin, M., 2000. Boston Harbor Sediment Study, Report Submitted to the U.S. Army Corps of Engineers, New England District.

Roberts, J., Jepsen, R., Gotthard, D., & Lick, W. (1998). Effects of particle size and bulk density on erosion of quartz particles. *Journal of Hydraulic Engineering*.

Rodrigue, J., Slack, B., & Notteboom, T. (n.d.). *The Geogrophy of Transport Systems*: *Port Terminals.* Retrieved May 15, 2014, fro http://people.hofstra.edu/geotrans/eng/ch4en/conc4en/ch4c3en.html

Ruddy, G., Turley, C., & Jones, T. (1998). Ecological interaction and sediment transport on an intertidal mudflat I. Evidence for a biologically mediated sediment-water interface. Geological Society, London, *Special Publications, 139* (1), 135–148.

Ryan, N., & Cooper, J. (1998). Spatial variability of tidal flats in response to wave exposure: examples from Strangford lough, Co. Down, Northern Ireland. Geological Society, London, *Special Publications, 139* (1), 221–230.

Sanford, L. P. (2006). Uncertainties in sediment erodibility estimates due to a lack of standards for experimental protocols and data interpretation. *Integrated environmental assessment and management, 2* (1), 29–34.

Sanford, L. P., & Maa, J. P.-Y. (2001). A unified erosion formulation for fine sediments. *Marine Geology, 179* (1), 9–23.

Schlichting, H. (n.d.). 1979, boundary layer theory, mcgraw-hill. *New York*.

Stein, A., Riley, J., & Halberg, N. (2001). Issues of scale for environmental indicators. *Agriculture, Ecosystems & Environment, 87* (2), 215–232.

Subramanian, V. (1993). Sediment load of Indian rivers. CURRENT SCIENCE-BANGALORE-, *CURRENT SCIENCE ASSOC/INDIAN ACADEMY OF SCIENCES, 64*, 928–928.

Sutherland, T., Amos, C. L., & Grant, J. (1998). The erosion threshold of biotic sediments: a comparison of methods. *Geological Society, London, Special Publications, 139* (1), 295–307.

Syvitski, J. P. (2003). Supply and flux of sediment along hydrological pathways: research for the 21st century. *Global and Planetary Change, 39* (1), 1–11.

Uncles, R., Stephens, J., & Harris, C. (1998). Seasonal variability of subtidal and intertidal sediment distributions in a muddy, macrotidal estuary: the Humber-Ouse, UK. *Geological Society, London, Special Publications, 139* (1), 211–219.

Unknown. (2003). *Collection and preparation of bottom sediment samples for analysis of radionuclides and trace elements* (Tech. Rep.). International Atomic Energy Agency.

Valette-Silver, N. J. (1993). The use of sediment cores to reconstruct historical trends in contamination of estuarine and coastal sediments. *Estuaries, 16* (3), 577–588.

Van der Lee, W. (1998). The impact of fluid shear and the suspended sediment concentration on the mud floc size variation in the Dollard estuary, The Netherlands. Geological Society, London, *Special Publications, 139* (1), 187–198.

Van Prooijen, B., & Winterwerp, J. (2010). A stochastic formulation for erosion of cohesive sediments. Journal of Geophysical Research: *Oceans (1978–2012), 115* (C1).

Webster, R., & Oliver, M. A. (2007). *Geostatistics for environmental scientists*. John Wiley &

Whitehouse, R., Soulsby, R., Roberts, W., & Mitchener, H. (2009). *Dynamics of estuarine muds. Institution of Civil Engineers.*

Whitehouse, R. J., & Mitchener, H. J. (1998). Observations of the morphodynamic behaviour of an intertidal mudflat at different timescales. *Geological Society, London, Special Publications, 139* (1), 255–271.

Widdows, J., Brown, S., Brinsley, M., Salkeld, P., & Elliott, M. (2000). Temporal changes in intertidal sediment erodability: influence of biological and climatic factors. *Continental Shelf Research, 20* (10), 1275–1289.

Wilson, T. P. (2006). Results of Cross-Channel Monitoring During the Lower Passaic River Environmental Dredging Pilot Program on the Lower Passaic River, December 1 to 12, 2005. *USGS Report, West Trenton, New Jersey Page intentionally left blank*.

Wiltshire, K. H., Tolhurst, T., Paterson, D., Davidson, I., & Gust, G. (1998). Pigment fingerprints as markers of erosion and changes in cohesive sediment surface properties in simulated and natural erosion events. *Geological Society, London, Special Publications, 139* (1), 99–114.

Winterwerp, J., Kesteren, W., Prooijen, B., & Jacobs, W. (2012). A conceptual framework for shear flow–induced erosion of soft cohesive sediment beds. *Journal of Geophysical Research: Oceans (1978–2012), 117* (C10).

Winterwerp, J. C., & Van Kesteren, W. G. (2004). *Introduction to the physics of cohesive sediment dynamics in the marine environment* (Vol. 56). Elsevier Science.

Witt, O., & Westrich, B. (2003). Quantification of erosion rates for undisturbed contaminated cohesive sediment cores by image analysis. In *The Interactions between Sediments and Water* (pp. 271-276). Springer Netherlands.

Wood, E. F., Sivapalan, M., Beven, K., & Band, L. (1988). Effects of spatial variability and scale with implications to hydrologic modeling. *Journal of Hydrology, 102* (1), 29–47.

Wu, W., & Wang, S. S. (n.d.). An introduction to latest developments in soil erosion and sediment transport modeling.

Xiao, H. (2009). *Experimental and numerical modeling of wave-induced sediment transport and soil responses*. Princeton University.

ZHANG, X., DRAKE, N. A., & WAINWRIGHT, J. (2005). Environmental modelling: Finding simplicity in complexity. In J. Wainwright & M. Mulligan(Eds.), (p. 319-334). John Wiley & Sons.

Zreik, D. A., Krishnappan, B. G., Germaine, J. T., Madsen, O. S., & Ladd, C. C. (1998). Erosional and mechanical strengths of deposited cohesive sediments. Journal of Hydraulic Engineering, 124 (11), 1076–1085.